# The roles of α-synuclein in biomolecular condensates implicated in neuronal physiology and disease

Inaugural-Dissertation
to obtain the academic degree
Doctor rerum naturalium (Dr. rer. nat.)

submitted to the Department of Biology, Chemistry, Pharmacy
of Freie Universität Berlin

by

Roberto Sansevrino

2023

August 2023

Freie Universität Berlin

1st reviewer:

Dr. Dragomir Milovanovic

AG Molecular Neuroscience

Deutsches Zentrum für Neurodegenerative Erkrankungen (DZNE)

Charitéplatz 1, 10117 Berlin

2nd reviewer:

Prof. Dr. Stephan Sigrist

AG Genetics

Institute of Biology, Freie Universität Berlin

Takustr. 6, Raum 216, 14195 Berlin

Date of defense: 02/02/2024

# DECLARATION OF INDEPENDENCE

Herewith I certify that I have prepared and written my thesis independently and that I have not used any sources and aids other than those indicated by me.

I also declare that I have not submitted the dissertation in this or any other form to any other institution as a dissertation.

Berlin, 31.08.2023
Roberto Sansevrino

# Table of Contents

# ACKNOWLEDGMENTS

I am profoundly grateful to have reached this significant milestone in my academic journey, and I would like to extend my heartfelt appreciation to all those who have supported and guided me along the way.

First and foremost, I would like to express my deepest gratitude to my thesis advisor, Dr. Dragomir Milovanovic for his unwavering support, invaluable guidance, and insightful feedback throughout the entire research process. I am thankful for the great opportunity he gave me to experience this adventure from the first day when the lab started and built up over time. Is it always going to be a great example of mentorship, determination, ambition, and pure love for science. His expertise and encouragement have been instrumental in shaping the direction of this thesis.

I am also grateful to Prof. Dr. Stephan Sigrist for his supervision and for enhancing the quality of my work. His availability and trust have allowed us to carry out this work in the best possible way.

I extend my appreciation to the entire Drago's Lab (Christian, Brana, Beppe, Han, Marko, Gerard, Akshita, Johannes, Chiny, Franzi, Linda, Lona, Ema, Florian, Sila, Gwenni, Yasat, Nela, Jean-Baptiste, Robin, Luka, Paula, Mahmoud, and Aleksandrand,) fellow colleagues who have provided a network of encouragement, stimulating discussions, and moments of respite during this challenging endeavor. Over the past years, your companionship has made this journey both rewarding and memorable.

I would also like to spend some extra words for some special fellows with whom I shared my journey:

Christian: Everything started that early morning entering the lab for the first time, crazy time ☺. You can't imagine how precious your guidance has been in these years and how much I've learned from you. I asked myself many times how it was possible that this guy always had if not the answer, at least the right suggestion for any scientific challenge. Your professional and personal attitude it's something that I tried to emulate many times. I enjoyed

so much doing extra hours in your company, one time spending the night at the microscope, or another time trying to complete the protein purification, when possible in a companion of a couple of great German beers.

Marta: Scrivere questa parte in inglese avrebbe forse reso la comunicazione più facile, ma in questi ultimi anni il tuo livello di pugliese è migliorato molto. Dove cominciare se non: "Come avrei fatto a Berlino questi anni senza di te?!"…mi sembra chiaro che sarebbe stato tutto molto più cupo e ostico (come se già ci si ammazzi di risate a fare il dottorato). Grazie per i mille caffè, cene, sigarette, FATTI e ABBOTTAMENTI che abbiamo condiviso in questi anni. La tua presenza è stata quella che più di ogni altra ha arricchito il mio percorso a Berlino. Sei una scienziata incredibilmente appassionata e ambiziosa e questo è stato di grande stimolo per me in questi anni. Ti auguro di diventare la capa suprema che mondo scienza e perdona loro che non sanno quello che fanno intorno a te nel tuo percorso :D.

Franzi: My dearest desk mate for so long that I still imagine looking over my screen and seeing you there with a post-it saying "Buongiorno". How many chats, food, and Berlin tours we shared together? You really helped me to see the lab as a family place where I was happy to go and start another day. Beppe and I worked so much teaching you Italian that I expect big things from you. Joking apart, after hearing your "Oggi ammazzo qualcuno" you are the best student of Italian I've ever had.

Max: Maaaan, how fun is microscopy??! It has been nice sharing suggestions and opinions on data analysis as much as time spent at your house parties!! I wish the best to you and Giulia, keep going with your Italian recipes and I trust that you will be good at Burraco, one day or the other :D.

Alvaro: Here it starts the Mediterranean side (we don't count Marta of course). Having someone who can understand how it is living in a personal time zone is something that made me feel at home. Always ready for an improvised trip (and we collected quite a lot of them), you helped me to realize how close I can be to the Spanish culture. I enjoyed all your "Mama Alvaro meals", our looong looong loooong conversations, and our dinner started at 10 p.m. and finished at 6 a.m. Your secret Domínguez Baquero sauce it's in safe hands.

Dimitra: Dìmitra or Dimìtra, or Dimitrà. More commonly used Dimitraaaaaaaa. Here the Mediterranean style gets an upgrade. The loudest of the upgrades as someone can confirm in Ireland. After countless cigarettes up the terrace, spent talking about the shitty weather in Berlin, I got to know you better and it has been great to share countless chat about art, music, and movies, but also debatable Italian food. The trips were a great occasion to have fun and discover new "so Dimitra" aspects (a prayer to all the lost things in every journey). One last thing. Do you know one thing that the Greeks didn't invent? Driving, especially on the left-hand side of the road :D. Love pistachio, love cats, and Peace.

Bilge: ALLORA, where do we start? I loved every laughing session when Dory's mode was on. Throughout the tough first years in Berlin, having a cozy and familiar environment made me happy, spending the evenings on your couch under the heavy weight of the wooden blanket. Nevertheless, I will miss the chats in the cell culture (oh wait I'm counting) and the moments of forced seriousness during the meetings. I wish the best for you and Yigit and hope you can love a cat someday☺. Don't forget: Italy's jerseys are blue and Turkey's are red.

Last but not least, I am indebted to my family. Their unending support, encouragement, and understanding have been my constant source of strength. Your belief in me has been my driving force.

In conclusion, this thesis would not have been possible without the collective efforts, encouragement, and guidance of all those mentioned above. While the list is not exhaustive, every contribution has left an indelible mark on my academic and personal growth. Thank you all for being a part of this journey.

# SUMMARY

Eukaryotic cells employ membrane-bound compartments to spatially organize their internal components. However, the recent discovery of biomolecular condensates, liquid-like structures not limited by a membrane, has emerged as a novel mechanism for cellular organization. These condensates often assemble by liquid-liquid phase separation (LLPS), a phenomenon in which an initially homogeneous liquid mixture spontaneously separates into two (or more) distinct liquid phases. LLPS is emerging as an important principle for understanding the organization and dynamics at the synapse and cellular pathology in neurodegeneration. For instance, synaptic vesicle (SV) clusters are shown to assemble via condensation of synapsins, a highly abundant family of synaptic phosphoproteins, and SVs. This thesis investigates the roles of α-synuclein, a protein involved in the SV cycle and implicated in the pathology of Parkinson's disease (PD), in modulating biomolecular condensates and their interplay with membrane-bound organelles. The first part of the thesis examines the contribution of α-synuclein to maintaining SV clusters. α-Synuclein enriches the liquid phase of SVs/synapsin, preserving their biophysical properties while maintaining high mobility. The results show that the presence of SVs enhances the condensation rate between synapsin and α-synuclein, indicating that SVs act as catalysts for synapsin condensate formation. Importantly, α-synuclein alone is unable to cluster isolated SVs under physiological conditions, emphasizing the importance of the synapsin/α-synuclein molar ratio in assembling functional and physiological condensates. The second part of the thesis focuses on understanding the aberrant LLPS process that leads to the formation of α-synuclein-containing protein aggregates, specifically Lewy bodies (LBs). LBs are associated with synucleinopathies like PD. By employing a minimal system comprising α-synuclein and synphilin 1, another protein implicated in PD, LB-like structures (LBLs) are recapitulated. Remarkably, synphilin 1 can independently form fluid condensates, while α-synuclein envelops these condensates, forming a core-shell structure resembling LBs. Additionally, LBLs disrupt the fibrillar actin network and accumulate membrane-bound organelles, leading to mitochondrial collapse and their accumulation at the interface of the aggregates. These observations highlight the connection between α-synuclein-driven aberrant phase separation and the formation of membrane-containing inclusions. Together, this thesis contributes to our understanding of the intricate dynamics and functional consequences of biomolecular condensates, specifically focusing on the role of α-synuclein in modulating their formation and interplay with membrane-bound organelles. The findings presented here deepen our understanding of the molecular mechanisms underlying neurodegenerative disorders, particularly PD, and pave the way for future research aimed at developing therapeutic interventions targeting these aberrant processes.

# ZUSAMMENFASSUNG

Zellen verwenden membranbegrenzte Kompartimente, um ihre internen Bestandteile räumlich zu organisieren. Allerdings hat sich die jüngste Entdeckung von biomolekularen Kondensaten, flüssigkeitsartigen Strukturen, die nicht durch eine Membran begrenzt sind, als ein neuer Mechanismus für die zelluläre Organisation herausgestellt. Diese Kondensate bilden sich oft durch Flüssig-Flüssig-Phasentrennung (LLPS), ein Phänomen, bei dem eine zunächst homogene Flüssigkeitsmischung spontan in zwei (oder mehr) unterschiedliche Flüssigkeitsphasen aufgeteilt wird. LLPS gewinnt als wichtiges Prinzip an Bedeutung für das Verständnis der Organisation und Dynamik an der Synapse sowie der zellulären Pathologie bei neurodegenerativen Erkrankungen. Beispielsweise wurde gezeigt, dass sich synaptische Vesikel (SV) durch Kondensation von Synapsinen, einer hochabundanten Familie von synaptischen Phosphoproteinen, und SVs zu Clustern zusammensetzen. Diese Dissertation untersucht die Rolle von α-Synuclein, einem Protein, das am SV-Zyklus beteiligt ist und mit der Pathologie der Parkinson-Krankheit (PD) in Verbindung gebracht wird, bei der Modulation von biomolekularen Kondensaten und deren Zusammenspiel mit membranbegrenzten Organellen. Der erste Teil der Dissertation untersucht den Beitrag von α-Synuclein zur Aufrechterhaltung von SV-Clustern. α-Synuclein bereichert die Flüssigphase von SVs/Synapsin und bewahrt ihre biophysikalischen Eigenschaften bei gleichzeitig hoher Mobilität. Die Ergebnisse zeigen, dass das Vorhandensein von SVs die Kondensationsrate zwischen Synapsin und α-Synuclein erhöht, was darauf hinweist, dass SVs als Katalysatoren für die Bildung von Synapsin-Kondensaten fungieren. Wichtig ist, dass α-Synuclein allein unter physiologischen Bedingungen nicht in der Lage ist, isolierte SVs zu clustern, was die Bedeutung des Synapsin/ α-Synuclein-Molverhältnisses bei der Bildung funktionaler und physiologischer Kondensate unterstreicht. Der zweite Teil der Dissertation konzentriert sich auf das Verständnis des fehlerhaften LLPS-Prozesses, der zur Bildung von α-Synuclein-haltigen Proteinaggregaten, speziell Lewy-Körperchen (LB), führt. LBs werden mit Synukleinopathien wie PD in Verbindung gebracht. Durch den Einsatz eines minimalen Systems, bestehend aus α-Synuclein und Synphilin 1, einem weiteren Protein, das mit PD in Verbindung gebracht wird, werden LB-ähnliche Strukturen (LBL) nachgebildet. Bemerkenswerterweise können Synphilin 1 unabhängig flüssige Kondensate bilden, während α-Synuclein diese Kondensate umhüllt und eine Kern-Hülle-Struktur bildet, die LBs ähnelt. Darüber hinaus stören LBLs das faserige Aktinnetzwerk und akkumulieren membranbegrenzte Organellen, was zu einem Zusammenbruch der Mitochondrien führt und zu ihrer Anreicherung an der Grenzfläche der Aggregate. Diese Beobachtungen verdeutlichen den Zusammenhang zwischen einer von α-Synuclein angetriebenen fehlerhaften Phasentrennung und der Bildung von membranhaltigen Einschlüssen. Insgesamt trägt diese Dissertation zu unserem Verständnis der komplexen Dynamik und funktionalen Konsequenzen von biomolekularen Kondensaten bei und konzentriert sich dabei speziell auf die Rolle von α-Synuclein bei ihrer Bildung und ihrem Zusammenspiel mit membranbegrenzten Organellen. Die hier vorgestellten Ergebnisse vertiefen unser Verständnis der molekularen Mechanismen, die neurodegenerative Erkrankungen, insbesondere PD, zugrunde liegen, und bahnen den Weg für zukünftige Forschung zur Entwicklung therapeutischer Interventionen, die diese fehlerhaften Prozesse zum Ziel haben.

# ABBREVIATIONS

| | |
|---|---|
| AD | Alzheimer's disease |
| AD/ALB | Alzheimer's disease with Amygdalar Restricted Lewy Bodies |
| ADP | Adenosine diphosphate |
| ALPS | Amphipathic lipid packing sensor |
| ALS | Amyotrophic lateral sclerosis |
| ANK | Ankyrin repeat domain |
| APS | Ammonium persulfate |
| ATP | Adenosine triphosphate |
| $CaCl_2$ | Calcium chloride |
| CaMKII | Ca2+/calmodulin-dependent protein kinase |
| Cdk1/5 | Cyclin-dependent kinase |
| CLEM | Correlative light and electron microscopy |
| $CO_2$ | Carbon dioxide |
| DIV 14 | Day in vitro 14 |
| DLB | Lewy bodies dementia |
| DMEM | Dulbecco’s modified eagle medium |
| DNA | Deoxyribonucleic Acid |
| EDTA | Ethylene-diamine-tetra-acetic acid |
| EM | Electron microscopy |
| ERK | Extracellular signal-regulated kinase |
| FUS | Fluorescence recovery after photobleaching |
| Grb 2 | Growth factor receptor-bound protein 2 |
| GTP | Guanosine triphosphate |
| HCl | Hydrogen chloride |
| HEK 293 | Human embryonic kidney 293 cells |
| HEPES | 4-(2-hydroxyethyl)-1-piperazineethanesulfonic acid |
| HIS | Histidine |
| IDRs | Intrinsically disordered regions |
| KCl | Potassium chloride |
| KOH | Potassium hydroxide |
| LBLs | Lewy bodies-like structures |
| LBs | Lewy bodies |
| LLPS | Liquid-liquid phase separation |
| LNs | Lewy neurites |
| LRRK2 | Leucine-rich repeat kinase 2 |
| MAPK | Mitogen-activated protein kinase |
| $MgCl_2$ | Magnesium chloride |
| MSA | Multiple system atrophy |
| $Na_2HPO_4$ | Disodium phosphate |
| NAC | Non-amyloid-component |
| NaCl | Sodium chloride |

| | |
|---|---|
| NBR1 | Neighbor of BRCA1 gene 1 protein |
| NSF | N-ethylmaleimide-sensitive factor |
| PBS | Phosphate-buffered saline |
| PCR | Polymerase chain reaction |
| PD | Parkinson's disease |
| PEG | Polyethylene glycol |
| pI | Isoelectric point |
| PKA | AMP-dependent protein kinase A |
| PrDOS | Protein disordered prediction system |
| PRM | Proline-rich motifs |
| PSD-95 | Postsynaptic density protein 95 |
| PTMs | Post-translational modifications |
| rDNA | Ribosomal DNA |
| RIM | Rab3-interacting molecule |
| RIM-BP | Rim-binding protein |
| RNA | Ribonucleic acid |
| RNP | Ribonucleoprotein |
| ROI | Region of interest |
| rRNA | Ribosomal RNA |
| RRP | Readily releasable pool |
| SDHA | Succinate dehydrogenase complex |
| SDS-PAGE | Sodium Dodecyl Sulphate - polyacrylamide Gel Electrophoresis |
| SH3 | Src homology 3 |
| SNARE | Soluble N-ethylmalemide sensitive factor-attachment protein receptor ] |
| SNpc | Substantia nigra pars compacta |
| SUMO | Small Ubiquitin-like Modifier |
| SVs | Synaptic vesicles |
| TCEP | Tris(2-carboxyethyl) phosphine |
| TDP-43 | TAR DNA-binding protein 43 |
| TEM | Transmission electron microscopy |
| TEMED | Tetramethylethylenediamine |
| TKO | Triple knockout |
| TRIS | Tris(hydroxymethyl)aminomethane |
| VAMP2 | Vesicle-associated membrane protein 2 |
| WT | Wild type |

# 1. INTRODUCTION

## 1.1. Liquid-liquid phase separation

### 1.1.1. Principles of LLPS

Eukaryotic cells are mostly composed of water (~70% of the total volume). This aqueous environment contains hundreds of thousands of different molecules such as proteins, nucleic acids, and lipids, leading to the definition of this space as a crowded, multicomponent fluid mixture (Moran et al., 2010). All of these biomolecules carry out their biological functions by interacting with one another and with their surroundings. The regulation of this interaction is crucial to organize and orchestrating in space and time biological reactions in a such crowded environment (Quiroz et al., 2020; Sontag et al., 2017). To do so, the cells use different strategies to create the most optimal condition for reactions to take place, for example, to generate compartments that allow the local concentration of specific reagents while excluding the others (Alberts et al., 2002). These compartments are called organelles (e.g., nucleus, secretory vesicles, mitochondria, and lysosome to name a few) and are surrounded by a lipid bilayer because of which, we refer to these as membrane-bound organelles. Thus, the interior and exterior of classical organelles are physically separated, and organelle compositions are regulated through specialized membrane transport machinery.

Recently another class of organelles called membrane-less organelles or biomolecular condensates has been described (Brangwynne et al., 2009; Hyman et al., 2014; Shin and Brangwynne, 2017). These condensates have a different chemical composition than the surroundings but are not wrapped by membranes (Banani et al., 2017). Oftentimes, such condensates form via Liquid-Liquid Phase Separation (LLPS), a process driven by low-affinity, multivalent interactions (Brangwynne et al., 2015). LLPS is a phenomenon in which one or multiple components, segregate from each other into distinct phases (Tang, 2019) (Figure. 1.1.).

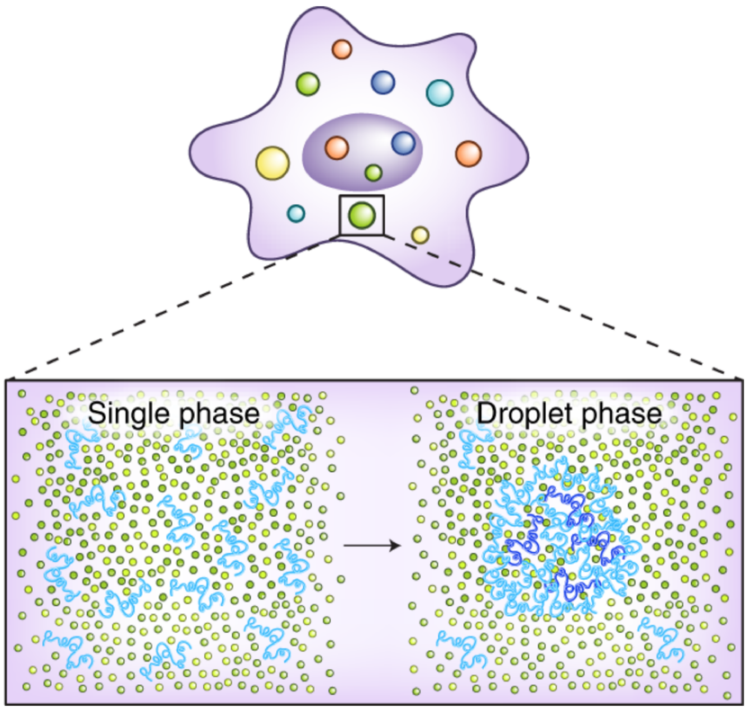


**FIGURE 1.1. Graphic representation of Intracellular liquid–liquid phase separation**. Modified from Tang, 2019.

As a result, these molecules are concentrated into compartments without a delimitating border, free to transiently interact with each other and separate from the surrounding aqueous environment. Different liquids have different material properties, such as viscosity, surface tension, and chemical composition (Alberti et al., 2019). These properties determine the interactions between the liquids, which in turn determines whether they will mix. Factors such as temperature, salt concentration, and the presence of other interacting partners can affect LLPS (Cinar et al., 2019). One classical example of LLPS is the separation of oil and water. Oil is less dense than water and does not mix with it, so when oil and water are combined, they will separate into two distinct layers. Low surface tension indicates that particle exchange with the surrounding is fast since there is less resistance to enter or leave the droplet (Wang et al., 2021). Because of their frequent round shape and small size, biomolecular condensates are often referred to as droplets.

### 1.1.2. Molecular features for LLPS

The molecules which undergo liquid phase separation have several distinct key features: (i) high local concentrations and the ability to engage in (ii) multivalent, (iii) low-affinity interaction (Li et al., 2012). Usually, LLPS is driven by Intrinsically Disordered

Regions (IDRs), sequences of proteins that lack a well-defined, stable three-dimensional structure under physiological conditions (Pak et al., 2016). Interestingly, IDRs of at least 50 amino acids in length are found in around one-third of eukaryotic proteins (Van der Lee et al., 2014). IDRs have been found to have a high degree of flexibility and a low level of hydrophobicity, which allows them to interact with other IDRs through low-affinity interactions and form a liquid droplet (Babu, 2016). This process is driven by the entropy gain and is dependent on the local chemical environment and the solvent (Pritišanac et al., 2019). IDRs that drive phase transitions are typically low-complexity sequences—the regions of protein with a low amino acid diversity. These sequences are frequently repetitive and rich in polar sidechains such as glycine (G), glutamine (Q), asparagine (N), and serine (S), positively charged sidechains such as arginine (R) and lysine (K), negatively charged side chains such as aspartic acid (D) and glutamic acid (E), and aromatic sidechains such as phenylalanine (F) and tyrosine (Y). For instance, YG/S-, FG-, RG-, GY-, KSPEA-, SY, and Q/N-rich regions, as well as blocks of alternating charges, are frequently found in sequences of interest (Uversky, 2013).

Therefore, molecules that undergo LLPS have specific properties, and many studies in the last years try to better characterize those features. In an early study, the relevance of the interaction between multivalent molecules and how concentration influences LLPS was extensively investigated by analyzing the Src Homology (SH3) domain and the proline-rich-motif (PRM) ligand: the two protein domains widely conserved in signaling proteins able to interact with each other (Figure. 1.2.). Modulating the number of these protein domains and the amount of proteins, they showed that concentrations needed for phase transition are directly related to the valency of the interacting species (Li et al., 2012). The condensates reconstituted in the study show some important liquid properties (Berry et al., 2018): (1) Condensates are typically spherical due to the high surface tension between phases; (2) They exhibit coalescence, which means they fuse upon contact; (3) They exchange particles with the environment through diffusion; (4) Despite behaving like a liquid, the condensate does not mix with its surroundings and retains a distinct composition from them. (5) To form a two-phase system, condensates require a certain concentration of specific proteins to be reached, so-called the critical concentration.

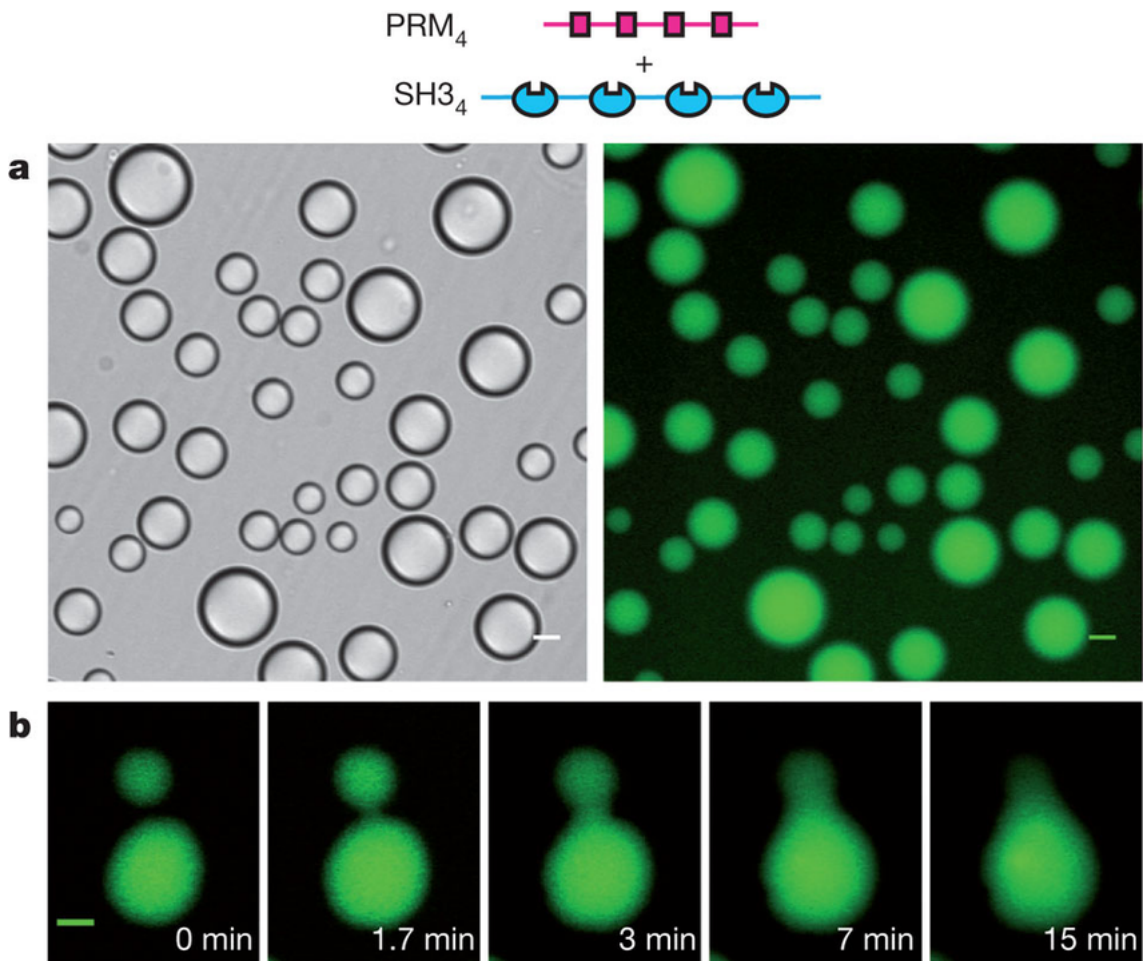


**FIGURE 1.2. Phase transitions in multivalent SH3/Prolin Rich Motifs (PRMs) systems.** (A) Liquid droplets observed by differential interference contrast microscopy (left) and widefield fluorescence microscopy (right) when 300 μM $SH3_4$, 300 μM $PRM_4$ (module concentrations; molecule concentrations are 75 μM), and 0.5 μM OG-$SH3_4$ are mixed. (B) Time-lapse imaging of merging droplets formed as in a. Modified from Li et al., 2012.

### 1.1.3. LLPS functions in a biological system

In biology, LLPS plays an important role in many cellular processes. For example, it is involved in the formation of intracellular compartments such as the nucleolus, where specific proteins and RNA molecules are concentrated to form a liquid droplet (Boija et al., 2018). This allows for the efficient assembly of these molecules for the formation of ribosomes, the cell's protein synthesis machinery (Boisvert et al., 2007). Another example is the phase separation of cytoskeletal proteins such as actin and microtubules, which form liquid droplets that can be converted into solid-like structures to provide structural support and shape to cells (Koppers et al., 2020). Condensates are also involved in important cellular processes such as cell division and movement (Ong and Torres, 2020; Curtis, 2021). Other examples such as P-bodies, are formed by the phase separation of specific proteins and RNA

molecules, which allows for the sequestration and regulation of these molecules (Luo et al., 2018).

Notably, the mechanisms of phase separation are size independent and not only restricted to nucleic acids and proteins but also include cohorts of organelles such as the stack of secretory vesicles (Gallo et al., 2020), Golgi apparatus (Ziltener et al., 2020; Rebane et al., 2020), and the synaptic vesicles (Milovanovic et al., 2018; Milovanovic and De Camilli, 2017a, Pechstein et al., 2020). Overall, LLPS is a widespread phenomenon in living cells and plays a role in various cellular processes such as gene expression, protein synthesis and degradation, and intracellular transport. Moreover, condensate formation and dissolution are extremely sensitive to external parameters near the critical point (Hohenberg and Halperin, 1977). This makes them an ideal tool for detecting differences in environmental conditions, such as those found in stress granules (Wippich et al., 2013; Alberti and Carra, 2018) or receptor clusters (Zhao and Zhang, 2020; Jaqaman and Ditlev, 2021). By keeping reactants in different phases, a high local concentration of certain molecules can speed up reactions and suppress certain reaction pathways (Peeples and Rosen, 2021; Lyon et al., 2021); additionally, a high concentration of molecules can enable processes that would be impossible in a well-mixed cytosol.

Moreover, biomolecular condensates exhibit liquid-like behavior such as wetting, which refers to a liquid's capacity to retain contact with a solid surface as a result of intermolecular interactions when the two are brought together (Murata and Tanaka, 2010). The wetting behavior can be used to direct condensate nucleation at specific sites, such as microtubules (Setru et al., 2021). Concentrating tubulin, for example, can induce microtubule nucleation in a condensates (Woodruff et al., 2017). As a result, microtubules only nucleate above a tubulin concentration that is exceeded in condensates but not in the cytosol. The compositions of the two phases formed by LLPS are fixed so, changing the total amount of protein in the two-phase region changes the condensate size while keeping the condensate and surrounding phase composition constant (Klosin et al., 2020). Force generation is another possible function of condensates. Condensates can exert forces on the cytoskeleton due to their surface tension and elastic properties (Böddeker et al., 2022).

Interestingly, condensates can be used to 'sort' proteins in multiphase systems. As a result, molecules partition into different phases based on their affinity (Feric et al., 2016). This was demonstrated in the nucleus where the sub-compartments within the nucleolus represent distinct, coexisting liquid phases. This multiphase droplet structure formed by ribosome assembly, rRNA processing, and rDNA transcription is caused by the difference in surface tension of droplets, which is in turn driven by the sequence-encoded features of their macromolecular components (Feric et al., 2016). These findings suggest that phase separation can produce multilayered liquids, which may improve consecutive RNA processing processes in a variety of RNP bodies (Figure. 1.3.). The multi-layered structure of the nucleolus is thought to facilitate assembly line processing of rRNA. Nascent rRNA transcripts are processed sequentially by enzymes that localize to various compartments before entering the nucleolus and being exported for final ribosome assembly in the cytoplasm.

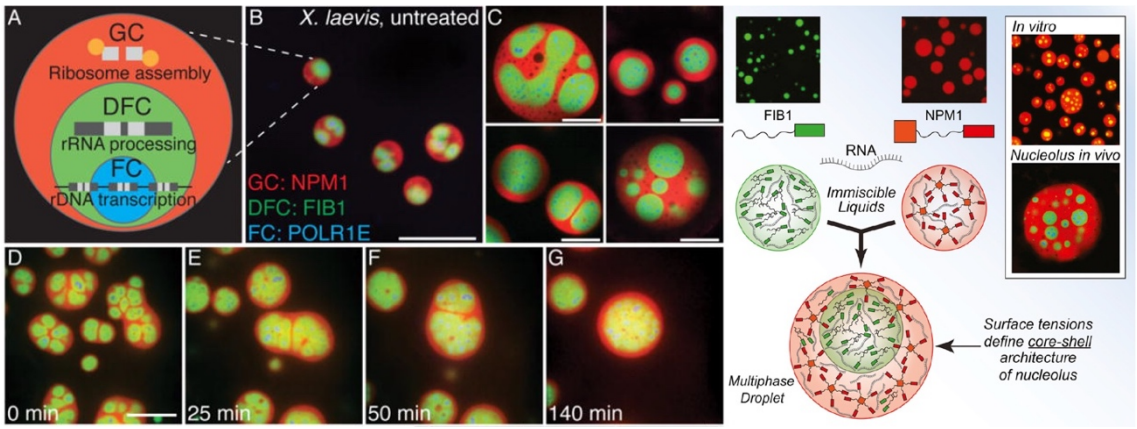


**FIGURE 1.3. Liquid-like behavior of biophysically distinct nucleolar subcompartments.** (A) Schematic diagram of ribosome biogenesis in the nucleolus. (B) Nucleoli in an untreated X. laevis nucleus. Scale bar = 20 µm. For all images, the granular component (GC) is visualized with NPM1 (red), dense fibrillar component (DFC) with FIB1 (green), and fibrillar center (FC) with POLR1E (blue). (C) Examples of nucleoli after coarsening in X. laevis nuclei treated with Lat-A. Scale bar = 20 µm. (D–G) Time-course of nucleolar component fusion after actin disruption by Lat-A. Scale bar = 20 µm. Modified from Feric et al., 2016.

## 1.2. Neurotransmitter release and synaptic vesicle cycle

### 1.2.1 Synaptic transmission

Neurons communicate using a combination of electrical and chemical signals. Neuronal communication takes place at particular locations known as synapses, where specialized portions of two cells (i.e., presynaptic and postsynaptic neurons) meet within a few nanometers of one another to allow for chemical transmission (Ziv and Fisher-Lavie, 2014). Neurons rely on the temporal and spatial architecture of the synapse to ensure rapid and precise neurotransmitter release in response to a stimulus (Jahn and Fasshauer, 2012; Südhof, 2013) A presynaptic neuron secrets neurotransmitters, which are chemicals that act as messengers and are stored in synaptic vesicles (SVs) (Heuser and Reese, 1973; Fernández-Busnadiego et al., 2010). A membrane depolarization at the presynaptic end causes calcium influx, which sets off a chain of coordinated processes resulting in SVs exocytosis at the active zone of the synapse, thereby releasing stored neurotransmitters into the synaptic cleft. Following exocytosis, SVs are recycled by endocytosis and reutilized for subsequent SVs trafficking cycles. Neurotransmitter molecules released in the synaptic cleft attach to receptor proteins, cause their conformational change and trigger depolarization of the postsynaptic neuronal cell (Sudhof, 2004). This coordinated sequence of reactions allows for signal propagation and neuronal communication.

Most neurons have more than 500 presynaptic nerve terminals, which are frequently detached from the neuronal cell bodies. Based on super-resolution microscopy and mass spectrometry a single synapse has an average volume of ~ 0.4 $\mu m^3$ in a total surface of ~ 2.3 $\mu m^2$, of which ~ 0.07$\mu m^2$ constitute the active zone surface. The average synapse contained a quantity of ~ 400 SVs, which are ~ 45 nm in diameter and had an inter-vesicle distance of ~ 60 nm (Wilhelm et al., 2014). SVs are densely packed, however, while being confined together in these clusters, vesicles are extremely mobile, allowing them to be rapidly attracted to the neuronal plasma membrane and released upon neuron activation (Rizzoli and Betz, 2004; Joensuu et al., 2016). Despite the classical representation of the presynaptic terminal is an extremely crowded environment in which all the molecule coexists in a narrow space (Wilhelm et al., 2014). In this environment, the neurons need to carefully orchestrate the synaptic transmission and the maintenance of the SVs pool.

### 1.2.2 Synaptic vesicle cycle

The central feature of the synaptic terminal is the existence of SVs functional pools, that is the collection of SVs that are available to be released even if only a limited number of vesicles are connected to the presynaptic membrane, with the remaining residing in an adjacent cluster (Rizzoli and Betz, 2005; Denker and Rizzoli, 2010). Based on the release kinetics upon neurons depolarization, the SVs have been divided into a vesicle-pool model (Elmqvist and Quastel, 1965):

i. The readily releasable pool (RRP) consists of a few vesicles (~1% of total SVs) immediately available on stimulation since are assumed to be docked to the presynaptic active zone (Kaeser and Regehr, 2017; Rettig and Neher, 2002).

ii. The recycling pool (significantly smaller ~10–15% of total SVs) maintains release on moderate stimulation (Neves and Lagnado, 1999; Qiu et al., 2015).

iii. The reserve pool (up ~80–90% of the total SV's pool), in which vesicles are drawn more slowly, refills and exchange SVs with the more proximal portion of the active zone, and release are only triggered during intense, repetitive stimulation (Denker et al., 2011).

SVs are involved in all presynaptic actions, either directly or indirectly. In the nerve terminal, SVs go through a trafficking cycle that may be divided into subsequent steps (Figure. 1.4.): Neurotransmitters are actively transported into SVs and cluster in front of the active zone (step 1). The SVs then attach to the active zone through docking (step 2), where they are primed (step 3) to become competent for $Ca^{2+}$-triggered fusion-pore opening (step 4). Following the fusion-pore opening, SVs endocytose and recycle via one of three possible pathways: (a) Without undocking, vesicles are reacidified and supplied with neurotransmitters, remaining in the readily releasable pool (named "kiss-and-stay"); (b) vesicles undock and recycle locally (named "kiss-and-run") to reacidify and refill neurotransmitters; or vesicles endocytose via clathrin-coated pits and either (c) directly or (d) after passing through an endosomal intermediate reacidify and refill with neurotransmitters (step 6) (Sudhof, 2004).

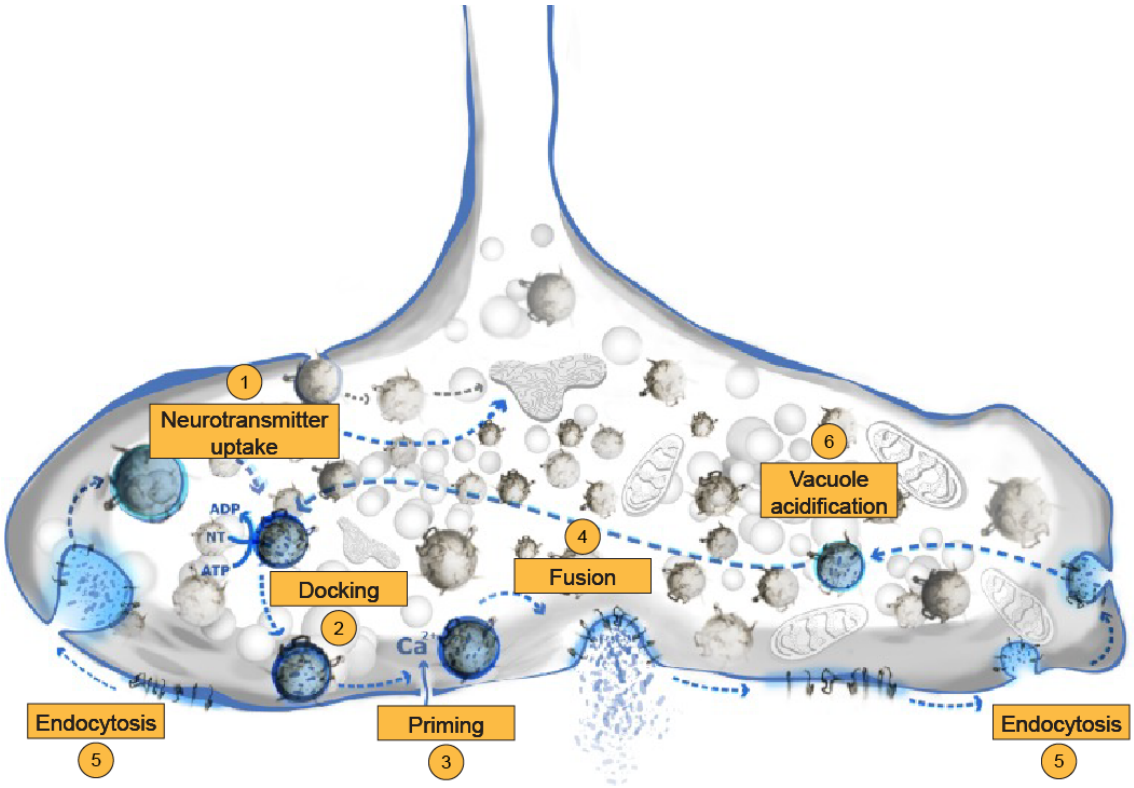


**FIGURE 1.4. The classical synaptic vesicle cycle (blue shade) includes neurotransmitter loading, docking, priming, calcium-triggered release, subsequent engulfing, and recycling of vesicles.** Modified from Milovanovic and Jahn, 2015.

### 1.2.3 Synaptic vesicle associated proteins

Biochemical studies involving purified SVs identified more than 1000 proteins to participate in the maintenance of the presynaptic architecture and hundreds of those are estimated to be involved in SV's exocytosis (Sudhof, 2004). Among those, the functions carried out by these proteins include trafficking proteins, transporter, and channel proteins, cytoskeletal proteins, cell-surface proteins, and signaling proteins. Many proteins associated with SVs are likely to be present just on a subset of vesicles or bind transiently to the vesicles, and the number of proteins constituting all SVs may be fairly limited (less than 50). Proteins linked to SVs perform several functions. Some proteins, like vesicular neurotransmitter transporters and a vacuolar ATPase, are responsible for neurotransmitter uptake. Synaptotagmins detect calcium, Rab proteins help with vesicle docking, and SNARE proteins are crucial for the vesicle fusion (Takamori et al., 2006).

However, it is also important to incorporate low-abundance synaptic proteins in research investigations. Recently, research utilizing subcellular proteomics discovered multiple synaptic proteins with various important activities previously gone unnoticed due to their low quantity or structural similarity to abundant proteins (Taoufiq et al., 2020). Identifying proteins and their activities in SV trafficking can give information on various other trafficking pathways used by cells. Several proteins, including SNAREs and Rab GTPases, have been proven to be members of conserved protein families that are essential for all trafficking mechanisms (Taoufiq et al., 2020). Different research has led to the identification of the synapse proteome, but much remains to be learned about their control during SV budding, transit, target recognition, docking, fusion, and recycling.

Several characteristics of SV's clusters indicate that they have fluid properties, with one component being vesicles and the other being a protein in an interwoven matrix (Milovanovic and De Camilli, 2017b). For example, despite the absence of a particular barrier, SV clusters have uniform morphologies with strong borders and exclude other organelles (Milovanovic and De Camilli, 2017b). Similarly, despite being closely packed, SVs appear to be highly mobile both inside and between clusters and surrounding cytoplasm (Rizzoli and Betz, 2004). This mobility has been observed in the EM studies of nerve terminals from the central and peripheral nervous systems after endocytic labeling with external tracers and luminal SV membrane ligands (Ceccarelli et al., 1973; Kraszewski et al., 1996). SV clustering is not dependent on active zone proteins, since the ablation of active zone components does not eliminate SV clustering upstream (Acuna et al., 2016; Wang et al., 2016). As a result, understanding the physiological features of the SVs cycle and pre-synaptic plasticity requires understanding the activities of numerous protein-protein interactions and neurotransmitters found in vesicles.

## 1.3. Synapsin-mediated LLPS of SVs

### 1.3.1 Synapsin structure and domains

Synapsins are a family of highly conserved phosphoproteins associated with SVs that play a role in neurotransmitter release regulation (Greengard et al., 1993). Synapsins are encoded by three genes in vertebrates (synapsins 1, 2, and 3), each with various splice variants (Südhof et al., 1989; De Camilli et al., 1990). Synapsin 1 and 2 are the most abundant with an estimated total concentration above 120 μM in the nerve terminals (Wilhelm et al., 2014). In 1990, the human SYN1 gene and protein structure was described and its product synapsin 1 was found as the first presynaptic protein, initially known as phospho-protein I (Südhof, 1990). Shortly before, two unique isoforms of synapsin 1a and 1b were found, with differing C-terminal ends due to alternative splicing of the same source transcript. Simultaneously, the synapsin isoforms 2a and 2b were described as homologs (Nestler and Greengard, 1984). Multiple isoforms of synapsin 1a-b, 2a-b, and 3a-f can be produced in humans via an alternative splicing (Südhof, 1990). They all share three N-terminal domains (A, B, and C), indicating that they are highly conserved. The C-terminal portions of the protein, on the other hand, differ, suggesting that these isoforms could have diverse functions in neurons (Südhof et al., 1989). Figure 1.5. shows an overview of the synapsin 1 domain for *Mus musculus* gene translation.


**FIGURE 1.5. Domain organization of synapsin 1.** Letters A to E indicate the specific functional domains. Modified from Milovanovic et al., 2018.

**Domain A** is the first N-terminal domain that all synapsin isoforms share. Cyclic AMP-dependent protein kinase A (PKA) and calcium/calmodulin-dependent protein kinase I (CaMKI/IV) phosphorylate site 1 in domain A (Huttner et al., 1981; Kao et al., 1999). These kinases, by phosphorylating Site 1, can inhibit synapsin interactions with phospholipids (Masahiro Hosaka and Südhof, 1999), which has been linked to the regulation of interactions with SVs (Bonanomi et al., 2005; Chi et al., 2001; Chi et al., 2003).

**Domain B** serves as a linker between domains A and C. This region has an evolutionary conserved amphipathic lipid packing sensor (ALPS) motif with numerous polar hydrophilic and hydrophobic residues (Krabben et al., 2011). When ALPS comes into touch with a membrane, it can fold into amphipathic α-helices, implying interactions with highly curved SV membranes (Drin et al., 2007). Domain B also contains two target phosphorylation sites for mitogen-activated protein kinase (MAPK)/Extracellular signal-regulated kinase (ERK) (Erk) (Jovanovic et al., 1996).

**Domain C** is the only folded region of synapsin 1 and the most conserved region of all synapsins. The crystal structure C domain of *Bos taurus* revealed a compact elliptical shape composed of α-helices and β-sheets, as well as a disordered area at the C-terminus (Esser et al., 1998). This structure not only resembles an ATP-binding characteristic, but it can also bind ATP and ADP with varying degrees of affinity (Hosaka and Südhof, 1998a). Calcium can facilitate ATP binding to synapsin 1 but prevent ATP binding to synapsin 3 (Hosaka and Südhof, 1998a; Hosaka and Südhof, 1998b). Furthermore, domain C promotes synapsin homo- and heterodimerization and mediates the protein's binding to actin and SV phospholipids (M. Hosaka and Südhof, 1999; Esser et al., 1998). A tyrosine residue in this domain of synapsin 1 (Tyr301, site 8) is phosphorylated by SVs-associated c-Src (Onofri et al., 2007). Following domain C, the domains differ amongst orthologues but are all proline-rich.

**Domain D** contains numerous Src homology 3 (SH3) domain-binding motifs (McPherson et al., 1994; Onofri et al., 2000) This motif can help synapsin and intersectin interact, which has been shown to sort SVs from a reserve pool into a rapidly releasable pool (RRP) (Gerth et al., 2017). Domain D contains phosphorylation sites 2 and 3, which are CaMKII targets (Czernik et al., 1987), as well as phosphorylation sites 6 and 7, which are MAPK/ERK and Cdk1/5 targets (Jovanovic et al., 1996; Matsubara et al., 1996)).

**Domain E** is present in the C-terminus of all synapsin 'a' isoforms and is highly conserved. Early research on domain E revealed the relevance of synapsin in SV clustering and fusing. Peptides corresponding to domain E were administered into the squid's large presynaptic terminals, effectively inhibiting transmitter release (Hilfiker et al., 1998; Monaldi et al., 2010). A peptide containing the most conserved area of domain E, which was

studied in conjunction with liposomes and other presynaptic protein partners, was found to have an extra influence on synapsin 1 oligomerization (Monaldi et al., 2010).

### 1.3.2 Phase separation of synapsins

Synapsin 1 has been shown to contain a large IDR portion as confirmed by PrDOS (protein disordered prediction system) bioinformatics tool prediction tool (Ishida and Kinoshita, 2007) (Figure. 1.6.).

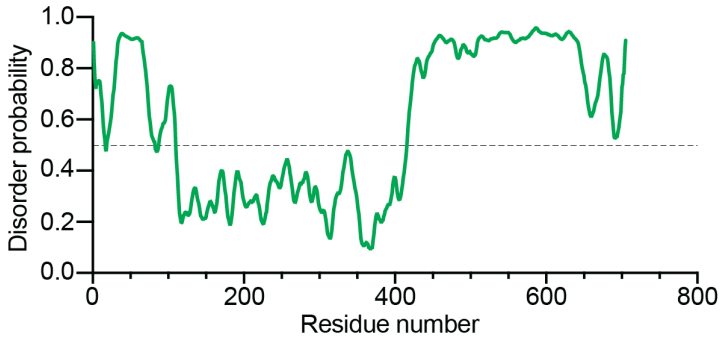


**FIGURE 1.6. Disorder prediction of synapsin 1 using PrDOS.**

The prediction shows a high propensity in correspondence of domains A, B, D, and E with a disorder probability above 0.5. In the *in vitro* reconstitutions using purified protein, synapsin 1 was shown to undergo LLPS by sequestering lipid vesicles and producing a separate liquid phase in an aqueous environment (Milovanovic et al., 2018). The most crucial aspect of LLPS is that it is reversible (Milovanovic et al., 2018). Post-translational changes such as phosphorylation and dephosphorylation by kinases and phosphatases are commonly used to achieve reversibility (Henkel et al., 1996; Kraszewski et al., 1996).

Droplets of synapsin 1 display all of the typical liquid phase properties: they merge and recover after photobleaching, implying a rapid exchange into and out of synapsin 1 droplets (Fig 1.7. A). Furthermore, synapsin 1 binding scaffolding proteins like Grb 2 and Intersectin influence this phase but are not required for its creation. Importantly, EM experiments demonstrated that synapsin 1 can attract small lipid vesicles into its phase: synapsin/liposomes biocondensates contained clusters of small vesicles, but liposomes do not form such clusters in the absence of synapsin 1 (Figure. 1.7. B).

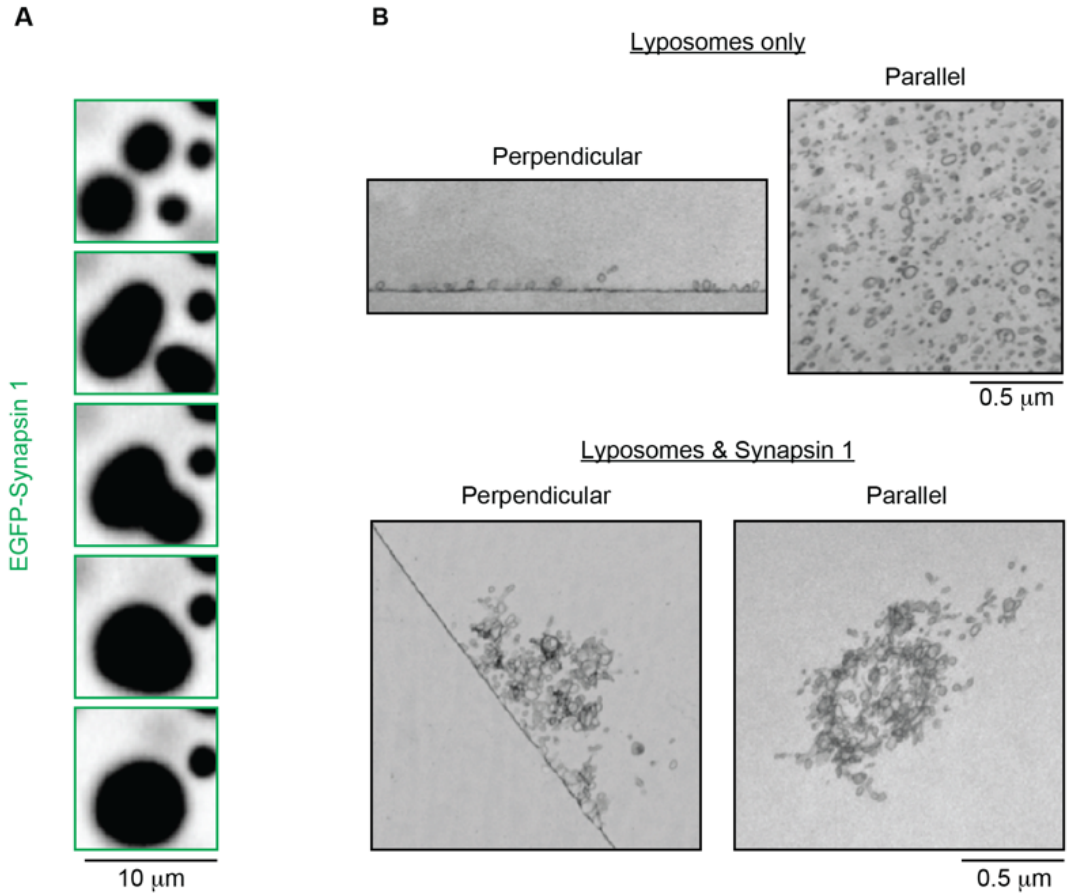


**FIGURE 1.7. Synapsin forms liquid condensates that actively sequester lipid vesicles. (**A) 10 μM of purified EGFP-tagged synapsin 1 forms liquid condensates in a buffer with physiological salt concentration. (B) EM images of reconstituted lipid vesicles without (top) and with Synapsin 1 (bottom). Modified from Milovanovic et al., 2018.

### 1.3.3 Synapsins are the master regulators of SVs cluster

Injecting anti-synapsin antibodies into the large reticulospinal synapse of *Lampetra fluviatilis* causes SV dispersion both at rest (Pechstein et al., 2020) and during depolarization (Pieribone et al., 1995) (Figure. 1.8. A, B). Only the pool of vesicles closer to the active zones, which is most likely cross-linked by other factors, persists. Similarly, chronic synapsin depletion in mice - i.e., synapsin gene deletions - leads to fewer vesicles accumulating at the synaptic bouton and more dispersed SVs inside the bouton than in wildtype synapses, both in cultured neurons and in brain slices (Milovanovic et al., 2018; Rosahl et al., 1995; Orenbuch et al., 2012; Gitler et al., 2004) (Figure. 1.8. C). These functional data strongly suggest that synapsin is a major regulator of SV clusters.

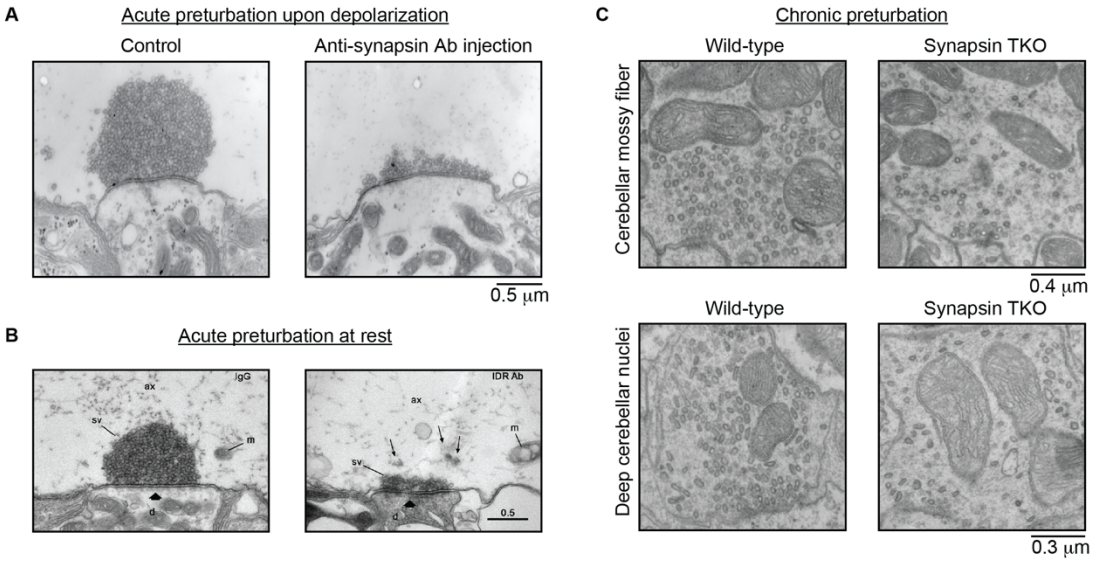


**FIGURE 1.8. Acute and chronic depletion of synapsins results in the dispersion of SVs from the synaptic bouton.** Electron microscopy (EM) images upon injection of anti-synapsin antibodies both upon depolarization (A) and at rest (B) in the giant axon of the lamprey show a full dispersion of SVs. Note that only SVs adjacent to the presynaptic plasma membrane remains, probably kept by the active zone proteins. (C) EM images of synapses from cerebellar mossy fibers obtained from adult wild-type (WT, top) and synapsin triple-knockout (synTKO, bottom) mice. Note that both the number and packing of SVs at the synaptic bouton dropped in synTKO animals. Modified from Milovanovic et al., 2018, Pechstein et al., 2020 and Pieribone et al., 1995.

## 1.4. Synucleins – impact on synaptic function and pathology

### 1.4.1. Synucleins family

Apart from synapsins, the highly abundant protein family in the nerve terminal is the family of synucleins, present largely in brain tissue and accounts for 1% of the total cytosolic protein (Clayton and George, 1998). In 1988, an antiserum against cholinergic vesicles was used to identify α-synuclein from *Torpedo californica* (an electric ray). Because the protein was found in the nuclear envelope and presynaptic nerve terminals of neurons, it was given the name synuclein (Maroteaux et al., 1988). The synuclein family comprises α-, β-, and γ-synuclein. The family members share a domain organization and are 55-62% identical in sequence (Goedert, 2001). Synucleins are extremely conserved throughout vertebrate species (Clayton and George, 1998). During the past three decades, α-synuclein has been the focus of research due to its association with neurodegenerative disorders known as synucleinopathies, although its precise physiological function is still unknown (Burré et al., 2018). Synucleinopathies are a diverse set of neurodegenerative illnesses, among which the most known is Parkinson's disease (PD), which is defined by excess amounts of aggregated α-synuclein in Lewy bodies (LBs) (Goedert et al., 2017; Jellinger, 2003).

### 1.4.2. α-Synuclein structure

With only 140 amino acids, the protein is an intrinsically disordered (or natively unfolded), with little or no organized structure in an aqueous environment (Eliezer et al., 2001; Uversky, 2003; Uversky et al., 2001; Weinreb et al., 1996). Although structurally unfolded in solution, it has been shown to form an α-helix upon binding to negatively charged membranes (Jo et al., 2000; Chandra et al., 2003). Different isoforms of α-synuclein (SNCA140, SNCA126, SNCA112, and SNCA98) are produced by alternate splicing of exons 3 and 5 (Beyer, 2006). The full-length α-synuclein protein can be divided into three domains: the N-terminal domain, the NAC region, and the C-terminal domain (Cookson, 2005) (Figure. 1.9. A).

- **N-terminal domain**: The highly conserved amphipathic N-terminal domain (residues 1-60) contains a series of 11-amino acid repeats. These repeats include the consensus sequence KTKEGV, which has a structural α-helix propensity and is highly similar to apolipoprotein lipid-binding motifs. Thus, this region adopts an α-helical secondary structure when bound to phospholipids (Davidson et al., 1998). This domain contains the three missense mutations linked to familial PD (A30P, E46K, and A53T).

- **Non-Amyloid-Component (NAC) domain:** The centrally hydrophobic NAC region (residues 61-95) of α-synuclein is linked to the protein's propensity to adopt a β-sheet configuration and form amyloid fibrils (Bodles et al., 2001). Other members of the synuclein family lack the NAC area and do not form aggregates efficiently (Goedert, 2001), which emphasizes the importance of this region for α-synuclein aggregation.

- **C-terminal domain:** The highly acidic and proline-rich C-terminal tail (residues 96-140) is predominantly negatively charged and fully lacks a stable tertiary structure. The acidic glutamate-rich C-terminal region (Asp98-Ala140) was demonstrated to behave as a highly mobile tail. It remained unstructured even in the presence of membranes (Jao et al., 2004; Ulmer and Bax, 2005) becoming insensitive to protease digestion when the micelle-bound α-synuclein is exposed to calcium (de Laureto et al., 2006). The prediction using PrDOS (Ishida and Kinoshita, 2007) shows that α-synuclein, in solution, has a structure almost completely disordered, with a score over the entire sequence always above 0.3 and maximum values in correspondence of the acidic tail contained in the C-terminal domain of about 0.8-1. (Figure. 1.9. B)

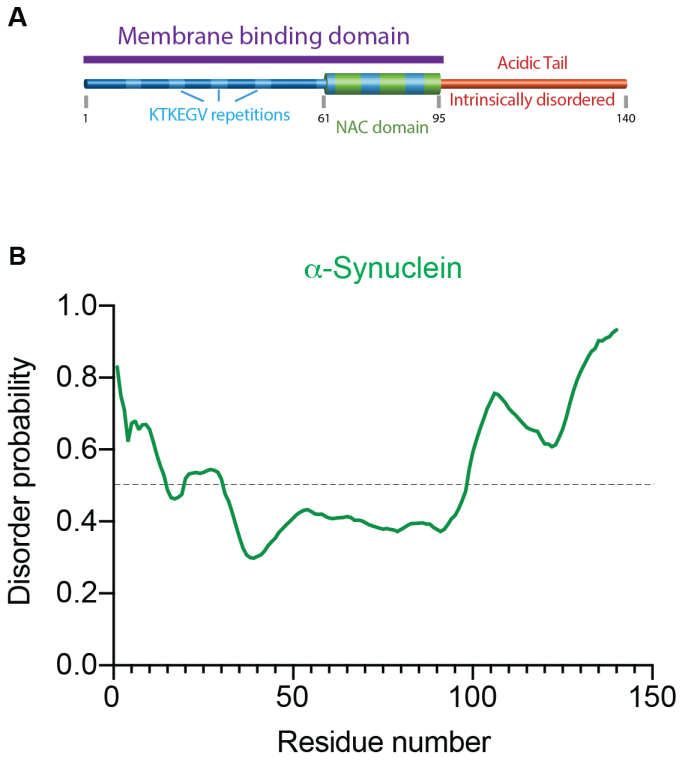


**FIGURE 1.9. α-Synuclein is intrinsically disordered.** (A) Domain organization and (B) disorder prediction of α-synuclein. Prediction performed using PrDOS bioinformatics tool.

### 1.4.3. α-Synuclein physiological functions

α-Synuclein is an intriguing synaptic protein for a variety of reasons. It has been linked to several functions, including vesicular transport, interactions with membranes and lipids, and protein-protein interaction (Emamzadeh, 2016). Monomeric α-synuclein resides in the presynaptic boutons in an equilibrium between free and plasma membrane- or vesicle-bound forms (McLean et al., 2000), with roughly 15% of α-synuclein being membrane-bound (Lee et al., 2002). Because of its tight relationship with vesicular structures, it has been proposed that α-synuclein may govern vesicular release and/or turnover, as well as other synaptic activities in the central nervous system (Burré et al., 2010; Clayton and George, 1998; Clayton and George, 1999). *In vitro* and *in vivo*, α-synuclein binds directly to the SNARE protein synaptobrevin-2/vesicle-associated membrane protein 2 (VAMP2) promoting the formation of SNARE-complex assembly and facilitating exocytosis (Burré et al., 2010; Burré et al., 2014). Furthermore, α-synuclein is believed to play a physiological role in controlling vesicle availability in distinct pools and impacts vesicle docking and

fusion under normal conditions. Functionally, elevated α-synuclein levels or mutant E46K or A53T α-synuclein, on the other hand, might cause a decrease in the dopamine release (Clayton and George, 1998) by disrupting a late phase in exocytosis or by decreasing vesicle availability in the recycling pool due to poor vesicle endocytosis (Simón-Sánchez et al., 2009).

α-Synuclein interacts stably with negatively charged synthetic phospholipid vesicles (Jo et al., 2000; Ramakrishnan et al., 2003), different phospholipid membranes, fatty acids, detergent micelles (Zhu and Fink, 2003; Zhu et al., 2003; Kim et al., 2006), and biological membranes such as crude brain vesicles (Jensen et al., 1998), general cellular membranes (McLean et al., 2000), lipid rafts (Fortin et al., 2004), and lipid droplets (Cole et al., 2002). The protein shows a stronger affinity for small vesicles, which could be due to the pronounced curvature (i.e., high surface-to-volume ratio) of small vesicles (Zhu et al., 2003). The association of α-synuclein with negatively charged membranes promotes the formation of α-helix form even if is structurally unfolded in solution (Jo et al., 2000; Chandra et al., 2003). α-Synuclein is abundant at the SV clusters in both cultured live synaptic boutons and minimally reconstituted systems where was demonstrated to form oligomers on the surface of SVs (Reshetniak et al., 2020; Perego et al., 2020). Pathologically high quantities of α-synuclein, independently of SVs, can cause aggregation via LLPS (Ray et al., 2020) (Hardenberg et al., 2021). Finally, α-synuclein interacts with β- and γ-synucleins for SV binding (Carnazza et al., 2022), raising the overall concentration of synucleins at the SV surface locally. These findings imply that α-synuclein influences the structure of membrane lipid components.

Interestingly, in animals, the genetic deletion of all three synucleins resulted in the exact opposite phenotype as the deletion of synapsins (Figure. 1.10. A-C). *In situ* investigations of nerve terminals in animals lacking all three synucleins revealed a highly organized three-dimensional packing of SVs, in contrast to the wild-type situation (Vargas et al., 2017).

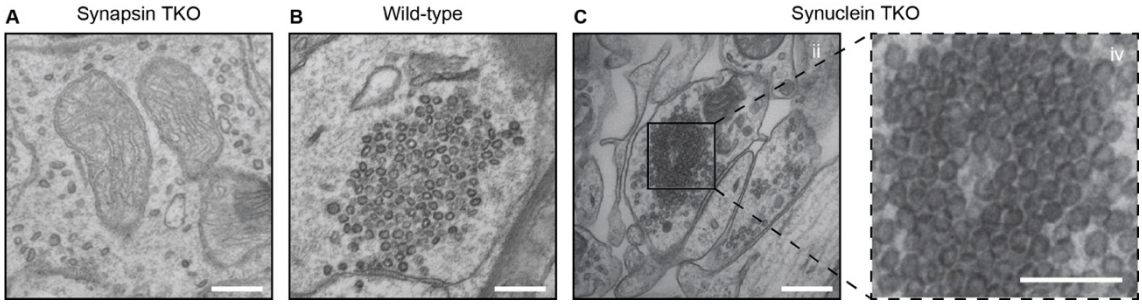


**FIGURE 1.10. Synapsin/Synuclein interaction affects the architecture of SV condensates** (A) Presynaptic terminal of synapsin TKO mouse contains dispersed SVs. (B) A nerve terminal of a wild-type mouse with the representative SV cluster. (C) SVs are tightly packed with highly-ordered structures in synuclein TKO synapse. Modified from Milovanovic et al., 2018, Milovanovic and De Camilli, 2017b, Vargas et al., 2017 and Sansevrino et al., 2023.

The presence of SV clusters is not surprising given that these synuclein triple-knockout (TKO) animals still expressed synapsin (Greten-Harrison et al., 2010), which is both necessary and sufficient for SV cluster formation. Synuclein TKO animals have smaller terminals (Greten-Harrison et al., 2010), which could in part explain the tight packing in part; nonetheless, the highly-ordered architecture of these clusters reveals a crucial change in their material properties. It might be that SV membranes provide a direct platform for synapsin and α-synuclein interaction, particularly via their IDRs. The overexpression of α-synuclein in wild-type mouse synapses reduces SV release and recycling (Nemani et al., 2010). However, when α-synuclein is overexpressed in neurons generated from synapsin TKO mice, this phenotype is missing (Atias et al., 2019). This suggests that SV mobility and cluster density are dependent on a delicate equilibrium of synapsin and α-synuclein concentrations (see Hypothesis).

### 1.4.4. α-Synuclein role in synucleinopathies

Several mutations in the α-synuclein gene (SNCA) have been related to familial PD. The initial mutations were discovered in Italian and Greek families with a dominantly inherited form of PD (Polymeropoulos et al., 1997). In the study, they found a G209A missense mutation causing an A53T (alanine to threonine) amino acid exchange. Subsequently, more point mutations in the SNCA gene linked to autosomal dominant PD were discovered. In German PD patients, the G88C missense mutation causes an A30P (alanine to proline) amino acid swap (Krüger et al., 1998). The G188A mutation resulted in an E46K (glutamic acid to lysine) amino acid swap, resulting in autosomal dominant PD in a Spanish family (Zarranz et al., 2004). The G188A mutation induced the E46K (glutamic

acid to lysine) amino acid swap in these patients, resulting in autosomal dominant PD. Furthermore, duplication and triplication of the SNCA locus have been reported in families with an autosomal dominant inheritance pattern (Chartier-Harlin et al., 2004; Singleton et al., 2003), supporting the critical involvement of α-synuclein in illness etiology. Surprisingly, a gene dosage impact was discovered, as individuals with SNCA triplication had an earlier disease onset and more severe symptoms (Fuchs et al., 2007).

Because α-synuclein is significant in the pathogenesis of PD and other synucleinopathies, it is critical to understand the underlying process of soluble protein aggregation into amyloid fibrils. The formation of α-synuclein fibrils is a multistep process that involves the structural transition of the protein from a random coil to a β-sheet-rich confirmation, and then the self-association of these β-sheets, forming oligomers and fibrils. As α-synuclein unfolds in an aqueous solution with a random coil structure (Li et al., 2002), it may expose hydrophobic surfaces (which would otherwise be hidden or masked within structured proteins) that can potentially interact with one other or other proteins in the environment. According to *in vitro* studies, the onset of aggregation is dependent on specific intermolecular interactions between folding intermediates (Wetzel, 1996) or the disturbance of equilibria between unfolded monomeric α-synuclein and its other intermediate conformations, such as the globular pre-molten state. Point mutations associated with familial variants of PD, such as the A53T and A30P α-synuclein mutants, might disrupt the protein's native shape and enhance the chance of self-association and aggregation (Bertoncini et al., 2005).

This destabilization of monomeric α-synuclein, combined with certain interactions between intermediate conformations, may increase the molecule's propensity to form micro aggregates like dimers, oligomers, tiny spherical particles, or protofibrils, which eventually group together to form larger, macromolecular deposits like highly ordered amyloid fibrils (Caughey and Lansbury, 2003). Furthermore, micro aggregates frequently serve as 'seeds' for the aggregation reaction, boosting the tendency of the different molecules to aggregate into amyloid fibrils and so reach an energetically favorable equilibrium. As a result, the development of α-synuclein amyloid-like fibrils is a complex process including one or more discrete stages such as low molecular weight oligomers, protofibrils, and finally mature fibrils, all of which have been demonstrated to generate toxicity to varied degrees (Conway et al., 2000; Harper et al., 1999; Poirier et al., 2002). The amyloid fibrils formed in this

process are the most energetically stable (or almost irreversible) forms. They are also, predictably, the most common and easily detectable aggregates in PD brain tissue.

Recent research suggests that α-synuclein oligomers and protofibrils are cytotoxic and that fibrillar aggregates of α-synuclein may constitute a cytoprotective mechanism in PD (Smith et al., 2010). In a Drosophila model of PD, an increase in the number of α-synuclein aggregates correlates with decreased toxicity of α-synuclein (Chen and Feany, 2005). In rats, inhibiting the proteasome causes the production of α-synuclein inclusions but prevents dopaminergic neuronal cell death (Sawada et al., 2004).

## 1.5. Lewy bodies: a hallmark structure in Parkinson's diseases and other Synucleinopathies

### 1.5.1. Synucleinopathies and Parkinson's disease

Synucleinopathies are a set of neurodegenerative disorders characterized by aggregated α-synuclein inclusions in neurons and glia. Pathologically, synucleinopathies are classified into several categories: Parkinson's disease (PD), Lewy bodies dementia (DLB), and multiple system atrophy (MSA) (Koga et al., 2021). Furthermore, postmortem studies have revealed that approximately 6% of sporadic Alzheimer's Disease (AD) patients have α-synuclein-positive Lewy pathology and are classified as Alzheimer's Disease with Amygdalar Restricted Lewy Bodies (AD/ALB). Lewy body disease is a pathological term for a neurodegenerative disease characterized by proteinaceous aggregation of α-synuclein in neurons soma (Lewy bodies, LBs) and neurites (Lewy neurites, LNs). The most prevalent of the previous is PD, named after James Parkinson, who described it for the first time in 1817 (Parkinson, 2002).

PD is the second most common neurodegenerative disease, after AD, affecting 1% of the population over the age of 60 years (Samii et al., 2004). While disease symptoms show a mean age of 57 years (Koller et al., 1987), around 5% of people diagnosed with PD are under the age of 40 (early-onset PD) (Gershanik and Nygaard, 1990). The motor manifestations of PD are referred to as 'parkinsonism'. Resting tremors, involuntary shaking, akinesia, bradykinesia (slowness of movement), impaired spontaneous movement, rigidity, balance problems, trouble walking, postural disturbances, and hypomimia (reduced facial expression) are among them. Fatigue, sleep disturbances, constipation, and gastric dysmotility are examples of non-motor symptoms (Tanner et al., 2009). As the disease progresses, PD patients may experience autonomic, behavioral, and mental issues such as depression and anxiety (Chaudhuri and Schapira, 2009). Slowness in memory and cognition, for example, worsens with age and disease progression (Levy, 2007).

Over 90% of PD cases are thought to be sporadic, meaning that there is no specific known cause or origin of the disease, hence PD has historically been classified as a non-genetic disorder (Klein and Westenberger, 2012). However, an estimated 5-10% of all

parkinsonian cases are familial; and 15% of people with PD have a first-degree relative who has the disease (Shulman et al., 2011). The first cause of symptoms that arise is the progressive death of dopaminergic neurons in the substantia nigra pars compacta (SNpc) (Braak and Braak, 2000) which results in depigmentation of the region in post-mortem brains of PD patients (Forno and Alvord, 1974) (Figure. 1.11.).

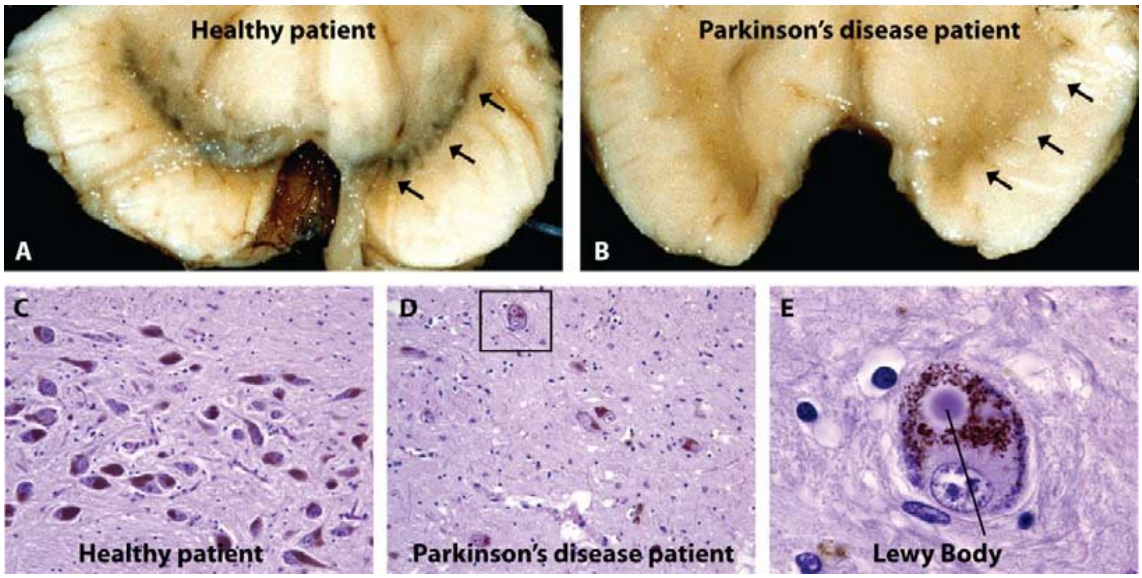


**FIGURE 1.11. Loss of substantia nigra pars compacta (SNpc) causes Parkinson's disease.** Pathological examination of a healthy patient (A) reveals typical pigmented dopaminergic neurons (arrows); in contrast, loss of SNpc neurons leads to pigment disappearance in the PD brain (B, arrow). Magnification of the SNpc area reveals a dense network of melanin-pigmented SNpc neurons in a healthy brain (C) while most of the DNpc neurons are lost in PD (D). Some of the remaining neurons in PD contain insoluble cytoplasmic LBs (E). The melanin-containing granules have a red-brown hue and are distributed in the cytosol of all SNpc neurons (C-E). The picture in E is the higher magnification of the dark-boxed area in D. Modified from Forno and Alvord, 1974, and Aron, 2023.

While major disease symptoms appear after significant loss of dopaminergic neurons projecting from the SNpc to the striatum (Samii et al., 2004), PD pathology is not limited to the nigrostriatal pathway, with LBs also found in the cortex, amygdala, locus coeruleus, and, in the enteric nervous system innervating the gut (Dickson et al., 2009; Wolters, 2009). Indeed, as the pathology advances diverse components of the autonomic, limbic, and somatomotor systems become particularly badly damaged (Braak et al., 2004).

### 1.5.2 Lewy bodies in Parkinson's disease

The histopathological hallmark of PD is the presence of fibrillar aggregates referred to as LBs, in which α-synuclein is a major constituent (Wakabayashi et al., 2013). The first evidence of α-synuclein enrichment in LBs came in 1997 with the employment of the first

α-synuclein antibody on isolated substatia nigra of PD patients (Spillantini et al., 1997). These peculiar inclusions were initially identified by Friederich H. Lewy in the dorsal vagal nucleus and the nucleus basalis of Meynert in PD patients and were termed LBs in his honor by Tretiakoff, who verified their existence in the substantia nigra (Lees et al., 2008; Tretiakoff, 1919). An examination of post-mortem brain tissue from patients that helps to recognize and differentiate these proteinaceous inclusions is haematoxylin and eosin staining. While positively charged haematoxylin stains nuclei of a blue or dark purple, eosin, a negatively charged acidic stain, colors cytoplasm, proteins, and extracellular matrix components such as collagen in up to five shades of pink (Chan, 2014). There are two main types of LBs related to their localization: brainstem LBs and cortical LBs (Fares et al., 2021). Brainstem LBs can be easily revealed using light microscopic examination of haematoxylin and eosin-stained sections highlighting intracytoplasmic, single or multiple, round or elongated, eosinophilic aggregates with a dense core and a peripheral halo (Beyer, 2006). Cortical LBs and LNs, on the other hand, were difficult to detect with haematoxylin and eosin staining and lacked a central halo, indicating that they had different ultrastructural features. Another type of LB often reported in the cytoplasm of pigmented neurons are Pale Bodies displaying well-defined, less eosinophilic, rather glassy areas without a halo.

Many studies indicate that pale bodies are a stage in the formation of the LBs (Saito et al., 2003). Although both brainstem and cortical LBs have a similar underlying ultrastructure of filamentous fibrillar proteins mixed with lipids, the organization of fibrils differs between the two LB subtypes, according to experiments using transmission electron microscopy (TEM) (Fares et al., 2021). Cortical LBs have a more widespread dispersion of disordered filamentous fibrils, whereas brainstem LBs have a compact core with a halo of irradiating filaments (Baba et al., 1998; Wakabayashi et al., 1998). The presence of large quantities of insoluble β-sheet-rich fibrillar components in cortical and brainstem LBs and LNs showed that these filaments have amyloid-like features, such as the cross-structure found in amyloid plaques, neurofibrillary tangles, and other amyloid-like deposits (Fares et al., 2021). Subsequent research revealed that amyloid-specific dyes, such as thioflavin S (ThS), that detect this unique cross-structure, consistently demonstrate high reactivity with both brainstem and cortical LBs (Irwin et al., 2013). Several researchers have speculated that LBs formation is an aggresome-related process. Aggresomes are proteinaceous inclusions that originate at the centrosome and segregate within distinct regions of the cytosol helping in the clearance of damaged, mutant, and cytotoxic proteins (Olanow et al.,

2004; McNaught et al., 2002). LBs and pale bodies are also immunopositive for autophagic adaptor proteins (p62 and NBR1) (Odagiri et al., 2012), which may sequester soluble hazardous proteins containing oligomeric-synuclein into inclusions.

Mutations or multiplications of the SNCA gene causing familial PD, have been directly related to LB and LN production (Klein and Westenberger, 2012; Binolfi et al., 2006). The change of α-synuclein from its soluble form to fibrillated pathogenic inclusions involves a sequence of events that go beyond a simple increase in protein levels. Post-translational modifications (PTMs) such as phosphorylation and ubiquitination, have been implicated in affecting α-synuclein misfolding and aggregation, as well as the processes of inclusion formation and maturation (Fujiwara et al., 2002; Anderson et al., 2006; Duda et al., 2000; Li et al., 2005). Furthermore, LBs and LNs are complex structures rich in lipids, cytoskeletal proteins, organelles, and membranous fragments, and the dynamics of α-synuclein interactions with these structures are likely to play an important role in regulating the process of inclusion formation, the biochemical and organizational heterogeneity of the formed inclusions, and the downstream consequences of neurodegeneration (Jensen et al., 2000; Ikenaka et al., 2019; Mahul-Mellier et al., 2020). Indeed, α-synuclein pathology in PD brain tissue is highly polymorphic, and LBs have various morphological, structural, and molecular components across different brain regions and patient subpopulations (Forno and Norville, 1976; Kuusisto et al., 2003). As a result, it is unclear if the variability of LBs and α-synuclein immunoreactive inclusions reflect separate diseases or a continuum of conformations corresponding to different stages of LB creation, maturation, and processing throughout time (Sekiya et al., 2019; Roberts et al., 2015).

### 1.5.3. Stages of Parkinson's disease progression and Lewy bodies formation

The creation of aberrant proteinaceous LBs and LNs inside the brain begins at known induction sites and progresses in a topographically predictable manner. Based on post-mortem analysis of hundreds of brains from individuals with PD at different stages of the disease, PD pathology was classified into six neuropathological phases (Figure. 1.12.), each of which is distinguished by the continuous development of various inclusion bodies (Braak et al., 2003).

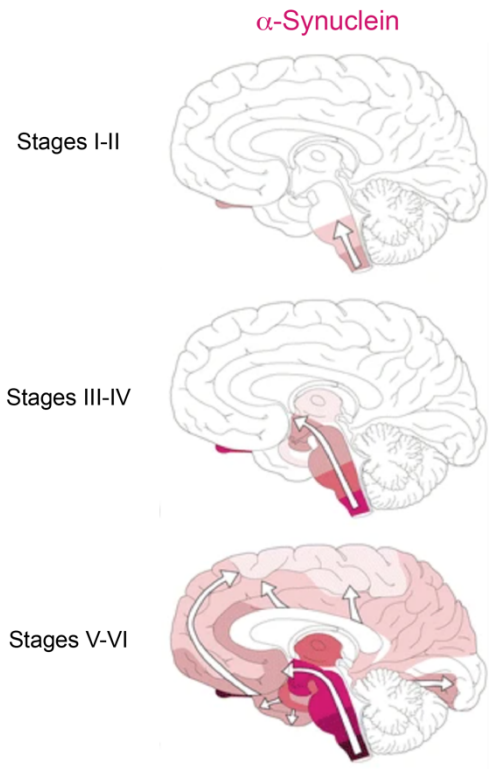


**FIGURE 1.12. Temporal and spatial spreading of α-synuclein-positive lesions in the process of Parkinson's disease and dementia with Lewy bodies.** 6 stages (I–VI) of α-synuclein pathology can be distinguished. The first inclusions appear in the olfactory bulb, the anterior olfactory nucleus, and the dorsal motor nucleus of the vagal and glossopharyngeal nerves in the medulla oblongata (Stages I and II). From the brainstem, the inclusions take an ascending path to the lower raphe nuclei, the gigantocellular reticular nucleus, and the locus coeruleus. In Stages III and IV, they reach the amygdala, the cholinergic nuclei of the basal forebrain, and the substantia nigra. The cerebral cortex also becomes affected, starting with the anteromedial temporal mesocortex. In Stages V and VI, the inclusions spread to the higher-order sensory association and prefrontal areas, the first-order sensory association areas, the premotor area, and the primary sensory and motor fields. The shading intensities of the areas colored in red are proportional to the severity of α-synuclein pathology. Modified from Braak et al., 2003 and Goedert et al., 2014.

During presymptomatic phases I-II, the appearance of inclusion is limited to the medulla oblongata/pontine tegmentum and olfactory bulb/anterior olfactory nucleus. The inclusions take an ascending path from the brainstem to the lower raphe nuclei, the gigantocellular reticular nucleus, and the locus coeruleus. In stages III-IV, they reach the amygdala, the cholinergic nuclei of the basal forebrain, and the substantia nigra which become the focus of initially mild, then severe degenerative alterations. The cerebral cortex is also damaged, beginning with the anteromedial temporal mesocortex. Most patients crossed the barrier into the symptomatic phase of the illness by this stage. Inclusions expand to the higher-order sensory association and prefrontal areas, the first-order sensory association areas, the premotor area, and the primary sensory and motor fields in Stages V and VI and the disease emerges in all of its clinical characteristics (Braak et al., 2004; Braak et al., 2003; Goedert et al., 2014).

These stages describing PD pathology can also be related to the higher complexity of LB's inclusions. Because of the structural differences between cortical and brainstem LBs, these two LB subtypes have been staged individually (Fares et al., 2021) (Figure. 1.13.).

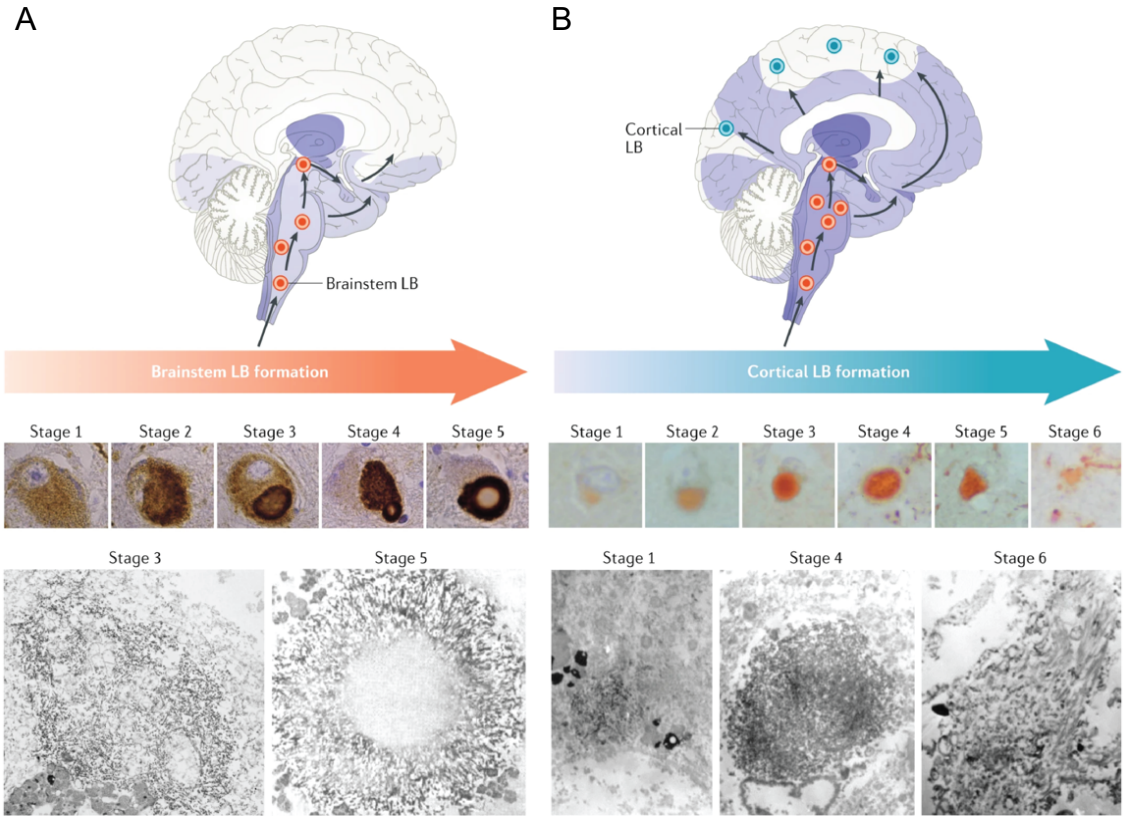


**FIGURE 1.13. Stages of LBs formation in brainstem and cortex.** (A) Brainstem LBs have been proposed to go through five stages before reaching maturity. The upper panel shows the anatomical distribution of brainstem LBs and proposed routes for their spreading, the middle panel shows α-synuclein-immunostained human neurons at different stages and the lower panels show transmission electron microscopy (TEM) analysis of accumulations at early and late stages. Stage 1 features abnormal cytoplasmic accumulations of α-synuclein, which become irregularly shaped, large structures in stage 2. Stage 3 is characterized by well-defined pale bodies that lack a halo and consist of a granular, vesicular, and filamentous ultrastructure. In stage 4, pale bodies exhibit peripheral condensation into smaller LBs having a halo. Stage 5 features large mature LBs having a central core and a surrounding halo of α-synuclein-immunopositive fibrils. (B) Six stages have been proposed to underlie cortical LB formation. The upper panel shows the anatomical distribution of brainstem and cortical LBs and proposed routes for LB spreading, the middle panel shows α-synuclein-immunostained human neurons at different stages and the lower panels show TEM analysis of accumulations at early, intermediate, and late stages. In stage 1, the abnormal α-synuclein accumulations are loose, granular, and intermingled with organelles. In stages 2 and 3, the structures are more well-defined and show intense staining for α-synuclein but they exhibit granular ultrastructures with few filaments. By stage 4, the structures have an irregular shape, consist of a dense granulofilamentous ultrastructure and are associated with curly neurites. In stages 5 and 6, the accumulations are ill-defined, exhibit a looser granulofilamentous structure, and show weaker reactivity with anti-α-synuclein immunostaining (stage 6). Modified from (Fares et al., 2021; Halliday et al., 2011; Wakabayashi et al., 2013b; Wakabayashi et al., 1998; Baba et al., 1998; Katsuse et al., 2003)

For brainstem LBs (Figure. 1.13. A), five stages of LB maturation based on morphological and ultrastructural alterations have been proposed. Neurons in the first stage exhibit granular α-synuclein accumulations in the cytoplasm, which subsequently becomes large, irregularly shaped structures (stage 2). These structures subsequently aggregate to create pale bodies, which usually lack a halo and are made up of granular, vesicular, and filamentous ultrastructures (stage 3). Following that, certain pale bodies show evidence of peripheral condensation, and one or more small LBs (with halos) arise from these condensations (stage 4). Subsequently, these 'early' LBs grow into larger LBs with the classic ring-like staining with a central core that is highly ubiquitin-positive and surrounded by an irradiating fibril-positive halo (stage 5).

Cortical LB staging differs significantly so these inclusions go through six stages before reaching maturity (Figure. 1.13. B). At the first stage, aberrant somatic α-synuclein accumulations that are loose, granular, and mixed with organelles are detected, similar to brainstem LBs. With stage advancement, they become more distinct and highly stained for α-synuclein, forming granular structures with few filaments (stages 2 and 3). These structures are then found to be connected with granular and curly neurites, which later become irregular in shape and comprise a dense granulofilamentous ultrastructure (stage 4). Later stages of these accumulations become ill-defined, have a looser granulofilamentous structure (stage 5), and eventually show minimal reactivity to α-synuclein antibodies (stage 6). This last finding is explained by the involvement of astroglial mechanisms that may degrade LBs into extracellular components. It is crucial to note that α-synuclein inclusions observed at each stage of the brainstem and cortical LBs have diverse shapes, heterogeneous content, and differential antibody staining patterns (C. Warren Olanow, 2011; Fujiwara et al., 2002; Mamais et al., 2013; Fares et al., 2021).

### 1.5.4. Lewy bodies composition

Even though α-synuclein is a key component of LBs, immunohistochemical studies have revealed that LBs include more than 90 molecules, including PD-linked gene products (DJ-1, LRRK2, Synphilin 1, parkin, and PINK-1), mitochondria-related proteins, and molecules implicated in the ubiquitin–proteasome system, autophagy, and aggresome formation (Wakabayashi et al., 2013). These molecules can be classified into different categories according to their function (Wakabayashi et al., 2007) (Table 1.1):

Table 1.1. Classification of Lewy bodies composition

| | |
|---|---|
| **1: Structural elements of the LB fibril** as α-synuclein (Spillantini et al., 1997; Fujiwara et al., 2002) and neurofilaments (Goldman et al., 1983). | **8: Molecules associated with protein phosphorylation** as CaMKII (Iwatsubo et al., 1991), LRRK2 (Zhu et al., 2006), or PINK-1 (Gandhi et al., 2006); and signal transduction as IκBα, NFκB (Noda et al., 2005) and p35 (Nakamura et al., 1997). |
| **2: α-Synuclein-binding proteins** as MAP1B (Jensen et al., 2000; Gai et al., 1996), synphilin 1 (Wakabayashi et al., 2000; Wakabayashi et al., 2002; Bandopadhyay et al., 2005) and tau (Galloway et al., 1989; Ishizawa et al., 2003). | **9: Cytoskeletal proteins** as MAP1B (Jensen et al., 2000; Gai et al., 1996), MAP2 (D'Andrea et al., 2001; Fukuda et al., 1993), tau (Galloway et al., 1989; Ishizawa et al., 2003), neurofilaments (Goldman et al., 1983), and tubulin (Galloway et al., 1988). |
| **3: Synphilin 1-binding proteins** as α-synuclein (Spillantini et al., 1997; Fujiwara et al., 2002), dorfin (Hishikawa et al., 2003; Ito et al., 2003) , parkin (Schlossmacher et al., 2002), and SIAH-1 (Liani et al., 2004). | **10: Mitochondria-related proteins** such as Cox IV (Itoh et al., 1997), cytochrome C (Hashimoto et al., 1999), and PINK-1 (Gandhi et al., 2006). |
| **4: Proteins implicated in the ubiquitin-proteasome system** such as ubiquitin (Kuzuhara et al., 1988), ubiquitin-activating enzyme (E1) (McNaught et al., 2002), and proteasome subunits 26 S (Fergusson et al., 1996). | **11: Cell cycle proteins** such as cyclin B (Lee et al., 2003) and retinoblastoma protein (Jordan-Sciutto et al., 2003). |
| **5: Protein implicated in the autophagosome-lysosome system** as LC3 (Tanji et al., 2011; Crews et al., 2010) and NBR1 (Odagiri et al., 2012). | **12: Cytosolic proteins passively diffuse into LBs** as APP (Arai et al., 1992), synaptophysin (Nishimura et al., 1994), synaptotagmin (Huynh et al., 2003), and tyrosine hydroxylase TH (Dugger and Dickson, 2010). |
| **6: Aggresome-related proteins** as γ-tubulin (McNaught et al., 2002) and HDAC6 (Kawaguchi et al., 2003).<br>3/6/24 11:48:00 AM | **13: Other components** including complement protein (Loeffler et al., 2006), immunoglobulin (Orr et al., 2005) and lipids (Gai et al., 2000) |
| **7: Proteins implicated in cellular responses** as molecular chaperone Hsp70-interacting protein (Y et al., 2005), heat-shock protein (Auluck et al., 2002), and oxidative stress (Kokoulina and Rohn, 2010; Bandopadhyay et al., 2004) | |

Moreover, because this method has a low throughput for investigating biological pathways involved in or influenced by LB formation and maturation during disease pathogenesis, a few studies used mass spectrometry to obtain complete, unbiased proteomic profiles of LBs from people with PD brains. Proteomic analyses of isolated cortical LBs, for example, revealed 296 proteins involved in a variety of cellular processes, including the ubiquitin-proteasome system, folding and intracellular trafficking, oxidative stress, synaptic transmission, and vesicular transport, signal transduction, and apoptosis (Leverenz et al., 2007; Basso et al., 2004; Licker et al., 2014) Membranous fragments, organelles, vesicular structures, and other subtypes of lipid contents later emerged as major components of LBs, and their presence was proven by a variety of techniques, including immunohistochemistry and Fourier transform infrared spectroscopy (Gai et al., 2000; Araki et al., 2015).

Interestingly, recent studies used correlative light and electron microscopy (CLEM) to investigate the ultrastructure of LBs in non-fixed post-mortem brains from people with PD, in which researchers obtained highly resolute images of LB structures enriched in lipids and membranous structures, including mitochondria (Shahmoradian et al., 2019). By adopting this method and expanding it using serial block-face scanning EM, the authors were able to find specific vesicle clusters in the center of LBs that was coated in high local quantities of non-fibrillar α-synuclein molecules, which may explain how α-synuclein staining appeared punctate in previous neuropathological analyses. Surprisingly, only around 20% of all LBs and NLs seemed to have large amyloid fibrils associated with them, showing that α-synuclein amyloid formation is not as important in PD pathogenesis as previously thought. Furthermore, the morphological investigation revealed the presence of multiple lysosomal vesicles connected with the core and additional mitochondrial membranes at the LB's periphery.

Following studies using a similar approach revealed that the formation of LB-like inclusions necessitates the formation of α-synuclein fibrils, which undergo significant remodeling and PTMs and interact with membranous structures as they transform into LB-like inclusions composed of proteins, fragmented membranes, vesicular structures, and dysmorphic organelles (mitochondria, lysosomes, and autophagosomes) (Mahul-Mellier et al., 2020).

## 1.6. Synphilin 1 – role in Lewy bodies formation

### 1.6.1. Synphilin 1 structure

Synphilin 1 was identified as α-synuclein interacting protein in a yeast two-hybrid screen (Neystat et al., 2002; Engelender et al., 1999) . Synphilin 1 has been linked with PD because of its interaction with α-synuclein and for its abundance in the LB (Wakabayashi et al., 2013; Wakabayashi et al., 2000). The translation product of its gene SNCAIP is a 919-amino acid protein containing several protein domains, including six ankyrin-like repeats, a coiled-coil domain, and a putative ATP/GTP binding motif (Krüger, 2004) (Figure. 1.14.).


**FIGURE 1.14. Domain organization of synphilin 1.** Modified from Krüger, 2004.

At the amino acid level, the human protein is 86% identical to its mouse counterpart (O'Farrell et al., 2002). The core part of the protein, which contains the ankyrin-like repeats and the coiled-coil domain, has a 96.5% homology (O'Farrell et al., 2002). These domains are known to be present in a wide range of proteins that mediate protein-protein interactions (Mosavi et al., 2004). Indeed, several studies established the interaction of synphilin 1 with α-synuclein, parkin, and dorfin (Neystat et al., 2002). For instance, a segment including amino acid residues 349-555 is both essential and sufficient to induce contact with α-synuclein (Nagano et al., 2003; Liani et al., 2004). Synphilin 1 and α-synuclein interact not just through their C-termini, but also through their N-termini (Kawamata et al., 2001). The overexpression of synphilin 1 in HEK 293 cells induced the formation of small puncta and together with α-synuclein was also found to form cytoplasmic inclusions (O'Farrell et al., 2001). Indeed, recent studies found that the interaction of the central coiled-coil domain of Synphilin 1 with the N-terminal stretch of α-synuclein induces the creation and accumulation of cellular inclusions (Xie et al., 2010).

Human brain extracts revealed synphilin 1 as a largely soluble 90 kDa protein, but a less soluble 120 kDa form, as well as fragments of 65 kDa and 50 kDa, were also found, indicating that alternative splicing (or post-translational processing) may play a role in synphilin 1 function or distribution (Murray et al., 2003). Indeed, synphilin 1 is found to be expressed in the central nervous system primarily in large neurons including Purkinje, nigral and pyramidal neurons, but also several peripheral tissues such as the heart, lungs, kidneys, liver, and blood cells (Engelender et al., 2000). Analysis of its aminoacidic sequence with PrDOS as a disordered prediction tool (Ishida and Kinoshita, 2007) revealed synphilin 1 to be intrinsically disordered with scores above 0.5 for a large part of the N-terminal and C-terminal, involving part of the coiled-coil domain and ANK 5 and 6 (Figure. 1.15.).

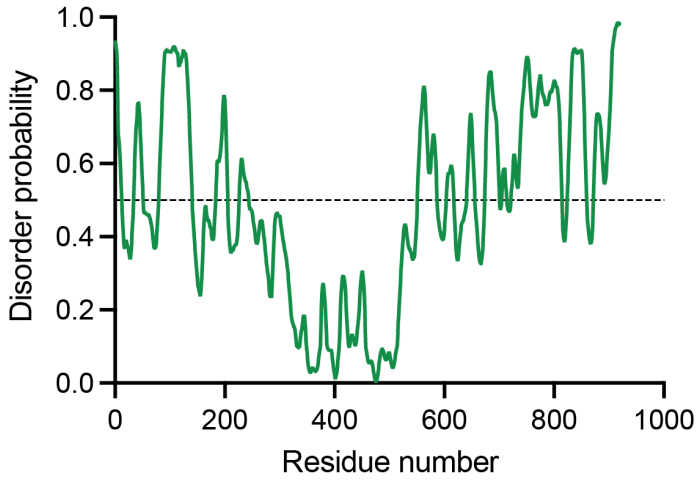


**FIGURE 1.15. Synphilin 1 is intrinsically disordered.** Disorder prediction for Synphilin 1. Prediction performed using PrDOS bioinformatics tool.

Nevertheless, Synphilin 1A is a splice variant of synphilin 1 that was found in LBs and detergent-insoluble fractions of brain protein samples. These findings are corroborated by the discovery of altered mRNA expression levels of Synphilin 1 isoforms in PD. Furthermore, synphilin 1A was found in both PD and DLBD patients' LBs, implying a role for synphilin 1A in the etiology of different synucleinopathies (Eyal et al., 2006).

The overexpression of synphilin 1 in HEK 293 cells induced the formation of small puncta and together with α-synuclein was also found to form cytoplasmic inclusions (O'Farrell et al., 2001) (Fig 1.16.).

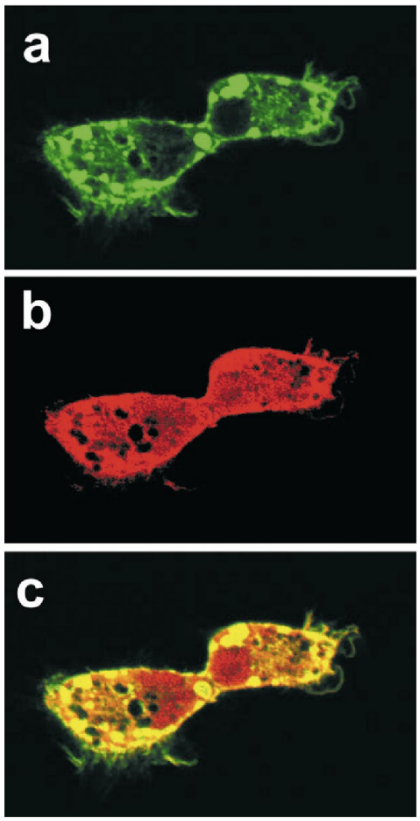


**FIGURE 1.16. Co-localization of α-synuclein and synphilin 1.** Cells were co-transfected with α-synuclein and EGFP–synphilin 1 as described above and into cells stained for α-synuclein (a–c). EGFP fluorescence was monitored using FITC optics (a) and α-synuclein immunoreactivity was identified using secondary antibodies conjugated to AlexaFluor 568 (b). Merged images (c) show that there are significant areas of overlap between the synphilin 1 inclusions and α-synuclein immunoreactivity. Modified from O'Farrell et al., 2001.

Synphilin 1 and α-synuclein interact not just through their C-termini, but also through their N-termini (Kawamata et al., 2001). On the other hand, recent studies found that the interaction of the central coiled-coil domain of synphilin 1 with the N-terminal stretch of α-synuclein induces the creation and accumulation of cellular inclusions (Xie et al., 2010).

### 1.6.2 Synphilin 1 function

Although the physiological function is currently unknown, synphilin 1 has been reported to interact with several E3-Ubiquitin-ligases and with the protein kinase LRRK2 involved in both autosomal dominant and sporadic PD (Smith et al., 2006; Szargel et al., 2008). During development, synphilin 1 is predominantly expressed in neurons and is enriched in presynaptic nerve terminals, which may represent its role in the synaptic maturation (Ribeiro et al., 2002). The presence of synphilin 1 in lipid fractions of brain extracts is associated with a role as an SVs-binding protein, as shown in several biochemical studies (Murray et al., 2003). The binding of synphilin 1 to SVs has been reported to be negatively regulated by α-synuclein (Ribeiro et al., 2002). These findings were further

corroborated by EM studies on the nature of these synphilin 1 inclusions demonstrating membrane-bound lamellar-like phospholipid accumulations (O'Farrell et al., 2001).

In familial forms of PD, the only accountable genetic mutation in SNCAIP related to PD leads to R621C substitution in synphilin 1 (Marx et al., 2003). Mice overexpressing the mutant synphilin 1 had an elevated neurotoxic impact and a motor phenotype compared to mice overexpressing the wild-type protein (Nuber et al., 2010). However, the frequency of the R621C substitution was shown to be the same in PD and control participants, raising doubts about the mutation's role in PD physiopathology (Myhre et al., 2008). Nevertheless, R621C-modified Synphilin 1 does not change its binding to α-synuclein (Marx et al., 2003).

The synphilin 1 function as an SVs binding protein is consistent with biochemical evidence showing the presence of synphilin 1 in lipid fractions of brain extracts (Murray et al., 2003). Moreover, functional implications are suggested by the apparent intracellular co-localization with the associated α-synuclein protein. There is evidence that α-synuclein adversely regulates synphilin 1 binding to SVs (Ribeiro et al., 2002). Furthermore, it has been proposed that synphilin 1 mediates the synaptic activities of α-synuclein, maybe by anchoring α-synuclein to the vesicle membrane. Observations of cultured cells have provided support for the importance of the carefully controlled interaction with α-synuclein and of binding to synaptic vesicles. According to this research, casein kinase II phosphorylates synphilin 1, which decreases its capacity to bind with α-synuclein and create cytoplasmic inclusions (Lee et al., 2004).

Subsequent studies of synphilin 1 inclusions produced in cell culture revealed that they resemble so-called aggresomes, which are perinuclear inclusion bodies commonly detected after a misfolded protein production (Kopito, 2000). Key properties of aggresomes, such as positive staining for vimentin, gamma-tubulin, ubiquitin, and proteasomal subunits, have been observed in synphilin 1-positive inclusions (Tanaka et al., 2004; Ito et al., 2003; Wahl et al., 2008). Aggresomes interact with lysosomal structures, suggesting that autophagy may be used to remove accumulated proteins (Fortun et al., 2003). These discoveries have crucial implications for the unresolved mechanism of PD since characteristic LB in the brains of PD patients exhibit several hallmarks of aggresomes as a result of proteasomal inhibition. These characteristics include the presence of α-synuclein

and other elements of the protein degradation and refolding machinery, as well as a core and halo organization (Junn et al., 2002).

It is widely acknowledged that synphilin 1 is a part of LBs in the brains of sporadic PD patients despite quantitatively varying results depending on the different antibodies used in the immunohistochemistry (Iseki et al., 2002; Wakabayashi and Takahashi, 2003). Up to 90% of LBs in PD patients have been shown to have synphilin 1. Its significant central core localization points to a crucial function in the LB development (Wakabayashi et al., 2000) (Figure. 1.17.). Synphilin 1 is found in DLB (Katsuse et al., 2003) and in glial cytoplasmic inclusions in MSA (Murray et al., 2003), both of which occur in parallel with the presence of alpha-synuclein. This may be due to its role in the development of cytoplasmic inclusions and neurodegeneration more generally (Wakabayashi and Takahashi, 2003).

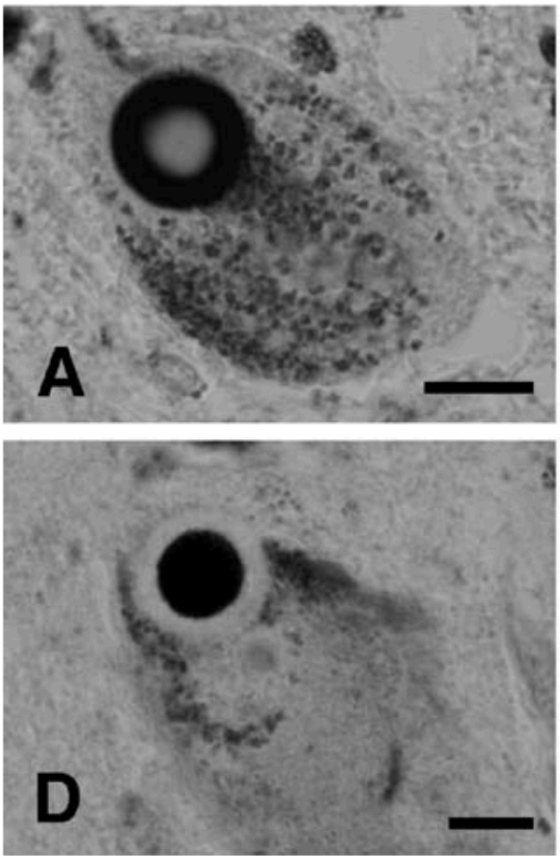


**FIGURE 1.17. Synphilin-1 localize in the core of LB.** Immunoreactivity of α-synuclein (A) and synphilin 1 (D). Modified from Wakabayashi and Takahashi, 2003.

## 1.7. LLPS as an emerging concept for understanding neuronal physiology and pathology

Particularly interesting for my work in this thesis are the particular examples described in the context of neurons, particularly referring to the LLPS at the synapse and in neurodegenerative diseases (Figure. 1.18.).

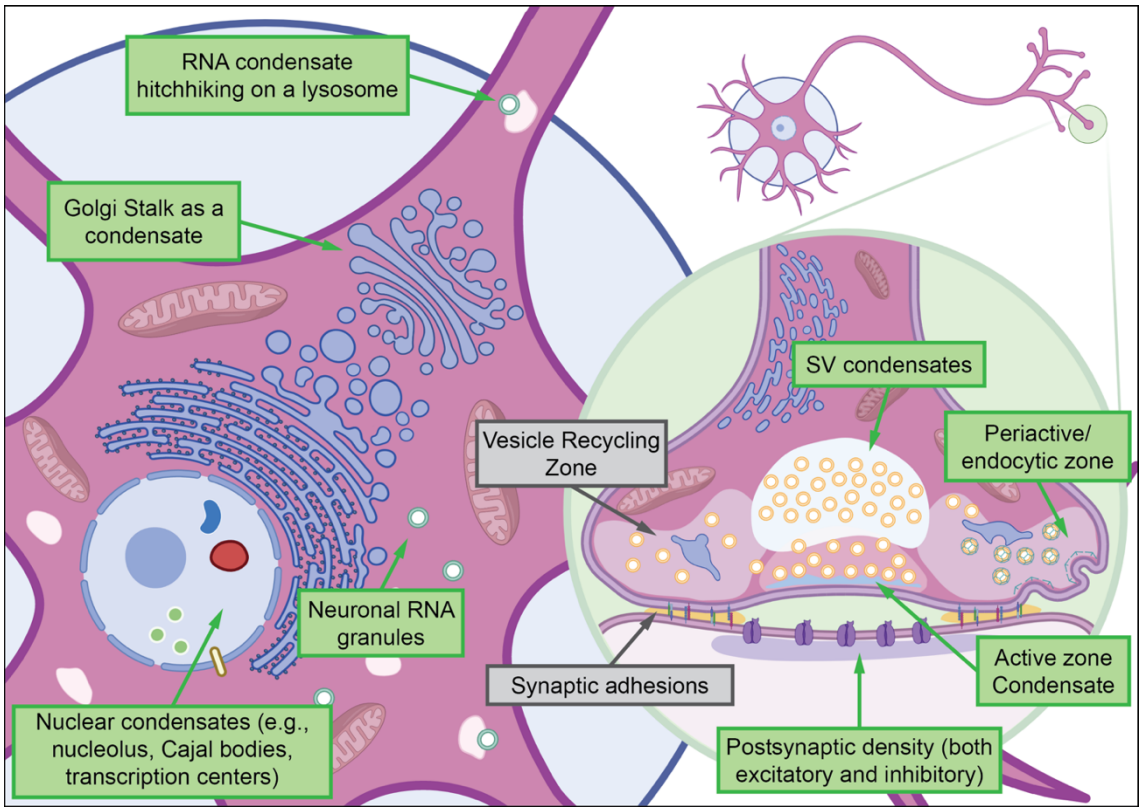


**FIGURE 1.18. Biomolecular condensates as an organizing principle in neuronal- and synaptic biology.** Scheme of a neuron. Blue: focus on the soma where several structures in the nucleus (e.g., nucleolus, Cajal bodies) and cytoplasm (e.g., neuronal RNA granules, Golgi stalk, secretory vesicles) are shown to assemble by LLPS. Green: focus on the synapse with an emphasis on several membrane-less condensates both at the presynapse (e.g., SV condensates, active zone, endocytic sites) and postsynapse (e.g., excitatory PSD 95-containing condensates, inhibitory gephyrin sheets. Putative regions that might form by LLPS at the synapse are highlighted in gray.

At the synapse, LLPS helps to maintain the SV's pool forming SVs condensates, active zone condensates, and periactive zone condensates at the presynaptic compartment. Purified synapsin 1 has been described undergo LLPS *in vitro* in a manner recapitulating its *in vivo* properties (Milovanovic et al., 2018). As discussed above, synapsin condensate can capture liposomes and are dispersed upon phosphorylation by CaMKII (Milovanovic et al.,

2018). LLPS of proteins that bind to intracellular areas of membrane proteins can also influence the clustering of membrane surface proteins (Ramella et al., 2022). Two active zone proteins, Rab3-interacting molecule (RIM) and RIM-Binding Protein (RIM-BP), which interact with voltage-gated $Ca^{2+}$ channels, facilitate $Ca^{2+}$ channel clustering through LLPS (Wu et al., 2019; Wu et al., 2021).

Looking at the postsynapse, *in vitro* mixing of Homer and Shank results in the formation of macromolecular complexes. Shank and Homer are both multimeric proteins. The protein complex acquires a high-order meshwork structure as a result of this multimer-multimer interaction, and this is the postulated underlying framework of the PSD at the excitatory synapse (Hayashi et al., 2009). Similarly, SynGAP, a postsynaptic Ras-activating protein, is a trimeric protein with a PDZ binding motif (Zeng et al., 2016). PSD-95, a postsynaptic scaffolding protein, multimerizes *in vitro* (Zeng et al., 2018). When purified SynGAP and PSD-95 are combined, they form a macromolecular complex. The resultant complex has droplet-like structures (Zeng et al., 2016).

Many implications and recent findings are highlighting the role of LLPS in how protein aggregates in neurodegenerative disorders. Some early examples include TDP-43, FUS, and TIA1, which are all RNA-binding proteins involved in the onset of amyotrophic lateral sclerosis (ALS) (Mackenzie and Neumann, 2016). The proteins all contain a prion-like domain, an IDR that can promote uncontrolled protein aggregation (Zbinden et al., 2020; Conicella et al., 2020), and it is often the site of disease-causing mutations (Mackenzie et al., 2017; Kim et al., 2013). Tau, implicated in AD forms liquid droplets through the interaction of its microtubule-binding domains, which are rich in positively charged amino acids, with negatively charged phospholipids in the membrane (Boyko and Surewicz, 2022; Wegmann, 2019; Vogels et al., 2020). Changes in tau protein, such as phosphorylation, ubiquitination, or the presence of mutations, can affect the thermodynamic stability of tau droplets and promote the formation of aggregates (Zeng et al., 2021). Along the same line, α-Synuclein can also undergo LLPS in the presence of extremely high protein concentration and high crowding conditions (Ray et al., 2020; Luna and Luk, 2015). This may be linked to the formation of aggregates known as LBs, toxic to nerve cells that contribute to the degeneration and death of dopamine-producing neurons.

## 1.8. Overarching Goal and Specific Aims

The overarching aim of this thesis is to investigate the intricate interaction between α-synuclein-containing condensates with the membrane-bound organelles in physiological and pathological contexts.

My first hypothesis was that α-synuclein affects the LLPS of SVs clusters, which are a central component of neuronal communication. LLPS of SVs/synapsin and α-synuclein ensures a proper compartmentalization and spatial arrangement within the presynaptic terminal allowing for efficient storage, release, and recycling of neurotransmitters.

My second hypothesis was that the formation of α-synuclein-containing pathological inclusions arises from the disruption of normal LLPS processes. When LLPS of α-synuclein becomes dysregulated, it can lead to the formation of aberrant intracellular inclusions similar to Lewy bodies, a key hallmark observed in PD patients.

**The specific aims of the thesis were to:**

1. Determine how α-synuclein influences the assembly, organization, and properties of SV condensates. By deciphering the impact of α-synuclein on SV condensates, I sought to gain insights into the mechanisms underlying SV dynamics and explore and examine the effects of α-synuclein on the physical properties of SV condensates.

2. Reconstitute the minimal machinery that recapitulates the key characteristics and processes associated with α-synuclein-containing inclusions observed in PD and other Lewy body-associated diseases.

3. Characterize the factors that contribute to the recruitment of membrane-bound organelles to α-synuclein-containing inclusions. This includes assessing the impact on organelle integrity, dynamics, and cellular homeostasis. Dissecting these interactions allows us to uncover the underlying mechanisms that contribute to the pathological processes associated with α-synuclein aggregation and neurodegeneration.

# 2. MATERIALS AND METHODS

## 2.1. Materials and equipment

### 2.1.1. General equipment

- Brand™ Blaubrand® Counting Chamber, Sigma-Aldrich, Germany
- Centrifuge 5430 R, Eppendorf, Germany
- $CO_2$ Incubator, Schubert & Weiss, Germany
- Eclipse Ti Nikon Spinning Disk Confocal, CSU-X microscope, Nikon, Japan
- Gas burner Fuego basic, WLD-TEC, Germany
- Incubation Shaker, INCU-Line IL56 Schubert & Weiss, Germany
- Magnetic Stirrer, Heidolph, Germany
- Microwave, Severin, Germany
- Nanodrop, One Thermo Scientific, USA
- pH meter, SevenCompact Mettler-Toledo, Germany
- Rotilab®-Mini Centrifuge, Roth, Germany
- SDS PAGE Chamber System, Bio-Rad, USA
- Thermal Cycler C1000 Touch, Bio-Rad, USA
- Thermal Shaker, Thermo Scientific, USA
- Vortex-Genie® 2, Scientific Industries, USA
- Waterbath, Phoenix instrument, Germany

### 2.1.2. Consumable supplies

- Bacteria dishes (100 mm, 150 mm) Sarstedt, Germany
- Eppendorf tubes (5 mL, 2 mL, 1.5 mL) Sarstedt, Germany
- Expi flasks, Life Technologies, USA
- Falcon tubes (50 mL, 15 mL), Corning, USA
- Filtropur Filter bottles (250 mL, 500 mL), Sarstedt, Germany
- Glass bottom dish, Cellvis, USA
- 15-well 3D glass bottom slide, Ibidi, Germany
- PCR 8er-SoftStrips (0.2 mL), Biozym, Germany
- Pierce™ Concentrator 30K MWCO, 0.5 mL, Thermo Scientific, USA

- Pierce™ Concentrator 30K MWCO, 2-6 mL, Thermo Scientific, USA
- Pipette tips (1000 µL, 200 µL, 10 µL), Sarstedt, Germany
- Serological pipettes (25 mL, 10 mL, 5 mL), Sarstedt, Germany
- Syringes (20 mL), Schubert & Weiss, Germany
- Syringes (5 mL), Roth, Germany
- Syringes (50 mL), VWR, USA
- T75 flasks, Corning, USA
- Whatman™ Filter Unit (2 µm), Th.Geyer, Germany

### 2.1.3. Enzymes, enzyme buffers, and PCR components

- 10X Buffer R, Thermo Scientific, USA
- 10x Ligase Buffer, Thermo Scientific, USA
- 5x Phusion® HF Reaction Buffer, Thermo Scientific, USA
- DNaseI, AppliChem, Germany
- dNTP mix (10 mM each), Thermo Scientific, USA
- DpnI, Thermo Scientific, USA
- FastAP, Thermo Scientific, USA
- HindIII, Thermo Scientific, USA
- Papaine, Sigma-Aldrich, Germany
- Phusion® DNA Polymerase, Thermo Scientific, USA
- Primers (100 µM), Sigma-Aldrich, Germany
- T4 DNA Ligase, Thermo Scientific, USA

### 2.1.4. Chemical and substances

- 1,6-Hexanediol, Sigma-Aldrich, Germany
- 1,3-Propanediol, Sigma-Aldrich, Germany
- Agar-Agar, Roth, Germany
- Boric Acid, Sigma-Aldrich, Germany
- Calcium chloride ($CaCl_2$), Roth, Germany
- Ethanol absolute, VWR, USA
- Ethylene-diamine-tetra-acetic acid (EDTA) free
- Protease inhibitor cocktail pill, Roche, Switzerland
- GelRed®, Biotium, USA

- Glucose, Sigma-Aldrich, Germany
- HEPES, Roth, Germany
- Imidazole, Schubert & Weiss, Germany
- InstantBlue® Coomassie Protein Stain (ISB1L), Abcam, United Kingdom
- Kanamycin Sulfate, AppliChem, Germany
- L-Cysteine hydrochloride monohydrate, Sigma-Aldrich, Germany
- Magnesium chloride ($MgCl_2$), Roth, Germany
- Natriumchlorid (NaCl), Roth, Germany
- Polyethylene glycol (PEG), Roth, Germany
- Potassium chloride (KCl), Roth, Germany
- Rotiphorese® Gel 30 (37,5:1), Acrylamide Roth, Germany
- SDS ultra-pure, Roth, Germany
- Sodium hydroxide (NaOH), Roth, Germany
- TCEP, Sigma-Aldrich, Germany
- TEMED, Roth, Germany
- TRIS, Roth, Germany
- Trypton/ Pepton ex casein, Roth, Germany
- Yeast extract, Roth, Germany

### 2.1.5. Media and solution

- B-27™ Supplement (50X), Gibco life technologies, USA
- Expi293F™ Expression Medium, Gibco life technologies, USA
- Fetal Bovine Serum, Sigma-Aldrich, Germany
- GlutaMAX™, Gibco life technologies, USA
- Hank's Balanced Salt Solution (HBSS), Gibco life technologies, USA
- HEPES, Gibco life technologies, USA
- Neurobasal™-A Medium, Gibco life technologies, USA
- Opti-MEM™, Gibco life technologies, USA
- Phosphate-Buffered Saline (PBS), Gibco life technologies, USA
- Penicillin/ Streptomycin, Gibco life technologies, USA
- Poly-L-lysine, Sigma-Aldrich, Germany
- Sodium Pyruvate, Gibco life technologies, USA
- Trypan Blue stain, Sigma-Aldrich, Germany

### 2.1.6. Fluorescent dyes

- FM 4-64, Invitrogen, USA
- SPY-Actin, Switzerland
- SiR-Actin, Spirochrome, Switzerland
- Sir-Tubulin, Spirochrome, Switzerland
- Lysotracker™ Deep Red, Invitrogen, USA
- Mitotracker™ Deep Red, Invitrogen, USA

### 2.1.7. Commercial Kits

- ExpiFectamine 293 Transfection Kit, Gibco life technologies, USA
- Lipofectamine® 2000 Transfection Kit, Invitrogen, USA
- NucleoBond® Xtra Midi EF, Macherey-Nagel, Germany
- NucleoSpin® Plasmid DNA purification, Macherey-Nagel, Germany
- Silica Bead DNA Gel Extraction Kit, Thermo Scientific, USA

### 2.1.8. Columns for protein purification

- Ni-NTA column (5 mL HisTrap™HP) GE, Healthcare, USA
- Superdex™ 200 Increase 10/300 GE, Healthcare, USA
- PD-10 column for protein NHS-protein labeling

### 2.1.9. Markers and loading dyes

- GeneRuler 1 kb DNA Ladder, Thermo Scientific, USA
- 6X Orange DNA Loading Dye, Thermo Scientific, USA
- PageRuler™ Prestained Protein Ladder, Thermo Scientific, USA

### 2.1.10. Human cell lines

- Expi293F™, Thermo Scientific, USA
- HEK 293, DSMZ, ACC 305, Germany

### 2.1.11. Mouse cell lines

C57BL/6, License T 0074/20. All animal experiments were approved by the Institutional Animal Welfare Committees of the Charité University Clinic (Berlin, DE) and Max Planck Institute for Biophysical Chemistry (Gottingen, DE).

### 2.1.12. Software

- Adobe Illustrator (v25.4.3)
- Biometra BioDocAnalyze (v2.67.5.0)
- Geneious prime (v11.0.9+11)
- GraphPad Prism 9 (v9.0.0)
- FIJI ImageJ2 (v2.3.0/1/53q)(NIH)
- Microsoft Excel (v2111)
- Nikon acquisition software NIS Elements (v5.21.02)

# 2.2. Methods

## 2.2.1. Molecular Biology/Cloning

### 2.2.1.1. Primer design

Primers were designed using the software Geneious Prime® 2021.0.3, 11.0.9+11 (64-bit) and purchased from Sigma Aldrich. Primers were dissolved in dd$H_2O$ (100 µM stock concentration) and stored at -20 °C. All primers used in this study are shown in the appendix table 2.1

Table 2.1. Primers list

| Name | Primer #pDML | Sequence | $T_m$ |
|---|---|---|---|
| 2F5_SNCA-BFP_fwd | 0079 | 5'-ATCACTCGAGCGCCACCATGGACGTGTTCATGAAGGG-3' | 71.1 °C |
| 2F5_SNCA-BFP_rev | 0080 | 5'-ATCAGGATCCGCGGCCTCGGGCTCGTAG-3' | 70.3 °C |
| 5G6_SNCA(A140C)_fwd | 0463 | 5'-CGAGCCCGAGTGTTGATAAGCGGCCGCACTCGAG-3' | 72.3 °C |
| 5G6_SNCA(A140C)_rev | 0464 | 5'-CGGCCGCTTATCAACACTCGGGCTCGTAGTCCTG-3' | 70.5 °C |
| 6B2_SNCA-BFP ΔF_fwd | 0486 | 5'-AAAAGAAGGCGTGAAGAAGGACCAGCTGGGCAAGAAC-3' | 69.0 °C |
| 6B2_SNCA-BFP ΔF_rev | 0487 | 5'-CCTTCTTCACGCCTTCTTTTGTCTTGCCAGCGGCTTC-3' | 69.8 °C |
| 6B4_SNCA-BFP ΔC_fwd | 0492 | 5'-CGGCTTTGTGGCGGATCCACCACCGGTCATGAGCGAGCTG-3' | 75.4 °C |
| 6B4_SNCA-BFP ΔC_fwd | 0493 | 5'-GTGGATCCGCCACAAAGCCGGTGGCAGCGGCGATAG-3' | 74.8 °C |
| 6G1_SNCA-BFP(A53T)_fwd | 0510 | 5'-GCACGGCGTGACCACCGTGGCCGAGAAAAC-3' | 72.0 °C |
| 6G1_SNCA-BFP(A53T)_rev | 0511 | 5'-CGGCCACGGTGGTCACGCCGTGCACCACC-3' | 75.2 °C |
| 6G2_SNCA-BFP(A30P)_fwd | 0512 | 5'-GCCGAAGCCCCTGGCAAGACAAAAGAAGG-3' | 67.3 °C |
| 6G2_SNCA-BFP(A30P)_rev | 0513 | 5'-TTGTCTTGCCAGGGGCTTCGGCCACCCC-3' | 71.5 °C |
| 6G7_SNCA-BFP(S129A)_fwd | 0522 | 5'-CGAGATGCCTGCCGAAGAGGGCTACCAGGAC-3' | 69.7 °C |
| 6G7_SNCA-BFP(S129A)_rev | 0523 | 5'-GCCCTCTTCGGCAGGCATCTCGTAGGCCTCG-3' | 71.4 °C |
| 6G8_SNCA-BFP(S129E)_fwd | 0524 | 5'-CGAGATGCCTGAGGAAGAGGGCTACCAGGAC-3' | 67.6 °C |
| 6G8_SNCA-BFP(S129E)_rev | 0537 | 5'-GCCCTCTTCCTCAGGCATCTCGTAGGCCTCG-3' | 69.4 °C |
| 3F8_HALO-SYN1_fwd | 0195 | 5'-ATCAACCGGTGCCACCATGGCAGAAATCGGTACTGG-3' | 70.3 °C |
| 3F8_HALO-SYN1_rev | 0196 | 5'-TGATAGATCTGCTGCCGCTGCCGGAAATCTCGAGCGTC-3' | 71.8 °C |
| 3F8_HALO-SYN1(6xHis)_fwd | 0438 | 5'-CTAGCGCCACCATGCATCACCATCACCATCACA-3' | 68.4 °C |
| 3F8_HALO-SYN1(6xHis)_rev | 0439 | 5'-CCGGTGTGATGGTGATGGTGATGCATGGTGGCG-3' | 70.5 °C |

### 2.2.1.2. PCR amplification

For PCR amplification of target sequences from plasmids, the Phusion® High-Fidelity DNA Polymerase was used. Reactions were prepared in 0.2 mL PCR tubes on ice. Final primer concentration was 0.2 µM. For amplification from plasmid DNA approximately 50 ng template DNA was used. All components were mixed and transferred to a PCR cycler. The standard pipetting scheme and PCR program is shown in table 2.2 and 2.3. After amplification, reactions were analyzed by agarose gel electrophoresis (2.2.1.7).

Table 2.2. Pipetting scheme for standard PCR amplification

| Component | Amount µL |
|---|---|
| $ddH_2O$ | 35 |
| 5x Phusion® HF Reaction Buffer | 10 |
| dNTP mix (10 mM each) | 1.5 |
| Primer Fwd 10 µM | 1 |
| Primer Rev 10 µM | 1 |
| Template DNA | 1 (approx. 50ng) |
| Phusion® HF DNA Polymerase | 0.5 (1 U) |
| Total volume | 50 |

Table 2.3. PCR program for standard PCR amplification

| Temperature | Time | Cycles |
|---|---|---|
| 98 °C | 5’ | 1 |
| 98 °C | 10’’ | 25 |
| 56 °C | 30’’ | |
| 72 °C | 15’’-30’’/kb | |
| 72 °C | 10’ | 1 |
| 4 °C | ∞ | 1 |

#### 2.2.1.3. Restriction digests

Class-II restriction enzymes are recognizing their specific palindromic recognition site and perform cleavage of the phosphodiester bond of the DNA. Restriction digests were performed either on a preparative or an analytical scale. For an analytical digest, proximately 150 ng plasmid DNA was used and analyzed for fragment patterning by agarose gel electrophoresis (2.2.1.7). For molecular cloning, preparative digests were performed to produce compatible ends of PCR products and vector plasmid backbones. Typically, 1 µg of vector plasmid was digested with 10 U of restriction enzyme for at least 1 hour. Buffers, supplements, and incubation temperatures were chosen accordingly to the manufacturer's instructions for each restriction enzyme. Double digests conditions were examined using the DoubleDigest tool from Thermo Scientific (http://www.thermoscientificbio.com/webtools/doubledigest/). Prior to PCR digest, the product was purified from the PCR mixture using the Silica Bead DNA Gel Extraction Kit (#K0513, www.thermoscientific.com/onebio) according to the manufacturer's instructions.

#### 2.2.1.4. Ligation of DNA molecules

In molecular biology, the term ligation stands for the formation of a covalent phosphodiester bond between DNA fragments that possess a free 3' hydroxyl and a 5' phosphate group in their backbone. Ligases are enzymes catalyzing this reaction. Ligations can be performed between compatible ends of DNA molecules such as digested PCR fragments and vector backbones. For a standard ligation, 1 U of the bacteriophage T4 DNA Ligase was used in a total volume of 10 µL. Usually, 50 ng of digested vector were mixed with a 3-molar excess of insert DNA (molar insert:vector ratio 3:1). In cases where the insert amount could not be determined, 50 ng of the digested vector with the maximum amount of insert was used. Reactions were carried out for 1 hour at 37 °C or overnight at room temperature.

#### 2.2.1.5. Transformation of bacteria

A standard calcium chloride protocol was used to achieve chemically competent DH10B Escherichia coli cells. These cells are able to take up DNA from their environment upon a heat shock. This ability is used to transform Escherichia coli cells with DNA of interest. Ligation reactions (5-10 mL) or purified plasmids (10-100 ng) were mixed with thawed competent cells on ice (ratio 1:10 (v/v). The mixture was kept on ice for 10 minutes and subsequently subjected to heat shock for 2 minutes at 42 °C. After heat shock, the cells were incubated for another 10 minutes on ice. Recovery was performed in 700 µL of LB medium

without antibiotics and incubated at 37 °C in a thermomixer (800 rpm) for approximately 45 minutes. Following recovery, 150 µL were spread on agar plates containing the appropriate antibiotics for selection. The residual cells were pelleted by centrifugation and spread on a second agar plate with appropriate antibiotics. Plates were incubated at 37 °C until colonies were grown.

#### 2.2.1.6. Preparation of plasmids

Preparation of plasmid DNA from Escherichia coli was done using the Silica Bead DNA Gel Extraction Kit (#K0513, www.thermoscientific.com/onebio), according to the manufacturer's instructions. Bacterial colonies were incubated in 4 mL LB media containing appropriate antibiotics. Cultures were kept at 37 °C in a shaker (approx. 210 rpm) for at least 16 hours. Cells were harvested by centrifugation in a table-top centrifuge at full speed. The cell pellet was subjected to plasmid preparation as described in the manual. The purification principle is based upon the DNA property of binding to silica gel under high chaotropic salt conditions and subsequent elution under low salt conditions. The DNA was finally eluted with 50 µL elution buffer and concentration was determined using UV spectroscopy at 260 nm. Plasmids were stored at -20 °C or subjected to downstream methods such as restriction digest or sequencing.

#### 2.2.1.7. Agarose gel electrophoresis

Gel electrophoresis can be either performed as a preparative gel, used for isolating DNA fragments of interest, or as an analytical gel utilized for the analysis of restriction patterns of test digests. The overall negative charge of DNA which is proportional to the molecular weight and thereby the length of the DNA can be used to separate a mixture of nucleic acid fragments in a solidified gel matrix made out of agarose. Applying a vector electric field to the matrix results in the separation of fragments of different sizes due to different migration distances. The fragments can be stained with fluorescent dyes which are present in the solidified gel matrix. Bands can be visualized by illumination of these dyes and pictures can be taken with a CCD camera. The agarose concentration of the solidified gel matrix determines a suitable separation range of nucleic acids (table 2.4).

Table 2.4. Agarose concentrations and suitable separation length used in gel electrophoresis

| Separation range | Agarose concentration (w/v) |
|---|---|
| 1 - 30 kb | 0.5 % |
| 0.8 - 12 kb | 0.7 % |
| 0.5 - 7 kb | 1.0 % |
| 0.4 - 6 kb | 1.2 % |
| 0.3 - 3 kb | 1.5 % |
| 0.1 - 2 kb | 2.0 % |

According to this table, an agarose/0.5xTBE solution was boiled in a microwave until the agarose was completely dissolved. The solution was cooled down and 4 µL of GelRed Nucleic Acid Stain (10,000x) per 100 mL molten agarose solution was added. After mixing, the solution was poured into the gel-casting unit. The solidified gel was either used directly for electrophoresis with 0.5x TBE buffer or stored wrapped in cling film at 4 °C. Samples were substituted with DNA Loading Dye to 1 x final concentration. For size determination, a commercially available DNA standards were used. Running conditions (voltages and times) were adapted to different gel casts, agarose percentages, and separation lengths. Gel analysis and imaging were performed using the GelDoc™ 2000 from Bio-Rad.

### 2.2.1.8. Extraction of DNA from agarose gel

In the case of preparative electrophoresis, the band of the agarose gel was cut out and purified with the Silica Bead DNA Gel Extraction Kit. The DNA fragment of the agarose gel was excised with a clean and sharp scalpel. The weight of the gel piece was determined, mixed with an equal volume of Binding Buffer (100 mg ~ 100 µL), and dissolved at 55 °C using a thermomixer. Binding of DNA, washing, and elution was performed according to the manufacturer's instructions. The DNA was eluted with elution buffer and subjected to downstream applications such as restriction digest or ligation. The Silica Bead DNA Gel Extraction Kit was used for the purification of restriction digests, as well as for PCR reactions. Therefore, a PCR reaction was mixed with an equal volume of Binding Buffer and purified as described above. The elution volume varied due to different downstream applications.

### 2.2.1.9. Synapsin 1 cloning

The open reading frame of human Synapsin 1 was inserted into the pmCherry-C1 or pEGFP-C1 vector using BglII-SacI restriction sites (Genscript). pmCherry-C1 and pEGFP-C1 were modified through NheI-XhoI sites to encode the His6-tag, according to Milovanovic, 2018. All the vectors contain CMV promoter and SV40 terminator.

### 2.2.1.10. α-Synuclein cloning

C-terminally tagged α-synuclein-BFP plasmid preparation (pBFP-N1 SNCA) is described in Hoffmann and Sansevrino, 2021. In principle, α-Synuclein (Addgene #51437) was PCR sub-cloned into a BFP-N1 vector (kind gift from Geert van den Bogaart) using restriction sites BamHI-XhoI sites as shown in table 2.5.

Table 2.5. α-Synuclein-BFP primer sequences for cloning and specific RE sites.

| | |
|---|---|
| #DML0079+0080 (*XhoI*, *BamHI*) ASYN | FW: ATCACTCGAGCGCCACCATGGACGTGTTCATGAAGGG<br>RV: ATCAGGATCCGCGGCCTCGGGCTCGTAG |

To obtain the truncated version, α-Synuclein ΔF and α-Synuclein ΔC, I used single-fragment Gibson Assembly cloning. Truncated α-synuclein-BFP was amplified from template pBFP-N1 SNCA by PCR with primers 0486 & 0487 for ΔF, or 0492 & 0493 for ΔC respectively (Table 2.1 and 2.6). The methylated template plasmid was digested with 10 U DpnI for at least 1 hour at 37 °C. Reactions were analyzed on preparative 1% agarose gel electrophoresis. The desired products were isolated from agarose gel as described in 2.2.1.8. Subsequently, 50 ng of the PCR product was used in Gibson Assembly reaction using an in-house mix (0.03 U/µL Phusion® 0.005 U/µL T5-exonuclease, 5.3 U/µL Taq-DNA ligase in 100 mM Tris-HCl pH 7.5, 5 mM $MgCl_2$, 0.2 mM dNTP each, 10 mM DTT, 2.5% (w/v) PEG 8000 and 1 mM $NAD^+$) incubated for 1 hour at 50 °C.

Table 2.6. Truncated version of α-Synuclein-BFP(ΔF &ΔC) primer sequences for cloning.

| | |
|---|---|
| #DML0486+0487 ASYN_ΔF | FW: AAAAGAAGGCGTGAAGAAGGACCAGCTGGGCAAGAAC<br>RV: CCTTCTTCACGCCTTCTTTTGTCTTGCCAGCGGCTTC |
| #DML0492+0493 ASYN_ΔC | FW: CGGCTTTGTGGCGGATCCACCGGTCATGAGCGAGCTG<br>RV: GTGGATCCGCCACAAAGCCGGTGGCAGCGGCGATAG |

To obtain single-point mutated versions of α-synuclein (A53T, A30P, S129A, S129E) the α-synuclein-BFP was amplified from template pBFP-N1 SNCA by mutagenesis PCR with primers 0510 & 0511 for A53T, 0512 & 0513 for A30P, 0522 & 0523 for S129A and 0524 & 0537 for S129E respectively (Table 2.1 and 2.7).

Table 2.7. Single-point mutated versions of α-synuclein (A53T, A30P, S129A, S129E) primer sequences for cloning.

| | |
|---|---|
| #DML0510+0511<br>ASYN_**A53T** | FW: GCACGGCGTG**ACC**ACCGTGGCCGAGAAAAC<br>RV: CGGCCACGGT**GGT**CACGCCGTGCACCACC |
| #DML0512+0513<br>ASYN_**A30P** | FW: GCCGAAGCC**CCT**GGCAAGACAAAAGAAGG<br>RV: TTGTCTTGCC**AGG**GGCTTCGGCCACCCC |
| #DML0522+0523<br>ASYN_**S129A** | FW: CGAGATGCCT**GCC**GAAGAGGGCTACCAGGAC<br>RV: GCCCTCTTC**GGC**AGGCATCTCGTAGGCCTCG |
| #DML0524+0537<br>ASYN_**S129E** | FW: CGAGATGCCT**GAG**GAAGAGGGCTACCAGGAC<br>RV: GCCCTCTTC**CTC**AGGCATCTCGTAGGCCTCG |

All reactions were directly used for the transformation of chemically competent bacteria as in 2.2.1.5. All the vectors contain CMV promoter and SV40 terminator. The plasmid sequence was verified by Sanger DNA sequencing.

For α-Synuclein purification from bacteria, WT and 140C α-Synuclein were expressed from pET28 plasmid accordingly with Huang et al., 2005. The pET28 expression vector was created by subcloning α-Synuclein (Addgene #51437) with restriction enzyme sites NcoI-NotI into the pET28 vector. For subsequent fluorescent labeling, alanine 140 was replaced with cysteine by mutagenesis PCR (A140C) according to standard lab protocol (2.2.1.1) using primers 0463 & 0464, as reported in table 2.8.

Table 2.8. α-synuclein(140C) primer sequences for cloning.

| | |
|---|---|
| #DML0463+0464<br>ASYN_**A140C** | FW: CGAGCCCGAG**TGT**TGATAAGCGGCCGCACTCGAG<br>RV: CGGCCGCTTATCA**ACA**CTCGGGCTCGTAGTCCTG |

### 2.2.1.11. Synphilin 1 cloning (EGFP-synphilin 1 and His-SUMO-EGFP-synphilin1)

Plasmid for EGFP-synphilin 1 was a kind gift from Tiago Outiero containing the human sequence for synphilin 1 CDS with an N-terminal EGFP tag in a classic pEGFP-C1 backbone (DNA sequence table 1). For protein purification of synphilin 1 in mammalian cells (Expi293F™), the sequence of EGFP from the synphilin 1 plasmid was replaced using restriction enzyme sub-cloning with AgeI-XhoI by an expression cassette consisting of a 14X Histidine affinity, SUMO_Eu1- and EGFP cassette tag. The His-14-SUMO_Eu1 tag was taken from pAV0279 (Addgene 149688) as in Vera Rodriguez et al., 2019 (DNA sequence table 1).

### 2.2.1.12. Halo-Synapsin 1

Halo sequence was amplified from Lyn-Halo (kind gift of Helge Ewers) and cloned with restriction enzyme BglI-AgeI into EGFP-synapsin 1 as in Milovanovic, 2018, replacing the EGFP tag (primers 0195 & 0196). The 6XHis tag was reintroduced by primer annealing cloning upstream to the Halo tag using NheI-AgeI restriction enzymes (primers 0438 & 0439), as reported in table 2.9.

Table 2.9. Halo-SYN1 primer sequences for cloning and specific RE sites.

| | |
|---|---|
| #DML0195+0196 (*Age*I, *Bgl*II) HALO-SYN 1 | FW: ATCA**ACCGGT**GCCACCATGGCAGAAATCGGTACTGG<br>RV: TGAT**AGATCT**GCTGCCGCTGCCGGAAATCTCGAGCGTC |
| #DML0438+0439 (*Nhe*I, *Age*I) HALO-SYN 1 (6xHIS) | FW: **CTAGC**GCCACCATGCATCACCATCACCATCAC**A**<br>RV: **CCGGT**GTGATGGTGATGGTGATGCATGGTGGC**G** |

### 2.2.1.13. Additional plasmids

Synaptophysin-EGFP (kind gift of Pietro De Camilli) and FUS-EGFP plasmid (Addgene 60362) were both in the pEGFP-N1 vector (DNA sequence table 1).

DNA sequence table 1

| DNA sequence of EGFP-synphilin-1:<br>…cmv-EGFP-LINKER-synphilin 1-*SV40*… |
| --- |
| …gcaaatgggcggtaggcgtgtacggtgggaggtctatataagcagagctggtttagtg<br>aaccgtcagatcCGCTAGCGCTACCGGTCGCCACCATGGTGAGCAAGGGCGAGGAGCTG<br>TTCACCGGGGTGGTGCCCATCCTGGTCGAGCTGGACGGCGACGTAAACGGCCACAAGTT<br>CAGCGTGTCCGGCGAGGGCGAGGGCGATGCCACCTACGGCAAGCTGACCCTGAAGTTCA<br>TCTGCACCACCGGCAAGCTGCCCGTGCCCTGGCCCACCCTCGTGACCACCCTGACCTAC<br>GGCGTGCAGTGCTTCAGCCGCTACCCCGACCACATGAAGCAGCACGACTTCTTCAAGTC<br>CGCCATGCCCGAAGGCTACGTCCAGGAGCGCACCATCTTCTTCAAGGACGACGGCAACT<br>ACAAGACCCGCGCCGAGGTGAAGTTCGAGGGCGACACCCTGGTGAACCGCATCGAGCTG<br>AAGGGCATCGACTTCAAGGAGGACGGCAACATCCTGGGGCACAAGCTGGAGTACAACTA<br>CAACAGCCACAACGTCTATATCATGGCCGACAAGCAGAAGAACGGCATCAAGGTGAACT<br>TCAAGATCCGCCACAACATCGAGGACGGCAGCGTGCAGCTCGCCGACCACTACCAGCAG<br>AACACCCCCATCGGCGACGGCCCCGTGCTGCTGCCCGACAACCACTACCTGAGCACCCA<br>GTCCGCCCTGAGCAAAGACCCCAACGAGAAGCGCGATCACATGGTCCTGCTGGAGTTCG<br>TGACCGCCGCCGGGATCACTCTCGGCATGGACGAGCTGTACAAGTCCGGACTCAGATCT<br>CGAGCTCAAGCTTCGAATTCTGCAGTCGACAGATGTTCCGCCACCATGGAAGCCCCTGA<br>ATACCTTGATTTGGATGAAATTGACTTTAGTGATGACATATCTTATTCAGTCACATCAC<br>TCAAGACGATCCCAGAACTGTGCCGAAGATGTGATACGCAAAACGAAGACAGATCAGCT<br>TCTAGCTCTAGCTGGAATTGTGGCATCTCAACTCTTATTACAAACACGCAAAAGCCCAC<br>AGGAATCGCTGATGTGTACAGTAAGTTCCGCCCAGTGAAGCGGGTTTCGCCACTGAAAC<br>ATCAGCCAGAGACTCTGGAGAACAATGAAAGTGATGACCAAAAGAACCAGAAAGTGGTT<br>GAGTACCAGAAAGGGGGTGAGTCTGACCTGGGCCCCCAGCCTCAGGAGCTTGGCCCTGG<br>AGATGGAGTGGGCGGCCCACCAGGTAAGAGCTCTGAGCCCAGCACATCGCTGGGTGAAC<br>TGGAGCACTACGACCTCGACATGGATGAGATTCTGGATGTGCCTTATATTAAATCCAGT<br>CAGCAGCTTGCCTCTTTTACCAAGGTGACTTCAGAAAAAAGAATTTTGGGCTTATGCAC<br>AACCATCAATGGCCTTTCTGGCAAAGCCTGCTCTACAGGAAGTTCTGAGAGCTCATCAT<br>CCAACATGGCACCATTTTGTGTTCTTTCTCCCGTGAAAAGCCCTCACTTGAGAAAAGCA<br>TCAGCTGTCATCCACGACCAGCACAAGCTGTCCACTGAAGAAACCGAGATCTCACCTCC<br>TCTGGTTAAATGTGGCTCTGCATATGAGCCTGAAAACCAGAGTAAAGACTTCCTAAACA<br>AGACATTTAGTGATCCTCATGGTCGAAAAGTTGAGAAGACAACACCAGACTGCCAGCTC<br>AGGGCCTTCCACCTACAATCCTCAGCAGCAGAATCCAAACCAGAAGAGCAGGTCAGTGG<br>CCTAAACCGGACCAGCTCCCAAGGCCCAGAAGAAAGGAGTGAGTATCTGAAAAAAGTGA |

AAAGCATCTTGAACATTGTTAAAGAAGGACAGATCTCTCTCCTGCCACACCTAGCTGCA
GACAATCTAGACAAAATTCACGACGAAAATGGAAACAATCTATTACATATTGCGGCGTC
ACAGGGACACGCAGAGTGTCTACAGCACCTCACTTCTTTGATGGGAGAAGACTGCCTCA
ATGAGCGCAACACTGAGAAGTTGACTCCAGCAGGCCTGGCCATTAAGAATGGTCAGTTG
GAGTGCGTACGCTGGATGGTGAGCGAAACAGAAGCCATTGCAGAACTGAGTTGTTCTAA
GGATTTTCCAAGCCTTATTCATTACGCAGGTTGCTATGGCCAGGAAAAGATTCTTCTGT
GGCTTCTTCAGTTTATGCAAGAACAGGGCATCTCGTTGGATGAAGTAGACCAGGATGGC
AACAGTGCCGTTCACGTAGCCTCACAGCATGGCTACCTTGGATGCATACAGACCTTGGT
TGAATATGGAGCAAATGTCACCATGCAGAACCACGCTGGGGAAAAGCCCTCCCAGAGCG
CCGAGCGGCAGGGGCACACCCTGTGCTCCAGGTACCTGGTGGTGGTGGAGACCTGCATG
TCGCTGGCCTCTCAAGTGGTGAAGTTAACCAAGCAGCTAAAGGAACAAACAGTAGAACG
TGTCACGCTGCAGAACCAACTCCAACAATTTCTAGAAGCCCAGAAATCAGAGGGCAAGT
CACTCCCTTCTTCACCCAGTTCACCATCCTCACCTGCCTCCAGAAAGTCCCAGTGGAAA
TCTCCAGATGCAGATGATGATTCTGTAGCCAAAAGCAAGCCAGGAGTCCAAGAGGGGAT
TCAGGTTCTTGGAAGCCTGTCAGCCTCCAGCCGGGCTAGACCCAAAGCAAAAGATGAAG
ATTCTGATAAAATCTTACGCCAGTTATTGGGAAAGGAAATCTCAGAAAATGTCTGCACC
CAGGAAAAACTGTCCTTGGAATTCCAGGATGCTCAGGCTTCCTCTAGAAATTCTAAAAA
GATCCCACTGGAGAAGAGGGAACTGAAGTTAGCCAGGCTGAGACAGCTGATGCAGAGGT
CACTGAGTGAGTCTGACACAGACTCCAACAACTCTGAGGACCCCAAGACTACCCCAGTG
AGGAAGGCTGACCGACCAAGGCCGCAGCCCATTGTAGAAAGCGTAGAGAGTATGGACAG
CGCAGAAAGCCTGCACCTGATGATTAAGAAACACACCTTGGCATCAGGGGGACGCAGGT
TTCCTTTCAGCATCAAGGCCTCCAAATCCCTGGATGGCCACAGCCCATCTCCCACCTCA
GAGAGCAGCGAACCAGACTTAGAATCCCAGTATCCAGGCTCAGGGAGTATTCCTCCAAA
CCAGCCCTCTGGTGACCCTCAGCAGCCCAGCCCTGACAGTACTGCTGCCCAGAAAGTTG
CCACAAGTCCCAAGAGTGCCCTCAAGTCTCCATCTTCCAAGCGTAGGACATCTCAGAAC
TTAAAACTGAGAGTTACCTTTGAGGAGCCTGTGGTGCAGATGGAGCAGCCTAGCCTTGA
ACTGAATGGAGAAAAAGACAAAGATAAGGGCAGGACTCTCCAGCGGACCTCCACAAGTA
ACGAATCGGGGGATCAACTGAAAAGGCCTTTTGGAGCCTTTCGATCTATCATGGAGACA
CTAAGTGGCAACCAAAACAATAATAATAACTACCAGGCAGCCAACCAGCTGAAAACCTC
TACATTGCCCTTGACCTCACTTGGGAGGAAGACAGATGCCAAGGGAAACCCTGCCAGCT
CCGCTAGCAAAGGAAAGAATAAGGCAGCGGATCCACCGGATCTAGATAACTGA*TCATAA*
*TCAGCCATACCACATTTGTAGAGGTTTTACTTGCTTTAAAAAACCTCCCACACCTCCCC*
*CTGAACCTGAAACATAAAATGAATGCAA…*

Extract of His14-SUMO_Eu1-EGFP-synphilin-1 expression cassette:

…cmv-His14-SUMO_Eu1-EGFP-LINKER-synphilin 1…

…gcaaatgggcggtaggcgtgtacggtgggaggtctatataagcagagctggtttagtg
aaccgtcagatcCGCTAGCGCTACCGGTCGCCACCATGAGCAAGCATCACCATCATTCAGG
CCATCACCATACCGGACACCACCATCATTCAGGCAGTCATCACCATTCCGGATCTGCTGCGGGT
GGCGAAGAAGATAAGAAACCGGCAGGTGGCGAAGGTGGCGGTGCCCATATCAACCTGAAAGTGA
AAGGTCAAGACGGCAACGAAGTCTTTTTCCGCATCAAACGTTCTACCCAGCTGAAAAAGCTGAT
GAACGCATACTGTGACCGTCAGTCTGTAGACATGAAGGCAATTGCTTTCCTCTTTAAGGGTCGT
CGCCTACGTGCGGAAAGGACCCCGGATGAACTGGAAATGGAAGATGGCGACGAAATCGACGCAA
TGCTGCACCAGACTGGAGGCAGATCCGTGAGCAAGGGCGAGGAGCTGTTCACCGGGGTGGTGCC
CATCCTGGTCGAGCTGGACGGCGACGTAAACGGCCACAAGTTCAGCGTGTCCGGCGAGGGCGAG
GGCGATGCCACCTACGGCAAGCTGACCCTGAAGTTCATCTGCACCACCGGCAAGCTGCCCGTGC
CCTGGCCCACCCTCGTGACCACCCTGACCTACGGCGTGCAGTGCTTCAGCCGCTACCCCGACCA
CATGAAGCAGCACGACTTCTTCAAGTCCGCCATGCCCGAAGGCTACGTCCAGGAGCGCACCATC
TTCTTCAAGGACGACGGCAACTACAAGACCCGCGCCGAGGTGAAGTTCGAGGGCGACACCCTGG
TGAACCGCATCGAGCTGAAGGGCATCGACTTCAAGGAGGACGGCAACATCCTGGGGCACAAGCT
GGAGTACAACTACAACAGCCACAACGTCTATATCATGGCCGACAAGCAGAAGAACGGCATCAAG
GTGAACTTCAAGATCCGCCACAACATCGAGGACGGCAGCGTGCAGCTCGCCGACCACTACCAGC
AGAACACCCCCATCGGCGACGGCCCCGTGCTGCTGCCCGACAACCACTACCTGAGCACCCAGTC
CGCCCTGAGCAAAGACCCCAACGAGAAGCGCGATCACATGGTCCTGCTGGAGTTCGTGACCGCC
GCCGGGATCACTCTCGGCATGGACGAGCTGTACAAGTCCGGACTCAGATCTCGAGCTCAAGC
TTCGAATTCTGCAGTCGACAGATGTTCCGCCACCATGGAAGCCCCTGAATACCTTGATTTG
GATGAAATTGACTTTAGTGATGACATATCTTATTCAGTCACATCACTCAAGACGATCCCAGAAC
TGTGCCGAAGATGTGATACGCAAAACGAAGACAGATCAGCTTCTAGCTCTAGCTGGAATTGTGG
CATCTCAACTCTTATTACAAACACGCAAAAGCCCACAGGAATCGCT…

DNA sequence of Synaptophysin-EGFP:

…cmv-LINKER-Synaptophysin-LINKER -EGFP...

…gcaaatgggcggtaggcgtgtacggtgggaggtctatataagcagagctggtttagtg
aaccgtcagatcCGCTAGCGCTACCGGACTCAGATCTCGAGCTCAAGCTTGCCACCATG
GACGTGGTGAATCAGCTGGTGGCTGGGGGTCAGTTCCGGGTGGTCAAGGAGCCCCTTGG
CTTCGTGAAGGTGCTGCAGTGGGTCTTTGCCATCTTCGCCTTTGCTACGTGCGGCAGCT
ACACCGGAGAGCTTCGGCTGAGCGTGGAGTGTGCCAACAAGACGGAGAGTGCCCTCAAC
ATCGAAGTCGAATTTGAGTACCCATTCAGGCTGCACCAAGTGTACTTTGATGCACCCTC
CTGCGTTAAAGGGGGCACTACCAAGATCTTCCTAGTTGGTGACTACTCCTCCTCGGCTG
AATTCTTTGTCACCGTGGCTGTGTTTGCCTTCCTCTACTCCATGGGGGCCCTGGCCACC
TACATCTTCCTGCAGAACAAGTACCGAGAGAACAACAAAGGGCCAATGATGGACTTCCT
GGCCACAGCAGTGTTCGCTTTCATGTGGCTAGTTAGCTCATCCGCCTGGGCCAAAGGCC
TGTCCGATGTGAAGATGGCCACTGACCCAGAGAACATTATCAAGGAGATGCCTATGTGC
CGCCAGACAGGAAACACATGCAAGGAACTGAGGGACCCTGTGACTTCAGGACTCAACAC
CTCGGTGGTGTTTGGCTTCCTGAACCTGGTGCTCTGGGTTGGCAACCTATGGTTCGTGT
TCAAGGAGACAGGCTGGGCCGCCCCATTCATGCGCGCACCTCCAGGCGCCCCAGAAAAG
CAACCAGCTCCTGGCGATGCCTACGGCGATGCGGGCTATGGGCAGGGCCCCGGAGGCTA
TGGGCCCCAGGACTCCTACGGGCCTCAGGGTGGTTATCAACCCGATTACGGGCAGCCAG
CCAGCGGCGGTGGCGGTGGCTACGGGCCTCAGGGCGACTATGGGCAGCAAGGCTACGGC
CAACAGGGTGCGCCCACCTCCTTCTCCAATCAGATGTCGGATCCACCGGTCGCCACCAT
*GGTGAGCAAGGGCGAGGAGCTGTTCACCGGGGTGGTGCCCATCCTGGTCGAGCTGGACG*
*GCGACGTAAACGGCCACAAGTTCAGCGTGTCCGGCGAGGGCGAGGGCGATGCCACCTAC*
*GGCAAGCTGACCCTGAAGTTCATCTGCACCACCGGCAAGCTGCCCGTGCCCTGGCCCAC*
*CCTCGTGACCACCCTGACCTACGGCGTGCAGTGCTTCAGCCGCTACCCCGACCACATGA*
*AGCAGCACGACTTCTTCAAGTCCGCCATGCCCGAAGGCTACGTCCAGGAGCGCACCATC*
*TTCTTCAAGGACGACGGCAACTACAAGACCCGCGCCGAGGTGAAGTTCGAGGGCGACAC*
*CCTGGTGAACCGCATCGAGCTGAAGGGCATCGACTTCAAGGAGGACGGCAACATCCTGG*
*GGCACAAGCTGGAGTACAACTACAACAGCCACAACGTCTATATCATGGCCGACAAGCAG*
*AAGAACGGCATCAAGGTGAACTTCAAGATCCGCCACAACATCGAGGACGGCAGCGTGCA*
*GCTCGCCGACCACTACCAGCAGAACACCCCCATCGGCGACGGCCCCGTGCTGCTGCCCG*
*ACAACCACTACCTGAGCACCCAGTCCGCCCTGAGCAAAGACCCCAACGAGAAGCGCGAT*
*CACATGGTCCTGCTGGAGTTCGTGACCGCCGCCGGGATCACTCTCGGCATGGACGAGCT*
*GTACAAGTAA*…

### 2.2.2. Cell culture and transfection

#### 2.2.2.1. HEK 293 cells

Human embryonic kidney (HEK 293) cells were cultured in a humidified incubator at 37 °C with 5% $CO_2$ using Dulbecco's Modified Eagle Medium (DMEM) containing 4.5 g/L D Glucose (Gibco) supplemented with 10% heat-inactivated FBS (FACS), 1% Penicillin/Streptavidin and 1% MEM medium (non-essential amino acids) (Sigma). When reaching a confluency of 80–90%, cells were passaged using standard trypsinization techniques. For live-cell imaging experiments, HEK 293 cells were either grown on glass coverslips (25 mm) or in glass bottom dishes until reaching a confluency of 50–70%.

#### 2.2.2.2 Transfection using Lipofectamine 2000

HEK 293 cells were transfected by Lipofectamine 2000 (Thermo Fisher) following the manufacturer's instructions. Briefly, 3 µl of lipofectamine 2000 was mixed with 2 µg of total DNA in 200 µl OptiMEM (Gibco). The transfection mix was incubated for 30 minutes at room temperature, then added to the cells. Cells were transfected and incubated overnight (37 °C and 5% $CO_2$). The day after the medium was fully replaced with fresh-supplemented DMEM.

#### 2.2.2.3. Hippocampal primary neurons

Hippocampal neurons were prepared from P0 wild-type mice (C57BL6/J). Brains were manually dissected and hippocampi were collected in cold Hank's balanced salt solution (HBSS, Gibco) containing 10 mM Hepes buffer (Gibco), 1 mM Pyruvic Acid (Gibco), 0.5% Penicillin/Streptomycin and 5.8 mM Magnesium Chloride. After dissection, hippocampi were enzymatically digested with Papaine (Sigma) in HBSS for 20 min at 37 °C. Papaine was removed with repeated HBSS washing, and the plating medium was added (Neurobasal Medium A [NB-A, Gibco], supplemented with 5% FBS, 1% B27, 1x Glutamax, and 1% Penicillin/Streptomycin). The final cell suspension was obtained through mechanical dissociation with a P1000 pipette. Cells were seeded on glass coverslips coated with 0.1 mg/mL poly-L-lysine (PLL; Sigma). Neurons were maintained at 37 °C and 5% $CO_2$ in Neuronal Media (NB-A supplemented with 1% B27, 1% Glutamax, and 0.5% penicillin/streptomycin) and half-media changed every other day.

#### 2.2.2.4 Transfection using Calcium Phosphate

Hippocampal neurons were seeded on a glass coverslip and transfected using the Calcium Phosphate protocol as follows. The coverslips were transferred from their original petri dish into a clean petri dish with 1 mL of current (conditioned) growth medium supplemented with kynurenic acid to a final concentration of 4 mM (Sigma K3375, stock: 20 mM in Neurobasal Medium A not supplemented) and placed back into the incubator. Calcium Phosphate precipitates solution was prepared by mixing 2 µg of each DNA construct in 1x TE to a final volume of 22.5 µL ((Tris-EDTA buffer) 10 mM Tris-HCl pH 7.3, 1 mM EDTA). The mix was supplemented with 2.5 µl $CaCl_2$ solution to a final concentration of 250 mM (stock: 10 mM HEPES (pH 7.2), 2.5 M $CaCl_2$). The DNA-CaCl2-mix was added dropwise to 25 µl of 2x HEBS solution (42 mM HEPES (pH 7.2) 274 mM NaCl, 10 mM KCl, 1.4 mM $Na_2HPO_4$, 10 mM glucose) with vortexing between the addition of each drop and incubated for 20 minutes at room temperature. The transfection mix was added dropwise to the seeded neurons and left to incubate for 1-2 hours in the incubator at 37 °C and 5% $CO_2$. After the incubation, the coverslips were washed with 1 mL prewarmed washing medium (Neurobasal medium (not supplemented) with 4 mM kynurenic acid supplemented with HCl to 2.5 mM final concentration). The wash was performed by incubating the seeded neurons in the incubator for 15 minutes (37°C, 5% $CO_2$). The coverslip was placed back in the original culture dish containing its own conditioned medium.

### 2.2.3. Protein expression and purification

#### 2.2.3.1. SDS Polyacrylamide electrophoresis of proteins

SDS-PAGE with a Tris-Glycine buffer system was used to separate the mixture of proteins based on their molecular weight. The composition of the prepared polyacrylamide gels is shown in table 2.10. These gels consist of two layers, including the lower acrylamide percentage stacking gel on top of the higher acrylamide percentage resolving gel. Samples were mixed with 4 x sample buffer and usually boiled at 95 °C for 10 minutes. Debris was removed by centrifugation at 13.000 rpm in a table-top centrifuge for 2 minutes and the supernatant was loaded. The gels were run in 1 x Tris-Glycine buffer. Electrophoresis was performed at a constant current of 45 mA per gel. The duration of electrophoresis depended on the desired separation range (usually 45-90 minutes).

Table 2.10. SDS-PAGE composition – components with stock solutions; amounts are given as final concentrations; gel solutions were prepared with $ddH_2O$

| Component | Stacking gel | Component | Resolving gel |
|---|---|---|---|
| **0.625 M Tris-HCl pH 6.8** | 0.125 M | 1.5 M Tris-HCl pH 8.8 | 0.375 M |
| **10% SDS** | 0.1 % | 10% SDS | 0.1 % |
| **TEMED** | 0.12 % | TEMED | 0.12 % |
| **10% APS** | 0.05 % | 10% APS | 0.1 % |

#### 2.2.3.2. EGFP-Synapsin 1, Halo-Synapsin 1, and mCherry-Synapsin 1

EGFP-Synapsin 1, Halo-synapsin 1, and mCherry-synapsin 1 were expressed in Expi293F™ cells (Thermo Fisher Scientific) from the pEGFP-C1, pHalo, and pmCherry_DM-C1 vector respectively for three days following enhancement. Cells were harvested and lysed in a buffer that contained 25 mM Tris–HCl (pH 7.4), 300 mM NaCl, 25 mM imidazole, 0.5 mM TCEP (buffer A), and protease inhibitor (Complete EDTA-free, Roche). All purification steps were carried out at 4 °C. The lysates were centrifuged for 1 hour at 20,000g, followed by a two-step purification. The first step was affinity purification on a Ni-NTA column (HisTrap™HP, GE Healthcare) using 25 mM imidazole for binding proteins, 40 mM during wash steps and 400 mM imidazole for elution of proteins (all in buffer A). Eluates were concentrated and subjected to size exclusion chromatography (Superdex™200 Increase 10/300, GE Healthcare) in 25 mM Tris-HCl (pH 7.4), 150 mM NaCl, and 0.5 mM TCEP (buffer B). Proteins were snap-freezed in liquid nitrogen and stored at -80 C° until further use.

#### 2.2.3.3. Labeling of Halo-Synapsin 1

For fluorescent labeling of Halo-synapsin 1, 250 µg purified protein was incubated with 0.7 µg Janelia Fluor® HaloTag® ligand (JF549, Promega GA111A; stock: 0.13 µg/µL in DMSO) for 1 hour at room temperature (25 mM Tris-HCl (pH7.4), 150 mM NaCl, 0.5 mM TCEP). The reaction was applied to PD-10 columns (Sephadex G-25, Cytiva) equilibrated with 25 mM Tris-HCl (pH 7.4), 150 mM NaCl, and 0.5 mM TCEP. Elution fractions containing labeled His-Halo(JF549)-synapsin 1 protein were concentrated using a 30K MWCO protein concentrator (Pierce) and snap-frozen in liquid nitrogen for storage at -80°C until use.

#### 2.2.3.4. α-Synuclein WT and A140C

Untagged human α-synuclein and untagged human α-synuclein-A140C were expressed from the pET17b vector (Novagen) in Escherichia coli BL21 cells and purified essentially as described in Huang et al., 2005. Shortly, the expression of the protein was induced at 37 °C for 3 hours, cells pelleted and periplasm proteins released by incubation in the osmotic shock buffer (40% v/v sucrose in 25 mM Tris-HCl pH 7.2, 2 mM EDTA) at room temperature for 10 min and subsequently in ice-cold 2 mM $MgCl_2$ for 3 min. The periplasmic extract was loaded on the strong anion-exchange column HiPrep Q FF (GE Healthcare) and bound synuclein was eluted by running a 0–500 mM NaCl gradient. Synuclein-containing fractions were pooled, and concentrated using 3 kDa cutoff-filters (Vivaspin 15R, Sartorius) and loaded on the gel filtration column HiLoad Superdex 200 16/600 (GE Healthcare). The relevant fractions were concentrated using Vivaspin 15R, heated at 95 °C for 30 min, and precipitates were separated by centrifugation. The remaining supernatant was gel-filtrated again. Synuclein concentration was determined at 280 nm by applying a molar extinction coefficient of 5960 $M^{-1}$ $cm^{-1}$. Proteins were snap-freeze in liquid nitrogen and stored at -80 C° until further use.

#### 2.2.3.5. Labeling of α-synuclein

**NHS-labeling.** For chemical labeling of α-synuclein, the NHS-ester reactive fluorescent Alexa 647 dye from Thermo Scientific was used (Alexa647-NHS-Ester, 10 mg/mL). Labeling was performed in PBS (pH 8,3 with NaHCO3) for 1 hour at room temperature with a 10 times molar excess of NHS-ester dye. Not-conjugated dye was removed from labeled α-synuclein by running the labeling reaction over a PD-10 column and elution with PBS (SephadexTMG-25 M, GE Healthcare).

**Maleimide labeling.** α-synuclein-A140C was thiol-maleimide conjugated with fluorescent Alexa 568 and Alexa 647 dyes from Thermo Scientific (Alexa Fluor™ 568 C5 Maleimide and Alexa Fluor™ 647 C2 Maleimide, 10 mg/mL). The labeling reaction was carried out in a buffer containing 150 mM NaCl, 25 mM Tris-HCl pH 7.2, and 1.3 mM TCEP for 2 hours at RT with a 3 times molar excess of Maleimide dye. The unconjugated remaining dye was removed by running the labeling reaction over a PD-10 column and elution with PBS (SephadexTMG-25 M, GE Healthcare). The degree of protein labeled was determined using the molar extinction coefficient and maximum absorbance length of respective dyes.

#### 2.2.3.6. EGFP-Synphilin 1

His-SUMO-EGFP-synphilin 1 was expressed in Expi293F™ cells (Thermo Fisher Scientific) from the pCMV vector for 3 days following enhancement. Cells were harvested and lysed in a buffer that contained 25 mM Tris–HCl (pH 7.4), 300 mM NaCl, 0.5 mM TCEP (buffer A), and protease inhibitor (Complete EDTA-free, Roche). All purification steps were carried out at 4 °C. The lysates were centrifuged for 1 hour at 20,000g, followed by a two-step purification. The first step was affinity purification on a Ni-NTA column (HisTrapTMHP, GE Healthcare) using 25 mM imidazole for the binding of proteins, 40 mM during wash steps, and 400 mM imidazole for elution of proteins (all in buffer A). Eluates were concentrated and subjected to size exclusion chromatography (SuperdexTM200 Increase 10/300, GE Healthcare) in 25 mM Tris-HCl (pH 7.4), 300 mM NaCl, and 0.5 mM TCEP (buffer B). The His-SUMO tag was removed using SUMO proteases ($SENP1^{EUB}$) (1:100) overnight at 4 °C and the two components were separated by running a His-exclusion using His-pure Ni-NTA resin (BRAND).

### 2.2.4. Confocal live cell imaging

#### 2.2.4.1. Spinning disk confocal

Spinning disk confocal (SDC) microscopy was carried out on an Eclipse Ti Nikon Spinning Disk Confocal CSU-X, equipped with OkoLab Live-cells incubator (for control of temperature at 37 °C, 5% $CO_2$), 2 EM-CCD cameras (AndorR iXon 888-U3 ultra EM-CCD), Andor Revolution SD System (CSU-X), objectives PL APO 60 /1.4NA oil immersion lens. Excitation wavelengths were: 405-nm for BFP, 488-nm for EGFP, 561-nm for mCherry, Halo, AlexaFluor568, FM 4-64, SPY555-Actin and 647-nm for AlexaFluor647, Lysotracker™ Deep Red, Mitotracker™ Deep Red FM, SiR-Actin, SiR-Tubulin. For imaging, one or more constructs were transfected in HEK 293 cells or primary hippocampal neurons. During imaging, glass coverslips (1.5 thickness, 25 mm diameter) for in cell experiments or 15-well 3D glass bottom slides for *in vitro* experiments were placed in a microscopy adaptor and then placed on the objective stage. Exposure time 200 ms, gain 300 (EM gain 20 mHz 16-bit) and Piezo stage z-motor were used to collect z-series. Images were acquired using Acquisition software NIS Elements 5.21.02 and then analyzed with FIJI ImageJ2 (NIH).

#### 2.2.4.2. FRAP *in vitro*

Fluorescence recovery after photobleaching (FRAP) experiments were performed *in vitro* as follows. Purified EGFP-Synapsin 1 and α-synuclein-647 were reconstituted *in vitro* and the bleach region of interest (ROI) was fixed to approx. 1.5 μm diameter and bleached at 100% transmission intensity (488 nm = 3.9 mW, 640 nm = 4.7 mW) for 500 ms. Recording was carried out starting with a prebleach sequence, followed by the bleach event and post-bleach images were acquired up to 160 s (250 ms frame rate). In reconstitution of EGFP-synphilin 1 and α-synuclein-568 the bleach ROI was placed in correspondence of the shell of LBLs where the proteins overlap. The bleach ROI was fixed to approx. 0.45 μm of diameter and bleached at 100% transmission intensity (488 nm = 3.9 mW, 561 nm = 4.1mW) for 500 ms. Recording was carried out starting with a prebleach sequence, followed by the bleach event and post-bleach images were acquired up to 180 s (1 s frame rate). Intensity recovery traces obtained from the regions of interest were background corrected and all traces were normalized. For all experiments, data are from three independent reconstitutions and presented as mean ± s.e.m.

#### 2.2.4.3. FRAP *in cells*

In fluorescence recovery after photobleaching (FRAP) experiments performed in HEK 293 cells expressing α-synuclein-BFP and mCherry-synapsin 1, the bleach ROI was fixed to 1.12 μm in diameter and bleached at 100% transmission intensity (405 nm = 3.5 mW and 561 nm = 4.1mW) for 500 ms. In cells expressing EGFP-synphilin 1, α-synuclein-BFP, and mCherry-synapsin 1 in all their presented combinations, the bleach ROI was fixed to approx. 0.45 μm in diameter and positioned in correspondence on the shell of LBLs where the proteins overlap (if not indicated differently). For the experiments, the bleaching was obtained using 100% transmission intensity (488 nm = 3.8 mW, 405 nm = 3.5 mW and 561 nm = 4.1mW) for 500 ms. Reference ROIs were defined in the cytosol of the same cell, and the Background ROIs were defined outside of the cell. Recordings were carried out starting with 1 picture pre-bleach, followed by a bleaching event, and post-bleach time-laps images were collected (1 s frame rate) up to 180 s. Each FRAP experiment was performed in at least 3 independent biological replications (different transfections). Intensity recovery traces obtained from the regions of interest were background corrected and all traces were normalized. The average trace was fitted to a simple linear regression function (Prism 9, GraphPad) obtaining the half-time of recovery. All data are presented as mean ± s.e.m.

### 2.2.5 Isolation of synaptic vesicles (By Gonzalo, Morabito, Hoffmann)

Synaptic vesicles (SVs) were isolated according to previous publications (Nagy et al., 1976; Huttner et al., 1983; Takamori et al., 2006). Briefly, 20 rat brains were homogenized in ice-cold sucrose buffer (320 mM sucrose, 4 mM HEPES-KOH, pH 7.4 supplemented with 0.2 mM phenylmethylsulfonylfluoride and 1 mg/mL pepstatin A). Cellular debris was removed by centrifugation (10 min at 900$g_{Av}$, 4 °C) and the resulting supernatant was further centrifuged for 10 min at 12,000$g_{Av}$, 4 °C. The pellet containing synaptosome was washed once by carefully resuspending it in sucrose buffer and further centrifuged for 15 min at 14,500$g_{Av}$, 4 °C. Synaptosomes were lysed by hypo-osmotic shock, and free released SVs were obtained after centrifugation of the lysate for 20 min at 14,500$g_{Av}$, 4 °C. The supernatant containing the SVs was further ultracentrifuged for 2 hours, yielding a crude SVs pellet. SVs were purified by resuspending the pellet in 40 mM sucrose followed by centrifugation for 3 hours at 110,880$g_{Av}$ on a continuous sucrose density gradient (50–800 mM sucrose). SVs were collected from the gradient and subjected to size-exclusion chromatography on controlled pore glass beads (300 nm diameter), equilibrated in glycine buffer (300 mM glycine, 5 mM HEPES, pH 7.40, adjusted using KOH), to separate SVs from residual larger membrane contaminants. SVs were pelleted by centrifugation for 2 hours at 230,000$g_{Av}$ and resuspended in sucrose buffer by homogenization before being aliquoted into single-use fractions and snap-frozen in liquid nitrogen. The molar concentration of SVs was determined by measuring the total protein concentration where ~100 ng/µL of total SV protein corresponds to ~10 nM of SVs, according to previously established quantitative relationship (Shin and Brangwynne, 2017).

#### 2.2.5.1. Western blot of contaminants and synaptic vesicle proteins

Proteins were transferred from a Tris-Glycine SDS-PAGE gel onto an Amersham Hybond LFP membrane (0.2 mm, Cytiva). The wet transfer was done after standard protocol for either 1.5 hours at 80 V at room temperature or overnight at 10 V at 4 °C. For washing and blocking steps TBS was used. Blocking was performed for 1 hour at room temperature, while the blocking agent (3% BSA or 5% MLK in TBS) depended upon the primary antibody combination. Incubation with primary antibody was typically performed overnight with shaking: (Synaptophysin 1 [1:4000 in 3% BSA/TBS, Sysy 101 011], Synaptobrevin 2 [1:8000 in 3% BSA/TBS, Sysy 104 211], NSF [1:5000 in 3% BSA/TBS, Sysy 123 011], Synaptotagmin [1:1000 in 5% MLK/TBS, Sysy 105 011], PSD95 [1:1000 in 5% MLK/TBS, Sysy 124 011], SDHA [1:1000 in 5% MLK/TBS, Abcam ab14715], Na+/K+-ATPase

[1:1000 in 5%MLK/TBS, Merck/Millipore 05-369]). For fluorescent detection, Cy3-conjugated secondary antibodies (goat-a-mouse-IgG-Cy3) from the Amersham ECL PlexTMDetection kit were used according to manufacturer's instructions (1:2500 in 5%MLK/TBS, Cytiva). Fluorescence detection was performed using a Typhoon Trio Variable Imager System (GE Healthcare) by Cy3 excitation with the green laser (532 nm) and Cy3 emission filter settings (580 nm BP 30 nm).

### 2.2.6. *In vitro* reconstitution assays

#### 2.2.6.1. Synapsin 1 and α-synuclein reconstitution and imaging

For obtaining the synapsin 1/ α-synuclein condensates *in vitro*, a mixture of 6 μM EGFP-Synapsin 1 and 2 μM of α-synuclein (equimolar amounts of unlabeled and Alexa Fluor 647-labeled) was incubated with 25 mM Tris–HCl (pH 7.4), 150 mM NaCl, 0.5 mM TCEP. After the addition of 3% PEG 8000 (final concentration), the condensation reaction was transferred to a 15-well 3D glass bottom slide (Ibidi) for imaging. Three independent reconstitutions were performed for each experiment. For examining the effect of increasing concentration of α-synuclein, the final protein concentration was fixed at 8 μM in which synapsin 1 and α-synuclein were mixed at 3:1, 1:1, or 1:3 molar ratios. SVs were added at 23 nM, following the average physiological molar ratio of synapsin to SVs (Wilhelm et al., 2014; Takamori et al., 2006). The condition where the molar ratio of synapsin 1, α-synuclein, and SVs mimicked the physiological (6 μM, 2 μM, and 23 nM, respectively) was used as a reference for normalizing the remaining curves in Figure 3.6 E. Three independent measurements (each containing a unique isolation of SVs) were done for each sample; all the data are represented as a mean ± standard error of the mean.

#### 2.2.6.2. Turbidity assay (by Hoffmann)

Fluorescence (excitation at 440 nm, emission at 484 nm) was measured every 20 minutes for 50 hours at 37 °C, double orbital shaking (425 cpm, 3 mm) for 5 s prior to recording, by using a Synergy H1 Hybrid Multi-Mode Microplate Reader (BioTek Instruments). A 30 mL reaction mixture was set up at 4 °C and transferred to a 384-well microtiter plate (Greiner Bio-One, #781906). All the measurements were done in the following buffer: 25 mM Tris–HCl (pH 7.4), 150 mM NaCl, 0.5 mM TCEP.

#### 2.2.6.3. Reconstitution of synphilin 1 and phase diagram

For phase separation experiment, purified EGFP-synphilin 1 was mixed in different concentrations (1 μM, 5 μM, 10 μM), and different percentages of PEG 8000 (0%, 0.5%, 1%, 3%, 5%, and 10% final concentration) in 25 mM Tris-HCl (pH 7.4), 300 mM NaCl, 0.5 mM TCEP. The phase diagram was then plotted accordingly to the images collected from three independent reconstitutions, indicating no-phase separation (empty circle), partial phase separation (dot circle), and phase separation (solid circle). For reconstitution of LBLs *in vitro*, 10 μM of EGFP-synphilin 1 was mixed with 20 μM α-synuclein (molar dilution 1:10 of unlabeled and Alexa Fluor™ 568 C5 Maleimide-labeled) in 25 mM Tris-HCl (pH 7.4), 300 mM NaCl, 0.5 mM TCEP. In LBLs reconstitution presenting also synapsin 1 was mixed with 0.45 μM of EGFP-synphilin 1, 4.5 μM of Halo-synapsin 1, and 1.5 μM of α-synuclein (molar dilution 1:10 of unlabeled and Alexa Fluor™ 647 C2 Maleimide-labeled) incubated in 25 mM Tris-HCl (pH 7.4), 300 mM NaCl, 0.5 mM TCEP. For all the reconstitution experiments the condensation reaction was incubated 5 minutes at RT and transferred to a 15-well 3D glass bottom slide (Ibidi) for imaging.

### 2.2.7. Cell-based LLPS assays

#### 2.2.7.1. Effect of aliphatic alcohols

1,6-Hexanediol (Sigma) and 1,3-propanediol (Sigma) were dissolved in DMEM (0.3 g/mL stock solution). HEK 293 cells expressing α-synuclein-BFP and mCherry-synapsin 1 were added to a pre-warmed 1,6–hexanediol or 1,3-propanediol solution diluted to a final concentration of 3% in imaging solution and imaged for various times as indicated in the figures 3.4. and 3.5. All images from three independent transfections were analyzed with FIJI ImageJ2 (NIH).

#### 2.2.7.2. Modulation of osmotic pressure

HEK 293 cells expressing either only EGFP-synphilin 1 or in combination with α-synuclein-BFP were added to the hypotonic solution (5% DMEM in $H_2O$) or hypertonic solution (300 mM NaCl in $H_2O$). Images from three independent transfections were collected before and after 5 minutes from the addition of the solutions.

#### 2.2.7.3. Colocalization of synphilin 1 inclusions with organelles

HEK 293 cells expressing either only EGFP-synphilin 1 or in combination with α-synuclein-BFP were incubated with several fluorescent dyes in order to visualize subcellular lipid localization (FM™ 4-64 Dye, Thermo Scientific), lysosomes (LysoTracker™ Deep Red, Thermo Scientific) and mitochondria (MitoTracker™ Deep Red FM, Thermo Fisher). Fluorescent dyes were diluted 1:1000 in pre-warmed imaging solution and added to HEK 293 cells 30 min before imaging. The co-localization of synphilin 1 inclusion and LBLs with cellular organelles were analyzed from three independent transfections using FIJI ImageJ2 (NIH).

#### 2.2.7.4. Time-lapse imaging of synphilin 1 inclusions with cytoskeleton

HEK cells expressing EGFP-synphilin 1 and α-synuclein-BFP were incubated with either SPY555-actin (Spirochrome, 1 mM stock solution), SiR-Actin (Spirochrome, 1 mM stock solution), or Sir-Tubulin (Spirochrome, 1 mM stock solution). Fluorescent dyes were diluted to 1 µM (final concentration) in pre-warmed DMEM and incubated with HEK cells for 30 min. The staining procedure was initiated at different time points post-transfection (15.5 hours or 19.5 hours). Before imaging the staining, the solution was replaced by fresh live cell imaging solution (Thermo Fisher Scientific, A14291DJ) and images were collected every 10 minutes for 1 hour. For quantification of actin and tubulin enrichment within the condensates over time, a mask of the EGFP-synphilin 1 signal was created. The mean grey intensity value was extracted for the actin or tubulin channel and plotted as s.e.m. from three independent biological replicates (at least 3 condensates from each).

# 3. RESULTS

## 3.1. α-Synuclein is enriched in synapsin condensates

Initially, I aimed to evaluate and validate the specific localization of synapsin 1 and α-synuclein. To achieve this, I simultaneously expressed our fusion proteins mCherry-synapsin 1 and α-synuclein-BFP constructs along with synaptophysin-EGFP, a marker for synaptic vesicles (SVs), into fully mature hippocampal neurons derived from wild-type (WT) mice at 14 days *in vitro* (DIV 14). Through the utilization of confocal imaging techniques, we observed overlapping puncta of all three proteins, providing confirmation of their localization at synaptic boutons (Figure 3.1).

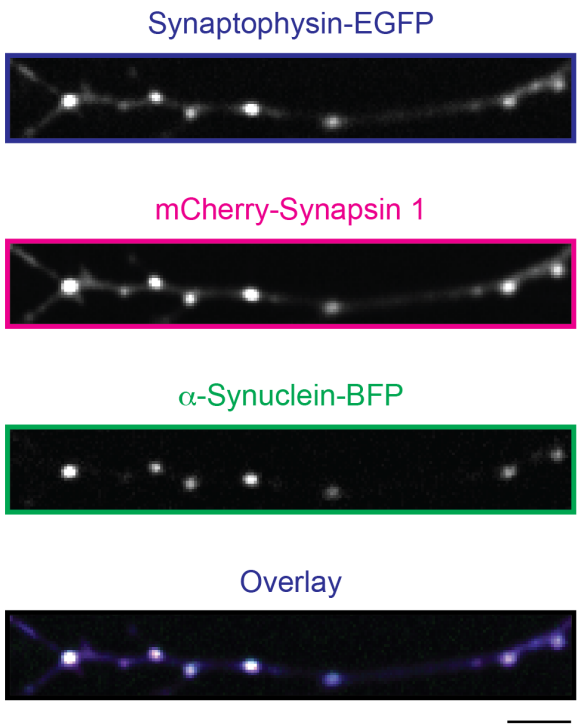


**Figure 3.1. Synapsin 1 and α-synuclein localize at the pre-synapse in mature hippocampal neurons.** Triple transfection of mature hippocampal neurons shows the colocalization of mCherry-synapsin 1 and α-synuclein-BFP with synaptophysin-EGFP (a marker for SVs). Scale bars, 5 µm

To examine the potential phase-separation capabilities of synapsin 1 and α-synuclein, I overexpressed either mCherry-synapsin 1 or α-synuclein-BFP into a heterologous cell system comprising HEK 293 cells (Figure 3.2. A-B). Based on confocal imaging data, when expressed individually, the proteins exhibited a dispersed signal indicative of solubility. Notably, mCherry-synapsin 1 displayed sporadic small puncta, while

α-synuclein-BFP was detected in both the nucleus and cytoplasm. In contrast, co-expression of mCherry-synapsin 1 and α-synuclein-BFP led to the emergence of large fluorescent condensates containing both proteins, as confirmed by the line profile analysis (Figure. 3.2. C), suggesting their propensity for phase-separation. The formation of these droplets was dependent on the quantity of mCherry-synapsin 1 introduced via plasmid transfection. Quantitative analysis revealed that approximately 50% of transfected cells exhibited droplet formation when 2 µg of the mCherry-synapsin 1 construct was transfected (Figure. 3.2. D). To determine the threshold concentration of mCherry-synapsin 1 required to induce phase-separation in HEK 293 cells, I utilized purified recombinant mCherry and imaged a dilution series of known concentrations using the same laser power employed during live-cell imaging (Figure. 3.2. E). By correlating the fluorescence intensity per square micrometer (µm²) with the calibration curve derived from the dilution series, I determined that a cellular concentration of 1 µM of mCherry-synapsin 1 is the threshold at which droplets start to appear (Figure. 3.2. F).

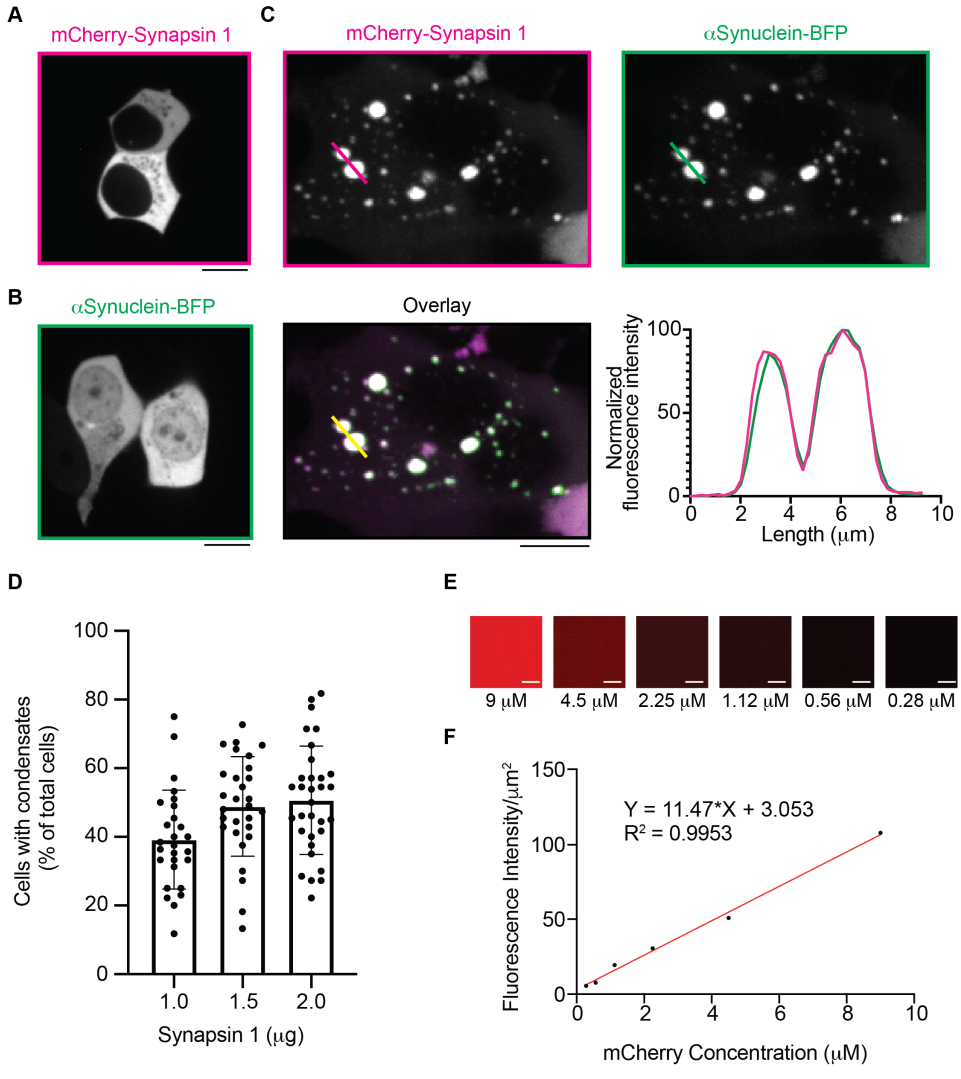

**Figure 2. Interaction of synapsin 1 and α-synuclein in cells.** Heterologous expression of mCherry-Synapsin 1 (A) and α-synuclein-BFP (B) in HEK 293 cells results in mostly diffuse distribution. (C) Co-expression of both mCherry-synapsin 1 and α-synuclein-BFP results in the formation of condensates. Line profiles indicate that both proteins co-localize in puncta. Scale bars, 10 μm. (D) The percentage of cells that contain condensates of both mCherry-synapsin 1 and α-synuclein-BFP increase with the increased amounts of transfected mCherry-synapsin 1 construct. Bars represent average values with ± standard error of the mean. Each dot is an individual experiment from four different rounds of transfections. (E) Fluorescence images of purified, recombinant mCherry at different concentrations under the same laser power as cells were imaged. Scale bar, 3 μm. (F) The calibration curve of fluorescence intensity was recorded for specific concentrations of mCherry, stimulated with the same laser power (0.15 mW) as in the live-cell imaging experiments.

To investigate the dynamic behavior of the formed condensates containing mCherry-synapsin 1 and α-synuclein-BFP, FRAP measurements were conducted. Photobleaching of both mCherry-synapsin 1 and α-synuclein-BFP condensates resulted in a rapid recovery of fluorescence intensity (Figure 3.3 A), indicating the fluidic nature of these condensates. To further explore the characteristics of the individual proteins within the condensates, a comparative analysis of fluorescence recovery rates was performed. Specifically, the recovery rate of mCherry-synapsin 1 was assessed within the condensate and in a cytoplasmic region where the signal appeared to be soluble. The results showed that mCherry-synapsin 1 only exhibited approximately 40% recovery of total fluorescence within the condensate (Figure 3.3 B). Conversely, α-synuclein-BFP demonstrated complete recovery of fluorescence both within the condensate and in the soluble pool (Figure 3.3 C). This discrepancy suggests that within the condensates, mCherry-synapsin 1 is composed predominantly of a highly immobile fraction, accounting for approximately 60% of the protein, which implies its potential role as a scaffold molecule contributing to the construction of the condensate structure. In contrast, α-synuclein-BFP displayed a high degree of mobility both inside and outside the condensates, with a fluorescence recovery rate of approximately 75%. These findings suggest that α-synuclein-BFP is transiently enriched within the condensates, rapidly exchanging with the soluble pool.

Overall, the FRAP analysis provided valuable insights into the dynamic nature of the mCherry-synapsin 1 and α-synuclein-BFP condensates. The differential recovery rates observed for the two proteins indicate distinct behaviors within the condensate structures, with mCherry-synapsin 1 exhibiting higher immobility and α-synuclein-BFP displaying greater mobility and dynamic exchange. These findings contribute to our understanding of the functional properties and regulatory mechanisms underlying the behavior of phase-separated condensates involving synapsin 1 and α-synuclein.

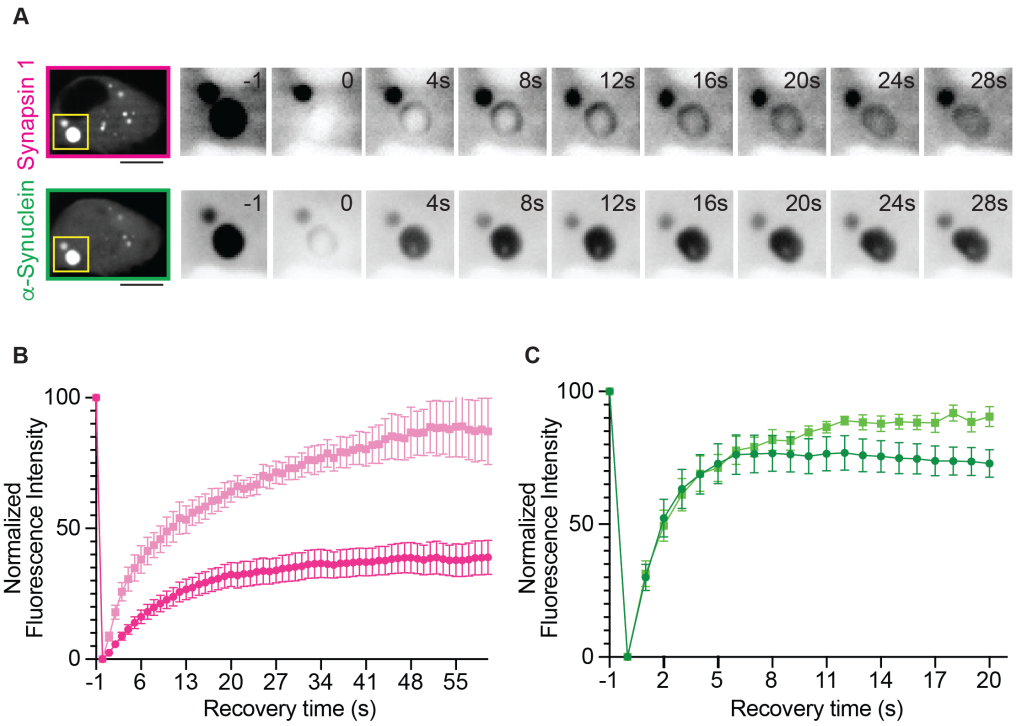


**Figure 3.3. α-Synuclein retains its mobility in synapsin 1 condensates.** (A) FRAP of mCherry-synapsin 1 (top) and α-synuclein-BFP (bottom) expressed in HEK 293 cells (droplet highlighted in yellow). (B) Recovery after bleaching of mCherry-synapsin 1 in droplets (dark magenta) and in the cytosol (light magenta). (B) Recovery after bleaching of α-synuclein-BFP in droplets (dark green) and in the cytosol (light green). Values are represented as average ± standard error of the mean. Data are from three independent biological replicates (ten cells each). Scale bars, 10 µm.

To distinguish between fluid condensates and insoluble aggregates, a valuable assay involves the utilization of the aliphatic alcohol 1,6-hexanediol. This compound disrupts weak hydrophobic interactions, particularly those involving aromatic residues, and is commonly employed to dissolve protein condensates both *in vitro* and within cellular environments. The reversible nature of phase separations can be demonstrated by the ability of 1,6-hexanediol to dissolve fluid condensates. Therefore, the addition of 1,6-hexanediol serves as a means to assess the fluidic nature of the condensates.

In the case of mCherry-synapsin 1 and α-synuclein-BFP condensates, the effect of 1,6-hexanediol was investigated. Upon the addition of a final concentration of 3% 1,6-hexanediol, the condensates dispersed, indicating their fluidic nature (Figure 3.4. A). Notably, the dissolution of the condensates resulted in an overall increase in soluble fluorescence signal within the cell, indicating that the proteins previously residing within the condensates became enriched in the soluble pool.

The observation of line profiles of mCherry-synapsin 1 and α-synuclein-BFP further supported the dissolution of the condensates. Over a time course of 30 seconds and 120 seconds, a progressive decrease in the fluorescent signal within the condensates was observed (Figure 3.4. B). Additionally, a dispersion profile analysis revealed that within 60 seconds, the condensates reached the minimum level of detectable fluorescence. Notably, α-synuclein-BFP exhibited a faster departure from the condensates compared to mCherry-synapsin 1, confirming its high mobility and dynamic behavior within the condensate structures.

These findings underscore the reversible and fluidic nature of the mCherry-synapsin 1 and α-synuclein-BFP condensates, as demonstrated by their dissolution upon the addition of 1,6-hexanediol. The observed increase in soluble fluorescence signal further highlights the redistribution of the proteins from the dissolved condensates to the soluble pool. Moreover, the differential dynamics between α-synuclein-BFP and mCherry-synapsin 1 within the condensates emphasize their distinct mobility properties and reinforce previous indications that α-synuclein-BFP has high mobility and rapid exchange behavior.

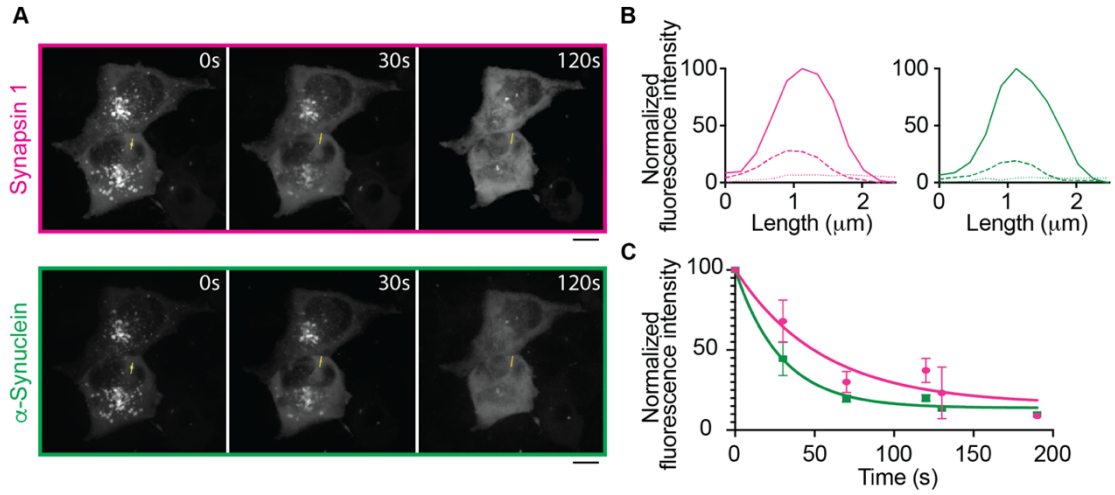


**Figure 3.4. 1,6-Hexanediol disperses synapsin 1/α-synuclein condensates.** (A) Confocal images of mCherry-synapsin 1 (top) and α-synuclein-BFP (bottom) in HEK 293 cells, before (0 s) and after loading 3% 1,6-hexanediol (final concentration). Scale bars, 10 μm. (B) Line profiles of mCherry-synapsin 1 (left) and α-synuclein-BFP (right) for different time points (full line – 0 s, dashed lines – 30 s, dotted line – 120 s). (C) Dispersion profiles of both mCherry-synapsin 1 and α-synuclein-BFP from four independent experiments.

The specificity of the observed effect on condensate dissolution was examined by comparing the impact of different aliphatic alcohols. In particular, the shorter aliphatic alcohol, 1,3-propanediol, was assessed for its potency in dissolving the condensates at an equivalent final concentration of 3% (Figure 3.5. A).

Interestingly, the results demonstrated that 1,3-propanediol exhibited lower efficacy in dissolving the condensates compared to 1,6-hexanediol. Line profiles of mCherry-synapsin 1 and α-synuclein-BFP further highlighted this distinction, revealing a reduction in the fluorescent signal by only approximately 50% after a time period of 130 seconds (Figure 3.5. B).

These findings support the specificity of 1,6-hexanediol in effectively dispersing the condensates while indicating that the shorter aliphatic alcohol, 1,3-propanediol, possess lower potency in dissolving the condensates at the same final concentration. The differential effects observed between these aliphatic alcohols further emphasize the importance of considering the specific properties and structures of different compounds when investigating their impact on the dissolution and dynamics of protein condensates.

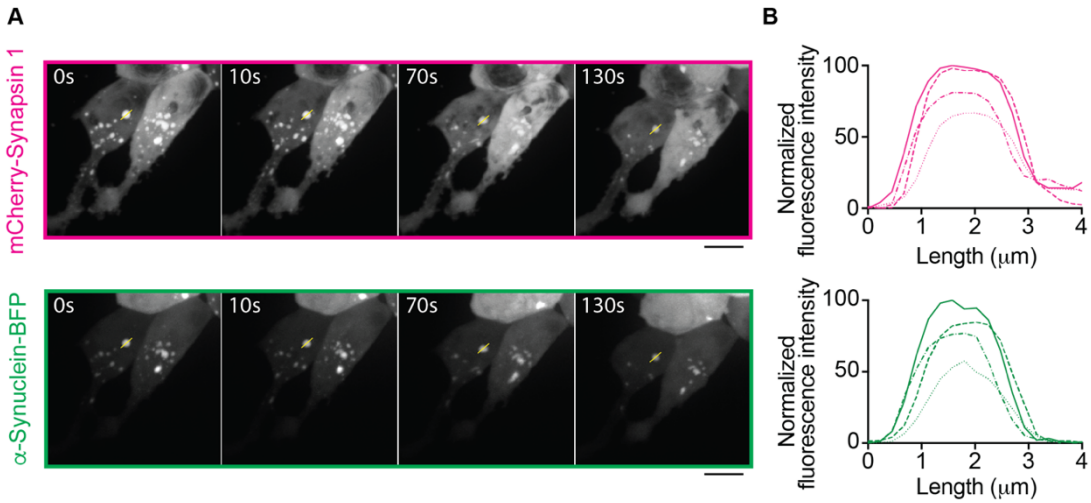


**Figure 3.5. 1,3-propanediol has a limited ability to disperse synapsin 1/α-synuclein condensates.** (A) Confocal images of mCherry-synapsin 1 (top) and α-synuclein-BFP (bottom) in HEK 293 cells, before (0 s) and after loading 3% 1,3-propanediol (final concentration). Scale bar, 10 μm. (B) Line profiles of mCherry-synapsin 1 (top) and α-synuclein-BFP (bottom) for different time points (full line – 0 s, dashed lines – 10 s, two dashed lines – 70 s, dotted line – 130 s).

In order to investigate the contribution of synaptic vesicles (SVs) in inducing phase separation, I shifted my focus to a minimal reconstitution system utilizing recombinant proteins and native SVs isolated from rats. The characterization of condensates formed through the ectopic co-expression of mCherry-synapsin 1 and α-synuclein-BFP provided valuable insights for this approach. Initially, confocal imaging was conducted on reconstituted EGFP-synapsin 1 (at a concentration of 6 μM) and α-synuclein chemically labeled with a far-red dye (Alexa Fluor 647) (at a concentration of 2 μM) under conditions of 3% PEG 8000 and physiological salt concentration (150 mM NaCl) at room temperature. The chosen ratio of synapsin 1 to α-synuclein was based on previous projections as the average physiological ratio at the synapse (Wilhelm et al., 2014). During the reconstitution process, droplets of EGFP-synapsin 1 were observed to recruit α-synuclein (AF 647), with α-synuclein progressively enriching the already formed synapsin 1 condensates. This ultimately led to the colocalization of α-synuclein within the condensates after a 10-minute incubation, as confirmed by line profiles (Figure 3.6. A). Subsequently, FRAP experiments were performed on the reconstituted condensates to further validate their fluidic nature *in vitro*. The photobleaching of either EGFP-synapsin 1 or α-synuclein (AF 647) resulted in a rapid recovery of fluorescent signal, exhibiting a similar recovery rate to the FRAP experiments conducted in cells. Notably, α-synuclein (AF 647) demonstrated complete recovery, whereas EGFP-synapsin 1 displayed a substantial immobile fraction, indicating its limited mobility within the condensates (Figure 3.6. B). This observation strongly suggests that α-synuclein is transiently recruited to the synapsin 1 droplets.

For the reconstitution experiments, EGFP-synapsin 1 was expressed in Expi293F™ cells to preserve the PTMs crucial for its liquid phase propensity, while α-synuclein was expressed in Escherichia coli BL21 cells. The successful purification of both recombinant proteins was confirmed by SDS-PAGE gel analysis (Figure 3.6. C), where the protein bands aligned with the predicted molecular weights of 102.26 kDa for EGFP-synapsin 1 and 14.46 kDa for α-synuclein. These findings provide evidence for the recruitment of α-synuclein by synapsin 1 droplets in the reconstitution system and support the fluidic nature of the formed condensates. The utilization of recombinant proteins and native SVs offers a valuable platform to explore the role of SVs in phase separation phenomena, furthering our understanding of the molecular mechanisms underlying synaptic function.

Throughout the SVs isolation process, we collected fractions and performed SDS-PAGE gel and immunoblotting analyses to separate and characterize the proteins present in each step, including the rat brain homogenate, pellet after osmotic lysis, supernatant after osmotic lysis, and pure SVs (Figure 3.6. D). The immunoblot results confirmed the successful isolation of pure SVs, which were enriched in characteristic integral membrane proteins such as Synaptophysin 1 and Synaptobrevin 2, as well as other SVs-associated proteins like NSF. Importantly, common SVs contaminants such as Na+/K+-ATPase, PSD95, and succinate dehydrogenase (SDHA) were absent in the pure SVs fraction (Figure 3.6. D).

Next, I utilized the isolated SVs (at a concentration of 23 nM) in combination with purified EGFP-synapsin 1 and α-synuclein, employing different molar ratios of α-synuclein to synapsin (1:1, 3:1, and 1:3) in the absence of any crowding reagent. The condensate formation was measured using turbidity measurements, specifically by monitoring the change in turbidity at 405 nm (Figure 3.6. E). The selection of 23 nM SVs concentration was based on the average physiological molar ratio of synapsin to SVs, which ranges between 1:100 and 1:1000 (Takamori et al., 2006; Wilhelm et al., 2014). Interestingly, α-synuclein alone, in the presence of SVs, was unable to form condensates on its own. However, EGFP-synapsin 1 alone, in the presence of SVs, exhibited a high rate of condensation, suggesting that SVs act as a catalyst for synapsin 1 phase separation. When EGFP-synapsin 1 was present at a higher or equimolar ratio to α-synuclein, the rate of condensation was comparable to that observed when EGFP-synapsin 1 was incubated alone with SVs. However, an excess of α-synuclein over EGFP-synapsin 1 resulted in a decrease in the rate of synapsin-mediated condensate formation. These findings indicate that the balance of molar ratios between synapsin 1 and α-synuclein is crucial for the equilibration of SVs packing at the nerve terminal under physiological conditions (Figure 3.6. F). These data highlight the significance of SVs in modulating the phase separation dynamics of synapsin 1 and α-synuclein, shedding light on the intricate molecular mechanisms underlying synaptic function and regulation.

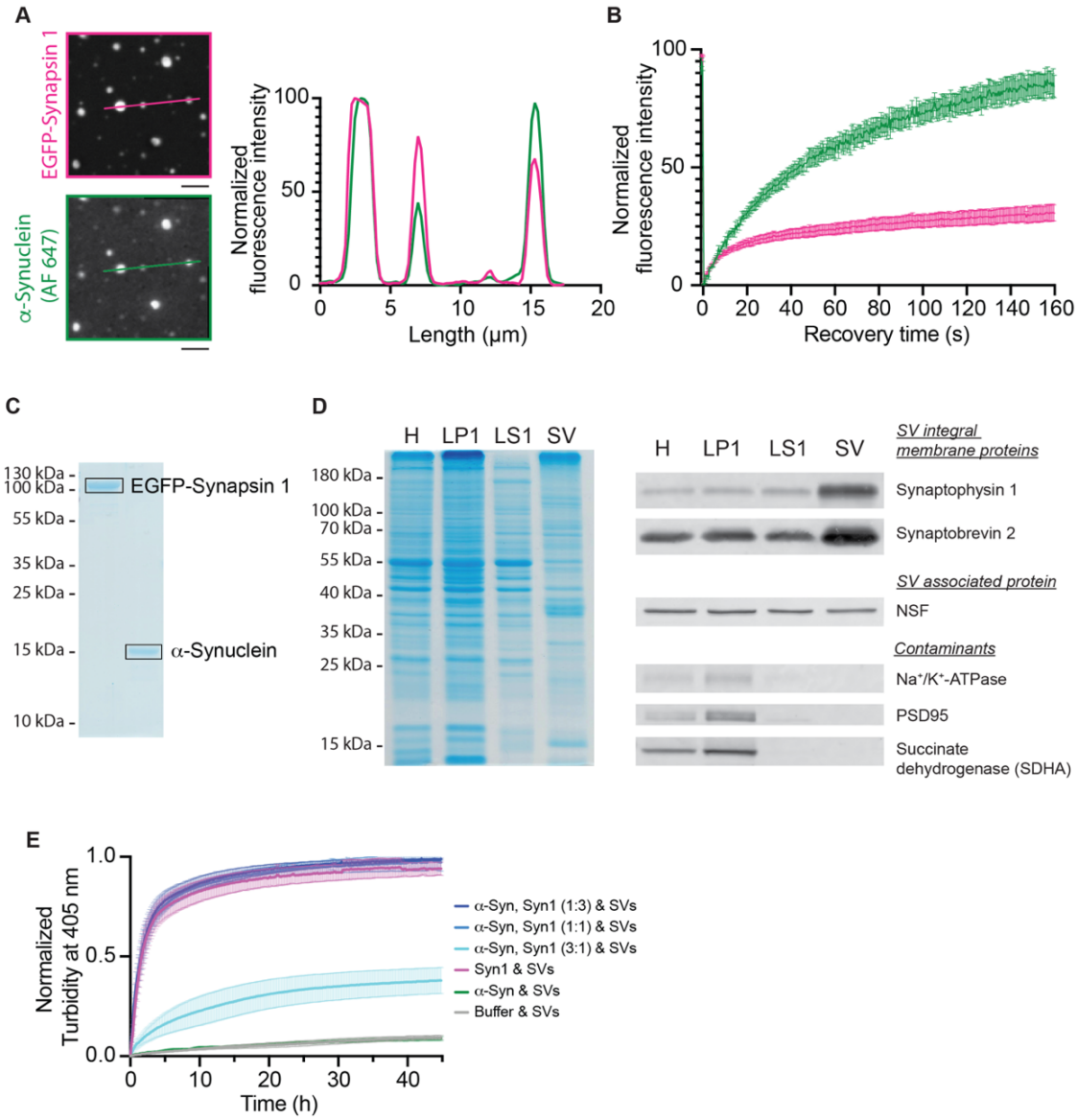


**Figure 3.6. Condensate formation of purified recombinant proteins.** (A) Colocalization of reconstituted condensates containing EGFP-synapsin 1 (6 µM) and α-synuclein (2 µM, chemically labeled with Alexa Fluor 647, AF 647) in 3% PEG, 8000 at RT. Scale bars, 5 µm. (B) Recovery after photobleaching of EGFP-synapsin 1 (magenta) and α-synuclein (AF 647) (green). Values are represented as average ± standard error of the mean. Data are from three independent reconstitutions. (C) SDS-page gel with recombinant proteins used in the *in vitro* assays. (D) Distribution profile of six proteins analyzed by immunoblotting of subcellular fractions. Each lane contains 5 µg/lane of protein of the respective fraction (H: rat brain homogenate, LP1: pellet after osmotic lysis, LS1: supernatant after osmotic lysis, SV: pure synaptic vesicles). Samples were separated on SDS-polyacrylamide gels (left) and transferred onto PVDF membranes (Amersham Hybond LFP 0.2 µm, Cytiva). The blots (right) were developed using Cy3-conjugated secondary antibodies (goat-anti-mouse IgG-Cy3, ECL Plex™) according to the manufacturer's instruction (Cytiva). The signals were recorded on a Typhoon Trio Variable Mode Imager System (GE Healthcare). (E) Condensate formation of purified recombinant proteins EGFP-synapsin 1 and α-synuclein (AF 647) in different molar ratios (curves in tones of blue), EGFP-synapsin 1 alone (magenta), α-synuclein (AF 647) alone (green) in presence of 23 nM SVs. The condensate formation was measured as a change of turbidity at 405 nm. Each value is shown as the average ± standard error of the mean, data are from three independent replicates (each time fresh isolation of native SVs). All experiments shown in Figure 3.6. were performed in collaboration with Dr.Christian Hoffmann.

## 3.2. α-Synuclein and synphilin-1 form biomolecular condensates

Intrigued by the impact of α-synuclein on the condensation behavior of synapsin and synaptic vesicles (SVs), I aimed to further investigate the role of α-synuclein in the condensation formation of another highly expressed protein at the synaptic terminal, synphilin 1. To assess the ability of synphilin 1 to form protein condensates in cells, I performed transfections of EGFP-synphilin 1 in both HEK 293 cells and mature hippocampal neurons. Through confocal imaging, I observed the formation of droplet-like and highly mobile inclusions of various sizes when EGFP-synphilin 1 was expressed in HEK 293 cells. In mature hippocampal neurons, puncta corresponding to synaptic boutons were observed (Figure. 3.7. A-B). Furthermore, analysis of sequential frames captured in HEK 293 cells revealed multiple fusion and fission events within the droplet-like structures, providing evidence for their dynamic and fluid nature (Figure. 3.7. C).

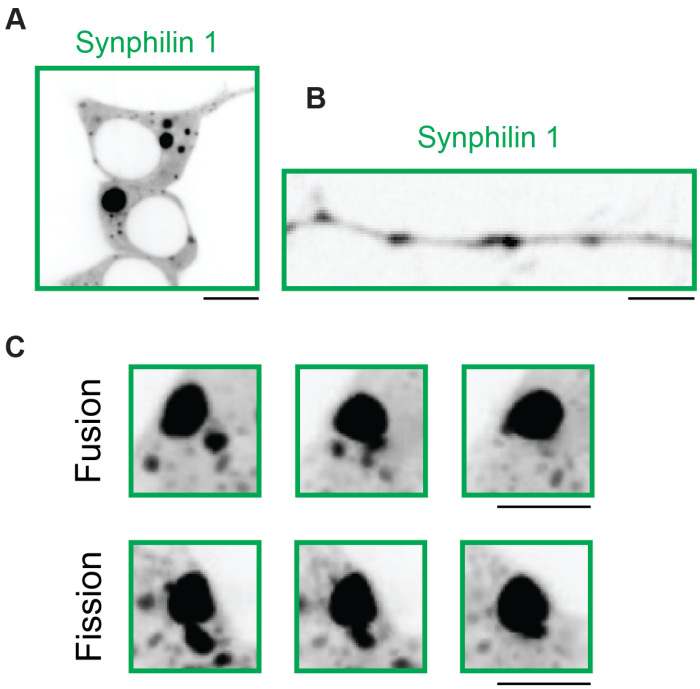


**Figure 3.7. Synphilin 1 forms condensates in cells.** (A) Heterologous expression of EGFP-synphilin 1 in HEK 293 cells results in condensate formation. Scale bars, 10 µm. (B) Transfection of mature hippocampal neurons shows the formation of condensates in correspondence with synaptic boutons. Scale bars, 5 µm. (C) Representative images of fusion (top) and fission (bottom) events of EGFP-synphilin 1 condensates in HEK 293 cells. Scale bars, 5 µm.

To investigate the LLPS properties of synphilin 1, I conducted a protein purification process and employed the purified protein for *in vitro* reconstitution experiments. Initially, I chose to purify synphilin 1 using a two-step purification approach involving affinity chromatography and size exclusion chromatography. In order to facilitate the cleavage of the tag and obtain a tag-free protein, I fused a His-SUMO tag with the EGFP-synphilin 1 construct (referred to as His-SUMO-EGFP-synphilin 1).

To begin the purification process, I expressed the His-SUMO-EGFP-synphilin 1 construct in Expi293F™ cells and obtained the cell lysate containing the target protein. Affinity purification was performed using a Ni-NTA column, with 4% imidazole used for wash steps and 100% imidazole for protein elution. The affinity purification chromatograph (Figure. 3.8. A) shows the removal of protein fractions associated with cell debris and non-specific bindings through the washing steps. Subsequently, I applied the elution buffer and collected three fractions enriched in proteins, corresponding to the rising phase of the peak (highlighted in yellow), as determined by absorbance at 280 nm. To further enhance the purity of the eluted protein and eliminate contaminants with molecular weights unrelated to our protein of interest, I concentrated the eluates and subjected them to size exclusion chromatography using Superdex™ 200 columns. The size-exclusion chromatograph (Figure. 3.8. B) demonstrates the collection of three eluted fractions belonging to the rising phase of the protein peak (highlighted in yellow), based on absorbance at 280 nm. Several other proteins with lower molecular weights were excluded during this step. Finally, I pooled together the fractions and incubated them overnight with SENP1EUB proteases, previously purified by Dr. Christian Hoffmann. This incubation allowed for the cleavage of the purified protein and separation of the His-SUMO tag from EGFP-synphilin 1. Following the cleavage step, I performed a His-exclusion process using His-pure Ni-NTA resin to separate the two components.

To assess the molecular weight of our protein and identify potential contaminants, I conducted an SDS-page gel analysis using the fractions collected at each step of the protein purification process (Figure. 3.8. C). The expected molecular weight for His-SUMO-EGFP-synphilin 1 is 143.70 kDa, while for EGFP-synphilin 1 alone it is 130.22 kDa. In the lanes corresponding to the cell lysate (L), pellet (P), and supernatant (S), an enriched protein band slightly higher than 130 kDa is observed, indicating the expression of His-SUMO-EGFP-

synphilin 1, along with several other bands representing the complex mixture of cellular debris.

The band corresponding to His-SUMO-EGFP-synphilin 1 disappears in the flow-through (FT) fraction of the affinity purification, while the most enriched lower molecular weight bands are still present, suggesting their exclusion from the eluted protein. In the His-eluate lane (HE), one band at 143.70 kDa, corresponding to our target protein, is visible, along with a second band at approximately 70 kDa, likely corresponding to HSP70. Some paler non-specific bands also appear in this lane. After pooling and concentrating the eluted fraction, the protein content becomes clearer, and additional bands representing contaminating proteins are observed in the SEC loading fraction (SL). In the pre-cleaved lane (PC), two major visible bands are present, one at 143.70 kDa, corresponding to our target protein, and a second at approximately 70 kDa, possibly corresponding to HSP70. In the cleaved not-reHis lane (CnH), the upper band now appears at 130.22 kDa, matching the predicted molecular weight of EGFP-synphilin 1. Additionally, a lower band around 35 kDa is visible, corresponding to the His-SUMO fragment, confirming the successful protease cleavage using SENP1EUB. After performing the re-his exclusion, the His-SUMO fragment is removed, and only two residual bands remain, which appear clean and are nicely enriched in protein.

Using the purified EGFP-synphilin 1, I conducted *in vitro* experiments to determine the conditions necessary for phase separation. I reconstituted the protein at different concentrations (1 μM, 5 μM, 10 μM) and varying percentages of PEG 8000 (0%, 0.5%, 1%, 3%, 5%, 10%). The reconstitution was performed in a buffer containing 25 mM Tris-HCl (pH 7.4), 300 mM NaCl, and 0.5 mM TCEP, followed by incubation for 5 mins at room temperature.

EGFP-synphilin 1 demonstrated the ability to undergo LLPS even at relatively low concentrations and low percentages of the crowding agent, as depicted in the phase diagram (Figure. 3.8. D). Representative images obtained from three independent reconstitutions using confocal microscopy (Figure. 3.8. E) illustrate the formation of droplet-like structures indicative of phase separation.

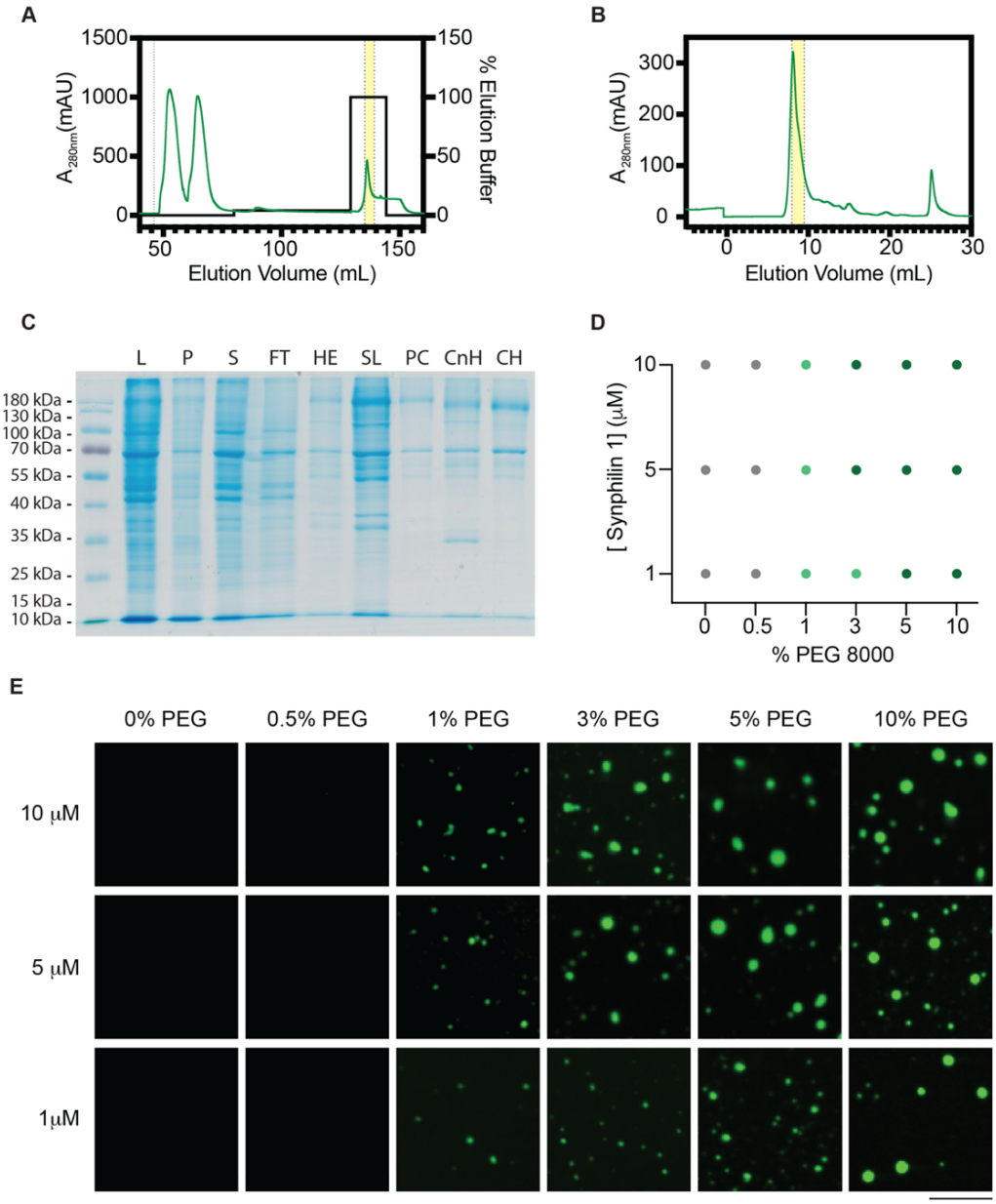


**Figure 3.8. Purification and phase diagram of EGFP-Synphilin 1. Purified recombinant Synphilin 1 undergoes LLPS.** (A) Chromatograph showing affinity chromatography of His-SUMO-EGFP-synphilin 1. Protein concentrations were measured as absorbance at 280nm and expressed in mAU (green line), while for protein elution the buffer employed is expressed as a percentage of elution buffer (black line). The fractions collected are highlighted (fractions 6-8). (B) Chromatograph showing S200 size-exclusion chromatography of His-SUMO-EGFP-synphilin 1. Protein concentrations were measured as absorbance at 280nm and expressed in mAU (green line). The fractions collected are highlighted (fractions 4-6). (C) SDS-page gel showing all steps of EGFP-synphilin 1 purification (L: cell lysate, P: pellet after osmotic lysis, S: supernatant after osmotic lysis, FT: Flow Through, HE: His-Eluate, SL: SEC load, PC: Pre-cleavage, CnH: Cleaved not re-His, CH: Cleaved re-His). (D) Phase diagram of EGFP-synphilin 1, referring to the images in e. Phase separation was determined as the appearance of droplets at the coverslip surface 5 min after the beginning of the incubation. Grey circles indicate no phase separation; Light green circles indicate the presence of small droplets; Dark green circles indicate the formation of condensates. Each condition was assessed by three independent reconstitutions. (E) Representative images of EGFP-synphilin 1 phase separation in different concentrations (1 μM, 5 μM, 10 μM) and increasing percentage of PEG 8000 (0%, 0.5%, 1%, 3%, 5%, 10%), reconstituted in 25 mM Tris-HCl (pH 7.4), 300 mM NaCl, 0.5 mM TCEP and incubated for 5 min at RT. Scale bars, 10 μm

Building upon previous findings regarding the interaction between synphilin 1 and α-synuclein, and their propensity for self-assembly, an *in vitro* approach was undertaken to further investigate their association and observe the formation of synphilin 1 condensates. For visualization purposes using confocal microscopy, a mixture of 10 μM purified EGFP-synphilin 1 and 20 μM chemically labeled α-synuclein (Alexa Fluor 568) was reconstituted in a buffer containing 25 mM Tris-HCl (pH 7.4), 300 mM NaCl, and 0.5 mM TCEP.

In the collected confocal images after a 5-minute incubation at room temperature (Figure. 3.9. A), α-synuclein (AF 568) appears both as a soluble form contributing to the background signal and enriched within EGFP-synphilin 1 condensates, exhibiting perfect colocalization. The line profile analysis further confirms this colocalization (Figure. 3.9. B). After a 10-minute incubation at room temperature, the high background signal diminishes, and α-synuclein (AF 568) segregates from EGFP-synphilin 1, accumulating at the periphery of the condensates, forming a rim-like structure referred to as "Core & Shell" (Figure. 3.9. C). The line profiles support this observation, showing the progressive translocation of α-synuclein from the center to the rim of the condensates (Figure. 3.9. D). This "Core & Shell" organization resembles the structure of LBs found in post-mortem brain slices of PD patients, where synphilin 1 forms the core and α-synuclein surrounds it in an enriched ring, so we named it after body-like structure (LBLs). To assess the fluidity of the LBLs and explore the mobility of their components, FRAP experiments were performed, with the region of interest (ROI) positioned at the condensate rim where the two proteins still overlap (Figure. 3.9. E). The results from FRAP analysis show that EGFP-synphilin 1 only partially recovers after photobleaching, while α-synuclein (AF 568) exhibits the ability to re-enrich the condensate, restoring its distinctive shell structure and display higher mobility compared to EGFP-synphilin 1 (Figure. 3.9. F).

Intrigued by these findings, I sought to investigate whether a similar structure could be recapitulated when the two proteins are ectopically expressed in cells. Through ectopic co-expression of EGFP-synphilin 1 and α-synuclein-BFP in HEK 293 cells, a single large condensate exhibiting the LBLs was formed (Figure. 3.9. G). Moreover, in mature hippocampal neurons co-transfected with EGFP-synphilin 1 and α-synuclein-BFP, multiple puncta enriched in both proteins were observed, localizing in correspondence with synaptic boutons (Figure. 3.9. H). These findings collectively indicate that synphilin 1 and α-

synuclein, in our experimental system, are capable of mediating and recapitulating the formation of LBLs.

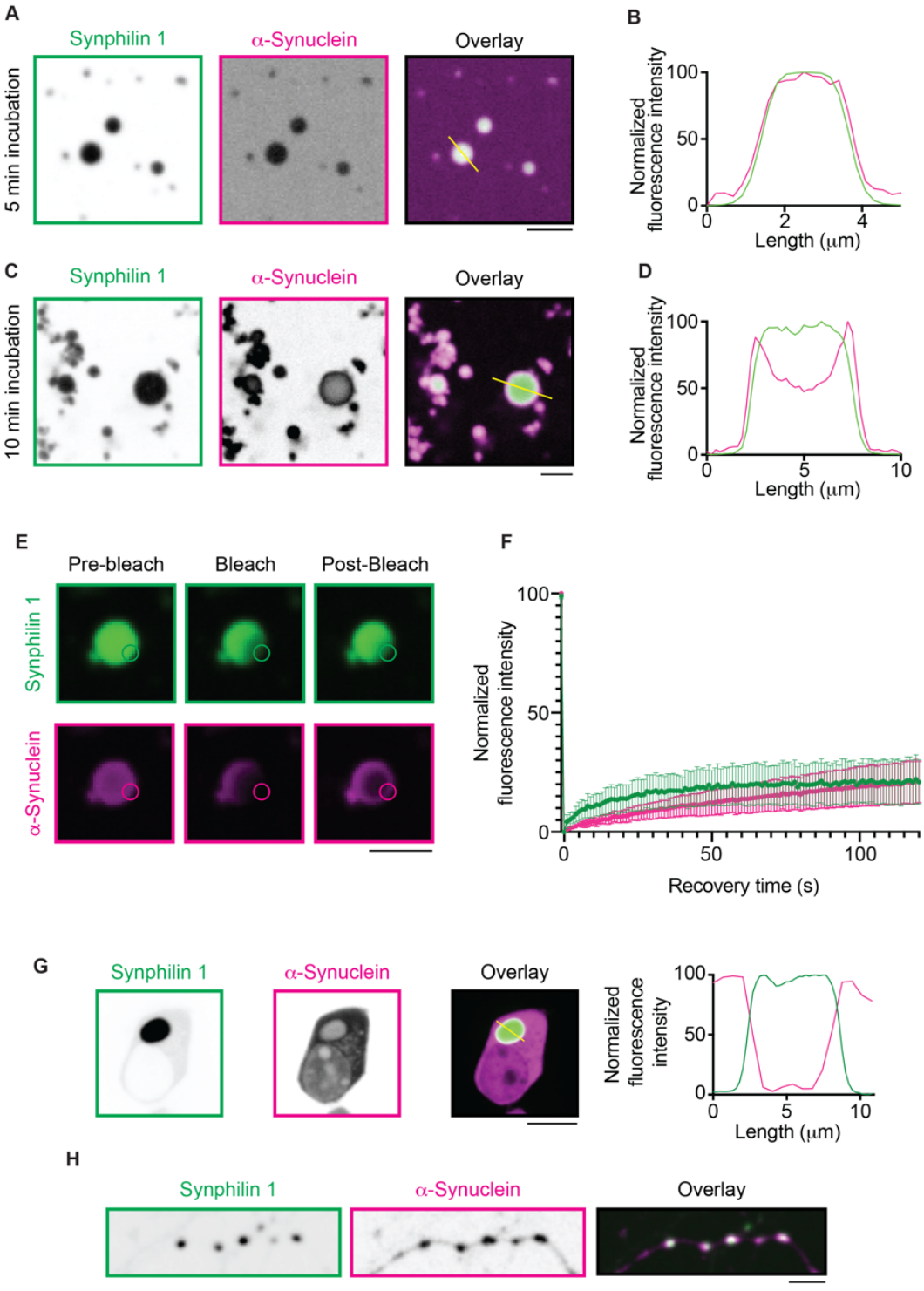

**Figure 3.9. Synphilin 1 and α-synuclein forms Lewy bodies-like structures (LBLs) *in vitro* and in cell.** (A, C) Reconstituted condensates containing EGFP-synphilin 1 (10 μM) and α-synuclein (20 μM, chemically labeled with Alexa Fluor 568 (AF 568) in 10% PEG, 8000 at RT, after 5 min (A) and 10 min (C) of incubation. Scale bars, 5 μm. (B, D) Line profiles of EGFP-synphilin 1 (green) and α-synuclein (AF 568) (magenta) indicate that both proteins co-localize in condensates after 5 min (B) and de-mix and reach the "Core & Shell" structure after 10 min (D). (E) FRAP at the rim of EGFP-synphilin 1 (top) and α-synuclein (AF 568) (bottom) showing pre-bleach (-1 s), bleaching (0 s), and post-bleaching (120 s). Scale bar, 10 μm. (F) Recovery after photobleaching of EGFP-synphilin 1 (green) and α-synuclein (AF 568) (magenta). Values are represented as average ± standard error of the mean. Data are from three independent reconstitutions. (G) Co-expression of both EGFP-synphilin 1 and α-synuclein-BFP in HEK 293 cells results in the formation of "Core & Shell" structure. Line profiles indicate that proteins de-mix in condensates. Scale bar, 10 μm. (H) Double transfection of mature hippocampal neurons shows the colocalization of EGFP-synphilin 1 and α-synuclein-BFP in correspondence with synaptic boutons. Scale bars, 5 μm

To investigate the role of synapsin 1 in the formation of synphilin 1/α-synuclein condensates, I performed *in vitro* reconstitution experiments to mimic the pre-synaptic environment. In these reconstituted condensates, EGFP-synphilin 1 colocalized with Halo-synapsin 1, enriching the core of the condensates, while α-synuclein labeled with Alexa Fluor 647 (AF 647) formed the characteristic shell, accumulating at the periphery (Figure. 3.10. A), as confirmed by the line profile analysis (Figure. 3.10. B). However, in HEK 293 cells co-expressing EGFP-synphilin 1, α-synuclein-BFP, and mCherry-synapsin 1, a different pattern emerged. The "Core & Shell" structure sequestered synapsin 1 at the rim of the condensates, depleting it from the core and following the pattern of α-synuclein (Figure. 3.10. C). It is worth noting that while the buffer used in the *in vitro* reconstitution contained 300 mM NaCl, the physiological salt concentration typically ranges around 150 mM NaCl. The higher NaCl concentration in the *in vitro* experiments may contribute to the observed differences in behavior between the *in vitro* and in-cell experiments, as higher NaCl concentrations generally increase protein solubility.

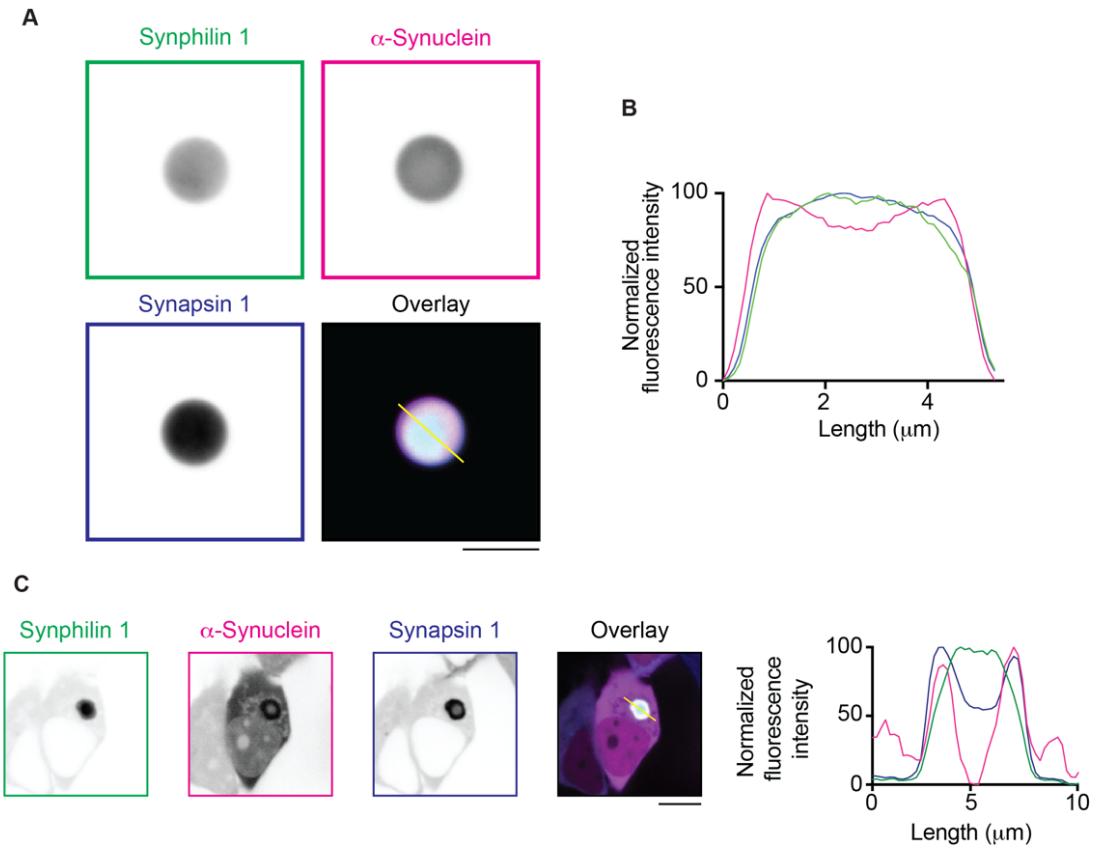


**Figure 3.10. Synapsin 1 enriches LBLs.** (A) Reconstituted condensates containing EGFP-synphilin 1 (0,05 μM), α-synuclein (6 μM, chemically labeled with Alexa Fluor 647 (AF 647), and Halo-synapsin 1 (0,7 μM) in 15% PEG, 8000 at RT, after 1 of incubation. Scale bars, 5 μm. (B) Line profiles of EGFP-synphilin 1 (green), α-synuclein (AF 647) (magenta), and Halo-synapsin 1 (blue) indicate that while synphilin 1 and synapsin 1 co-localize in condensates, α-synuclein enriches the periphery of the condensates. (C) Triple transfection using EFGP-synphilin 1, α-synuclein-BFP, and mCherry-synapsin 1 in HEK 293 cells. Scale bars, 10 μm.

After investigating the formation of LBLs *in vitro* and in cells, I focused on analyzing the dynamic properties of these multi-phase condensates, specifically examining the mobility of synphilin 1 and α-synuclein expressed in HEK 293 cells using FRAP experiments. When EGFP-synphilin 1 was expressed individually, it exhibited high mobility at the rim of the condensates, with a fluorescent intensity recovery of approximately 50% (Figure. 3.11. A). However, when co-transfected with α-synuclein-BFP, the mobility of EGFP-synphilin 1 significantly decreased, resulting in a lower fluorescent intensity recovery of only about 20% (Figure. 3.11. B).

To explore the effect of synphilin 1 on the balance between synapsin 1 and α-synuclein in terms of condensate mobility, I compared the dynamics under different transfection conditions (Figure. 3.11. C) and quantified the FRAP experiments (Figure. 3.11.

D). In all tested conditions, round droplet-like structures were formed, except for the co-transfection of synphilin 1 and synapsin 1, which resembled aggregated structures. The comparison revealed that the decrease in the mobility of EGFP-synphilin 1 occurred only when co-transfected with α-synuclein-BFP, while it maintained high recovery when co-transfected with mCherry-synapsin 1. These findings suggest that α-synuclein reduces the mobility of synphilin 1, likely acting as a physical barrier between the core of the condensates and the surrounding soluble pool.

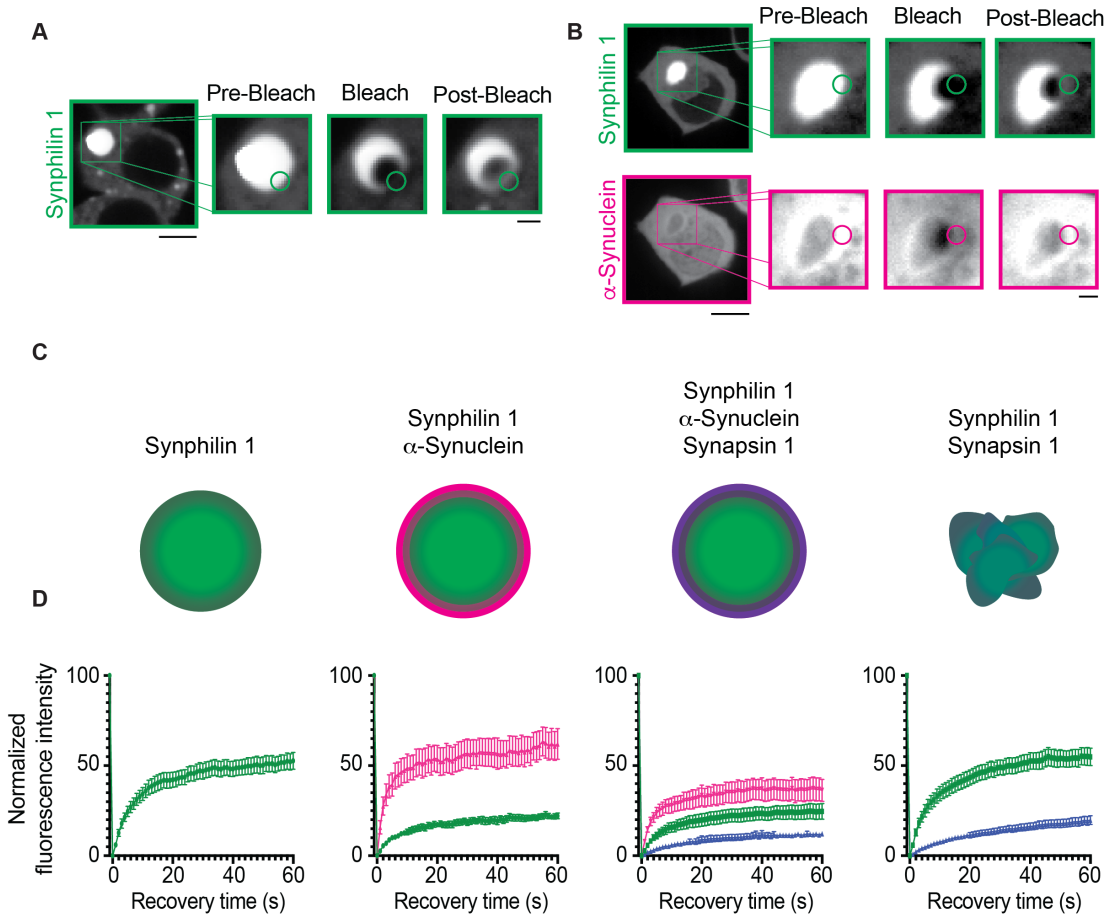


**Figure 3.11. α-Synuclein decreases the mobility of synphilin 1 in LBLs.** (A) Recovery after bleaching of EGFP-synphilin 1 (green) at the rim of condensates. Values are represented as average ± standard error if the mean. (B) FRAP at the rim of EGFP-synphilin 1 showing pre-bleach (-1 s), bleaching (0 s), and post-bleaching (60 s). Scale bar of cell, 10 µm; Scale bar of condensate, 2 µm. (C) Schematic representation of varying types of condensates resulting in transfection experiment in HEK 293 cells. (D) Recovery after photobleaching of EGFP-synphilin 1 (green) and α-synuclein-BFP (magenta) and mCherry-synapsin 1 at the rim of condensates. Values are represented as average ± standard error of the mean.

## 3.3. Maturation of α-synuclein/synphilin-1 condensates leads to Lewy body-like structures

High local concentration and ionic strength are two crucial factors that significantly impact the solubility and propensity for condensation of proteins. To evaluate their effects on LBLs condensation, I conducted a straightforward experiment by manipulating the ionic environment of cultured cells using hypotonic and hypertonic solutions. Firstly, I applied a hypotonic solution (5% DMEM in $H_2O$) to the cells, which decreased the extracellular salt concentration compared to the physiological level of 150 mM NaCl. This led to an osmotic gain of water inside the cells, causing them to swell and resulting in a reduction of protein concentration and internal ionic strength (Figure. 3.12. A, C).

In contrast, I applied a hypertonic solution (300 mM NaCl) to the cells, which increased the extracellular salt concentration. This caused the cells to lose water through osmosis, leading to cell shrinkage and an increase in protein concentration and ionic strength (Figure. 3.12. B, D). Upon exchange with the hypotonic solution, small and highly dynamic condensates of EGFP-synphilin 1 fully dissolved, indicating that they were not true condensates but rather aggregates (Figure. 3.12. A). However, large condensates persisted, suggesting that they were aggregated condensates. On the other hand, the application of the hypertonic solution increased the condensation in cells, as indicated by the higher number of newly formed fluorescence foci (Figure. 3.12. B). These findings demonstrate that both low and high ionic strength can influence the formation and dissolution of LBLs, highlighting the importance of ionic conditions in protein condensation.

Interestingly, in the presence of either hypotonic or hypertonic solutions, the condensates formed by synphilin 1 remain unchanged and appear insoluble. However, in HEK 293 cells co-transfected with EGFP-synphilin 1 and α-synuclein-BFP, α-synuclein undergoes de-mixing in the presence of hypotonic solution (Figure. 3.12. C, D). These observations suggest that while synphilin 1 alone retains its fluid nature when co-expressed with α-synuclein, it becomes insoluble. However, α-synuclein can still be recruited within synphilin 1 condensates under lower ionic strength conditions, indicating its high mobility. Conversely, at higher ionic strength, α-synuclein tends to localize at the periphery of the condensates, reinforcing the shell structure.

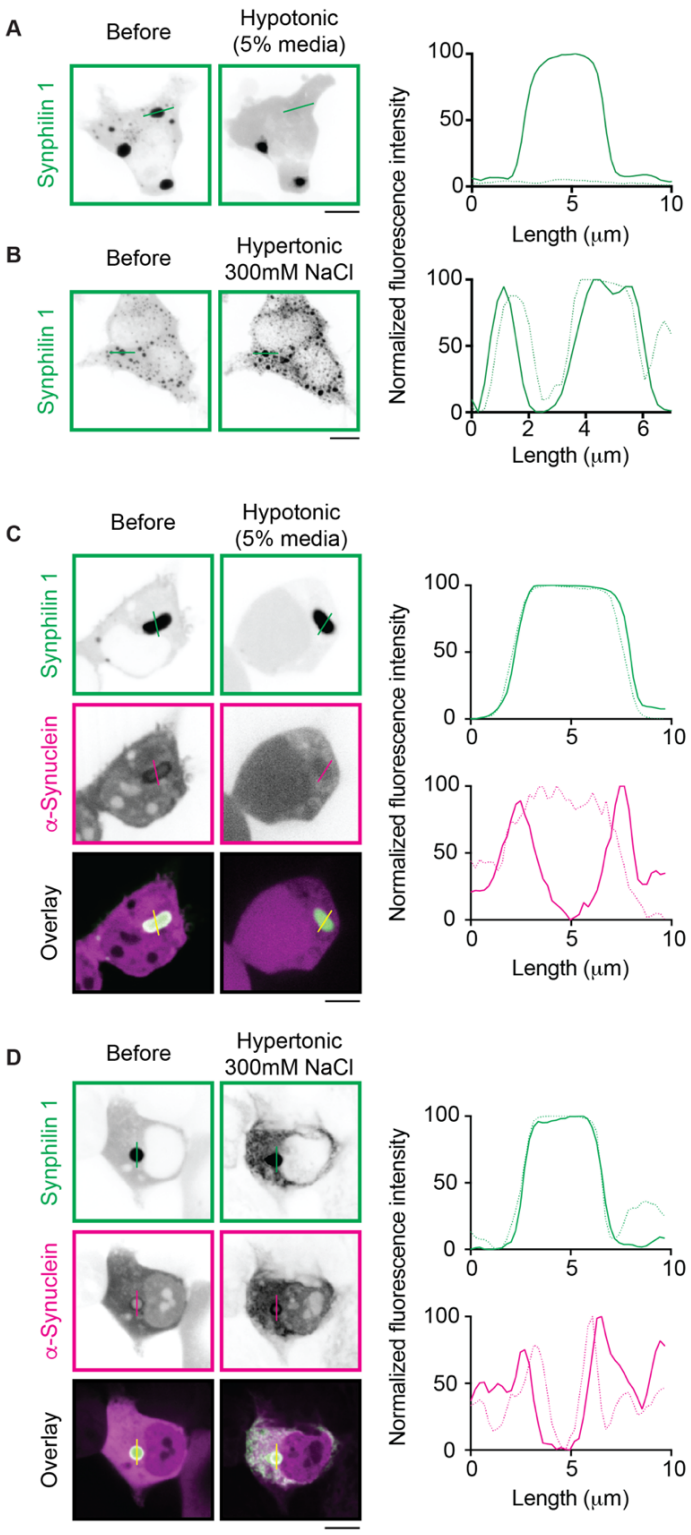


**Figure 3.12. Salt concentration modulates the strength of interaction between synphilin 1 and α-synuclein in LBLs.** Confocal images of HEK 293 cells expressing EGFP-synphilin 1, before and after the exchange of 5% DMEM in $H_2O$ (A) and before and after the exchange with 300 mM NaCl solution (B). Scale bars, 10 μm. Confocal images of HEK 293 cells expressing EGFP-synphilin 1 and α-synuclein-BFP, before and after the exchange of 5% DMEM in $H_2O$ (C) and before and after the exchange with 300 mM NaCl solution (D). Scale bars, 10 μm. For all line profiles, solid lines indicate the protein profile before treatment and dotted lines indicate the protein profile after treatment.

The primary risk factor for numerous neurodegenerative diseases, including PD, is aging. This is primarily attributed to the progressive and unregulated buildup of insoluble proteins, which ultimately form aggregates and contribute to the development of neurodegenerative pathology.

To investigate the impact of aging on the mobility of LBLs, I reconstituted them in HEK 293 cells and performed FRAP measurements. I focused on different time points post-transfection (12 hours, 24 hours, and 48 hours) to mimic various stages of protein accumulation, and analyzed the corresponding confocal images (Figure. 3.13 A). At early time points, the cells exhibited small, highly dynamic droplets as condensates. However, as time progressed, the condensates grew larger due to the continuous aggregation of proteins, resulting in fewer but larger condensates. This difference was clearly observed in the microscopy images, prompting me to quantitatively analyze the distribution of cells expressing no condensates, small condensates, and large condensates (Figure. 3.13. B). By measuring the surface area of the condensates, I found that the number of small condensates ($< 20\ \mu m^2$) decreased over time, while the number of large condensates ($> 20\ \mu m^2$) increased, reaching a peak at 48 hours post-transfection. The threshold size of $20\ \mu m^2$ was chosen based on the distribution plot of all detected sizes in the analyzed conditions (Figure. 3.13. C). To gain insights into the aggregation state of the condensates, their circularity was measured. Round condensates are indicative of liquid-like structures, while non-round condensates suggest solid aggregate structures.

Analyzing the aspect ratio at the middle plane of cells, I observed that low circular aggregates were more prominent at 24- and 48-hours post-transfection (Figure. 3.13. D), suggesting an increased tendency towards aggregation during the aging process. To further validate the mobility state of the condensates over time, FRAP experiments were performed. The results showed that EGFP-synphilin 1 condensates remained dynamic even at 48 hours post-transfection, but there was a progressive increase in the immobile fraction over time (Figure. 3.13. E).

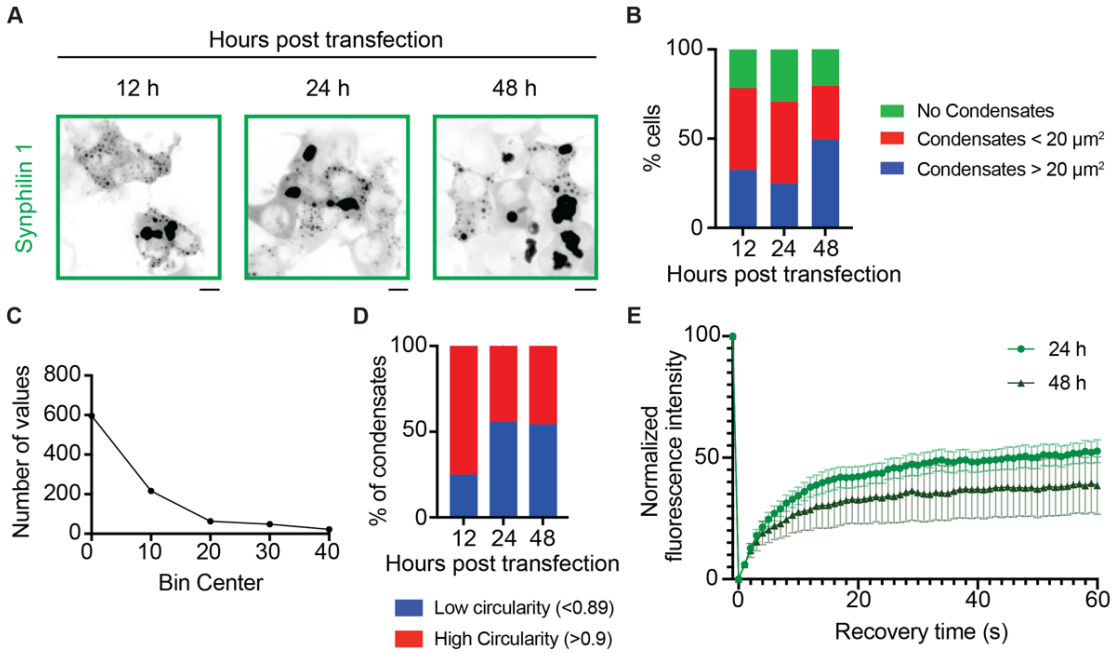


**Figure 3.13. Synphilin 1 condensates progressively age forming solid aggregates.** (A) Representative images of HEK 293 cells transfected with EGFP-synphilin 1 at 12 h, 24 h, and 48 h post-transfection. Z-projection of all cell planes at max intensity projection. Scale bars, 10 µm. (B) Histogram showing that EGFP-synphilin 1 condensates increase their size over time. (C) The distribution plot shows the threshold of EGFP-synphilin 1 condensates. (D) Histogram showing circularity of EGFP-synphilin 1 condensates between low circularity (< 0.89) and high circularity (> 0.9). (E) Recovery after bleaching of EGFP-synphilin 1 at the rim, 24 h, and 48 h post-transfection. Values are represented as average ± standard error if the mean.

Furthermore, EGFP-synphilin 1 and α-synuclein-BFP were ectopically expressed in HEK 293 cells, and confocal images were acquired at 12 hours, 24 hours, and 48 hours after transfection (Figure. 3.14 A). After 12 hours of expression, small condensates formed wherein the two proteins exhibited perfect colocalization, as evidenced by the line profile plot. This indicates that during the initial stages of LBLs formation, the proteins intermingle within the condensates. At 24 hours post-transfection, the LBLs became apparent, displaying a distinct "Core & Shell" organization, which was also observed at the 48-hour time point. Notably, starting from 48 hours after transfection, α-synuclein-BFP fluorescence predominantly localized at the center of LBLs, while EGFP-synphilin 1 appeared to be depleted in the same region. Although the percentage of transfected cells exhibiting co-localizing condensates enriched in both proteins decreased over time, the percentage of cells displaying LBLs increased from 12 hours to 48 hours post-transfection.

In general, the formation of co-localizing condensates and LBLs in transfected cells remains relatively limited, consistently observed in approximately 25% of the total

transfected cells across all time points (Figure. 3.14 B). Analysis of circularity further supports this observation, revealing that condensates appear more liquid-like and highly circular during the early stage (12 hours), while circularity decreases as LBLs form and exhibit lower circularity during the later stages (24 and 48 hours) (Figure. 3.14 C). Relative fluorescence intensity measurements (Figure. 3.14 D) were conducted for EGFP-synphilin 1 and α-synuclein-BFP within the condensates (small dots) and the entire cell (big dots). The results indicate that both proteins tend to converge at the initial nucleation point, resulting in reduced fluorescence intensity throughout the entire cell. This finding supports the notion of a maturation process involving the interaction between synphilin 1 and α-synuclein, where the proteins initially aggregate in droplets that subsequently undergo phase separation to form LBLs. These findings corroborate previous *in vitro* results (Figure. 3.9 A-D). Furthermore, the aging process of LBLs over 24 hours leads to an increased accumulation of α-synuclein in the central core. This suggests that α-synuclein has the ability to translocate from the enriched shell region across the synphilin 1 phase.

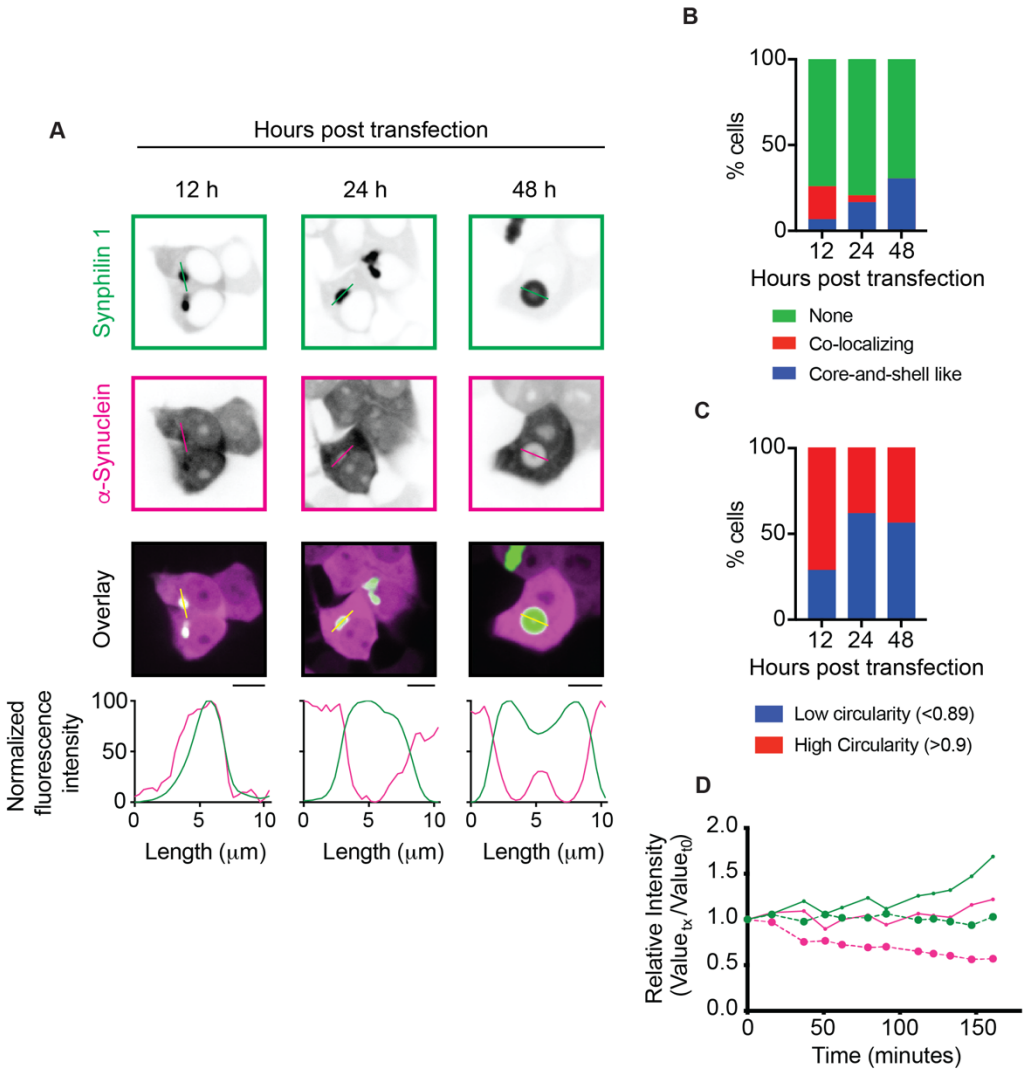

**Figure 3.14. The aging of LBLs leads to the formation of an α-synuclein nucleus.** (A) Representative images of HEK 293 cells transfected with EGFP-synphilin 1 and α-synuclein-BFP at 12 h, 24 h, and 48 h post-transfection. Single plane images. Scale bars, 10 μm. (B) Histogram showing the increase of LBLs appearing over time. (C) Histogram showing circularity of EGFP-synphilin 1 and α-synuclein-BFP condensates between low circularity (< 0.89) and high circularity (> 0.9). (D) The plot of the relative intensity of EGFP-synphilin 1 and α-synuclein-BFP fluorescence inside and outside condensates over time.

FRAP experiments were conducted to investigate the mobility of EGFP-synphilin 1 and α-synuclein-BFP within the shell region of LBLs at different time points of overexpression, specifically at 24 hours and 48 hours. The results of the FRAP experiments indicate that the mobility of EGFP-synphilin 1 (Figure. 3.15 A) and α-synuclein-BFP (Figure. 3.15 B) remains unchanged at both the 24-hour and 48-hour time points following transfection.

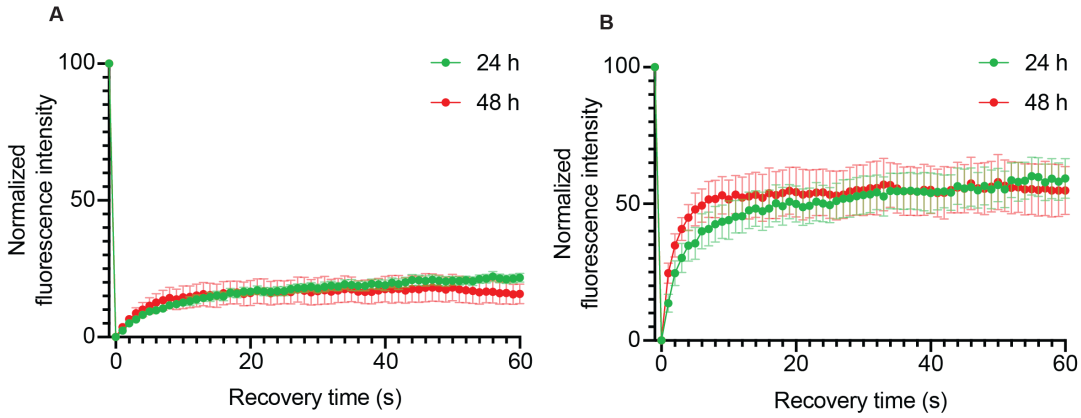


**Figure 3.15. Synphilin 1 and α-synuclein does not change mobility at the shell of LBLs after 48 hours.** (A) Recovery after bleaching of EGFP-synphilin 1 at the rim, 24 h and 48 h post-transfection. Values are represented as average ± standard error if the mean. (B) Recovery after bleaching of α-synuclein-BFP at the rim, 24 h, and 48 h post-transfection. Values are represented as average ± standard error if the mean.

The preceding observations were conducted to probe the characteristics of the multiphasic state observed in aged synphilin 1 and α-synuclein within LBLs. This involved delineating three distinct regions within the LBLs, namely the center, the interspace, and the rim, and subsequently conducting FRAP experiments. EGFP-synphilin 1 exhibited no fluorescence recovery in the center and interspace regions, suggesting that the enriched core of LBLs possesses solid-like properties. Conversely, partial fluorescence recovery was observed in the rim region, aligning with previous findings (Figure. 3.16 A-B). Remarkably, α-synuclein-BFP demonstrated significant fluorescence recovery in all three selected areas, indicating its ability to maintain high mobility through the entire LBLs (Figure. 3.16 C-D).

These results shed light on the distinct characteristics of EGFP-synphilin 1 and α-synuclein-BFP within LBLs. The lack of fluorescence recovery in the core and interspace of LBLs suggests a more rigid and structured arrangement of synphilin 1, while the partial recovery observed in the rim region indicates a less constrained environment. In contrast, the notable fluorescence recovery of α-synuclein-BFP across all three regions highlights its sustained mobility within the entirety of LBLs.

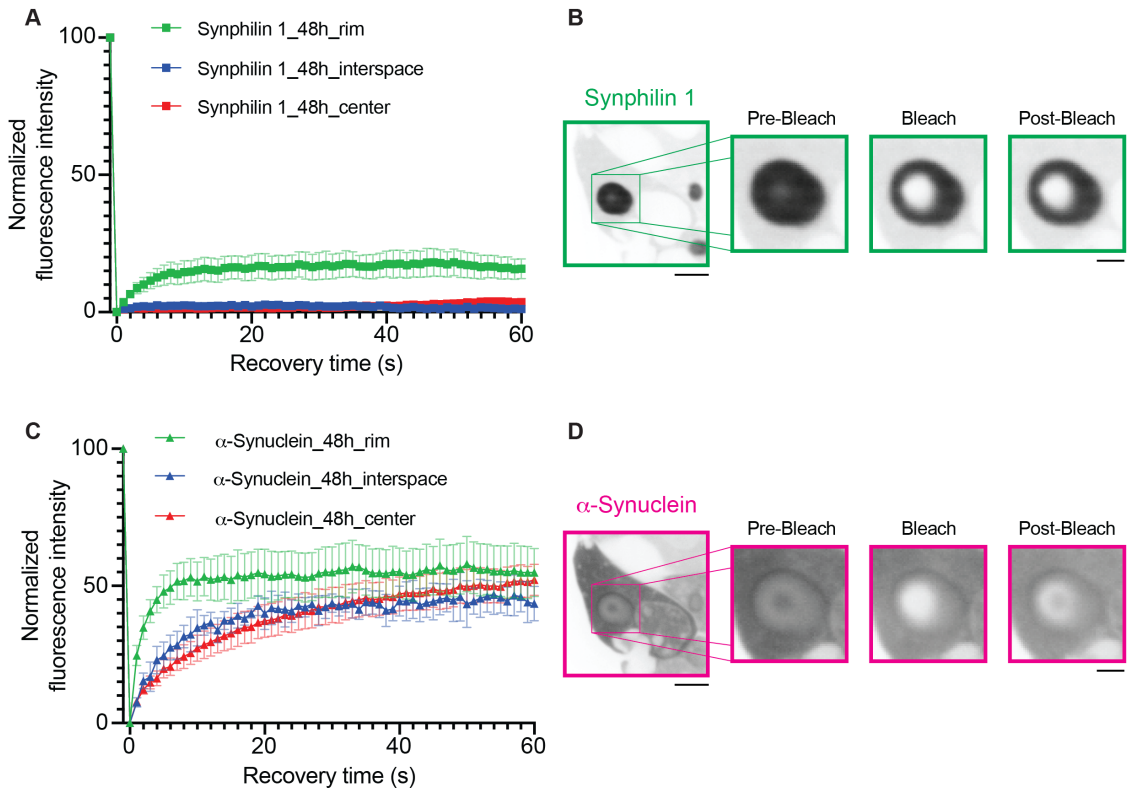


**Figure 3.16. Accumulation of α-synuclein in the center of LBLs is highly mobile.** (A) Recovery after bleaching of EGFP-synphilin 1 at the center, interspace, and rim at 48 hours post-transfection. Values are represented as average ± standard error if the mean. (B) FRAP at the center, interspace, and rim of EGFP-synphilin 1 showing pre-bleach (-1 s), bleaching (0 s), and post-bleaching (60 s). Large image scale bar, 10 μm; magnified images, scale bar 5 μm. (C) Recovery after bleaching of α-synuclein-BFP at the center, interspace, and rim at 48 hours post-transfection. Values are represented as average ± standard error if the mean. (D) FRAP at the center, interspace, and rim of α-synuclein-BFP showing pre-bleach (-1 s), bleaching (0 s), and post-bleaching (60 s). Large image scale bar, 10 μm; magnified images, scale bar 5 μm.

To investigate the interaction mechanism between synphilin 1 and α-synuclein and identify the specific functional domain of α-synuclein involved in driving the formation of LBLs, an alternative approach was employed. Truncated versions of the α-synuclein-BFP wild-type construct were generated for this purpose. Two constructs were cloned: 1) α-synuclein(ΔF)-BFP, which lacks a portion of the amphipathic N-terminal region and the entire central hydrophobic NAC domain (Δ37-94 AA), a domain known to be aggregation-prone and responsible for fibril formation; 2) α-synuclein(ΔC)-BFP, which lacks the C-terminal domain (Δ96-140 AA), including the acidic tail and the fully disordered sequence (Figure. 3.17 A).

Comparisons were made with the classic LBLs observed in the wild-type α-synuclein-BFP construct. Co-expression of EGFP-synphilin 1 and α-synuclein(ΔF)-BFP in HEK 293 cells resulted in the formation of canonical LBLs (Figure. 3.17 B, middle), similar to those observed with the wild-type construct (Figure. 3.17 B, top). On the other hand, co-expression of EGFP-synphilin 1 and α-synuclein(ΔC)-BFP showed only partial de-mixing of the two proteins, with a higher frequency of condensates that were homogenously enriched in both proteins (Figure. 3.17 B, bottom).

These findings indicate that the acidic tail of α-synuclein may play a crucial role in the multiphase organization of LBLs in conjunction with synphilin 1. The results suggest that the N-terminal and central hydrophobic regions of α-synuclein, which are absent in α-synuclein(ΔF)-BFP, are not essential for driving the formation of canonical LBLs. However, the C-terminal domain, including the acidic tail, is implicated in the proper phase separation and organization of LBLs when interacting with synphilin 1.

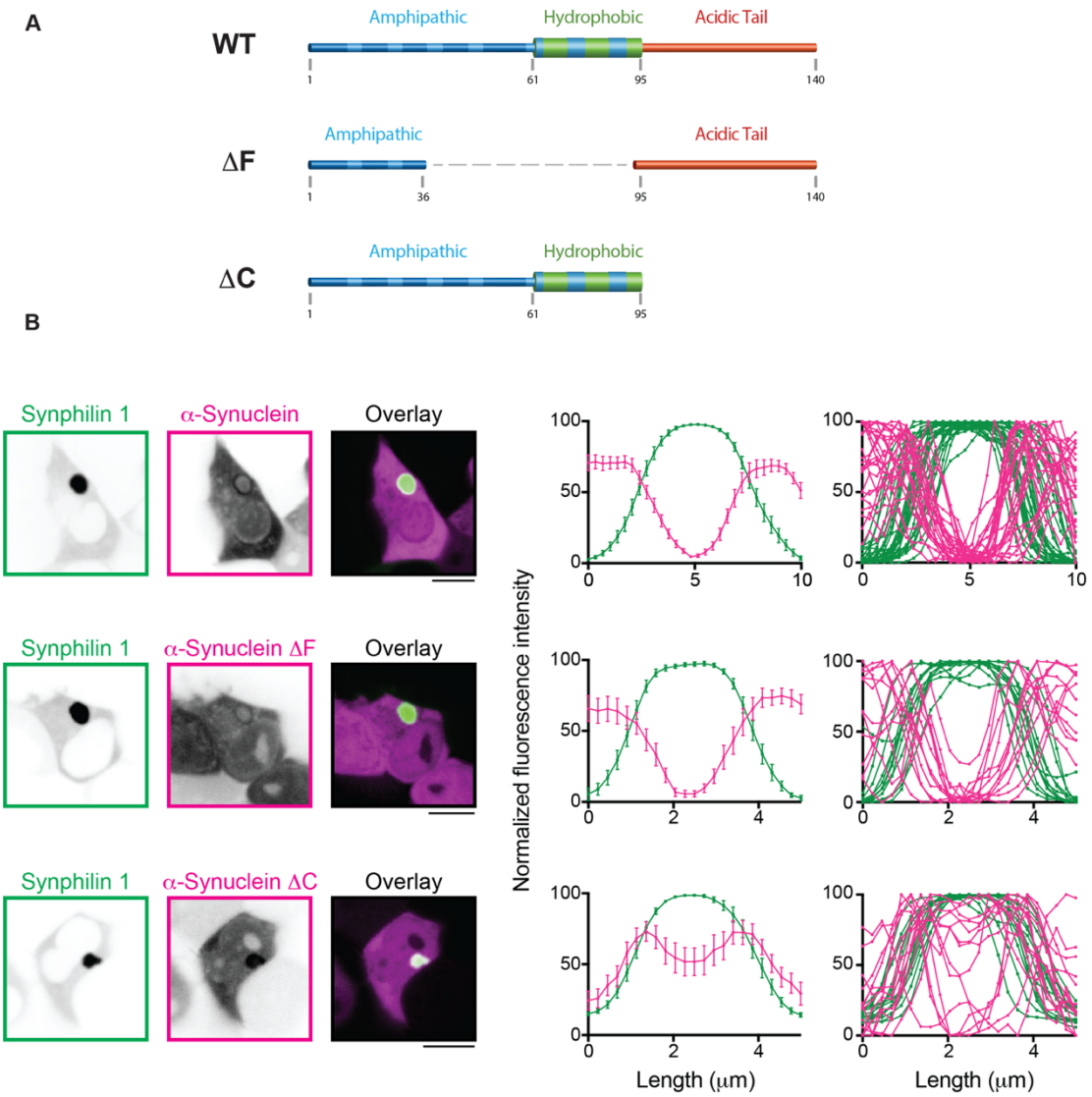


**Figure 3.17. The C-terminal acidic tail of α-synuclein is fundamental for the formation of LBLs.** (A) Cartoon representation for the truncated versions of α-synuclein (ΔF and ΔC) and its wild-type form (WT). (B) Representative images of HEK 293 cells co-transfected with EGFP-synphilin 1 and truncated version of α-synuclein (ΔF and ΔC) compared with the wild-type form (WT). The line profiles graph displays appearing of LBLs for WT and ΔF, but only a partial de-mix of proteins for ΔC. Values are represented as average ± standard error if the mean (left) or as single measurements (right). Scale bars, 10 μm.

Various single-point mutations associated with the genetic onset of PD have been identified as having an impact on the aggregation behavior of α-synuclein. To investigate whether these mutated versions of α-synuclein can influence the architecture of reconstituted LBLs in experimental system, I generated several α-synuclein-BFP mutants (A30P, A53T, S129A, and S129E) (Figure. 3.18 A) and co-transfected them with EGFP-synphilin 1.

The resulting LBLs exhibited a preserved "Core & Shell" structure, with distinct regions of enrichment. However, in the presence of the A30P mutation, there was a noticeable alteration in the inner depletion of α-synuclein within the core of the condensate (Figure. 3.18 B). This mutation disrupted the typical pattern of reduced α-synuclein accumulation in the core observed in the wild-type LBLs.

These findings suggest that the A30P mutation in α-synuclein can influence the organization and composition of LBLs, potentially altering the interaction dynamics between synphilin 1 and α-synuclein. It highlights the importance of specific mutations in α-synuclein in modulating the architecture of LBLs and provides further insight into the role of genetic variants in the pathogenesis of PD (Figure. 3.18 A-B).

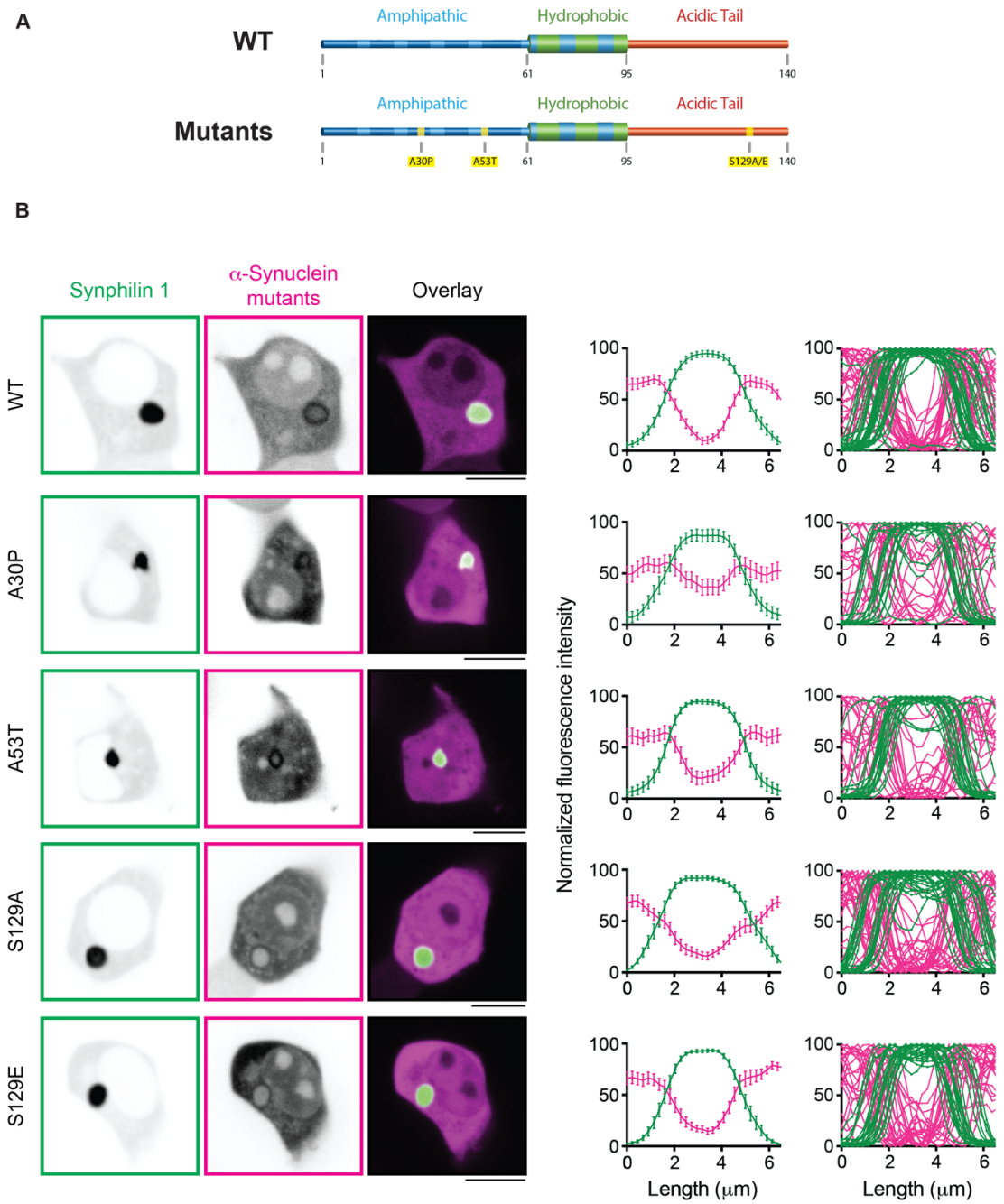


**Figure 3.18. α-Synuclein A30P leads to miss-localization α-synuclein in the core of LBLs.** (A) Cartoon representation for the mutated versions of α-synuclein (A30P, A53T, S129A, and S129E) and its wild-type form (WT). (B) Representative images of HEK 293 cells co-transfected with EGFP-synphilin 1 and mutated version of α-synuclein (A30P, A53T, S129A, and S129E) compared with the wild-type form (WT). The line profiles graph displays only a partial de-mix of α-synuclein(A30P) in the core of LBLs. Values are represented as average ± standard error if the mean (left) or as single measurements (right). Scale bars, 10 μm.

## 3.4. Lewy body-like structures disrupt intracellular organelles

An important characteristic of LBs in PD patients is their ability to sequester membrane organelles in their vicinity. To investigate whether this feature is also present in our reconstituted LBLs, I conducted experiments using FM4-64 staining on HEK 293 cells expressing either EGFP-synphilin 1 alone or co-expressing EGFP-synphilin 1 and α-synuclein-BFP to detect membrane infiltration (Figure. 3.19).

Upon analysis, it was observed that the synphilin 1 condensates and the reconstituted LBLs exhibited local enrichment in lipids at the periphery of the condensates, indicating membrane infiltration (Figure. 3.19 A-B). These lipids were found to be widely distributed and co-localized with mCherry-synapsin 1/synaptophysin condensates, which served as a control. The presence of lipids in these regions is indicative of the sequestration of synaptic vesicles (SVs) at the presynaptic space, as synaptophysin directly binds to lipids. This control experiment confirms the ability of our reconstituted LBLs to recapitulate the sequestering of membrane organelles, similar to the physiological process observed in PD-associated LBs (Figure. 3.19C).

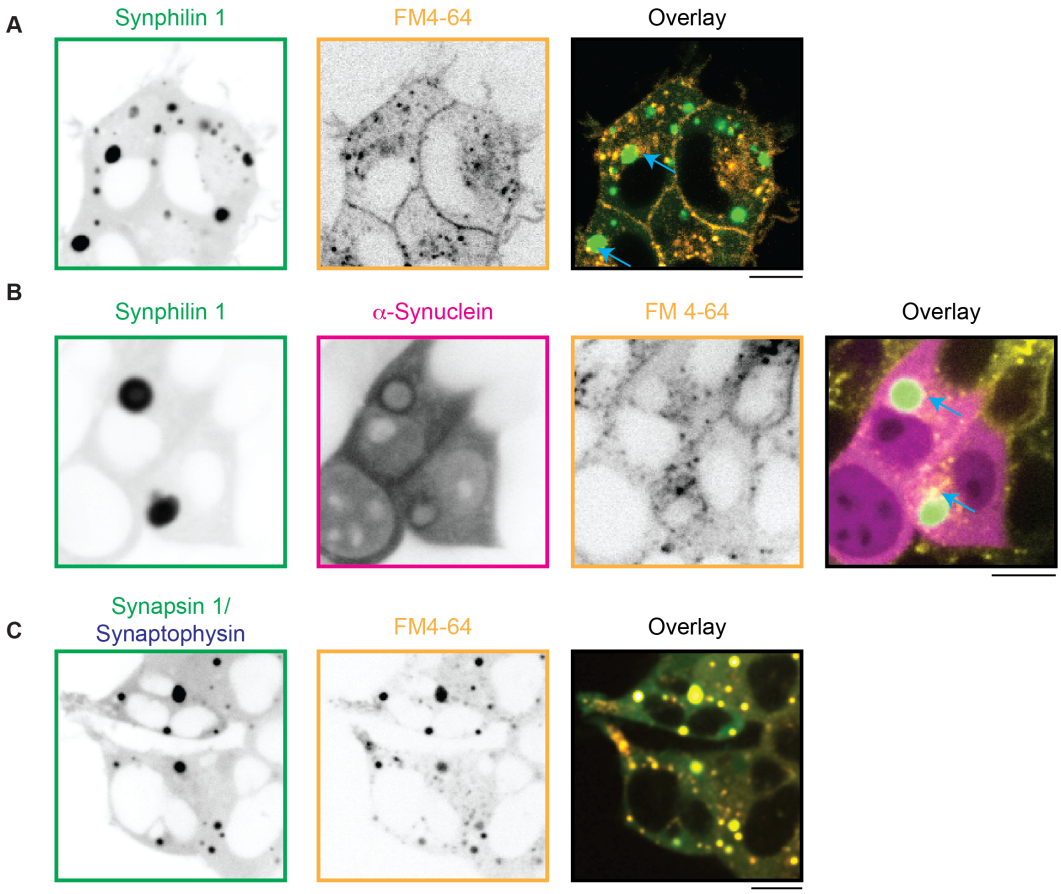

**Figure 3.19. Membrane infiltration occurs in correspondence with synphilin 1 condensates and LBLs.** Representative images of cells expressing mCherry-synapsin 1 and synaptophysin (A), only EGFP-synphilin 1 (B) or EGFP-synphilin 1 and α-synuclein-BFP (C) incubated with FM4-64 for 30 minutes before imaging. Scale bars, 10 μm.

In order to investigate the potential interactions between synphilin 1 condensates and LBLs with specific membrane organelles, I conducted experiments using lysotracker-647 and mitotracker-647 on HEK 293 cells expressing either EGFP-synphilin 1 alone or co-expressing EGFP-synphilin 1 and α-synuclein-BFP. The lysotracker-647 staining was used to detect the accumulation of lysosomes (Figure. 3.20 A). Interestingly, while lysosomes did not appear to localize with synphilin 1 condensates (Figure. 3.20 A, top), synphilin 1/α-synuclein co-expression (Figure. 3.20 A, middle), or synapsin 1/synaptophysin condensates (Figure. 3.20 A, bottom), there was a clear proximity of mitochondria observed in all of these conditions. To investigate the accumulation and proximity of mitochondria, mitotracker-647 staining was employed (Figure. 3.20 B). Notably, mitochondria were found to be in close proximity to synphilin 1 condensates and synapsin 1/synaptophysin condensates (Figure. 3.20 B, top and bottom), but they appeared to be in even closer association with the LBLs (Figure. 3.20 B, middle). Moreover, a morphological evaluation revealed that in the presence of LBLs, mitochondria appeared fragmented and exhibited signs of reduced health compared to the other conditions.

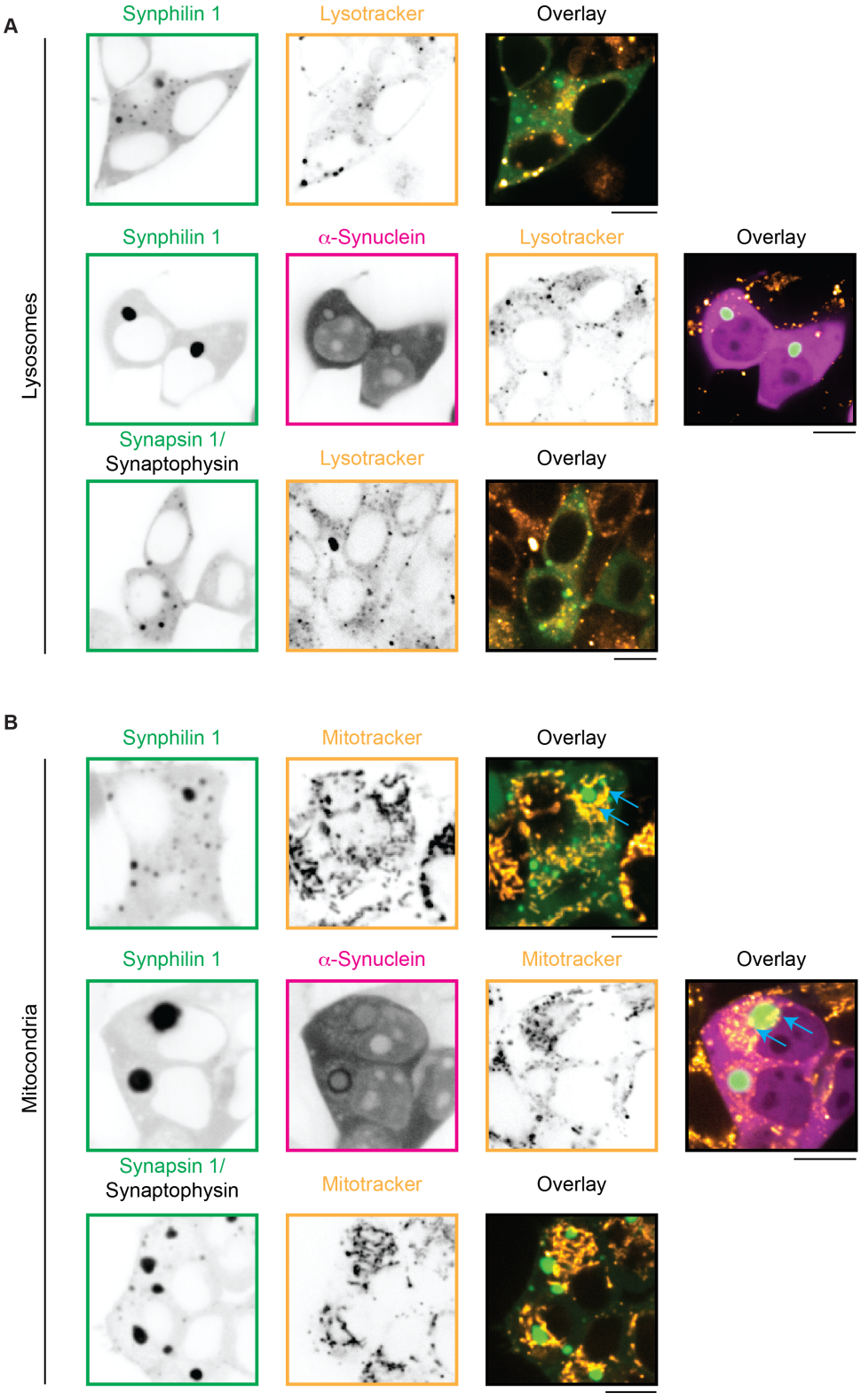


**Figure 3.20. Mitochondria but not lysosomes accumulate in the vicinity of synphilin 1 condensate and LBLs.** (A) Representative images of cells expressing mCherry-synapsin 1 and synaptophysin, EGFP-synphilin 1 or EGFP-synphilin 1 and α-synuclein-BFP incubated with Lysotracker-647 for 30 minutes before imaging. Scale bars, 10 µm. (B) Representative images of cells expressing mCherry-synapsin 1 and synaptophysin, EGFP-synphilin 1 or EGFP-synphilin 1 and α-synuclein-BFP incubated with Mitotracker-647 for 30 minutes before imaging. Scale bars, 10 µm.

Based on the previous observation that mitochondria accumulate at the surface of LBLs, my focus was to investigate the involvement of the cytoskeleton in this process. Initially, I aimed to determine if any specific cytoskeletal component directly interacts with LBLs. To achieve this, I co-transfected HEK 293 cells with EGFP-synphilin 1 and α-synuclein-BFP, which mimic the characteristics of LBLs. Subsequently, we incubated the cells with either Sir-Actin or Sir-Tubulin dyes for a duration of 30 minutes before conducting live cell imaging (Figure 3.21 A, D).

By monitoring the maturation of the condensates over time and capturing images every 10 minutes, we observed that actin progressively accumulates at the LBLs, reaching a plateau after 40 minutes of imaging, as quantified in the intensity plot and observed in the corresponding magnified images (Figure 3.21 B, C). Importantly, this enrichment is specific to actin, as tubulin is excluded by the LBLs, with its presence limited to the immediate vicinity of the condensates. Moreover, tubulin does not exhibit an increase in signal intensity, as quantified in the plot and depicted in the time-lapse images (Figure 3.21 E, F). Notably, the initial formation of condensates appears to be independent of actin enrichment, as the actin signal is negligible within the condensates at the initial stage of 16 hours post-transfection (Figure 3.21 G).

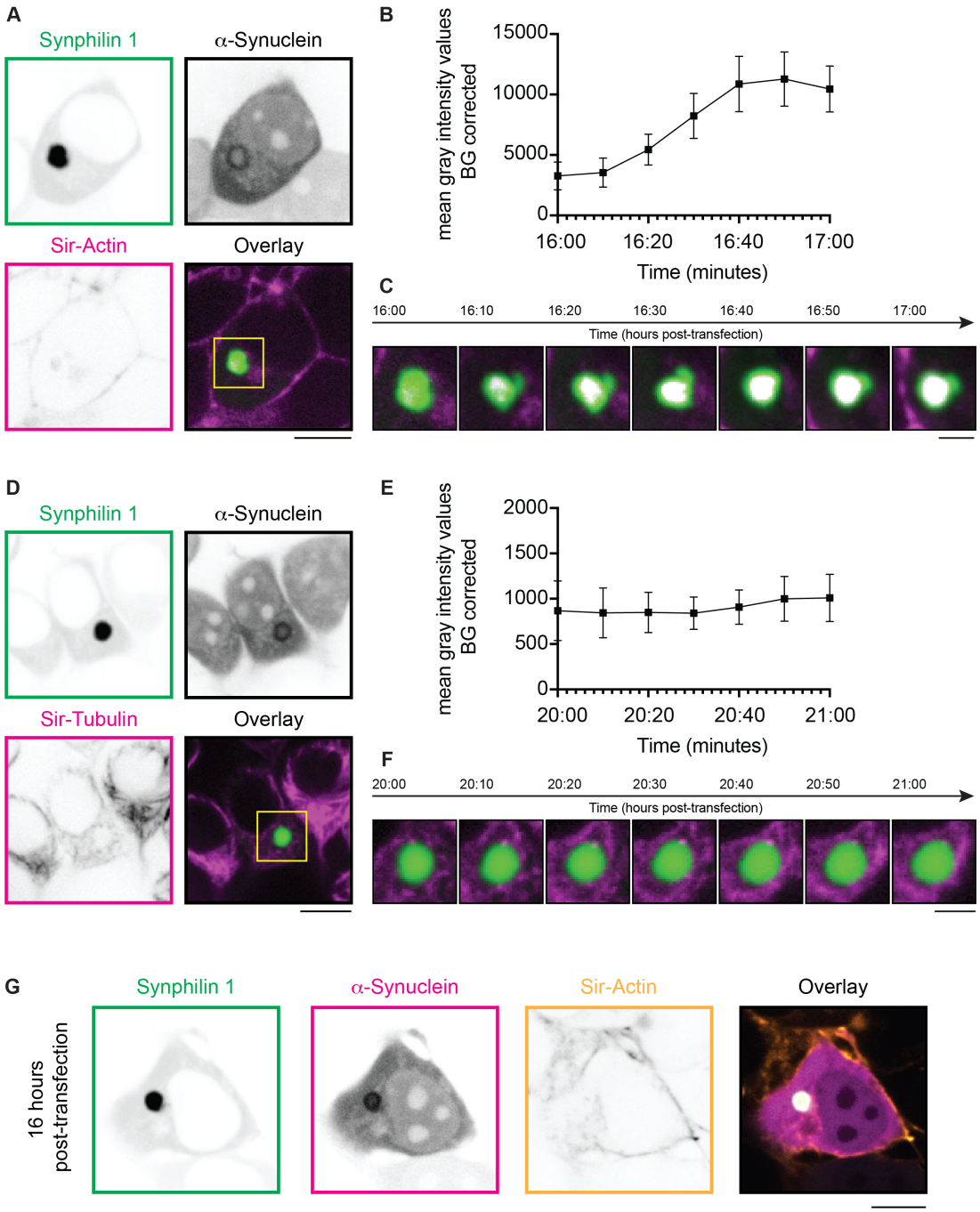


**Figure 3.21. Cytosolic actin, but not tubulin enriches LBLs.** (A) Representative images of cells expressing EGFP-synphilin 1 and α-synuclein-BFP 16 hours post-transfection showing EGFP-Synphilin in green; Sir-Actin in magenta; α-synuclein is not shown in overlay for clarity in the overlay. Highlighted condensate (yellow square) is magnified in C. Scale bar, 10 µm. (B) Quantification of Sir-Actin signal inside the condensates (three independent experiments fifteen condensates analyzed). Note the enrichment of actin signal inside the condensate. (C) Live-cell imaging demonstrates Sir-Actin enrichment inside the condensates. Scale bar, 5 µm. (D) Representative images of cells expressing EGFP-synphilin 1 and α-synuclein-BFP 20 hours post-transfection, showing EGFP-Synphilin in green; Sir-Tubulin in magenta; α-synuclein is not shown for clarity in the overlay. Highlighted condensate (yellow square) is magnified in F. Scale bar, 10 µm. (E) Quantification of Sir-Tubulin signal inside the condensates (three independent experiments fifteen condensates analyzed). Note the steady level (i.e., the absence) of Sir-Tubulin signal inside the condensates. (F) Live-cell imaging indicates no accumulation of Sir-Tubulin inside the condensates. Scale bar, 5 µm. (G) Representative images of cells expressing EGFP-synphilin 1 and α-synuclein-BFP 16 hours post-transfection, and incubated with Sir-Actin for 30 min before imaging showing no enrichment of actin at this early stage. Scale bar, 10 µm.

In light of the strong association between actin and mitochondria, I aimed to investigate the role of actin in the observed accumulation and fragmentation of mitochondria in the LBLs proximity, observed in the previous experiments. In fact, actin filaments are known to provide structural support and facilitate the movement of mitochondria within the cytoplasm (Moore et al., 2021). Moreover, actin has been implicated in regulating mitochondrial fission and fusion processes, which are crucial for maintaining mitochondrial morphology and function (Moore et al., 2016). In order to visualize mitochondria and actin dynamic, I conducted an experiment in which SPY-Actin and MitoTracker-647 dyes were incubated in HEK 293 cells co-expressing EGFP-synphilin 1 and α-synuclein allowing the formation of LBLs.

Analysis of the collected images revealed a clear disruption of the mitochondrial network upon sequestration of the actin cytoskeleton within the LBLs, resulting in fragmented mitochondria (Figure 3.22 A). Line profiles were utilized to visualize the overlap between the actin signal and the LBLs (Figure 3.22 B), as well as the close accumulation of fragmented mitochondria at the surface of these abnormal condensates (Figure 3.22 C). Multiple examples were collected and analyzed from independent replicates, demonstrating varying degrees of mitochondrial disruption and accumulation, as highlighted by the light blue arrows (Figure 3.22 D).

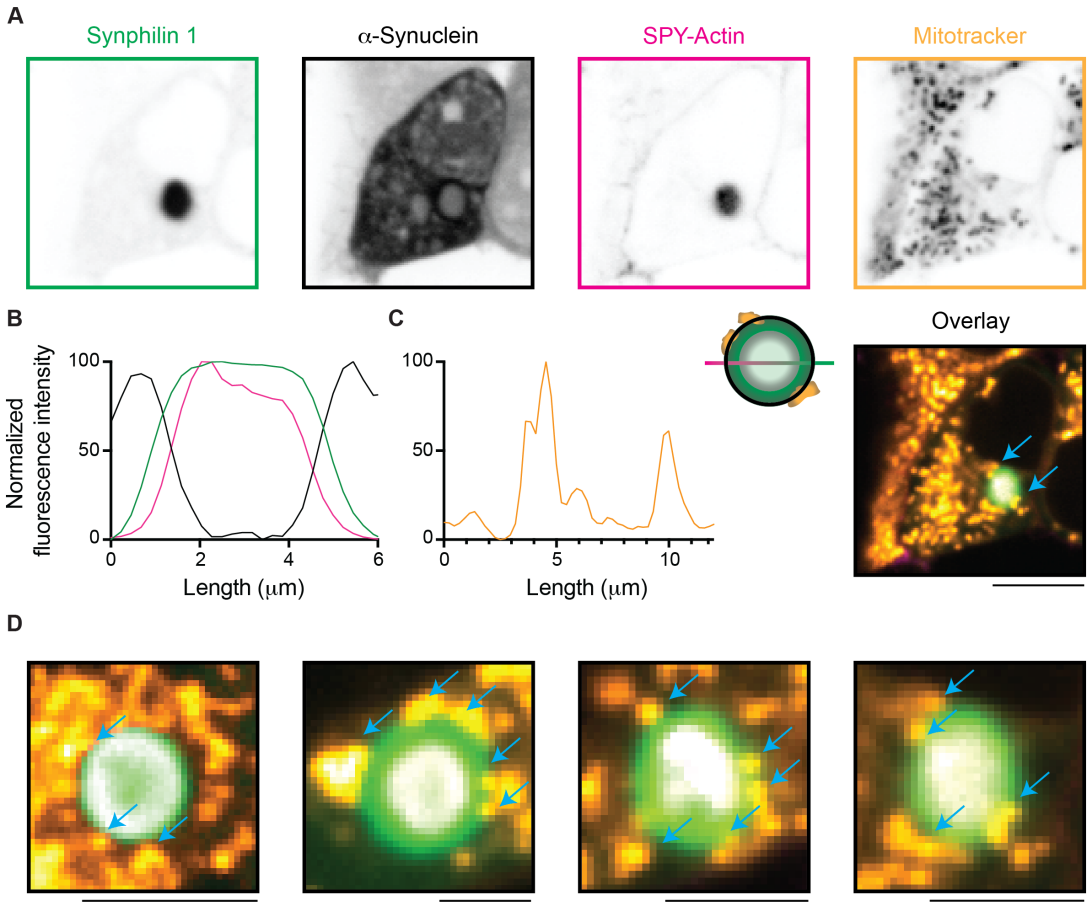


**Figure 3.22. LBLs sequester cytosolic actin causing the accumulation and disruption of mitochondria in the vicinity of condensates.** (A) Representative images of cells expressing EGFP-Synphilin 1 and α-synuclein-BFP, 24 hours post-transfection and incubated with SPY555-actin and mitotracker in far-red. Scale bar, 10 μm. (B) Line profile indicates the enrichment of SPY555-actin (magenta line) signal inside the condensate (synphilin, green line) and α-synuclein (black line) accumulating at the surface. (C) Line profile indicates the accumulation of mitochondria (orange line) at the interface of the condensate. (D) Four representative condensates, each from a separate experiment, of cells expressing LBLs (green, EGFP-synphilin 1) and incubated with mitotracker far-red (orange) and SPY555-actin (white in overlay). Scale bars, 2 μm.

# 4. DISCUSSION

Throughout the work presented in my thesis, I focused on understanding how α-synuclein affects condensates in the physiology and the pathology of synucleinopathies. In the first part, I show that a condensate of synapsin 1 can recruit α-synuclein affecting the maintenance of the SVs. Using heterologous cell systems and *in vitro* assays, I investigated the mobility in condensates and the role of the physiological molar ratio of these proteins to ensure the proper architecture of the SV clusters. In the second part of my thesis, I investigated how LLPS of α-synuclein may represent a starting point for the formation of protein condensates and organelle inclusions. My data show that overexpression of synphilin 1, another synaptic protein implicated in PD, leads to the aberrant phase separation forming an inclusion that is enriched with α-synuclein. These structures were morphologically reminiscent of LB inclusions in PD patients. I also analyzed which functional domains of α-synuclein are necessary to drive the formation of these LBLs and which pathology-related mutations in α-synuclein gene can influence the stability of these condensates. Employing heterologous cell systems and *in vitro* assays, I first described the LLPS features of LBLs and demonstrated their ability for membranous infiltration and mitochondria sequestering.

### 4.1. Synapsin/SV condensates recruit α-synuclein

Building upon the previously described characteristics of synapsin 1 to undergo LLPS and serve as a crucial regulator in maintaining the pool SVs (Milovanovic et al., 2018), I sought to understand how α-synuclein, another pivotal protein involved in the SV cycle, affects this process. The findings presented in this thesis demonstrate the ability of α-synuclein to undergo LLPS in the presence of synapsin 1 at physiological concentration. The low-affinity interaction between these two proteins represents an example of a liquid phase, as confirmed for example by the assay utilizing aliphatic alcohols. The underlying mechanism for these multivalent low-affinity interactions can be attributed to the electrostatic interactions between the positively charged C-terminal of synapsin 1, characterized by a pI of around 10, and the highly negatively charged tail of α-synuclein. Indeed, electrostatic interactions have been previously reported as a key mechanism also for interactions of other proteins undergoing LLPS (Kim et al., 2021; Boyko et al., 2019). Furthermore, the highly intrinsically disordered nature of these domains enhances the

accessibility and exposure of charged residues, thereby enabling the occurrence of low-affinity interactions. The lack of well-defined secondary or tertiary structures in these protein domains allows for increased flexibility and dynamics, leading to the exposure of charged amino acids.

Given the densely packed nature of the presynapse, it is reasonable to propose that additional multivalent low-affinity interactions contribute to the condensation of synaptic SVs in physiological cellular conditions (Li et al., 2012). Synaptobrevin 2, an integral protein of SVs known to interact with α-synuclein, represents one potential candidate (Diao et al., 2013; Sun et al., 2019). While α-synuclein and synaptobrevin 2 may play a role in promoting SV clustering (Diao et al., 2013), their presence alone is insufficient to induce mesoscale condensation of native SVs. Notably, neutral liposomes do not significantly impact condensation, but the acidity of SVs has been identified as a critical factor in the synapsin/lipid vesicle condensation (Milovanovic et al., 2018). The affinity of α-synuclein for negatively charged phospholipids is likely essential for the localized enrichment of α-synuclein within synapsin/SV condensates. Collectively, these findings support the notion that multiple multivalent low-affinity interactions, including the interactions between α-synuclein, synaptobrevin 2, and the acidic phospholipids of SVs, contribute to the formation and maintenance of synapsin-associated condensates within the SV cluster in physiological cellular environments.

Based on my results, synapsin 1 condensates have been found to recruit α-synuclein, and within these condensates, α-synuclein exhibits high mobility (Hoffmann and Sansevrino, 2021). The formation of these condensates is dependent on the presence and abundance of synapsin 1, suggesting that synapsin 1 functions as an essential scaffold for the transient recruitment of α-synuclein. The implication of these findings is that synapsin/SV condensates at nerve terminals have the ability to spatially concentrate α-synuclein. This observation aligns with the concept that SV clusters serve as a buffer for synaptic proteins, including α-synuclein (Shupliakov, 2009; Denker et al., 2011; Reshetniak et al., 2020). The spatial enrichment of α-synuclein within these condensates suggests its influence on the physiological functions and interactions with other synaptic components.

Indeed, it has been observed that upon stimulation, the dispersion of synapsin/SV condensates leads to the transient release of enriched proteins, including α-synuclein (Chi et

al., 2001). Subsequently, these released proteins have the ability to translocate to the plasma membrane, where they can exert their effects on various cellular processes. Specifically, α-synuclein has been shown to enhance endocytosis and SV recycling, thereby modulating synaptic transmission and neurotransmitter release (Vargas et al., 2014; Medeiros et al., 2017). This suggests that the formation of synapsin/SV condensate may represent a mechanism of local spatial enrichment of α-synuclein which ultimately plays a role in facilitating the dynamic recruitment and redistribution of α-synuclein, impacting synaptic function and vesicle recycling processes.

*In vitro* experiments described in this thesis utilizing isolated SVs provide evidence that SVs serve as triggers for the phase separation of synapsin 1. Specifically, the presence of SVs enhances the condensation process of synapsin/α-synuclein complexes since it has been observed that under physiological salt concentrations, α-synuclein alone does not have the ability to induce phase separation of native SVs that have been purified from rat brains. However, when SVs are present, they facilitate and accelerate the phase separation of synapsin/α-synuclein complexes. This suggests that SVs play a critical role in initiating and promoting the condensation of synapsin in the presence of α-synuclein, emphasizing the importance of SVs in modulating the phase separation behavior of these proteins.

Although it has been established that α-synuclein exhibits binding affinity towards small, acidic lipid vesicles (Georgieva et al., 2008; Bodner et al., 2009; Middleton and Rhoades, 2010; Diao et al., 2013) as well as SVs (Perego et al., 2020; Lautenschläger et al., 2018; Wang et al., 2014), the current findings demonstrate that α-synuclein alone, at physiological concentrations, does not induce LLPS of native SVs. However, under these protein and salt concentration conditions, the presence of vesicles promotes the formation of synapsin/α-synuclein condensates. Notably, the absence of any crowding reagent and the utilization of a concentration at which synapsin 1 does not undergo phase separation, combined with the physiological ratio of α-synuclein, highlights how SVs act as triggers for the phase separation process.

### 4.2. The molar ratio of synapsin 1/α-synuclein is important for maintaining the packing density of SV clusters

High local concentrations, along with valency and weak interactions, have all been recognized as crucial factors driving the process of phase separation (Li et al., 2012; Berry et al., 2018). In line with this, both synapsins and α-synuclein are highly concentrated at the neuro terminal, with estimated concentrations of approximately 120 μM and 50 μM, respectively (Wilhelm et al., 2014). Indeed, from the experiments in this thesis, it is evident that SVs condensation was sensitive to the concentration of both proteins. The crucial role of specific concentrations of synapsin 1 and α-synuclein in maintaining the liquid phase is highlighted by *in situ* experiments involving genetic deletions of either synapsins or synucleins. When all synapsins are deleted in cultured hippocampal neurons, SVs disperse away from the active zone without a reduction in their overall number (Milovanovic and De Camilli, 2017). This observation indicates that synapsin 1 serves as a scaffold protein essential for SV clustering. In contrast, the deletion of all synucleins leads to a tightly packed arrangement of SVs, forming a nearly crystalline structure (Vargas et al., 2017). These findings suggest that maintaining a balance between the functions of synapsin 1 and α-synuclein is critical in ensuring the proper fluidity required for SV clustering and supporting their efficient localization and release at the synapse (summarized in a scheme in Figure 4.1).

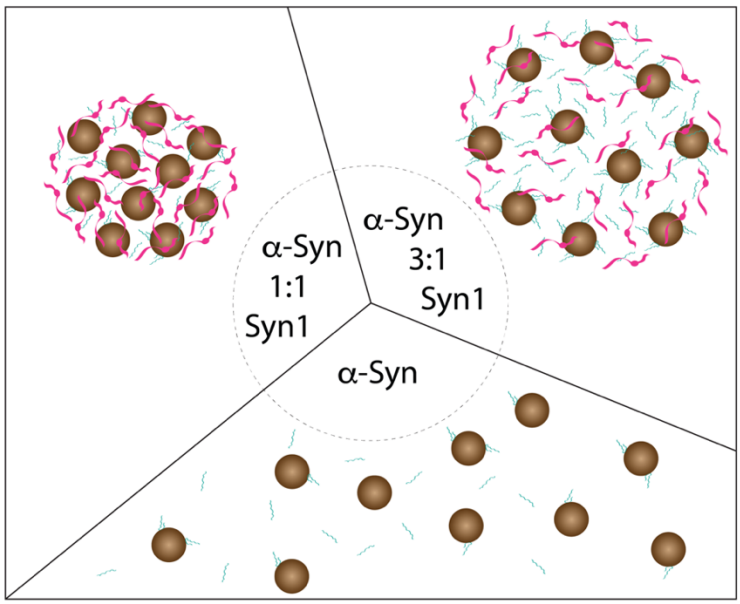


**FIGURE 4.1. Proposed model of the synapsin/SVs condensation in different molar ratios of α-synuclein.** α-synuclein-to-synapsin 1, 1:1 (left), and 3:1 (right), or in absence of synapsin 1 (bottom). Synapsin 1 molecules are represented in magenta, α-synuclein molecules are represented in turquoise and SVs are represented as brown spheres. Modified from Hoffmann, Sansevrino, et al., 2021.

In a series of *in vitro* assay, purified SVs were utilized, incorporating them at a physiological molar ratio of 3:1 or an equimolar ratio of 1:1 between synapsin 1 and α-synuclein (Hoffmann and Sansevrino, 2021). The experimental data clearly demonstrated a rapid rate of condensation, indicating the successful formation of functional biomolecular condensates. Conversely, when an excess molar ratio of α-synuclein is introduced, the formation of synapsin/SV condensates is delayed. These findings unveil that an elevated concentration of α-synuclein hampers the kinetics of native SV condensation, underscoring the importance of maintaining a precise balance between synapsin 1 and α-synuclein for the proper architecture and maintenance of SV clusters. The observed results emphasize the dynamic interplay between these two proteins and their impact on the organization and functionality of SVs, providing valuable insights into the molecular mechanisms governing synaptic vesicle dynamics.

### 4.3. Aberrant LLPS can represent an initial stage for α-synuclein aggregation

Recent studies have highlighted that α-synuclein undergoes LLPS to facilitate amyloid aggregation (Hardenberg et al., 2021; Ray et al., 2020). Phase separation of α-synuclein has been recognized as an initiating step for amyloid transition through seeding and nucleation processes (Xu et al., 2022; Stender et al., 2021). During LLPS, α-synuclein becomes concentrated in condensates, accelerating conformational changes and promoting amyloid formation (Wegmann et al., 2018; Pytowski et al., 2020; Xing et al., 2021). In the presented thesis, a multi-phase liquid system involving α-synuclein and its interacting partner synphilin 1 was investigated, resembling Lewy body-like structures (LBLs) observed in both cellular and *in vitro* contexts.

Notably, my data indicate that synphilin 1 alone can undergo LLPS, exhibiting characteristic features of phase-separating proteins such as the formation of spherical droplets, high fluorescence recovery after photobleaching, and dynamic fusion and fission events between droplets. The progressive accumulation and aberrant phase transition of synphilin 1 led to the sequestration of α-synuclein at the periphery of synphilin 1 condensates, significantly impairing its mobility. This experimental evidence indicates that α-synuclein enhances the insoluble fraction of synphilin 1 condensate, thereby promoting the formation of solid-like aggregates.

Multiple parameters and environmental factors can significantly impact the rate of protein aggregation. For instance, mildly acidic pH conditions have been shown to enhance the process of secondary nucleation, contributing to accelerated protein aggregation (Peduzzo et al., 2020; Buell et al., 2014). Additionally, ionic strength plays a crucial role in the aggregation of α-synuclein, with optimal fibrillation occurring at moderate NaCl concentrations (Ramis et al., 2020; Ziaunys et al., 2021). Supporting this, the data presented in this study indicates that a higher salt concentration (300 mM NaCl) leads to increased condensation of α-synuclein around the synphilin 1 core, suggesting that the interaction between these two proteins is primarily regulated by ionic interactions.

Furthermore, the maturation of protein condensates also influences the transition from a liquid to a solid state. In the cell experiments conducted here, the liquid condensates exhibited an increased propensity to form solid-like structures over time, as evidenced by a decreasing circularity value. Specifically, in cells expressing both synphilin 1 and α-synuclein, a progressive de-mixing of the components occurred, highlighting that time course is necessary for the formation of LBLs. Indeed, the analyzed early time point showed α-synuclein colocalizing homogeneously within the condensates suggesting a more dynamic fluid nature. From this data can be speculated that the gradual accumulation of α-synuclein, as observed in various instances of gene duplication and triplication associated with PD, can disrupt the dynamic equilibrium within liquid condensates, leading to an uncontrolled process of aggregation. This dysregulation can ultimately result in the sequestration of α-synuclein within the shell of these formed LBLs. The excessive accumulation of α-synuclein may perturb the normal interactions and balance of components within the condensates, causing a shift towards more solid-like aggregates and impairing the fluidity of the system. This disrupted equilibrium may contribute to the pathogenic mechanisms underlying α-synuclein aggregation and the formation of proteinaceous inclusions characteristic of PD. This implies that temporal factors are crucial for the maturation and stabilization of LBLs, leading to the emergence of more solid-like aggregates.

Previous studies on the kinetics of in vitro protein aggregation have revealed the existence of a conserved fibrillization pathway. This pathway is characterized by the sequential formation of organized prefibrillar aggregates exhibiting a wide range of morphologies. These aggregates, known as protofibrils, represent intermediate stages in the process of fibrillization and ultimately give rise to mature insoluble fibrils (Figure 4.2., top).

Protofibrils, initially discovered in studies on amyloid beta, have been found to be present in the aggregation process of various proteins (Harper and Lansbury, 1997; Walsh et al., 1999; Bucciantini et al., 2002). These intermediate aggregates, which typically consist of 15-40 monomers, exhibit a spherical morphology (Harper et al., 1999; Lashuel et al., 2002). Importantly, these distinct phases of aggregation have been shown to exhibit varying degrees of toxicity (Conway et al., 2000; Harper et al., 1999; Poirier et al., 2002). These spherical protofibrils then undergo annealing processes, leading to the formation of chainlike protofibrils (Nichols et al., 2002). Subsequently, these chainlike protofibrils can further evolve into annular or pore-like species, as well as mature amyloid fibrils (Ding et al., 2002; Lashuel et al., 2002). In the case of α-synuclein, in vitro fibrillization also follows a similar pattern, starting with the formation of spherical protofibrils, which rapidly progress into chainlike protofibrils before ultimately maturing into fibrils (Caughey and Lansbury, 2003).

In this thesis, I showed how LLPS is emerging as a step toward protein aggregation (Figure 4.2., bottom). When proteins phase separate and form droplets, they can concentrate to higher levels than they would normally do in a homogeneous solution, which can facilitate the formation of protein aggregates (Aguzzi and Altmeyer, 2016). Many neurodegenerative diseases such as amyotrophic lateral sclerosis (ALS), and frontotemporal dementia (FTD) have all been shown to have dysregulation of protein phase separation (Chou et al., 2018; Marrone et al., 2019). Various factors can contribute to the atypical condensation of proteins, such as mutations in genes encoding phase-separated proteins, compromised protein quality control mechanisms, and damage to cellular transportation networks. In particular, the aberrant phase transition of FUS, a protein associated with ALS, whether in its wild-type or mutant form, has been shown to result in the formation of insoluble aggregates during aging (Patel et al., 2015). Additionally, these aggregates have been found to sequester organelles such as lysosomes (Trnka et al., 2021) further highlighting the disruptive effects of aberrant protein condensation on cellular processes.

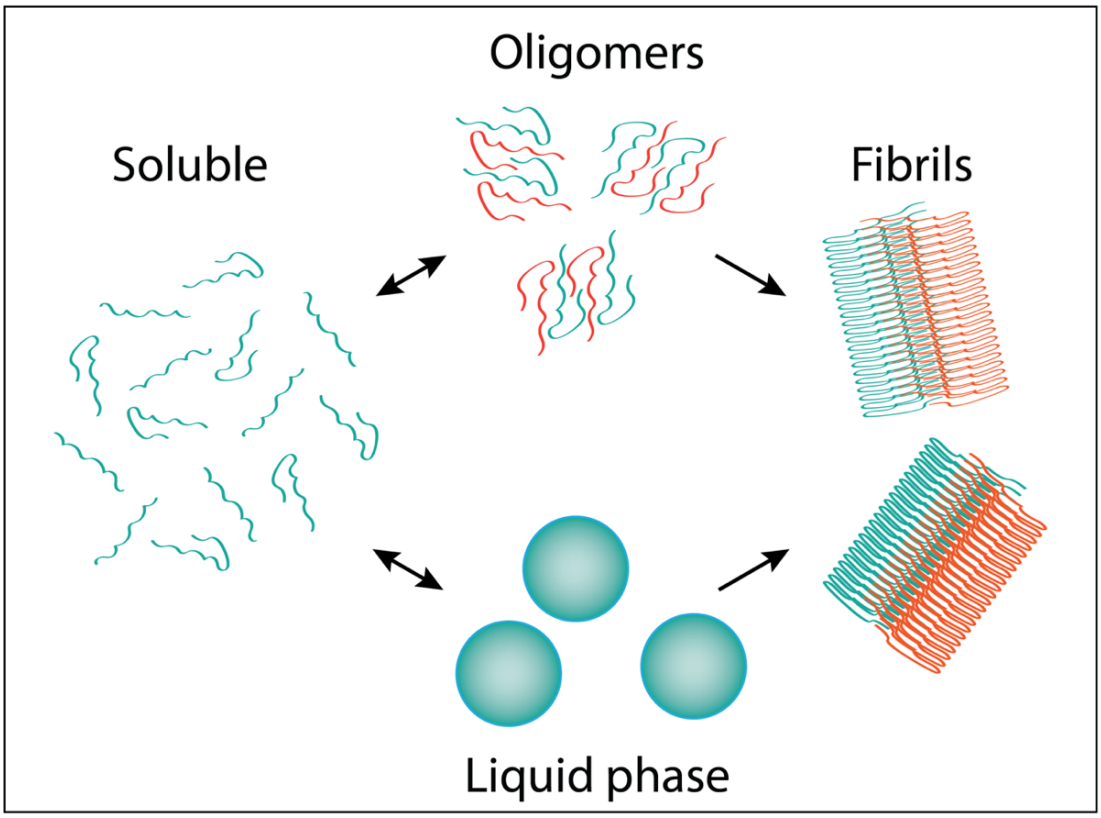


**FIGURE 4.2. Schematic representation of two coexisting pathways that could lead to a higher degree of aggregation through either oligomerization (top) or liquid-liquid phase separation (bottom).**

### 4.4. Acidic tail of α-synuclein is important for the demixing of synuclein from synphilin 1 condensate

While the interacting domain of synphilin 1 has been extensively studied and characterized (Nagano et al., 2003; Liani et al., 2004), the specific domain of α-synuclein responsible for mediating this interaction remains to be determined. In my experiments, I employed a heterologous cell system and investigated various truncated versions of α-synuclein to identify the crucial domain involved in the formation of LBLs. The data obtained in this thesis indicate that the C-terminal region of α-synuclein plays a significant role in stabilizing the "Core and Shell" architecture characteristic of LBs (Wakabayashi and Takahashi, 2003). It is worth noting that the NAC domain, which is essential for driving fibrillization (Giasson et al., 2001), is still present in the truncated α-synuclein protein used in the experiment. Therefore, it is tempting to speculate that α-synuclein-ΔC could still undergo a higher degree of aggregation, potentially forming protofibrils and fibrils, but failing to recapitulate the LB architecture observed in patients.

It has been observed that the C-terminal region of α-synuclein is highly enriched in LBs, which supports the notion that it can participate independently in LB formation (Huang et al., 2022). The pI of synphilin 1 varies across its specific domains, with the N-terminal domain having a pI of 4.5 and the ANK domain having a pI of 5.3. In contrast, the C-terminal region of synphilin 1 has a positively charged pI of 9.5, indicating a potential affinity for acidic phospholipids (Takahashi et al., 2006). The C-terminus of synphilin 1 may serve as a primary determinant for its binding capacity to phospholipids. Interestingly, the C-terminal region of α-synuclein is highly acidic and predominantly negatively charged (Mor et al., 2016; Furukawa et al., 2020) suggesting the possibility of low-affinity interactions driven by electrostatic charges between these sequences. It is tempting to speculate that these charge-based interactions contribute to the stabilization of the LBLs observed in this study.

### 4.5. The aberrant condensates of α-synuclein disrupt intracellular membrane trafficking

Immunohistochemical studies have identified over 90 different molecules that show reactivity in the context of protein aggregates (Wakabayashi et al., 2007). In addition, mass spectrometry analysis has revealed that these pathological aggregates consist of a complex mixture of components, including membranous fragments, vesicular structures, and various lipid species (Gai et al., 2000; Araki et al., 2015). The presence of various membranous structures in LBs has been associated with the ability of α-synuclein to bind to membranes, particularly lipids and fatty acids (Fanning et al., 2019) and synaptic vesicles (Wang et al., 2014). Based on these observations, several research groups have proposed a challenged view that vesicle binding can promote amyloid production, but rather the interactions of α-synuclein with membranes could play a critical role in the generation of aggregation-resistant forms of the protein (Rovere et al., 2018; Kim et al., 2018; Bartels, 2019; Fanning et al., 2020).

Inspired by previous studies of patient material using correlative light and electron microscopy that demonstrated the enrichment of mitochondria in the outer region of LBs in patients (Shahmoradian et al., 2019), I investigated the presence of membranous structures in reconstituted LBLs. My data presented here support the presence of high contact between LBLs and mitochondria. Moreover, mitochondria in cells expressing LBLs appeared to be fragmented, which is a common indication of mitochondrial dysfunction observed in various

neurodegenerative diseases (Knott et al., 2008). This effect may reflect defective mitochondrial respiration and the overproduction of reactive oxygen species (ROS), as observed in previous studies (Picca et al., 2021). Recent studies have made significant efforts to understand the link between vesicular structure, mitochondrial disruption, and impairment of neuronal communication in PD and other synucleinopathies (Alegre-Abarrategui et al., 2019). These interconnected processes play a critical role in the normal functioning of neurons, and their dysfunction can explain the development of cognitive and motor symptoms that worsen over time.

Finally, the experimental findings in this thesis indicate that there is an interplay between the sequestration of actin by LBLs and the accumulation of mitochondria, which ultimately affects the physiological function of mitochondria. Specifically, my data suggest that LBLs progressively sequester actin, leading to the collapse of the intracellular actin network. This phenomenon is accompanied by increased actin enrichment within the LBLs themselves. Furthermore, these results demonstrate a significant accumulation of mitochondria in association with LBLs. This accumulation suggests that the sequestration of actin by LBLs may play a role in influencing the positioning or distribution of mitochondria within the cell. The impaired physiological function of mitochondria may be a consequence of this altered distribution or other downstream effects resulting from actin sequestration. These findings provide insights into the potential mechanism by which actin dynamics and the cytoskeleton are involved in the sequestration of mitochondria and the subsequent impact on their function.

The ultrastructure analysis of α-synuclein-containing inclusions in patients done by several research groups have already provided valuable insights, revealing that these inclusions consist of a complex mixture of membrane-bound organelles (Shahmoradian et al., 2019; Mahul-Mellier et al., 2020; Lashuel, 2020). However, the specific mechanisms underlying the entrapment of mitochondria at the interface of α-synuclein inclusions remained unexplored. Although the presence of mitochondria within α-synuclein inclusions has been observed, further investigations are needed to elucidate the precise mechanisms by which these organelles become sequestered within the inclusions.

# 5. CONCLUSION AND FUTURE DIRECTIONS

Liquid-liquid phase separation is a growing concept that is changing the point of view on how biological systems can self-organize and compartmentalize within cells forming biomolecular condensates. SV condensates serve as a compelling example of this concept in neurobiology. Here, α-synuclein emerges as a major regulator of these condensates affecting neuronal communication in physiological conditions, and its dysregulation has been implicated in the pathogenesis of neurodegenerative disorders.

In the first part of this thesis, I demonstrated that α-synuclein is sequestered in synapsin/SV condensates. SVs catalyze the formation of the dynamic synapsin condensates, and α-synuclein can further modulate the packing density of SVs assembly of these condensates. Further investigations are needed to characterize how this system influences the dynamics of SV release during neurotransmission. For example, it is important to explore how the kinetics of this process can change the SVs availability under stress conditions. As both synapsins and synucleins are targets of many kinases and phosphatases, exploring the PTMs status of the proteins involved in neurotransmitter release can provide valuable insights into the regulation of this process. These effects can be investigated by selectively mutating phosphorylation sites and comparing the kinetics of SV release between wild-type and mutant proteins. In addition, advanced imaging techniques such as super-resolution microscopy or employing optogenetic tools to selectively control the activity of specific could allow for visualize the nanoscale organization of proteins involved in SV release and assess how alterations in protein localization affect release kinetics. By delving into these aspects, we can gain a deeper understanding of the regulatory mechanisms underlying neurotransmitter release and potentially identify novel avenues for modulating synaptic function.

An important advancement in expanding the research presented in this thesis would be to conduct experiments using animal models or human pluripotent stem cells (iPSCs). Furthermore, the utilization of alternative animal models, such as the lamprey, can provide notable benefits in investigating synaptic architecture due to their giant axons, considerably larger in size compared to mammalian axons. This enlarged axon dimension offers enhanced feasibility for experimental manipulations and cellular-level investigations on the synaptic

terminal facilitating localized administration of purified proteins, enabling precise examination of protein dynamics and their influence on synaptic processes.

In the second part of this work, Lewy bodies-like structures (LBLs), hallmark pathological inclusions in PD patients, are recapitulated in a minimal system containing α-synuclein and synphilin 1. Experiments have revealed that LBLs accumulate α-synuclein around the synphilin 1 core. The elevated expression of both α-synuclein and synphilin 1, along with the condensate maturation, serves as an illustrative example of how the LLPS system can undergo dysregulation, resulting in the formation of insoluble inclusions. This scenario provides insight into the underlying mechanism of LB biogenesis. Nevertheless, the formed LBLs prominently exhibit pathological characteristics, including the sequestration of membranes, particularly mitochondria, and the disruption of the actin cytoskeleton.

Transgenic mouse models of PD that overexpress human α-synuclein have been developed to replicate several features of the human disease and may be used in the future to validate this system. It is important to note that inclusions observed in the mouse models are fibrillar, in contrast to the LBs found in postmortem PD tissue which often lack α-synuclein fibrils. However, despite the valuable insights provided by these animal models, it is recognized that they do not fully capture the complexity of human neurodegenerative diseases. The significance of this study is closely tied to the need for appropriate models to investigate the pathology of LBs in their early stages and progression. The tissue samples available for neuropathological studies are typically obtained from clinically diagnosed cases, which represent the later stages of the disease. This limitation restricts the insights gained from neuropathological investigations. The reconstitution of early stages of LBs formation, resembling the preclinical stage of the disease, holds significant potential for providing vital insights into the causal relationship between LBs pathology and disease progression.

To further investigate the functional consequences of the interaction between LBLs and mitochondria, several lines of research could be pursued. For example, *in vitro* reconstituted LBLs could be used in combination with isolated mitochondria to elucidate additional features of this direct physical interaction. Additionally, experiments focused on quantifying mitochondrial respiration, such as measuring the rate of ATP production,

oxygen flux, oxygen consumption rate, and ROS production, could provide insights into the impact of LBLs on mitochondrial function. By conducting these experiments, one could understand the functional consequences of LBL-mitochondria interactions and their role in mitochondrial dysfunction observed in PD pathology. Finally, future studies employing advanced imaging techniques such as electron microscopy or soft-X-ray tomography will be instrumental in unraveling the intricate molecular events leading to mitochondrial trapping within α-synuclein inclusions.

Further work needs to be done to understand the complexity of LB pathogenesis, such as investigating the role of other pathways such as proteasome regulation and endo-lysosomal system. One additional advantage of the approach employed in this thesis is the potential to utilize the reconstituted LBLs as a platform for large-scale high-throughput screening. This platform can be used for the discovery and testing of new drugs or molecules with the ability to disrupt aberrant protein aggregates or slow down the onset of pathological phenotypes associated with LB formation. By employing high-throughput screening methods, a large number of compounds can be rapidly evaluated for their effectiveness in modulating LB-related processes. This approach holds promise for identifying potential therapeutic candidates that may be capable of mitigating LB pathology and potentially delaying or alleviating disease symptoms. Further exploration of this platform can lead to important insights and advancements in the development of novel treatments for LB-associated neurodegenerative diseases.

# 6. REFERENCES


Acuna, C., Liu, X., Südhof, T.C., 2016. How to Make an Active Zone: Unexpected Universal Functional Redundancy between RIMs and RIM-BPs. Neuron 91, 792–807. https://doi.org/10.1016/j.neuron.2016.07.042

Aguzzi, A., Altmeyer, M., 2016. Phase Separation: Linking Cellular Compartmentalization to Disease. Trends Cell Biol 26, 547–558. https://doi.org/10.1016/j.tcb.2016.03.004

Alberti, S., Carra, S., 2018. Quality Control of Membraneless Organelles. Journal of Molecular Biology, Phase Separation in Biology and Disease 430, 4711–4729. https://doi.org/10.1016/j.jmb.2018.05.013

Alberti, S., Gladfelter, A., Mittag, T., 2019. Considerations and Challenges in Studying Liquid-Liquid Phase Separation and Biomolecular Condensates. Cell 176, 419–434. https://doi.org/10.1016/j.cell.2018.12.035

Alberts, B., Johnson, A., Lewis, J., Raff, M., Roberts, K., Walter, P., 2002. Molecular Biology of the Cell, 4th ed. Garland Science.

Alegre-Abarrategui, J., Brimblecombe, K.R., Roberts, R.F., Velentza-Almpani, E., Tilley, B.S., Bengoa-Vergniory, N., Proukakis, C., 2019. Selective vulnerability in α-synucleinopathies. Acta Neuropathol 138, 681–704. https://doi.org/10.1007/s00401-019-02010-2

Anderson, J.P., Walker, D.E., Goldstein, J.M., de Laat, R., Banducci, K., Caccavello, R.J., Barbour, R., Huang, J., Kling, K., Lee, M., Diep, L., Keim, P.S., Shen, X., Chataway, T., Schlossmacher, M.G., Seubert, P., Schenk, D., Sinha, S., Gai, W.P., Chilcote, T.J., 2006. Phosphorylation of Ser-129 is the dominant pathological modification of alpha-synuclein in familial and sporadic Lewy body disease. J Biol Chem 281, 29739–29752. https://doi.org/10.1074/jbc.M600933200

Arai, H., Lee, V.M., Hill, W.D., Greenberg, B.D., Trojanowski, J.Q., 1992. Lewy bodies contain beta-amyloid precursor proteins of Alzheimer's disease. Brain Res 585, 386–390. https://doi.org/10.1016/0006-8993(92)91242-7

Araki, K., Yagi, N., Ikemoto, Y., Yagi, H., Choong, C.-J., Hayakawa, H., Beck, G., Sumi, H., Fujimura, H., Moriwaki, T., Nagai, Y., Goto, Y., Mochizuki, H., 2015. Synchrotron FTIR micro-spectroscopy for structural analysis of Lewy bodies in the brain of Parkinson's disease patients. Sci Rep 5, 17625. https://doi.org/10.1038/srep17625

Aron, L., 2023. Genetic analysis of dopaminergic neuron survival. GDNF/Ret signaling and the Parkinson's disease-associated gene DJ-1.

Atias, M., Tevet, Y., Sun, J., Stavsky, A., Tal, S., Kahn, J., Roy, S., Gitler, D., 2019. Synapsins regulate α-synuclein functions. Proc Natl Acad Sci U S A 116, 11116–11118. https://doi.org/10.1073/pnas.1903054116

Auluck, P.K., Chan, H.Y.E., Trojanowski, J.Q., Lee, V.M.Y., Bonini, N.M., 2002. Chaperone suppression of alpha-synuclein toxicity in a Drosophila model for Parkinson's disease. Science 295, 865–868. https://doi.org/10.1126/science.1067389

Baba, M., Nakajo, S., Tu, P.H., Tomita, T., Nakaya, K., Lee, V.M., Trojanowski, J.Q., Iwatsubo, T., 1998. Aggregation of alpha-synuclein in Lewy bodies of sporadic Parkinson's disease and dementia with Lewy bodies. Am J Pathol 152, 879–884.

Babu, M.M., 2016. The contribution of intrinsically disordered regions to protein function, cellular complexity, and human disease. Biochemical Society Transactions 44, 1185–1200. https://doi.org/10.1042/BST20160172

Bai, G., Wang, Y., Zhang, M., 2021. Gephyrin-mediated formation of inhibitory postsynaptic density sheet via phase separation. Cell Res 31, 312–325. https://doi.org/10.1038/s41422-020-00433-1

Banani, S.F., Lee, H.O., Hyman, A.A., Rosen, M.K., 2017. Biomolecular condensates: organizers of cellular biochemistry. Nat Rev Mol Cell Biol 18, 285–298. https://doi.org/10.1038/nrm.2017.7

Bandopadhyay, R., Kingsbury, A.E., Cookson, M.R., Reid, A.R., Evans, I.M., Hope, A.D., Pittman, A.M., Lashley, T., Canet-Aviles, R., Miller, D.W., McLendon, C., Strand, C., Leonard, A.J., Abou-Sleiman, P.M., Healy, D.G., Ariga, H., Wood, N.W., de Silva, R., Revesz, T., Hardy, J.A., Lees, A.J., 2004. The expression of DJ-1 (PARK7) in normal human CNS and idiopathic Parkinson's disease. Brain 127, 420–430. https://doi.org/10.1093/brain/awh054

Bandopadhyay, R., Kingsbury, A.E., Muqit, M.M., Harvey, K., Reid, A.R., Kilford, L., Engelender, S., Schlossmacher, M.G., Wood, N.W., Latchman, D.S., Harvey, R.J., Lees, A.J., 2005. Synphilin-1 and parkin show overlapping expression patterns in human brain and form aggresomes in response to proteasomal inhibition. Neurobiol Dis 20, 401–411. https://doi.org/10.1016/j.nbd.2005.03.021

Bartels, T., 2019. A traffic jam leads to Lewy bodies. Nat Neurosci 22, 1043–1045. https://doi.org/10.1038/s41593-019-0435-y

Basso, M., Giraudo, S., Corpillo, D., Bergamasco, B., Lopiano, L., Fasano, M., 2004. Proteome analysis of human substantia nigra in Parkinson's disease. Proteomics 4, 3943–3952. https://doi.org/10.1002/pmic.200400848

Berry, J., Brangwynne, C.P., Haataja, M., 2018. Physical principles of intracellular organization via active and passive phase transitions. Rep Prog Phys 81, 046601. https://doi.org/10.1088/1361-6633/aaa61e

Bertoncini, C.W., Fernandez, C.O., Griesinger, C., Jovin, T.M., Zweckstetter, M., 2005. Familial mutants of alpha-synuclein with increased neurotoxicity have a destabilized conformation. J Biol Chem 280, 30649–30652. https://doi.org/10.1074/jbc.C500288200

Beyer, K., 2006. Alpha-synuclein structure, post-translational modification and alternative splicing as aggregation enhancers. Acta Neuropathol 112, 237–251. https://doi.org/10.1007/s00401-006-0104-6

Binolfi, A., Rasia, R.M., Bertoncini, C.W., Ceolin, M., Zweckstetter, M., Griesinger, C., Jovin, T.M., Fernández, C.O., 2006. Interaction of alpha-synuclein with divalent metal ions reveals key differences: a link between structure, binding specificity and fibrillation enhancement. J Am Chem Soc 128, 9893–9901. https://doi.org/10.1021/ja0618649

Böddeker, T.J., Rosowski, K.A., Berchtold, D., Emmanouilidis, L., Han, Y., Allain, F.H.T., Style, R.W., Pelkmans, L., Dufresne, E.R., 2022. Non-specific adhesive forces between filaments and membraneless organelles. Nat. Phys. 18, 571–578. https://doi.org/10.1038/s41567-022-01537-8

Bodles, A.M., Guthrie, D.J., Greer, B., Irvine, G.B., 2001. Identification of the region of non-Abeta component (NAC) of Alzheimer's disease amyloid responsible for its aggregation and toxicity. J Neurochem 78, 384–395. https://doi.org/10.1046/j.1471-4159.2001.00408.x

Bodner, C.R., Dobson, C.M., Bax, A., 2009. Multiple tight phospholipid-binding modes of alpha-synuclein revealed by solution NMR spectroscopy. J Mol Biol 390, 775–790. https://doi.org/10.1016/j.jmb.2009.05.066

Boija, A., Klein, I.A., Sabari, B.R., Dall'Agnese, A., Coffey, E.L., Zamudio, A.V., Li, C.H., Shrinivas, K., Manteiga, J.C., Hannett, N.M., Abraham, B.J., Afeyan, L.K., Guo, Y.E., Rimel, J.K., Fant, C.B., Schuijers, J., Lee, T.I., Taatjes, D.J., Young, R.A., 2018. Transcription Factors Activate Genes through the Phase-Separation Capacity of Their Activation Domains. Cell 175, 1842-1855.e16. https://doi.org/10.1016/j.cell.2018.10.042

Boisvert, F.-M., van Koningsbruggen, S., Navascués, J., Lamond, A.I., 2007. The multifunctional nucleolus. Nat Rev Mol Cell Biol 8, 574–585. https://doi.org/10.1038/nrm2184

Bonanomi, D., Menegon, A., Miccio, A., Ferrari, G., Corradi, A., Kao, H.-T., Benfenati, F., Valtorta, F., 2005. Phosphorylation of Synapsin I by cAMP-Dependent Protein Kinase Controls Synaptic Vesicle Dynamics in Developing Neurons. J. Neurosci. 25, 7299–7308. https://doi.org/10.1523/JNEUROSCI.1573-05.2005

Boyko, S., Qi, X., Chen, T.-H., Surewicz, K., Surewicz, W.K., 2019. Liquid-liquid phase separation of tau protein: The crucial role of electrostatic interactions. J Biol Chem 294, 11054–11059. https://doi.org/10.1074/jbc.AC119.009198

Boyko, S., Surewicz, W.K., 2022. Tau liquid-liquid phase separation in neurodegenerative diseases. Trends Cell Biol 32, 611–623. https://doi.org/10.1016/j.tcb.2022.01.011

Braak, H., Braak, E., 2000. Pathoanatomy of Parkinson's disease. J Neurol 247 Suppl 2, II3-10. https://doi.org/10.1007/PL00007758

Braak, H., Del Tredici, K., Rüb, U., de Vos, R.A.I., Jansen Steur, E.N.H., Braak, E., 2003. Staging of brain pathology related to sporadic Parkinson's disease. Neurobiol Aging 24, 197–211. https://doi.org/10.1016/s0197-4580(02)00065-9

Brangwynne, C.P., Eckmann, C.R., Courson, D.S., Rybarska, A., Hoege, C., Gharakhani, J., Jülicher, F., Hyman, A.A., 2009. Germline P Granules Are Liquid Droplets That Localize by Controlled Dissolution/Condensation. Science 324, 1729–1732. https://doi.org/10.1126/science.1172046

Brangwynne, C.P., Tompa, P., Pappu, R.V., 2015. Polymer physics of intracellular phase transitions. Nature Phys 11, 899–904. https://doi.org/10.1038/nphys3532

Bucciantini, M., Giannoni, E., Chiti, F., Baroni, F., Formigli, L., Zurdo, J., Taddei, N., Ramponi, G., Dobson, C.M., Stefani, M., 2002. Inherent toxicity of aggregates implies a common mechanism for protein misfolding diseases. Nature 416, 507–511. https://doi.org/10.1038/416507a

Buell, A.K., Galvagnion, C., Gaspar, R., Sparr, E., Vendruscolo, M., Knowles, T.P.J., Linse, S., Dobson, C.M., 2014. Solution conditions determine the relative importance of nucleation and growth processes in α-synuclein aggregation. Proc Natl Acad Sci U S A 111, 7671–7676. https://doi.org/10.1073/pnas.1315346111

Burré, J., Sharma, M., Südhof, T.C., 2018. Cell Biology and Pathophysiology of α-Synuclein. Cold Spring Harb Perspect Med 8, a024091. https://doi.org/10.1101/cshperspect.a024091

Burré, J., Sharma, M., Südhof, T.C., 2014. α-Synuclein assembles into higher-order multimers upon membrane binding to promote SNARE complex formation. Proc Natl Acad Sci U S A 111, E4274-4283. https://doi.org/10.1073/pnas.1416598111

Burré, J., Sharma, M., Tsetsenis, T., Buchman, V., Etherton, M.R., Südhof, T.C., 2010. Alpha-synuclein promotes SNARE-complex assembly in vivo and in vitro. Science 329, 1663–1667. https://doi.org/10.1126/science.1195227

C. Warren Olanow, 2011. Parkinson's Disease: Non-Motor and Non-Dopaminergic Features | Wiley. ISBN: 978-1-444-39796-3

Carnazza, K.E., Komer, L.E., Xie, Y.X., Pineda, A., Briano, J.A., Gao, V., Na, Y., Ramlall, T., Buchman, V.L., Eliezer, D., Sharma, M., Burré, J., 2022. Synaptic vesicle binding of α-synuclein is modulated by β- and γ-synucleins. Cell Rep 39, 110675. https://doi.org/10.1016/j.celrep.2022.110675

Caughey, B., Lansbury, P.T., 2003. Protofibrils, pores, fibrils, and neurodegeneration: separating the responsible protein aggregates from the innocent bystanders. Annu Rev Neurosci 26, 267–298. https://doi.org/10.1146/annurev.neuro.26.010302.081142

Ceccarelli, B., Hurlbut, W.P., Mauro, A., 1973. TURNOVER OF TRANSMITTER AND SYNAPTIC VESICLES AT THE FROG NEUROMUSCULAR JUNCTION. Journal of Cell Biology 57, 499–524. https://doi.org/10.1083/jcb.57.2.499

Chan, J.K.C., 2014. The wonderful colors of the hematoxylin-eosin stain in diagnostic surgical pathology. Int J Surg Pathol 22, 12–32. https://doi.org/10.1177/1066896913517939

Chandra, S., Chen, X., Rizo, J., Jahn, R., Südhof, T.C., 2003. A broken alpha -helix in folded alpha -Synuclein. J Biol Chem 278, 15313–15318. https://doi.org/10.1074/jbc.M213128200

Chartier-Harlin, M.-C., Kachergus, J., Roumier, C., Mouroux, V., Douay, X., Lincoln, S., Levecque, C., Larvor, L., Andrieux, J., Hulihan, M., Waucquier, N., Defebvre, L., Amouyel, P., Farrer, M., Destée, A., 2004. Alpha-synuclein locus duplication as a cause of familial Parkinson's disease. Lancet 364, 1167–1169. https://doi.org/10.1016/S0140-6736(04)17103-1

Chaudhuri, K.R., Schapira, A.H.V., 2009. Non-motor symptoms of Parkinson's disease: dopaminergic pathophysiology and treatment. Lancet Neurol 8, 464–474. https://doi.org/10.1016/S1474-4422(09)70068-7

Chen, L., Feany, M.B., 2005. Alpha-synuclein phosphorylation controls neurotoxicity and inclusion formation in a Drosophila model of Parkinson disease. Nat Neurosci 8, 657–663. https://doi.org/10.1038/nn1443

Chi, P., Greengard, P., Ryan, T.A., 2003. Synaptic Vesicle Mobilization Is Regulated by Distinct Synapsin I Phosphorylation Pathways at Different Frequencies. Neuron 38, 69–78. https://doi.org/10.1016/S0896-6273(03)00151-X

Chi, P., Greengard, P., Ryan, T.A., 2001. Synapsin dispersion and reclustering during synaptic activity. Nat Neurosci 4, 1187–1193. https://doi.org/10.1038/nn756

Chou, C.-C., Zhang, Y., Umoh, M.E., Vaughan, S.W., Lorenzini, I., Liu, F., Sayegh, M., Donlin-Asp, P.G., Chen, Y.H., Duong, D.M., Seyfried, N.T., Powers, M.A., Kukar, T., Hales, C.M., Gearing, M., Cairns, N.J., Boylan, K.B., Dickson, D.W., Rademakers, R., Zhang, Y.-J., Petrucelli, L., Sattler, R., Zarnescu, D.C., Glass, J.D., Rossoll, W., 2018. TDP-43 pathology disrupts nuclear pore complexes and nucleocytoplasmic transport in ALS/FTD. Nat Neurosci 21, 228–239. https://doi.org/10.1038/s41593-017-0047-3

Cinar, H., Fetahaj, Z., Cinar, S., Vernon, R.M., Chan, H.S., Winter, R.H.A., 2019. Temperature, Hydrostatic Pressure, and Osmolyte Effects on Liquid–Liquid Phase Separation in Protein Condensates: Physical Chemistry and Biological Implications. Chemistry – A European Journal 25, 13049–13069. https://doi.org/10.1002/chem.201902210

Clayton, D.F., George, J.M., 1999. Synucleins in synaptic plasticity and neurodegenerative disorders. J Neurosci Res 58, 120–129.

Clayton, D.F., George, J.M., 1998. The synucleins: a family of proteins involved in synaptic function, plasticity, neurodegeneration and disease. Trends Neurosci 21, 249–254. https://doi.org/10.1016/s0166-2236(97)01213-7

Cole, N.B., Murphy, D.D., Grider, T., Rueter, S., Brasaemle, D., Nussbaum, R.L., 2002. Lipid droplet binding and oligomerization properties of the Parkinson's disease protein alpha-synuclein. J Biol Chem 277, 6344–6352. https://doi.org/10.1074/jbc.M108414200

Conicella, A.E., Dignon, G.L., Zerze, G.H., Schmidt, H.B., D'Ordine, A.M., Kim, Y.C., Rohatgi, R., Ayala, Y.M., Mittal, J., Fawzi, N.L., 2020. TDP-43 α-helical structure tunes liquid-liquid phase separation and function. Proc Natl Acad Sci U S A 117, 5883–5894. https://doi.org/10.1073/pnas.1912055117

Conway, K.A., Harper, J.D., Lansbury, P.T., 2000. Fibrils formed in vitro from alpha-synuclein and two mutant forms linked to Parkinson's disease are typical amyloid. Biochemistry 39, 2552–2563. https://doi.org/10.1021/bi991447r

Cookson, M.R., 2005. The biochemistry of Parkinson's disease. Annu Rev Biochem 74, 29–52. https://doi.org/10.1146/annurev.biochem.74.082803.133400

Crews, L., Spencer, B., Desplats, P., Patrick, C., Paulino, A., Rockenstein, E., Hansen, L., Adame, A., Galasko, D., Masliah, E., 2010. Selective molecular alterations in the autophagy pathway in patients with Lewy body disease and in models of alpha-synucleinopathy. PLoS One 5, e9313. https://doi.org/10.1371/journal.pone.0009313

Curtis, I. de, 2021. Biomolecular Condensates at the Front: Cell Migration Meets Phase Separation. Trends in Cell Biology 31, 145–148. https://doi.org/10.1016/j.tcb.2020.12.002

Czernik, A.J., Pang, D.T., Greengard, P., 1987. Amino acid sequences surrounding the cAMP-dependent and calcium/calmodulin-dependent phosphorylation sites in rat and

bovine synapsin I. Proc Natl Acad Sci U S A 84, 7518–7522. https://doi.org/10.1073/pnas.84.21.7518

D'Andrea, M.R., Ilyin, S., Plata-Salaman, C.R., 2001. Abnormal patterns of microtubule-associated protein-2 (MAP-2) immunolabeling in neuronal nuclei and Lewy bodies in Parkinson's disease substantia nigra brain tissues. Neurosci Lett 306, 137–140. https://doi.org/10.1016/s0304-3940(01)01811-0

Davidson, W.S., Jonas, A., Clayton, D.F., George, J.M., 1998. Stabilization of alpha-synuclein secondary structure upon binding to synthetic membranes. J Biol Chem 273, 9443–9449. https://doi.org/10.1074/jbc.273.16.9443

De Camilli, P., Benfenati, F., Valtorta, F., Greengard, P., 1990. The Synapsins. Annual Review of Cell Biology 6, 433–460. https://doi.org/10.1146/annurev.cb.06.110190.002245

de Laureto, P.P., Tosatto, L., Frare, E., Marin, O., Uversky, V.N., Fontana, A., 2006. Conformational properties of the SDS-bound state of alpha-synuclein probed by limited proteolysis: unexpected rigidity of the acidic C-terminal tail. Biochemistry 45, 11523–11531. https://doi.org/10.1021/bi052614s

Denker, A., Kröhnert, K., Bückers, J., Neher, E., Rizzoli, S.O., 2011. The reserve pool of synaptic vesicles acts as a buffer for proteins involved in synaptic vesicle recycling. Proc Natl Acad Sci U S A 108, 17183–17188. https://doi.org/10.1073/pnas.1112690108

Denker, A., Rizzoli, S., 2010. Synaptic Vesicle Pools: An Update. Frontiers in Synaptic Neuroscience 2.

Diao, J., Burré, J., Vivona, S., Cipriano, D.J., Sharma, M., Kyoung, M., Südhof, T.C., Brunger, A.T., 2013. Native α-synuclein induces clustering of synaptic-vesicle mimics via binding to phospholipids and synaptobrevin-2/VAMP2. Elife 2, e00592. https://doi.org/10.7554/eLife.00592

Dickson, D.W., Fujishiro, H., Orr, C., DelleDonne, A., Josephs, K.A., Frigerio, R., Burnett, M., Parisi, J.E., Klos, K.J., Ahlskog, J.E., 2009. Neuropathology of non-motor features of

Parkinson disease. Parkinsonism Relat Disord 15 Suppl 3, S1-5. https://doi.org/10.1016/S1353-8020(09)70769-2

Ding, T.T., Lee, S.-J., Rochet, J.-C., Lansbury, P.T., 2002. Annular alpha-synuclein protofibrils are produced when spherical protofibrils are incubated in solution or bound to brain-derived membranes. Biochemistry 41, 10209–10217. https://doi.org/10.1021/bi020139h

Drin, G., Casella, J.-F., Gautier, R., Boehmer, T., Schwartz, T.U., Antonny, B., 2007. A general amphipathic alpha-helical motif for sensing membrane curvature. Nat Struct Mol Biol 14, 138–146. https://doi.org/10.1038/nsmb1194

Duda, J.E., Giasson, B.I., Chen, Q., Gur, T.L., Hurtig, H.I., Stern, M.B., Gollomp, S.M., Ischiropoulos, H., Lee, V.M., Trojanowski, J.Q., 2000. Widespread nitration of pathological inclusions in neurodegenerative synucleinopathies. Am J Pathol 157, 1439–1445. https://doi.org/10.1016/S0002-9440(10)64781-5

Dugger, B.N., Dickson, D.W., 2010. Cell type specific sequestration of choline acetyltransferase and tyrosine hydroxylase within Lewy bodies. Acta Neuropathol 120, 633–639. https://doi.org/10.1007/s00401-010-0739-1

Eliezer, D., Kutluay, E., Bussell, R., Browne, G., 2001. Conformational properties of alpha-synuclein in its free and lipid-associated states. J Mol Biol 307, 1061–1073. https://doi.org/10.1006/jmbi.2001.4538

Elmqvist, D., Quastel, D.M., 1965. A quantitative study of end-plate potentials in isolated human muscle. The Journal of Physiology 178, 505–529. https://doi.org/10.1113/jphysiol.1965.sp007639

Emamzadeh, F.N., 2016. Alpha-synuclein structure, functions, and interactions. J Res Med Sci 21, 29. https://doi.org/10.4103/1735-1995.181989

Engelender, S., Kaminsky, Z., Guo, X., Sharp, A.H., Amaravi, R.K., Kleiderlein, J.J., Margolis, R.L., Troncoso, J.C., Lanahan, A.A., Worley, P.F., Dawson, V.L., Dawson, T.M.,

Ross, C.A., 1999. Synphilin-1 associates with alpha-synuclein and promotes the formation of cytosolic inclusions. Nat Genet 22, 110–114. https://doi.org/10.1038/8820

Engelender, S., Wanner, T., Kleiderlein, J.J., Wakabayashi, K., Tsuji, S., Takahashi, H., Ashworth, R., Margolis, R.L., Ross, C.A., 2000. Organization of the human synphilin-1 gene, a candidate for Parkinson's disease. Mamm Genome 11, 763–766. https://doi.org/10.1007/s003350010123

Esser, L., Wang, C.R., Hosaka, M., Smagula, C.S., Südhof, T.C., Deisenhofer, J., 1998. Synapsin I is structurally similar to ATP-utilizing enzymes. EMBO J 17, 977–984. https://doi.org/10.1093/emboj/17.4.977

Eyal, A., Szargel, R., Avraham, E., Liani, E., Haskin, J., Rott, R., Engelender, S., 2006. Synphilin-1A: an aggregation-prone isoform of synphilin-1 that causes neuronal death and is present in aggregates from alpha-synucleinopathy patients. Proc Natl Acad Sci U S A 103, 5917–5922. https://doi.org/10.1073/pnas.0509707103

Fanning, S., Haque, A., Imberdis, T., Baru, V., Barrasa, M.I., Nuber, S., Termine, D., Ramalingam, N., Ho, G.P.H., Noble, T., Sandoe, J., Lou, Y., Landgraf, D., Freyzon, Y., Newby, G., Soldner, F., Terry-Kantor, E., Kim, T.-E., Hofbauer, H.F., Becuwe, M., Jaenisch, R., Pincus, D., Clish, C.B., Walther, T.C., Farese, R.V., Srinivasan, S., Welte, M.A., Kohlwein, S.D., Dettmer, U., Lindquist, S., Selkoe, D., 2019. Lipidomic Analysis of α-Synuclein Neurotoxicity Identifies Stearoyl CoA Desaturase as a Target for Parkinson Treatment. Mol Cell 73, 1001-1014.e8. https://doi.org/10.1016/j.molcel.2018.11.028

Fanning, S., Selkoe, D., Dettmer, U., 2020. Parkinson's disease: proteinopathy or lipidopathy? NPJ Parkinsons Dis 6, 3. https://doi.org/10.1038/s41531-019-0103-7

Fares, M.B., Jagannath, S., Lashuel, H.A., 2021. Reverse engineering Lewy bodies: how far have we come and how far can we go? Nat Rev Neurosci 22, 111–131. https://doi.org/10.1038/s41583-020-00416-6

Fergusson, J., Landon, M., Lowe, J., Dawson, S.P., Layfield, R., Hanger, D.P., Mayer, R.J., 1996. Pathological lesions of Alzheimer's disease and dementia with Lewy bodies brains

exhibit immunoreactivity to an ATPase that is a regulatory subunit of the 26S proteasome. Neurosci Lett 219, 167–170. https://doi.org/10.1016/s0304-3940(96)13192-x

Feric, M., Vaidya, N., Harmon, T.S., Mitrea, D.M., Zhu, L., Richardson, T.M., Kriwacki, R.W., Pappu, R.V., Brangwynne, C.P., 2016. Coexisting Liquid Phases Underlie Nucleolar Subcompartments. Cell 165, 1686–1697. https://doi.org/10.1016/j.cell.2016.04.047

Fernández-Busnadiego, R., Zuber, B., Maurer, U.E., Cyrklaff, M., Baumeister, W., Lučić, V., 2010. Quantitative analysis of the native presynaptic cytomatrix by cryoelectron tomography. Journal of Cell Biology 188, 145–156. https://doi.org/10.1083/jcb.200908082

Forno, L.S., Alvord, E.C., 1974. Depigmentation in the nerve cells of the substantia nigra and locus ceruleus in Parkinsonism. Adv Neurol 5, 195–202.

Forno, L.S., Norville, R.L., 1976. Ultrastructure of Lewy bodies in the stellate ganglion. Acta Neuropathol 34, 183–197. https://doi.org/10.1007/BF00688674

Fortin, D.L., Troyer, M.D., Nakamura, K., Kubo, S., Anthony, M.D., Edwards, R.H., 2004. Lipid rafts mediate the synaptic localization of alpha-synuclein. J Neurosci 24, 6715–6723. https://doi.org/10.1523/JNEUROSCI.1594-04.2004

Fortun, J., Dunn, W.A., Joy, S., Li, J., Notterpek, L., 2003. Emerging role for autophagy in the removal of aggresomes in Schwann cells. J Neurosci 23, 10672–10680. https://doi.org/10.1523/JNEUROSCI.23-33-10672.2003

Fuchs, J., Nilsson, C., Kachergus, J., Munz, M., Larsson, E.-M., Schüle, B., Langston, J.W., Middleton, F.A., Ross, O.A., Hulihan, M., Gasser, T., Farrer, M.J., 2007. Phenotypic variation in a large Swedish pedigree due to SNCA duplication and triplication. Neurology 68, 916–922. https://doi.org/10.1212/01.wnl.0000254458.17630.c5

Fujiwara, H., Hasegawa, M., Dohmae, N., Kawashima, A., Masliah, E., Goldberg, M.S., Shen, J., Takio, K., Iwatsubo, T., 2002. alpha-Synuclein is phosphorylated in synucleinopathy lesions. Nat Cell Biol 4, 160–164. https://doi.org/10.1038/ncb748

Fukuda, T., Tanaka, J., Watabe, K., Numoto, R.T., Minamitani, M., 1993. Immunohistochemistry of neuronal inclusions in the cerebral cortex and brain-stem in Lewy body disease. Acta Pathol Jpn 43, 545–551. https://doi.org/10.1111/j.1440-1827.1993.tb03230.x

Furukawa, K., Aguirre, C., So, M., Sasahara, K., Miyanoiri, Y., Sakurai, K., Yamaguchi, K., Ikenaka, K., Mochizuki, H., Kardos, J., Kawata, Y., Goto, Y., 2020. Isoelectric point-amyloid formation of α-synuclein extends the generality of the solubility and supersaturation-limited mechanism. Curr Res Struct Biol 2, 35–44. https://doi.org/10.1016/j.crstbi.2020.03.001

Gai, W.P., Blumbergs, P.C., Blessing, W.W., 1996. Microtubule-associated protein 5 is a component of Lewy bodies and Lewy neurites in the brainstem and forebrain regions affected in Parkinson's disease. Acta Neuropathol 91, 78–81. https://doi.org/10.1007/s004010050395

Gai, W.P., Yuan, H.X., Li, X.Q., Power, J.T., Blumbergs, P.C., Jensen, P.H., 2000. In situ and in vitro study of colocalization and segregation of alpha-synuclein, ubiquitin, and lipids in Lewy bodies. Exp Neurol 166, 324–333. https://doi.org/10.1006/exnr.2000.7527

Gallo, R., Rai, A., Pelkmans, L., 2020. DYRK3-Controlled Phase Separation Organizes the Early Secretory Pathway. https://doi.org/10.1101/2020.02.10.941757

Galloway, P.G., Bergeron, C., Perry, G., 1989. The presence of tau distinguishes Lewy bodies of diffuse Lewy body disease from those of idiopathic Parkinson disease. Neurosci Lett 100, 6–10. https://doi.org/10.1016/0304-3940(89)90651-4

Galloway, P.G., Grundke-Iqbal, I., Iqbal, K., Perry, G., 1988. Lewy bodies contain epitopes both shared and distinct from Alzheimer neurofibrillary tangles. J Neuropathol Exp Neurol 47, 654–663. https://doi.org/10.1097/00005072-198811000-00008

Gandhi, S., Muqit, M.M.K., Stanyer, L., Healy, D.G., Abou-Sleiman, P.M., Hargreaves, I., Heales, S., Ganguly, M., Parsons, L., Lees, A.J., Latchman, D.S., Holton, J.L., Wood, N.W.,

Revesz, T., 2006. PINK1 protein in normal human brain and Parkinson's disease. Brain 129, 1720–1731. https://doi.org/10.1093/brain/awl114

George, J.M., 2002. The synucleins. Genome Biol 3, REVIEWS3002. https://doi.org/10.1186/gb-2001-3-1-reviews3002

Georgieva, E.R., Ramlall, T.F., Borbat, P.P., Freed, J.H., Eliezer, D., 2008. Membrane-bound alpha-synuclein forms an extended helix: long-distance pulsed ESR measurements using vesicles, bicelles, and rodlike micelles. J Am Chem Soc 130, 12856–12857. https://doi.org/10.1021/ja804517m

Gershanik, O.S., Nygaard, T.G., 1990. Parkinson's disease beginning before age 40. Adv Neurol 53, 251–258.

Gerth, F., Jäpel, M., Pechstein, A., Kochlamazashvili, G., Lehmann, M., Puchkov, D., Onofri, F., Benfenati, F., Nikonenko, A.G., Fredrich, K., Shupliakov, O., Maritzen, T., Freund, C., Haucke, V., 2017. Intersectin associates with synapsin and regulates its nanoscale localization and function. Proc Natl Acad Sci U S A 114, 12057–12062. https://doi.org/10.1073/pnas.1715341114

Giasson, B.I., Murray, I.V., Trojanowski, J.Q., Lee, V.M., 2001. A hydrophobic stretch of 12 amino acid residues in the middle of alpha-synuclein is essential for filament assembly. J Biol Chem 276, 2380–2386. https://doi.org/10.1074/jbc.M008919200

Gitler, D., Takagishi, Y., Feng, J., Ren, Y., Rodriguiz, R.M., Wetsel, W.C., Greengard, P., Augustine, G.J., 2004. Different presynaptic roles of synapsins at excitatory and inhibitory synapses. J Neurosci 24, 11368–11380. https://doi.org/10.1523/JNEUROSCI.3795-04.2004

Goedert, M., 2001. Alpha-synuclein and neurodegenerative diseases. Nat Rev Neurosci 2, 492–501. https://doi.org/10.1038/35081564

Goedert, M., Falcon, B., Clavaguera, F., Tolnay, M., 2014. Prion-like mechanisms in the pathogenesis of tauopathies and synucleinopathies. Curr Neurol Neurosci Rep 14, 495. https://doi.org/10.1007/s11910-014-0495-z

Goedert, M., Jakes, R., Spillantini, M.G., 2017. The Synucleinopathies: Twenty Years On. J Parkinsons Dis 7, S51–S69. https://doi.org/10.3233/JPD-179005

Goldman, J.E., Yen, S.H., Chiu, F.C., Peress, N.S., 1983. Lewy bodies of Parkinson's disease contain neurofilament antigens. Science 221, 1082–1084. https://doi.org/10.1126/science.6308771

Greengard, P., Valtorta, F., Czernik, A.J., Benfenati, F., 1993. Synaptic Vesicle Phosphoproteins and Regulation of Synaptic Function. Science 259, 780–785. https://doi.org/10.1126/science.8430330

Greten-Harrison, B., Polydoro, M., Morimoto-Tomita, M., Diao, L., Williams, A.M., Nie, E.H., Makani, S., Tian, N., Castillo, P.E., Buchman, V.L., Chandra, S.S., 2010. αβγ-Synuclein triple knockout mice reveal age-dependent neuronal dysfunction. Proc Natl Acad Sci U S A 107, 19573–19578. https://doi.org/10.1073/pnas.1005005107

Halliday, G., Lees, A., Stern, M., 2011. Milestones in Parkinson's disease--clinical and pathologic features. Mov Disord 26, 1015–1021. https://doi.org/10.1002/mds.23669

Hardenberg, M.C., Sinnige, T., Casford, S., Dada, S.T., Poudel, C., Robinson, E.A., Fuxreiter, M., Kaminksi, C.F., Kaminski Schierle, G.S., Nollen, E.A.A., Dobson, C.M., Vendruscolo, M., 2021. Observation of an α-synuclein liquid droplet state and its maturation into Lewy body-like assemblies. J Mol Cell Biol 13, 282–294. https://doi.org/10.1093/jmcb/mjaa075

Harper, J.D., Lansbury, P.T., 1997. Models of amyloid seeding in Alzheimer's disease and scrapie: mechanistic truths and physiological consequences of the time-dependent solubility of amyloid proteins. Annu Rev Biochem 66, 385–407. https://doi.org/10.1146/annurev.biochem.66.1.385

Harper, J.D., Wong, S.S., Lieber, C.M., Lansbury, P.T., 1999. Assembly of A beta amyloid protofibrils: an in vitro model for a possible early event in Alzheimer's disease. Biochemistry 38, 8972–8980. https://doi.org/10.1021/bi9904149

Hashimoto, M., Takeda, A., Hsu, L.J., Takenouchi, T., Masliah, E., 1999. Role of cytochrome c as a stimulator of alpha-synuclein aggregation in Lewy body disease. J Biol Chem 274, 28849–28852. https://doi.org/10.1074/jbc.274.41.28849

Hayashi, M.K., Tang, C., Verpelli, C., Narayanan, R., Stearns, M.H., Xu, R.-M., Li, H., Sala, C., Hayashi, Y., 2009. The postsynaptic density proteins Homer and Shank form a polymeric network structure. Cell 137, 159–171. https://doi.org/10.1016/j.cell.2009.01.050

Henkel, A.W., Simpson, L.L., Ridge, R.M., Betz, W.J., 1996. Synaptic vesicle movements monitored by fluorescence recovery after photobleaching in nerve terminals stained with FM1-43. J Neurosci 16, 3960–3967. https://doi.org/10.1523/JNEUROSCI.16-12-03960.1996

Heuser, J.E., Reese, T.S., 1973. EVIDENCE FOR RECYCLING OF SYNAPTIC VESICLE MEMBRANE DURING TRANSMITTER RELEASE AT THE FROG NEUROMUSCULAR JUNCTION. Journal of Cell Biology 57, 315–344. https://doi.org/10.1083/jcb.57.2.315

Hilfiker, S., Schweizer, F.E., Kao, H.T., Czernik, A.J., Greengard, P., Augustine, G.J., 1998. Two sites of action for synapsin domain E in regulating neurotransmitter release. Nat Neurosci 1, 29–35. https://doi.org/10.1038/229

Hishikawa, N., Niwa, J.-I., Doyu, M., Ito, T., Ishigaki, S., Hashizume, Y., Sobue, G., 2003. Dorfin localizes to the ubiquitylated inclusions in Parkinson's disease, dementia with Lewy bodies, multiple system atrophy, and amyotrophic lateral sclerosis. Am J Pathol 163, 609–619. https://doi.org/10.1016/s0002-9440(10)63688-7

Hoffmann, C., Milovanovic, D., 2021. Gephyrin: a scaffold that builds a phase at the inhibitory postsynapses. Cell Res 31, 245–246. https://doi.org/10.1038/s41422-020-00440-2

Hoffmann, C., Sansevrino, R., Morabito, G., Logan, C., Vabulas, R.M., Ulusoy, A., Ganzella, M., Milovanovic, D., 2021. Synapsin Condensates Recruit alpha-Synuclein. J Mol Biol 433, 166961. https://doi.org/10.1016/j.jmb.2021.166961

Hohenberg, P.C., Halperin, B.I., 1977. Theory of dynamic critical phenomena. Rev. Mod. Phys. 49, 435–479. https://doi.org/10.1103/RevModPhys.49.435

Hosaka, M., Südhof, T.C., 1999. Homo- and heterodimerization of synapsins. J Biol Chem 274, 16747–16753. https://doi.org/10.1074/jbc.274.24.16747

Hosaka, M., Südhof, T.C., 1998a. Synapsins I and II are ATP-binding proteins with differential Ca2+ regulation. J Biol Chem 273, 1425–1429. https://doi.org/10.1074/jbc.273.3.1425

Hosaka, M., Südhof, T.C., 1998b. Synapsin III, a novel synapsin with an unusual regulation by Ca2+. J Biol Chem 273, 13371–13374. https://doi.org/10.1074/jbc.273.22.13371

Huang, C., Ren, G., Zhou, H., Wang, C., 2005. A new method for purification of recombinant human alpha-synuclein in Escherichia coli. Protein Expr Purif 42, 173–177. https://doi.org/10.1016/j.pep.2005.02.014

Huang, S., Mo, X., Wang, J., Ye, X., Yu, H., Liu, Y., 2022. α-Synuclein phase separation and amyloid aggregation are modulated by C-terminal truncations. FEBS Lett 596, 1388–1400. https://doi.org/10.1002/1873-3468.14361

Huttner, W.B., DeGennaro, L.J., Greengard, P., 1981. Differential phosphorylation of multiple sites in purified protein I by cyclic AMP-dependent and calcium-dependent protein kinases. J Biol Chem 256, 1482–1488.

Huttner, W.B., Schiebler, W., Greengard, P., De Camilli, P., 1983. Synapsin I (protein I), a nerve terminal-specific phosphoprotein. III. Its association with synaptic vesicles studied in a highly purified synaptic vesicle preparation. J Cell Biol 96, 1374–1388. https://doi.org/10.1083/jcb.96.5.1374

Huynh, D.P., Scoles, D.R., Nguyen, D., Pulst, S.M., 2003. The autosomal recessive juvenile Parkinson disease gene product, parkin, interacts with and ubiquitinates synaptotagmin XI. Hum Mol Genet 12, 2587–2597. https://doi.org/10.1093/hmg/ddg269

Hyman, A.A., Weber, C.A., Jülicher, F., 2014. Liquid-Liquid Phase Separation in Biology. Annual Review of Cell and Developmental Biology 30, 39–58. https://doi.org/10.1146/annurev-cellbio-100913-013325

Ikenaka, K., Suzuki, M., Mochizuki, H., Nagai, Y., 2019. Lipids as Trans-Acting Effectors for α-Synuclein in the Pathogenesis of Parkinson's Disease. Front Neurosci 13, 693. https://doi.org/10.3389/fnins.2019.00693

Irwin, D.J., Lee, V.M.-Y., Trojanowski, J.Q., 2013. Parkinson's disease dementia: convergence of α-synuclein, tau and amyloid-β pathologies. Nat Rev Neurosci 14, 626–636. https://doi.org/10.1038/nrn3549

Iseki, E., Takayama, N., Furukawa, Y., Marui, W., Nakai, T., Miura, S., Uéda, K., Kosaka, K., 2002. Immunohistochemical study of synphilin-1 in brains of patients with dementia with Lewy bodies - synphilin-1 is non-specifically implicated in the formation of different neuronal cytoskeletal inclusions. Neurosci Lett 326, 211–215. https://doi.org/10.1016/s0304-3940(02)00418-4

Ishida, T., Kinoshita, K., 2007. PrDOS: prediction of disordered protein regions from amino acid sequence. Nucleic Acids Res 35, W460-464. https://doi.org/10.1093/nar/gkm363

Ishizawa, T., Mattila, P., Davies, P., Wang, D., Dickson, D.W., 2003. Colocalization of tau and alpha-synuclein epitopes in Lewy bodies. J Neuropathol Exp Neurol 62, 389–397. https://doi.org/10.1093/jnen/62.4.389

Ito, T., Niwa, J.-I., Hishikawa, N., Ishigaki, S., Doyu, M., Sobue, G., 2003. Dorfin localizes to Lewy bodies and ubiquitylates synphilin-1. J Biol Chem 278, 29106–29114. https://doi.org/10.1074/jbc.M302763200

Itoh, K., Weis, S., Mehraein, P., Müller-Höcker, J., 1997. Defects of cytochrome c oxidase in the substantia nigra of Parkinson's disease: and immunohistochemical and morphometric study. Mov Disord 12, 9–16. https://doi.org/10.1002/mds.870120104

Iwatsubo, T., Nakano, I., Fukunaga, K., Miyamoto, E., 1991. Ca2+/calmodulin-dependent protein kinase II immunoreactivity in Lewy bodies. Acta Neuropathol 82, 159–163. https://doi.org/10.1007/BF00294440

Jahn, R., Fasshauer, D., 2012. Molecular machines governing exocytosis of synaptic vesicles. Nature 490, 201–207. https://doi.org/10.1038/nature11320

Jao, C.C., Der-Sarkissian, A., Chen, J., Langen, R., 2004. Structure of membrane-bound alpha-synuclein studied by site-directed spin labeling. Proc Natl Acad Sci U S A 101, 8331–8336. https://doi.org/10.1073/pnas.0400553101

Jaqaman, K., Ditlev, J.A., 2021. Biomolecular condensates in membrane receptor signaling. Current Opinion in Cell Biology, Cell Signalling 69, 48–54. https://doi.org/10.1016/j.ceb.2020.12.006

Jellinger, K.A., 2003. Neuropathological spectrum of synucleinopathies. Mov Disord 18 Suppl 6, S2-12. https://doi.org/10.1002/mds.10557

Jensen, P.H., Islam, K., Kenney, J., Nielsen, M.S., Power, J., Gai, W.P., 2000. Microtubule-associated protein 1B is a component of cortical Lewy bodies and binds alpha-synuclein filaments. J Biol Chem 275, 21500–21507. https://doi.org/10.1074/jbc.M000099200

Jensen, P.H., Nielsen, M.S., Jakes, R., Dotti, C.G., Goedert, M., 1998. Binding of alpha-synuclein to brain vesicles is abolished by familial Parkinson's disease mutation. J Biol Chem 273, 26292–26294. https://doi.org/10.1074/jbc.273.41.26292

Jo, E., McLaurin, J., Yip, C.M., St George-Hyslop, P., Fraser, P.E., 2000. alpha-Synuclein membrane interactions and lipid specificity. J Biol Chem 275, 34328–34334. https://doi.org/10.1074/jbc.M004345200

Joensuu, M., Padmanabhan, P., Durisic, N., Bademosi, A.T.D., Cooper-Williams, E., Morrow, I.C., Harper, C.B., Jung, W., Parton, R.G., Goodhill, G.J., Papadopulos, A., Meunier, F.A., 2016. Subdiffractional tracking of internalized molecules reveals

heterogeneous motion states of synaptic vesicles. Journal of Cell Biology 215, 277–292. https://doi.org/10.1083/jcb.201604001

Jordan-Sciutto, K.L., Dorsey, R., Chalovich, E.M., Hammond, R.R., Achim, C.L., 2003. Expression patterns of retinoblastoma protein in Parkinson disease. J Neuropathol Exp Neurol 62, 68–74. https://doi.org/10.1093/jnen/62.1.68

Jovanovic, J.N., Benfenati, F., Siow, Y.L., Sihra, T.S., Sanghera, J.S., Pelech, S.L., Greengard, P., Czernik, A.J., 1996. Neurotrophins stimulate phosphorylation of synapsin I by MAP kinase and regulate synapsin I-actin interactions. Proc Natl Acad Sci U S A 93, 3679–3683. https://doi.org/10.1073/pnas.93.8.3679

Junn, E., Lee, S.S., Suhr, U.T., Mouradian, M.M., 2002. Parkin accumulation in aggresomes due to proteasome impairment. J Biol Chem 277, 47870–47877. https://doi.org/10.1074/jbc.M203159200

Kao, H.T., Porton, B., Hilfiker, S., Stefani, G., Pieribone, V.A., DeSalle, R., Greengard, P., 1999. Molecular evolution of the synapsin gene family. J Exp Zool 285, 360–377.

Katsuse, O., Iseki, E., Marui, W., Kosaka, K., 2003. Developmental stages of cortical Lewy bodies and their relation to axonal transport blockage in brains of patients with dementia with Lewy bodies. J Neurol Sci 211, 29–35. https://doi.org/10.1016/s0022-510x(03)00037-6

Kawaguchi, Y., Kovacs, J.J., McLaurin, A., Vance, J.M., Ito, A., Yao, T.P., 2003. The deacetylase HDAC6 regulates aggresome formation and cell viability in response to misfolded protein stress. Cell 115, 727–738. https://doi.org/10.1016/s0092-8674(03)00939-5

Kawamata, H., McLean, P.J., Sharma, N., Hyman, B.T., 2001. Interaction of alpha-synuclein and synphilin-1: effect of Parkinson's disease-associated mutations. J Neurochem 77, 929–934. https://doi.org/10.1046/j.1471-4159.2001.00301.x

Kim, G., Lee, S.-E., Jeong, S., Lee, J., Park, D., Chang, S., 2021. Multivalent electrostatic pi-cation interaction between synaptophysin and synapsin is responsible for the coacervation. Mol Brain 14, 137. https://doi.org/10.1186/s13041-021-00846-y

Kim, H.J., Kim, N.C., Wang, Y.-D., Scarborough, E.A., Moore, J., Diaz, Z., MacLea, K.S., Freibaum, B., Li, S., Molliex, A., Kanagaraj, A.P., Carter, R., Boylan, K.B., Wojtas, A.M., Rademakers, R., Pinkus, J.L., Greenberg, S.A., Trojanowski, J.Q., Traynor, B.J., Smith, B.N., Topp, S., Gkazi, A.-S., Miller, J., Shaw, C.E., Kottlors, M., Kirschner, J., Pestronk, A., Li, Y.R., Ford, A.F., Gitler, A.D., Benatar, M., King, O.D., Kimonis, V.E., Ross, E.D., Weihl, C.C., Shorter, J., Taylor, J.P., 2013. Mutations in prion-like domains in hnRNPA2B1 and hnRNPA1 cause multisystem proteinopathy and ALS. Nature 495, 467–473. https://doi.org/10.1038/nature11922

Kim, S., Yun, S.P., Lee, S., Umanah, G.E., Bandaru, V.V.R., Yin, X., Rhee, P., Karuppagounder, S.S., Kwon, S.-H., Lee, H., Mao, X., Kim, D., Pandey, A., Lee, G., Dawson, V.L., Dawson, T.M., Ko, H.S., 2018. GBA1 deficiency negatively affects physiological α-synuclein tetramers and related multimers. Proc Natl Acad Sci U S A 115, 798–803. https://doi.org/10.1073/pnas.1700465115

Kim, Y.S., Laurine, E., Woods, W., Lee, S.-J., 2006. A novel mechanism of interaction between alpha-synuclein and biological membranes. J Mol Biol 360, 386–397. https://doi.org/10.1016/j.jmb.2006.05.004

Klein, C., Westenberger, A., 2012. Genetics of Parkinson's disease. Cold Spring Harb Perspect Med 2, a008888. https://doi.org/10.1101/cshperspect.a008888

Klosin, A., Oltsch, F., Harmon, T., Honigmann, A., Jülicher, F., Hyman, A.A., Zechner, C., 2020. Phase separation provides a mechanism to reduce noise in cells. Science 367, 464–468. https://doi.org/10.1126/science.aav6691

Knott, A.B., Perkins, G., Schwarzenbacher, R., Bossy-Wetzel, E., 2008. Mitochondrial fragmentation in neurodegeneration. Nat Rev Neurosci 9, 505–518. https://doi.org/10.1038/nrn2417

Koga, S., Sekiya, H., Kondru, N., Ross, O.A., Dickson, D.W., 2021. Neuropathology and molecular diagnosis of Synucleinopathies. Mol Neurodegener 16, 83. https://doi.org/10.1186/s13024-021-00501-z

Kokoulina, P., Rohn, T.T., 2010. Caspase-cleaved transactivation response DNA-binding protein 43 in Parkinson's disease and dementia with Lewy bodies. Neurodegener Dis 7, 243–250. https://doi.org/10.1159/000287952

Koller, W., O'Hara, R., Weiner, W., Lang, A., Nutt, J., Agid, Y., Bonnet, A.M., Jankovic, J., 1987. Relationship of aging to Parkinson's disease. Adv Neurol 45, 317–321.

Kopito, R.R., 2000. Aggresomes, inclusion bodies and protein aggregation. Trends Cell Biol 10, 524–530. https://doi.org/10.1016/s0962-8924(00)01852-3

Koppers, M., Özkan, N., Farías, G.G., 2020. Complex Interactions Between Membrane-Bound Organelles, Biomolecular Condensates and the Cytoskeleton. Frontiers in Cell and Developmental Biology 8.

Krabben, L., Fassio, A., Bhatia, V.K., Pechstein, A., Onofri, F., Fadda, M., Messa, M., Rao, Y., Shupliakov, O., Stamou, D., Benfenati, F., Haucke, V., 2011. Synapsin I Senses Membrane Curvature by an Amphipathic Lipid Packing Sensor Motif. J. Neurosci. 31, 18149–18154. https://doi.org/10.1523/JNEUROSCI.4345-11.2011

Kraszewski, K., Daniell, L., Mundigl, O., De Camilli, P., 1996. Mobility of synaptic vesicles in nerve endings monitored by recovery from photobleaching of synaptic vesicle-associated fluorescence. J Neurosci 16, 5905–5913. https://doi.org/10.1523/JNEUROSCI.16-19-05905.1996

Krüger, R., 2004. The role of synphilin-1 in synaptic function and protein degradation. Cell Tissue Res 318, 195–199. https://doi.org/10.1007/s00441-004-0953-z

Krüger, R., Kuhn, W., Müller, T., Woitalla, D., Graeber, M., Kösel, S., Przuntek, H., Epplen, J.T., Schöls, L., Riess, O., 1998. Ala30Pro mutation in the gene encoding alpha-synuclein in Parkinson's disease. Nat Genet 18, 106–108. https://doi.org/10.1038/ng0298-106

Kuusisto, E., Parkkinen, L., Alafuzoff, I., 2003. Morphogenesis of Lewy bodies: dissimilar incorporation of alpha-synuclein, ubiquitin, and p62. J Neuropathol Exp Neurol 62, 1241–1253. https://doi.org/10.1093/jnen/62.12.1241

Kuzuhara, S., Mori, H., Izumiyama, N., Yoshimura, M., Ihara, Y., 1988. Lewy bodies are ubiquitinated. A light and electron microscopic immunocytochemical study. Acta Neuropathol 75, 345–353. https://doi.org/10.1007/BF00687787

Lashuel, H.A., 2020. Do Lewy bodies contain alpha-synuclein fibrils? and Does it matter? A brief history and critical analysis of recent reports. Neurobiol Dis 141, 104876. https://doi.org/10.1016/j.nbd.2020.104876

Lashuel, H.A., Hartley, D., Petre, B.M., Walz, T., Lansbury, P.T., 2002a. Neurodegenerative disease: amyloid pores from pathogenic mutations. Nature 418, 291. https://doi.org/10.1038/418291a

Lashuel, H.A., Petre, B.M., Wall, J., Simon, M., Nowak, R.J., Walz, T., Lansbury, P.T., 2002b. Alpha-synuclein, especially the Parkinson's disease-associated mutants, forms pore-like annular and tubular protofibrils. J Mol Biol 322, 1089–1102. https://doi.org/10.1016/s0022-2836(02)00735-0

Lautenschläger, J., Stephens, A.D., Fusco, G., Ströhl, F., Curry, N., Zacharopoulou, M., Michel, C.H., Laine, R., Nespovitaya, N., Fantham, M., Pinotsi, D., Zago, W., Fraser, P., Tandon, A., St George-Hyslop, P., Rees, E., Phillips, J.J., De Simone, A., Kaminski, C.F., Schierle, G.S.K., 2018. C-terminal calcium binding of α-synuclein modulates synaptic vesicle interaction. Nat Commun 9, 712. https://doi.org/10.1038/s41467-018-03111-4

Lee, G., Tanaka, M., Park, K., Lee, S.S., Kim, Y.M., Junn, E., Lee, S.-H., Mouradian, M.M., 2004. Casein kinase II-mediated phosphorylation regulates alpha-synuclein/synphilin-1 interaction and inclusion body formation. J Biol Chem 279, 6834–6839. https://doi.org/10.1074/jbc.M312760200

Lee, H.-J., Choi, C., Lee, S.-J., 2002. Membrane-bound alpha-synuclein has a high aggregation propensity and the ability to seed the aggregation of the cytosolic form. J Biol Chem 277, 671–678. https://doi.org/10.1074/jbc.M107045200

Lee, S.S., Kim, Y.M., Junn, E., Lee, G., Park, K.-H., Tanaka, M., Ronchetti, R.D., Quezado, M.M., Mouradian, M.M., 2003. Cell cycle aberrations by alpha-synuclein over-expression and cyclin B immunoreactivity in Lewy bodies. Neurobiol Aging 24, 687–696. https://doi.org/10.1016/s0197-4580(02)00196-3

Lees, A.J., Selikhova, M., Andrade, L.A., Duyckaerts, C., 2008. The black stuff and Konstantin Nikolaevich Tretiakoff. Mov Disord 23, 777–783. https://doi.org/10.1002/mds.21855

Leverenz, J.B., Umar, I., Wang, Q., Montine, T.J., McMillan, P.J., Tsuang, D.W., Jin, J., Pan, C., Shin, J., Zhu, D., Zhang, J., 2007. Proteomic identification of novel proteins in cortical lewy bodies. Brain Pathol 17, 139–145. https://doi.org/10.1111/j.1750-3639.2007.00048.x

Levy, G., 2007. The relationship of Parkinson disease with aging. Arch Neurol 64, 1242–1246. https://doi.org/10.1001/archneur.64.9.1242

Li, H.-T., Du, H.-N., Tang, L., Hu, J., Hu, H.-Y., 2002. Structural transformation and aggregation of human alpha-synuclein in trifluoroethanol: non-amyloid component sequence is essential and beta-sheet formation is prerequisite to aggregation. Biopolymers 64, 221–226. https://doi.org/10.1002/bip.10179

Li, P., Banjade, S., Cheng, H.-C., Kim, S., Chen, B., Guo, L., Llaguno, M., Hollingsworth, J.V., King, D.S., Banani, S.F., Russo, P.S., Jiang, Q.-X., Nixon, B.T., Rosen, M.K., 2012. Phase transitions in the assembly of multivalent signalling proteins. Nature 483, 336–340. https://doi.org/10.1038/nature10879

Li, W., West, N., Colla, E., Pletnikova, O., Troncoso, J.C., Marsh, L., Dawson, T.M., Jäkälä, P., Hartmann, T., Price, D.L., Lee, M.K., 2005. Aggregation promoting C-terminal truncation of alpha-synuclein is a normal cellular process and is enhanced by the familial

Parkinson's disease-linked mutations. Proc Natl Acad Sci U S A 102, 2162–2167. https://doi.org/10.1073/pnas.0406976102

Liani, E., Eyal, A., Avraham, E., Shemer, R., Szargel, R., Berg, D., Bornemann, A., Riess, O., Ross, C.A., Rott, R., Engelender, S., 2004. Ubiquitylation of synphilin-1 and alpha-synuclein by SIAH and its presence in cellular inclusions and Lewy bodies imply a role in Parkinson's disease. Proc Natl Acad Sci U S A 101, 5500–5505. https://doi.org/10.1073/pnas.0401081101

Licker, V., Turck, N., Kövari, E., Burkhardt, K., Côte, M., Surini-Demiri, M., Lobrinus, J.A., Sanchez, J.-C., Burkhard, P.R., 2014. Proteomic analysis of human substantia nigra identifies novel candidates involved in Parkinson's disease pathogenesis. Proteomics 14, 784–794. https://doi.org/10.1002/pmic.201300342

Loeffler, D.A., Camp, D.M., Conant, S.B., 2006. Complement activation in the Parkinson's disease substantia nigra: an immunocytochemical study. J Neuroinflammation 3, 29. https://doi.org/10.1186/1742-2094-3-29

Luna, E., Luk, K.C., 2015. Bent out of shape: α-Synuclein misfolding and the convergence of pathogenic pathways in Parkinson's disease. FEBS Lett 589, 3749–3759. https://doi.org/10.1016/j.febslet.2015.10.023

Luo, Y., Na, Z., Slavoff, S.A., 2018. P-Bodies: Composition, Properties, and Functions. Biochemistry 57, 2424–2431. https://doi.org/10.1021/acs.biochem.7b01162

Lyon, A.S., Peeples, W.B., Rosen, M.K., 2021. A framework for understanding the functions of biomolecular condensates across scales. Nat Rev Mol Cell Biol 22, 215–235. https://doi.org/10.1038/s41580-020-00303-z

Mackenzie, I.R., Nicholson, A.M., Sarkar, M., Messing, J., Purice, M.D., Pottier, C., Annu, K., Baker, M., Perkerson, R.B., Kurti, A., Matchett, B.J., Mittag, T., Temirov, J., Hsiung, G.-Y.R., Krieger, C., Murray, M.E., Kato, M., Fryer, J.D., Petrucelli, L., Zinman, L., Weintraub, S., Mesulam, M., Keith, J., Zivkovic, S.A., Hirsch-Reinshagen, V., Roos, R.P., Züchner, S., Graff-Radford, N.R., Petersen, R.C., Caselli, R.J., Wszolek, Z.K., Finger, E.,

Lippa, C., Lacomis, D., Stewart, H., Dickson, D.W., Kim, H.J., Rogaeva, E., Bigio, E., Boylan, K.B., Taylor, J.P., Rademakers, R., 2017. TIA1 Mutations in Amyotrophic Lateral Sclerosis and Frontotemporal Dementia Promote Phase Separation and Alter Stress Granule Dynamics. Neuron 95, 808-816.e9. https://doi.org/10.1016/j.neuron.2017.07.025

Mackenzie, I.R.A., Neumann, M., 2016. Molecular neuropathology of frontotemporal dementia: insights into disease mechanisms from postmortem studies. J Neurochem 138 Suppl 1, 54–70. https://doi.org/10.1111/jnc.13588

Mahul-Mellier, A.-L., Burtscher, J., Maharjan, N., Weerens, L., Croisier, M., Kuttler, F., Leleu, M., Knott, G.W., Lashuel, H.A., 2020. The process of Lewy body formation, rather than simply α-synuclein fibrillization, is one of the major drivers of neurodegeneration. Proc Natl Acad Sci U S A 117, 4971–4982. https://doi.org/10.1073/pnas.1913904117

Mamais, A., Raja, M., Manzoni, C., Dihanich, S., Lees, A., Moore, D., Lewis, P.A., Bandopadhyay, R., 2013. Divergent α-synuclein solubility and aggregation properties in G2019S LRRK2 Parkinson's disease brains with Lewy Body pathology compared to idiopathic cases. Neurobiol Dis 58, 183–190. https://doi.org/10.1016/j.nbd.2013.05.017

Maroteaux, L., Campanelli, J.T., Scheller, R.H., 1988. Synuclein: a neuron-specific protein localized to the nucleus and presynaptic nerve terminal. J Neurosci 8, 2804–2815. https://doi.org/10.1523/JNEUROSCI.08-08-02804.1988

Marrone, L., Drexler, H.C.A., Wang, J., Tripathi, P., Distler, T., Heisterkamp, P., Anderson, E.N., Kour, S., Moraiti, A., Maharana, S., Bhatnagar, R., Belgard, T.G., Tripathy, V., Kalmbach, N., Hosseinzadeh, Z., Crippa, V., Abo-Rady, M., Wegner, F., Poletti, A., Troost, D., Aronica, E., Busskamp, V., Weis, J., Pandey, U.B., Hyman, A.A., Alberti, S., Goswami, A., Sterneckert, J., 2019. FUS pathology in ALS is linked to alterations in multiple ALS-associated proteins and rescued by drugs stimulating autophagy. Acta Neuropathol 138, 67–84. https://doi.org/10.1007/s00401-019-01998-x

Marx, F.P., Holzmann, C., Strauss, K.M., Li, L., Eberhardt, O., Gerhardt, E., Cookson, M.R., Hernandez, D., Farrer, M.J., Kachergus, J., Engelender, S., Ross, C.A., Berger, K., Schöls, L., Schulz, J.B., Riess, O., Krüger, R., 2003. Identification and functional characterization

of a novel R621C mutation in the synphilin-1 gene in Parkinson's disease. Hum Mol Genet 12, 1223–1231. https://doi.org/10.1093/hmg/ddg134

Matsubara, M., Kusubata, M., Ishiguro, K., Uchida, T., Titani, K., Taniguchi, H., 1996. Site-specific phosphorylation of synapsin I by mitogen-activated protein kinase and Cdk5 and its effects on physiological functions. J Biol Chem 271, 21108–21113. https://doi.org/10.1074/jbc.271.35.21108

McLean, P.J., Kawamata, H., Ribich, S., Hyman, B.T., 2000. Membrane association and protein conformation of alpha-synuclein in intact neurons. Effect of Parkinson's disease-linked mutations. J Biol Chem 275, 8812–8816. https://doi.org/10.1074/jbc.275.12.8812

McNaught, K.S.P., Shashidharan, P., Perl, D.P., Jenner, P., Olanow, C.W., 2002. Aggresome-related biogenesis of Lewy bodies. Eur J Neurosci 16, 2136–2148. https://doi.org/10.1046/j.1460-9568.2002.02301.x

McPherson, P.S., Czernik, A.J., Chilcote, T.J., Onofri, F., Benfenati, F., Greengard, P., Schlessinger, J., De Camilli, P., 1994. Interaction of Grb2 via its Src homology 3 domains with synaptic proteins including synapsin I. Proc Natl Acad Sci U S A 91, 6486–6490. https://doi.org/10.1073/pnas.91.14.6486

Medeiros, A.T., Soll, L.G., Tessari, I., Bubacco, L., Morgan, J.R., 2017. α-Synuclein Dimers Impair Vesicle Fission during Clathrin-Mediated Synaptic Vesicle Recycling. Front Cell Neurosci 11, 388. https://doi.org/10.3389/fncel.2017.00388

Middleton, E.R., Rhoades, E., 2010. Effects of curvature and composition on α-synuclein binding to lipid vesicles. Biophys J 99, 2279–2288. https://doi.org/10.1016/j.bpj.2010.07.056

Milovanovic, D., De Camilli, P., 2017. Synaptic Vesicle Clusters at Synapses: A Distinct Liquid Phase? Neuron 93, 995–1002. https://doi.org/10.1016/j.neuron.2017.02.013

Milovanovic, D., Jahn, R., 2015. Organization and dynamics of SNARE proteins in the presynaptic membrane. Frontiers in Physiology 6.

Milovanovic, D., Wu, Y., Bian, X., De Camilli, P., 2018. A liquid phase of synapsin and lipid vesicles. Science 361, 604–607. https://doi.org/10.1126/science.aat5671

Monaldi, I., Vassalli, M., Bachi, A., Giovedì, S., Millo, E., Valtorta, F., Raiteri, R., Benfenati, F., Fassio, A., 2010. The highly conserved synapsin domain E mediates synapsin dimerization and phospholipid vesicle clustering. Biochem J 426, 55–64. https://doi.org/10.1042/BJ20090762

Moore, A.S., Coscia, S.M., Simpson, C.L., Ortega, F.E., Wait, E.C., Heddleston, J.M., Nirschl, J.J., Obara, C.J., Guedes-Dias, P., Boecker, C.A., Chew, T.-L., Theriot, J.A., Lippincott-Schwartz, J., Holzbaur, E.L.F., 2021. Actin cables and comet tails organize mitochondrial networks in mitosis. Nature 591, 659–664. https://doi.org/10.1038/s41586-021-03309-5

Moore, A.S., Wong, Y.C., Simpson, C.L., Holzbaur, E.L.F., 2016. Dynamic actin cycling through mitochondrial subpopulations locally regulates the fission-fusion balance within mitochondrial networks. Nat Commun 7, 12886. https://doi.org/10.1038/ncomms12886

Mor, D.E., Ugras, S.E., Daniels, M.J., Ischiropoulos, H., 2016. Dynamic structural flexibility of α-synuclein. Neurobiol Dis 88, 66–74. https://doi.org/10.1016/j.nbd.2015.12.018

Moran, U., Phillips, R., Milo, R., 2010. SnapShot: key numbers in biology. Cell 141, 1262-1262.e1. https://doi.org/10.1016/j.cell.2010.06.019

Mosavi, L.K., Cammett, T.J., Desrosiers, D.C., Peng, Z.-Y., 2004. The ankyrin repeat as molecular architecture for protein recognition. Protein Sci 13, 1435–1448. https://doi.org/10.1110/ps.03554604

Murata, K., Tanaka, H., 2010. Surface-wetting effects on the liquid–liquid transition of a single-component molecular liquid. Nat Commun 1, 16. https://doi.org/10.1038/ncomms1015

Murray, I.J., Medford, M.A., Guan, H.-P., Rueter, S.M., Trojanowski, J.Q., Lee, V.M.-Y., 2003. Synphilin in normal human brains and in synucleinopathies: studies with new antibodies. Acta Neuropathol 105, 177–184. https://doi.org/10.1007/s00401-002-0629-2

Myhre, R., Klungland, H., Farrer, M.J., Aasly, J.O., 2008. Genetic association study of synphilin-1 in idiopathic Parkinson's disease. BMC Med Genet 9, 19. https://doi.org/10.1186/1471-2350-9-19

Nagano, Y., Yamashita, H., Takahashi, T., Kishida, S., Nakamura, T., Iseki, E., Hattori, N., Mizuno, Y., Kikuchi, A., Matsumoto, M., 2003. Siah-1 facilitates ubiquitination and degradation of synphilin-1. J Biol Chem 278, 51504–51514. https://doi.org/10.1074/jbc.M306347200

Nagy, A., Baker, R.R., Morris, S.J., Whittaker, V.P., 1976. The preparation and characterization of synaptic vesicles of high purity. Brain Res 109, 285–309. https://doi.org/10.1016/0006-8993(76)90531-x

Nakamura, S., Kawamoto, Y., Nakano, S., Akiguchi, I., Kimura, J., 1997. p35nck5a and cyclin-dependent kinase 5 colocalize in Lewy bodies of brains with Parkinson's disease. Acta Neuropathol 94, 153–157. https://doi.org/10.1007/s004010050687

Nemani, V.M., Lu, W., Berge, V., Nakamura, K., Onoa, B., Lee, M.K., Chaudhry, F.A., Nicoll, R.A., Edwards, R.H., 2010. Increased expression of alpha-synuclein reduces neurotransmitter release by inhibiting synaptic vesicle reclustering after endocytosis. Neuron 65, 66–79. https://doi.org/10.1016/j.neuron.2009.12.023

Nestler, E.J., Greengard, P., 1984. Neuron-specific phosphoproteins in mammalian brain. Adv Cyclic Nucleotide Protein Phosphorylation Res 17, 483–488.

Neves, G., Lagnado, L., 1999. The kinetics of exocytosis and endocytosis in the synaptic terminal of goldfish retinal bipolar cells. J Physiol 515 (Pt 1), 181–202. https://doi.org/10.1111/j.1469-7793.1999.181ad.x

Neystat, M., Rzhetskaya, M., Kholodilov, N., Burke, R.E., 2002. Analysis of synphilin-1 and synuclein interactions by yeast two-hybrid beta-galactosidase liquid assay. Neurosci Lett 325, 119–123. https://doi.org/10.1016/s0304-3940(02)00253-7

Nichols, M.R., Moss, M.A., Reed, D.K., Lin, W.-L., Mukhopadhyay, R., Hoh, J.H., Rosenberry, T.L., 2002. Growth of beta-amyloid(1-40) protofibrils by monomer elongation and lateral association. Characterization of distinct products by light scattering and atomic force microscopy. Biochemistry 41, 6115–6127. https://doi.org/10.1021/bi015985r

Nishimura, M., Tomimoto, H., Suenaga, T., Nakamura, S., Namba, Y., Ikeda, K., Akiguchi, I., Kimura, J., 1994. Synaptophysin and chromogranin A immunoreactivities of Lewy bodies in Parkinson's disease brains. Brain Res 634, 339–344. https://doi.org/10.1016/0006-8993(94)91940-2

Noda, K., Kitami, T., Gai, W.P., Chegini, F., Jensen, P.H., Fujimura, T., Murayama, K., Tanaka, K., Mizuno, Y., Hattori, N., 2005. Phosphorylated IkappaBalpha is a component of Lewy body of Parkinson's disease. Biochem Biophys Res Commun 331, 309–317. https://doi.org/10.1016/j.bbrc.2005.03.167

Nuber, S., Franck, T., Wolburg, H., Schumann, U., Casadei, N., Fischer, K., Calaminus, C., Pichler, B.J., Chanarat, S., Teismann, P., Schulz, J.B., Luft, A.R., Tomiuk, J., Wilbertz, J., Bornemann, A., Krüger, R., Riess, O., 2010. Transgenic overexpression of the alpha-synuclein interacting protein synphilin-1 leads to behavioral and neuropathological alterations in mice. Neurogenetics 11, 107–120. https://doi.org/10.1007/s10048-009-0212-2

Odagiri, S., Tanji, K., Mori, F., Kakita, A., Takahashi, H., Wakabayashi, K., 2012. Autophagic adapter protein NBR1 is localized in Lewy bodies and glial cytoplasmic inclusions and is involved in aggregate formation in α-synucleinopathy. Acta Neuropathol 124, 173–186. https://doi.org/10.1007/s00401-012-0975-7

O'Farrell, C., Murphy, D.D., Petrucelli, L., Singleton, A.B., Hussey, J., Farrer, M., Hardy, J., Dickson, D.W., Cookson, M.R., 2001. Transfected synphilin-1 forms cytoplasmic inclusions in HEK293 cells. Brain Res Mol Brain Res 97, 94–102. https://doi.org/10.1016/s0169-328x(01)00292-3

O'Farrell, C., Pickford, F., Vink, L., McGowan, E., Cookson, M.R., 2002. Sequence conservation between mouse and human synphilin-1. Neurosci Lett 322, 9–12. https://doi.org/10.1016/s0304-3940(02)00068-x

Olanow, C.W., Perl, D.P., DeMartino, G.N., McNaught, K.S.P., 2004. Lewy-body formation is an aggresome-related process: a hypothesis. Lancet Neurol 3, 496–503. https://doi.org/10.1016/S1474-4422(04)00827-0

Ong, J.Y., Torres, J.Z., 2020. Phase Separation in Cell Division. Molecular Cell 80, 9–20. https://doi.org/10.1016/j.molcel.2020.08.007

Onofri, F., Giovedi, S., Kao, H.T., Valtorta, F., Bongiorno Borbone, L., De Camilli, P., Greengard, P., Benfenati, F., 2000. Specificity of the binding of synapsin I to Src homology 3 domains. J Biol Chem 275, 29857–29867. https://doi.org/10.1074/jbc.M006018200

Onofri, F., Messa, M., Matafora, V., Bonanno, G., Corradi, A., Bachi, A., Valtorta, F., Benfenati, F., 2007. Synapsin phosphorylation by SRC tyrosine kinase enhances SRC activity in synaptic vesicles. J Biol Chem 282, 15754–15767. https://doi.org/10.1074/jbc.M701051200

Orenbuch, A., Shalev, L., Marra, V., Sinai, I., Lavy, Y., Kahn, J., Burden, J.J., Staras, K., Gitler, D., 2012. Synapsin selectively controls the mobility of resting pool vesicles at hippocampal terminals. J Neurosci 32, 3969–3980. https://doi.org/10.1523/JNEUROSCI.5058-11.2012

Orr, C.F., Rowe, D.B., Mizuno, Y., Mori, H., Halliday, G.M., 2005. A possible role for humoral immunity in the pathogenesis of Parkinson's disease. Brain 128, 2665–2674. https://doi.org/10.1093/brain/awh625

Pak, C.W., Kosno, M., Holehouse, A.S., Padrick, S.B., Mittal, A., Ali, R., Yunus, A.A., Liu, D.R., Pappu, R.V., Rosen, M.K., 2016. Sequence Determinants of Intracellular Phase Separation by Complex Coacervation of a Disordered Protein. Molecular Cell 63, 72–85. https://doi.org/10.1016/j.molcel.2016.05.042

Parkinson, J., 2002. An essay on the shaking palsy. 1817. J Neuropsychiatry Clin Neurosci 14, 223–236; discussion 222. https://doi.org/10.1176/jnp.14.2.223

Patel, A., Lee, H.O., Jawerth, L., Maharana, S., Jahnel, M., Hein, M.Y., Stoynov, S., Mahamid, J., Saha, S., Franzmann, T.M., Pozniakovski, A., Poser, I., Maghelli, N., Royer, L.A., Weigert, M., Myers, E.W., Grill, S., Drechsel, D., Hyman, A.A., Alberti, S., 2015. A Liquid-to-Solid Phase Transition of the ALS Protein FUS Accelerated by Disease Mutation. Cell 162, 1066–1077. https://doi.org/10.1016/j.cell.2015.07.047

Pechstein, A., Tomilin, N., Fredrich, K., Vorontsova, O., Sopova, E., Evergren, E., Haucke, V., Brodin, L., Shupliakov, O., 2020. Vesicle Clustering in a Living Synapse Depends on a Synapsin Region that Mediates Phase Separation. Cell Rep 30, 2594-2602.e3. https://doi.org/10.1016/j.celrep.2020.01.092

Peduzzo, A., Linse, S., Buell, A.K., 2020. The Properties of α-Synuclein Secondary Nuclei Are Dominated by the Solution Conditions Rather than the Seed Fibril Strain. ACS Chem Neurosci 11, 909–918. https://doi.org/10.1021/acschemneuro.9b00594

Peeples, W., Rosen, M.K., 2021. Mechanistic dissection of increased enzymatic rate in a phase-separated compartment. Nat Chem Biol 17, 693–702. https://doi.org/10.1038/s41589-021-00801-x

Perego, E., Reshetniak, S., Lorenz, C., Hoffmann, C., Milovanović, D., Rizzoli, S.O., Köster, S., 2020. A minimalist model to measure interactions between proteins and synaptic vesicles. Sci Rep 10, 21086. https://doi.org/10.1038/s41598-020-77887-1

Ph, J., K, I., J, K., Ms, N., J, P., Wp, G., 2000. Microtubule-associated protein 1B is a component of cortical Lewy bodies and binds alpha-synuclein filaments. The Journal of biological chemistry 275. https://doi.org/10.1074/jbc.M000099200

Picca, A., Guerra, F., Calvani, R., Romano, R., Coelho-Júnior, H.J., Bucci, C., Marzetti, E., 2021. Mitochondrial Dysfunction, Protein Misfolding and Neuroinflammation in Parkinson's Disease: Roads to Biomarker Discovery. Biomolecules 11, 1508. https://doi.org/10.3390/biom11101508

Pieribone, V.A., Shupliakov, O., Brodin, L., Hilfiker-Rothenfluh, S., Czernik, A.J., Greengard, P., 1995. Distinct pools of synaptic vesicles in neurotransmitter release. Nature 375, 493–497. https://doi.org/10.1038/375493a0

Poirier, M.A., Li, H., Macosko, J., Cai, S., Amzel, M., Ross, C.A., 2002. Huntingtin spheroids and protofibrils as precursors in polyglutamine fibrilization. J Biol Chem 277, 41032–41037. https://doi.org/10.1074/jbc.M205809200

Polymeropoulos, M.H., Lavedan, C., Leroy, E., Ide, S.E., Dehejia, A., Dutra, A., Pike, B., Root, H., Rubenstein, J., Boyer, R., Stenroos, E.S., Chandrasekharappa, S., Athanassiadou, A., Papapetropoulos, T., Johnson, W.G., Lazzarini, A.M., Duvoisin, R.C., Di Iorio, G., Golbe, L.I., Nussbaum, R.L., 1997. Mutation in the alpha-synuclein gene identified in families with Parkinson's disease. Science 276, 2045–2047. https://doi.org/10.1126/science.276.5321.2045

Pritišanac, I., Vernon, R.M., Moses, A.M., Forman Kay, J.D., 2019. Entropy and Information within Intrinsically Disordered Protein Regions. Entropy 21, 662. https://doi.org/10.3390/e21070662

Pytowski, L., Lee, C.F., Foley, A.C., Vaux, D.J., Jean, L., 2020. Liquid-liquid phase separation of type II diabetes-associated IAPP initiates hydrogelation and aggregation. Proc Natl Acad Sci U S A 117, 12050–12061. https://doi.org/10.1073/pnas.1916716117

Qiu, X., Zhu, Q., Sun, J., 2015. Quantitative analysis of vesicle recycling at the calyx of Held synapse. Proceedings of the National Academy of Sciences 112, 4779–4784. https://doi.org/10.1073/pnas.1424597112

Quiroz, F.G., Fiore, V.F., Levorse, J., Polak, L., Wong, E., Pasolli, H.A., Fuchs, E., 2020. Liquid-liquid phase separation drives skin barrier formation. Science 367, eaax9554. https://doi.org/10.1126/science.aax9554

Ramakrishnan, M., Jensen, P.H., Marsh, D., 2003. Alpha-synuclein association with phosphatidylglycerol probed by lipid spin labels. Biochemistry 42, 12919–12926. https://doi.org/10.1021/bi035048e

Ramella, M., Ribolla, L.M., de Curtis, I., 2022. Liquid-Liquid Phase Separation at the Plasma Membrane-Cytosol Interface: Common Players in Adhesion, Motility, and Synaptic Function. J Mol Biol 434, 167228. https://doi.org/10.1016/j.jmb.2021.167228

Ramis, R., Ortega-Castro, J., Vilanova, B., Adrover, M., Frau, J., 2020. Unraveling the NaCl Concentration Effect on the First Stages of α-Synuclein Aggregation. Biomacromolecules 21, 5200–5212. https://doi.org/10.1021/acs.biomac.0c01292

Ray, S., Singh, N., Kumar, R., Patel, K., Pandey, S., Datta, D., Mahato, J., Panigrahi, R., Navalkar, A., Mehra, S., Gadhe, L., Chatterjee, D., Sawner, A.S., Maiti, S., Bhatia, S., Gerez, J.A., Chowdhury, A., Kumar, A., Padinhateeri, R., Riek, R., Krishnamoorthy, G., Maji, S.K., 2020. α-Synuclein aggregation nucleates through liquid-liquid phase separation. Nat Chem 12, 705–716. https://doi.org/10.1038/s41557-020-0465-9

Rebane, A.A., Ziltener, P., LaMonica, L.C., Bauer, A.H., Zheng, H., López-Montero, I., Pincet, F., Rothman, J.E., Ernst, A.M., 2020. Liquid–liquid phase separation of the Golgi matrix protein GM130. FEBS Letters 594, 1132–1144. https://doi.org/10.1002/1873-3468.13715

Reshetniak, S., Ußling, J.-E., Perego, E., Rammner, B., Schikorski, T., Fornasiero, E.F., Truckenbrodt, S., Köster, S., Rizzoli, S.O., 2020. A comparative analysis of the mobility of 45 proteins in the synaptic bouton. EMBO J 39, e104596. https://doi.org/10.15252/embj.2020104596

Rettig, J., Neher, E., 2002. Emerging Roles of Presynaptic Proteins in Ca++-Triggered Exocytosis. Science 298, 781–785. https://doi.org/10.1126/science.1075375

Ribeiro, C.S., Carneiro, K., Ross, C.A., Menezes, J.R.L., Engelender, S., 2002. Synphilin-1 is developmentally localized to synaptic terminals, and its association with synaptic vesicles is modulated by alpha-synuclein. J Biol Chem 277, 23927–23933. https://doi.org/10.1074/jbc.M201115200

Rizzoli, S.O., Betz, W.J., 2005. Synaptic vesicle pools. Nat Rev Neurosci 6, 57–69. https://doi.org/10.1038/nrn1583

Rizzoli, S.O., Betz, W.J., 2004. The Structural Organization of the Readily Releasable Pool of Synaptic Vesicles. Science 303, 2037–2039. https://doi.org/10.1126/science.1094682

Roberts, R.F., Wade-Martins, R., Alegre-Abarrategui, J., 2015. Direct visualization of alpha-synuclein oligomers reveals previously undetected pathology in Parkinson's disease brain. Brain 138, 1642–1657. https://doi.org/10.1093/brain/awv040

Rosahl, T.W., Spillane, D., Missler, M., Herz, J., Selig, D.K., Wolff, J.R., Hammer, R.E., Malenka, R.C., Südhof, T.C., 1995. Essential functions of synapsins I and II in synaptic vesicle regulation. Nature 375, 488–493. https://doi.org/10.1038/375488a0

Rovere, M., Sanderson, J.B., Fonseca-Ornelas, L., Patel, D.S., Bartels, T., 2018. Refolding of helical soluble α-synuclein through transient interaction with lipid interfaces. FEBS Lett 592, 1464–1472. https://doi.org/10.1002/1873-3468.13047

Saito, Y., Kawashima, A., Ruberu, N.N., Fujiwara, H., Koyama, S., Sawabe, M., Arai, T., Nagura, H., Yamanouchi, H., Hasegawa, M., Iwatsubo, T., Murayama, S., 2003. Accumulation of phosphorylated alpha-synuclein in aging human brain. J Neuropathol Exp Neurol 62, 644–654. https://doi.org/10.1093/jnen/62.6.644

Samii, A., Nutt, J.G., Ransom, B.R., 2004. Parkinson's disease. Lancet 363, 1783–1793. https://doi.org/10.1016/S0140-6736(04)16305-8

Sansevrino, R., Hoffmann, C., Milovanovic, D., 2023. Condensate biology of synaptic vesicle clusters. Trends Neurosci 46, 293–306. https://doi.org/10.1016/j.tins.2023.01.001

Sawada, H., Kohno, R., Kihara, T., Izumi, Y., Sakka, N., Ibi, M., Nakanishi, M., Nakamizo, T., Yamakawa, K., Shibasaki, H., Yamamoto, N., Akaike, A., Inden, M., Kitamura, Y., Taniguchi, T., Shimohama, S., 2004. Proteasome mediates dopaminergic neuronal degeneration, and its inhibition causes alpha-synuclein inclusions. J Biol Chem 279, 10710–10719. https://doi.org/10.1074/jbc.M308434200

Schlossmacher, M.G., Frosch, M.P., Gai, W.P., Medina, M., Sharma, N., Forno, L., Ochiishi, T., Shimura, H., Sharon, R., Hattori, N., Langston, J.W., Mizuno, Y., Hyman, B.T., Selkoe,

D.J., Kosik, K.S., 2002. Parkin localizes to the Lewy bodies of Parkinson disease and dementia with Lewy bodies. Am J Pathol 160, 1655–1667. https://doi.org/10.1016/S0002-9440(10)61113-3

Sekiya, H., Kowa, H., Koga, H., Takata, M., Satake, W., Futamura, N., Funakawa, I., Jinnai, K., Takahashi, M., Kondo, T., Ueno, Y., Kanagawa, M., Kobayashi, K., Toda, T., 2019. Wide distribution of alpha-synuclein oligomers in multiple system atrophy brain detected by proximity ligation. Acta Neuropathol 137, 455–466. https://doi.org/10.1007/s00401-019-01961-w

Setru, S.U., Gouveia, B., Alfaro-Aco, R., Shaevitz, J.W., Stone, H.A., Petry, S., 2021. A hydrodynamic instability drives protein droplet formation on microtubules to nucleate branches. Nat. Phys. 17, 493–498. https://doi.org/10.1038/s41567-020-01141-8

Shahmoradian, S.H., Lewis, A.J., Genoud, C., Hench, J., Moors, T.E., Navarro, P.P., Castaño-Díez, D., Schweighauser, G., Graff-Meyer, A., Goldie, K.N., Sütterlin, R., Huisman, E., Ingrassia, A., Gier, Y. de, Rozemuller, A.J.M., Wang, J., Paepe, A.D., Erny, J., Staempfli, A., Hoernschemeyer, J., Großerüschkamp, F., Niedieker, D., El-Mashtoly, S.F., Quadri, M., Van IJcken, W.F.J., Bonifati, V., Gerwert, K., Bohrmann, B., Frank, S., Britschgi, M., Stahlberg, H., Van de Berg, W.D.J., Lauer, M.E., 2019. Lewy pathology in Parkinson's disease consists of crowded organelles and lipid membranes. Nat Neurosci 22, 1099–1109. https://doi.org/10.1038/s41593-019-0423-2

Shin, Y., Brangwynne, C.P., 2017. Liquid phase condensation in cell physiology and disease. Science 357, eaaf4382. https://doi.org/10.1126/science.aaf4382

Shulman, J.M., De Jager, P.L., Feany, M.B., 2011. Parkinson's disease: genetics and pathogenesis. Annu Rev Pathol 6, 193–222. https://doi.org/10.1146/annurev-pathol-011110-130242

Shupliakov, O., 2009. The synaptic vesicle cluster: a source of endocytic proteins during neurotransmitter release. Neuroscience 158, 204–210. https://doi.org/10.1016/j.neuroscience.2008.03.035

Simón-Sánchez, J., Schulte, C., Bras, J.M., Sharma, M., Gibbs, J.R., Berg, D., Paisan-Ruiz, C., Lichtner, P., Scholz, S.W., Hernandez, D.G., Krüger, R., Federoff, M., Klein, C., Goate, A., Perlmutter, J., Bonin, M., Nalls, M.A., Illig, T., Gieger, C., Houlden, H., Steffens, M., Okun, M.S., Racette, B.A., Cookson, M.R., Foote, K.D., Fernandez, H.H., Traynor, B.J., Schreiber, S., Arepalli, S., Zonozi, R., Gwinn, K., van der Brug, M., Lopez, G., Chanock, S.J., Schatzkin, A., Park, Y., Hollenbeck, A., Gao, J., Huang, X., Wood, N.W., Lorenz, D., Deuschl, G., Chen, H., Riess, O., Hardy, J.A., Singleton, A.B., Gasser, T., 2009. Genome-wide association study reveals genetic risk underlying Parkinson's disease. Nat Genet 41, 1308–1312. https://doi.org/10.1038/ng.487

Singleton, A.B., Farrer, M., Johnson, J., Singleton, A., Hague, S., Kachergus, J., Hulihan, M., Peuralinna, T., Dutra, A., Nussbaum, R., Lincoln, S., Crawley, A., Hanson, M., Maraganore, D., Adler, C., Cookson, M.R., Muenter, M., Baptista, M., Miller, D., Blancato, J., Hardy, J., Gwinn-Hardy, K., 2003. alpha-Synuclein locus triplication causes Parkinson's disease. Science 302, 841. https://doi.org/10.1126/science.1090278

Smith, W.W., Liu, Z., Liang, Y., Masuda, N., Swing, D.A., Jenkins, N.A., Copeland, N.G., Troncoso, J.C., Pletnikov, M., Dawson, T.M., Martin, L.J., Moran, T.H., Lee, M.K., Borchelt, D.R., Ross, C.A., 2010. Synphilin-1 attenuates neuronal degeneration in the A53T alpha-synuclein transgenic mouse model. Hum Mol Genet 19, 2087–2098. https://doi.org/10.1093/hmg/ddq086

Smith, W.W., Pei, Z., Jiang, H., Dawson, V.L., Dawson, T.M., Ross, C.A., 2006. Kinase activity of mutant LRRK2 mediates neuronal toxicity. Nat Neurosci 9, 1231–1233. https://doi.org/10.1038/nn1776

Sontag, E.M., Samant, R.S., Frydman, J., 2017. Mechanisms and Functions of Spatial Protein Quality Control. Annual Review of Biochemistry 86, 97–122. https://doi.org/10.1146/annurev-biochem-060815-014616

Spillantini, M.G., Schmidt, M.L., Lee, V.M., Trojanowski, J.Q., Jakes, R., Goedert, M., 1997. Alpha-synuclein in Lewy bodies. Nature 388, 839–840. https://doi.org/10.1038/42166

Stender, E.G.P., Ray, S., Norrild, R.K., Larsen, J.A., Petersen, D., Farzadfard, A., Galvagnion, C., Jensen, H., Buell, A.K., 2021. Capillary flow experiments for thermodynamic and kinetic characterization of protein liquid-liquid phase separation. Nat Commun 12, 7289. https://doi.org/10.1038/s41467-021-27433-y

Strom, A.R., Emelyanov, A.V., Mir, M., Fyodorov, D.V., Darzacq, X., Karpen, G.H., 2017. Phase separation drives heterochromatin domain formation. Nature 547, 241–245. https://doi.org/10.1038/nature22989

Südhof, T.C., 2013. Neurotransmitter Release: The Last Millisecond in the Life of a Synaptic Vesicle. Neuron 80, 675–690. https://doi.org/10.1016/j.neuron.2013.10.022

Südhof, T.C., 2004. The Synaptic Vesicle Cycle. Annual Review of Neuroscience 27, 509–547. https://doi.org/10.1146/annurev.neuro.26.041002.131412

Südhof, T.C., 1990. The structure of the human synapsin I gene and protein. J Biol Chem 265, 7849–7852.

Südhof, T.C., Czernik, A.J., Kao, H.-T., Takei, K., Johnston, P.A., Horiuchi, A., Kanazir, S.D., Wagner, M.A., Perin, M.S., De Camilli, P., Greengard, P., 1989. Synapsins: Mosaics of Shared and Individual Domains in a Family of Synaptic Vesicle Phosphoproteins. Science 245, 1474–1480. https://doi.org/10.1126/science.2506642

Sun, J., Wang, L., Bao, H., Premi, S., Das, U., Chapman, E.R., Roy, S., 2019. Functional cooperation of α-synuclein and VAMP2 in synaptic vesicle recycling. Proc Natl Acad Sci U S A 116, 11113–11115. https://doi.org/10.1073/pnas.1903049116

Szargel, R., Rott, R., Engelender, S., 2008. Synphilin-1 isoforms in Parkinson's disease: regulation by phosphorylation and ubiquitylation. Cell Mol Life Sci 65, 80–88. https://doi.org/10.1007/s00018-007-7343-0

Takahashi, T., Yamashita, H., Nagano, Y., Nakamura, T., Kohriyama, T., Matsumoto, M., 2006. Interactions of Synphilin-1 with phospholipids and lipid membranes. FEBS Lett 580, 4479–4484. https://doi.org/10.1016/j.febslet.2006.07.019

Takamori, S., Holt, M., Stenius, K., Lemke, E.A., Grønborg, M., Riedel, D., Urlaub, H., Schenck, S., Brügger, B., Ringler, P., Müller, S.A., Rammner, B., Gräter, F., Hub, J.S., De Groot, B.L., Mieskes, G., Moriyama, Y., Klingauf, J., Grubmüller, H., Heuser, J., Wieland, F., Jahn, R., 2006. Molecular anatomy of a trafficking organelle. Cell 127, 831–846. https://doi.org/10.1016/j.cell.2006.10.030

Tanaka, M., Kim, Y.M., Lee, G., Junn, E., Iwatsubo, T., Mouradian, M.M., 2004. Aggresomes formed by alpha-synuclein and synphilin-1 are cytoprotective. J Biol Chem 279, 4625–4631. https://doi.org/10.1074/jbc.M310994200

Tang, L., 2019. Liquid phase separation. Nat Methods 16, 18–18. https://doi.org/10.1038/s41592-018-0269-7

Tanji, K., Mori, F., Kakita, A., Takahashi, H., Wakabayashi, K., 2011. Alteration of autophagosomal proteins (LC3, GABARAP and GATE-16) in Lewy body disease. Neurobiol Dis 43, 690–697. https://doi.org/10.1016/j.nbd.2011.05.022

Tanner, C.M., Ross, G.W., Jewell, S.A., Hauser, R.A., Jankovic, J., Factor, S.A., Bressman, S., Deligtisch, A., Marras, C., Lyons, K.E., Bhudhikanok, G.S., Roucoux, D.F., Meng, C., Abbott, R.D., Langston, J.W., 2009. Occupation and risk of parkinsonism: a multicenter case-control study. Arch Neurol 66, 1106–1113. https://doi.org/10.1001/archneurol.2009.195

Taoufiq, Z., Ninov, M., Villar-Briones, A., Wang, H.-Y., Sasaki, T., Roy, M.C., Beauchain, F., Mori, Y., Yoshida, T., Takamori, S., Jahn, R., Takahashi, T., 2020. Hidden proteome of synaptic vesicles in the mammalian brain. Proceedings of the National Academy of Sciences 117, 33586–33596. https://doi.org/10.1073/pnas.2011870117

Tretiakoff, 1919. Contribution a L'étude de L'anatomie Pathologique de Locus Niger de Soemmerling.

Trnka, F., Hoffmann, C., Wang, H., Sansevrino, R., Rankovic, B., Rost, B.R., Schmitz, D., Schmidt, H.B., Milovanovic, D., 2021. Aberrant Phase Separation of FUS Leads to

Lysosome Sequestering and Acidification. Front Cell Dev Biol 9, 716919. https://doi.org/10.3389/fcell.2021.716919

Ulmer, T.S., Bax, A., 2005. Comparison of structure and dynamics of micelle-bound human alpha-synuclein and Parkinson disease variants. J Biol Chem 280, 43179–43187. https://doi.org/10.1074/jbc.M507624200

Uversky, V.N., 2013. The alphabet of intrinsic disorder. Intrinsically Disordered Proteins 1, e24684. https://doi.org/10.4161/idp.24684

Uversky, V.N., 2003. A protein-chameleon: conformational plasticity of alpha-synuclein, a disordered protein involved in neurodegenerative disorders. J Biomol Struct Dyn 21, 211–234. https://doi.org/10.1080/07391102.2003.10506918

Uversky, V.N., Li, J., Fink, A.L., 2001. Evidence for a partially folded intermediate in alpha-synuclein fibril formation. J Biol Chem 276, 10737–10744. https://doi.org/10.1074/jbc.M010907200

van der Lee, R., Buljan, M., Lang, B., Weatheritt, R.J., Daughdrill, G.W., Dunker, A.K., Fuxreiter, M., Gough, J., Gsponer, J., Jones, D.T., Kim, P.M., Kriwacki, R.W., Oldfield, C.J., Pappu, R.V., Tompa, P., Uversky, V.N., Wright, P.E., Babu, M.M., 2014. Classification of Intrinsically Disordered Regions and Proteins. Chem. Rev. 114, 6589–6631. https://doi.org/10.1021/cr400525m

Vargas, K.J., Makani, S., Davis, T., Westphal, C.H., Castillo, P.E., Chandra, S.S., 2014. Synucleins regulate the kinetics of synaptic vesicle endocytosis. J Neurosci 34, 9364–9376. https://doi.org/10.1523/JNEUROSCI.4787-13.2014

Vargas, K.J., Schrod, N., Davis, T., Fernandez-Busnadiego, R., Taguchi, Y.V., Laugks, U., Lucic, V., Chandra, S.S., 2017. Synucleins Have Multiple Effects on Presynaptic Architecture. Cell Rep 18, 161–173. https://doi.org/10.1016/j.celrep.2016.12.023

Vera Rodriguez, A., Frey, S., Görlich, D., 2019. Engineered SUMO/protease system identifies Pdr6 as a bidirectional nuclear transport receptor. J Cell Biol 218, 2006–2020. https://doi.org/10.1083/jcb.201812091

Vogels, T., Leuzy, A., Cicognola, C., Ashton, N.J., Smolek, T., Novak, M., Blennow, K., Zetterberg, H., Hromadka, T., Zilka, N., Schöll, M., 2020. Propagation of Tau Pathology: Integrating Insights From Postmortem and In Vivo Studies. Biol Psychiatry 87, 808–818. https://doi.org/10.1016/j.biopsych.2019.09.019

Wahl, C., Kautzmann, S., Krebiehl, G., Strauss, K., Woitalla, D., Müller, T., Bauer, P., Riess, O., Krüger, R., 2008. A comprehensive genetic study of the proteasomal subunit S6 ATPase in German Parkinson's disease patients. J Neural Transm (Vienna) 115, 1141–1148. https://doi.org/10.1007/s00702-008-0054-3

Wakabayashi, K., Engelender, S., Tanaka, Y., Yoshimoto, M., Mori, F., Tsuji, S., Ross, C.A., Takahashi, H., 2002. Immunocytochemical localization of synphilin-1, an alpha-synuclein-associated protein, in neurodegenerative disorders. Acta Neuropathol 103, 209–214. https://doi.org/10.1007/s004010100451

Wakabayashi, K., Engelender, S., Yoshimoto, M., Tsuji, S., Ross, C.A., Takahashi, H., 2000. Synphilin-1 is present in Lewy bodies in Parkinson's disease. Ann Neurol 47, 521–523.

Wakabayashi, K., Hayashi, S., Kakita, A., Yamada, M., Toyoshima, Y., Yoshimoto, M., Takahashi, H., 1998. Accumulation of alpha-synuclein/NACP is a cytopathological feature common to Lewy body disease and multiple system atrophy. Acta Neuropathol 96, 445–452. https://doi.org/10.1007/s004010050918

Wakabayashi, K., Takahashi, H., 2003. α-Synuclein, synphilin-1 and inclusion body formation in α-synucleinopathies. International Congress Series, Advances in Brain Research. Cerebrovascular Disorders and Neurodegeneration. Proceedings of the 6th Hirosaki International Forum of Medical Science 1251, 149–156. https://doi.org/10.1016/S0531-5131(03)00115-8

Wakabayashi, K., Tanji, K., Mori, F., Takahashi, H., 2007. The Lewy body in Parkinson's disease: molecules implicated in the formation and degradation of alpha-synuclein

aggregates. Neuropathology 27, 494–506. https://doi.org/10.1111/j.1440-1789.2007.00803.x

Wakabayashi, K., Tanji, K., Odagiri, S., Miki, Y., Mori, F., Takahashi, H., 2013. The Lewy body in Parkinson's disease and related neurodegenerative disorders. Mol Neurobiol 47, 495–508. https://doi.org/10.1007/s12035-012-8280-y

Walsh, D.M., Hartley, D.M., Kusumoto, Y., Fezoui, Y., Condron, M.M., Lomakin, A., Benedek, G.B., Selkoe, D.J., Teplow, D.B., 1999. Amyloid beta-protein fibrillogenesis. Structure and biological activity of protofibrillar intermediates. J Biol Chem 274, 25945–25952. https://doi.org/10.1074/jbc.274.36.25945

Wang, H., Kelley, F.M., Milovanovic, D., Schuster, B.S., Shi, Z., 2021. Surface tension and viscosity of protein condensates quantified by micropipette aspiration. Biophysical Reports 1, 100011. https://doi.org/10.1016/j.bpr.2021.100011

Wang, L., Das, U., Scott, D.A., Tang, Y., McLean, P.J., Roy, S., 2014. α-synuclein multimers cluster synaptic vesicles and attenuate recycling. Curr Biol 24, 2319–2326. https://doi.org/10.1016/j.cub.2014.08.027

Wang, S.S.H., Held, R.G., Wong, M.Y., Liu, C., Karakhanyan, A., Kaeser, P.S., 2016. Fusion Competent Synaptic Vesicles Persist upon Active Zone Disruption and Loss of Vesicle Docking. Neuron 91, 777–791. https://doi.org/10.1016/j.neuron.2016.07.005

Wegmann, S., 2019. Liquid-Liquid Phase Separation of Tau Protein in Neurobiology and Pathology. Adv Exp Med Biol 1184, 341–357. https://doi.org/10.1007/978-981-32-9358-8_25

Wegmann, S., Eftekharzadeh, B., Tepper, K., Zoltowska, K.M., Bennett, R.E., Dujardin, S., Laskowski, P.R., MacKenzie, D., Kamath, T., Commins, C., Vanderburg, C., Roe, A.D., Fan, Z., Molliex, A.M., Hernandez-Vega, A., Muller, D., Hyman, A.A., Mandelkow, E., Taylor, J.P., Hyman, B.T., 2018. Tau protein liquid-liquid phase separation can initiate tau aggregation. EMBO J 37, e98049. https://doi.org/10.15252/embj.201798049

Weinreb, P.H., Zhen, W., Poon, A.W., Conway, K.A., Lansbury, P.T., 1996. NACP, a protein implicated in Alzheimer's disease and learning, is natively unfolded. Biochemistry 35, 13709–13715. https://doi.org/10.1021/bi961799n

Wetzel, R., 1996. For protein misassembly, it's the "I" decade. Cell 86, 699–702. https://doi.org/10.1016/s0092-8674(00)80143-9

Wilhelm, B.G., Mandad, S., Truckenbrodt, S., Kröhnert, K., Schäfer, C., Rammner, B., Koo, S.J., Claßen, G.A., Krauss, M., Haucke, V., Urlaub, H., Rizzoli, S.O., 2014. Composition of isolated synaptic boutons reveals the amounts of vesicle trafficking proteins. Science 344, 1023–1028. https://doi.org/10.1126/science.1252884

Wippich, F., Bodenmiller, B., Trajkovska, M.G., Wanka, S., Aebersold, R., Pelkmans, L., 2013. Dual Specificity Kinase DYRK3 Couples Stress Granule Condensation/Dissolution to mTORC1 Signaling. Cell 152, 791–805. https://doi.org/10.1016/j.cell.2013.01.033

Wolters, E.C., 2009. Non-motor extranigral signs and symptoms in Parkinson's disease. Parkinsonism Relat Disord 15 Suppl 3, S6-12. https://doi.org/10.1016/S1353-8020(09)70770-9

Woodruff, J.B., Gomes, B.F., Widlund, P.O., Mahamid, J., Honigmann, A., Hyman, A.A., 2017. The Centrosome Is a Selective Condensate that Nucleates Microtubules by Concentrating Tubulin. Cell 169, 1066-1077.e10. https://doi.org/10.1016/j.cell.2017.05.028

Wu, X., Cai, Q., Shen, Z., Chen, X., Zeng, M., Du, S., Zhang, M., 2019. RIM and RIM-BP Form Presynaptic Active-Zone-like Condensates via Phase Separation. Mol Cell 73, 971-984.e5. https://doi.org/10.1016/j.molcel.2018.12.007

Wu, X., Ganzella, M., Zhou, J., Zhu, S., Jahn, R., Zhang, M., 2021. Vesicle Tethering on the Surface of Phase-Separated Active Zone Condensates. Mol Cell 81, 13-24.e7. https://doi.org/10.1016/j.molcel.2020.10.029

Xie, Y.-Y., Zhou, C.-J., Zhou, Z.-R., Hong, J., Che, M.-X., Fu, Q.-S., Song, A.-X., Lin, D.-H., Hu, H.-Y., 2010. Interaction with synphilin-1 promotes inclusion formation of alpha-

synuclein: mechanistic insights and pathological implication. FASEB J 24, 196–205. https://doi.org/10.1096/fj.09-133082

Xing, Y., Nandakumar, A., Kakinen, A., Sun, Y., Davis, T.P., Ke, P.C., Ding, F., 2021. Amyloid Aggregation under the Lens of Liquid-Liquid Phase Separation. J Phys Chem Lett 12, 368–378. https://doi.org/10.1021/acs.jpclett.0c02567

Xu, B., Huang, S., Liu, Y., Wan, C., Gu, Y., Wang, D., Yu, H., 2022. Manganese promotes α-synuclein amyloid aggregation through the induction of protein phase transition. J Biol Chem 298, 101469. https://doi.org/10.1016/j.jbc.2021.101469

Y, S., J, K., C, P., Bt, H., Pj, M., 2005. The co-chaperone carboxyl terminus of Hsp70-interacting protein (CHIP) mediates alpha-synuclein degradation decisions between proteasomal and lysosomal pathways. The Journal of biological chemistry 280. https://doi.org/10.1074/jbc.M503326200

Zarranz, J.J., Alegre, J., Gómez-Esteban, J.C., Lezcano, E., Ros, R., Ampuero, I., Vidal, L., Hoenicka, J., Rodriguez, O., Atarés, B., Llorens, V., Gomez Tortosa, E., del Ser, T., Muñoz, D.G., de Yebenes, J.G., 2004. The new mutation, E46K, of alpha-synuclein causes Parkinson and Lewy body dementia. Ann Neurol 55, 164–173. https://doi.org/10.1002/ana.10795

Zbinden, A., Pérez-Berlanga, M., De Rossi, P., Polymenidou, M., 2020. Phase Separation and Neurodegenerative Diseases: A Disturbance in the Force. Dev Cell 55, 45–68. https://doi.org/10.1016/j.devcel.2020.09.014

Zeng, M., Chen, X., Guan, D., Xu, J., Wu, H., Tong, P., Zhang, M., 2018. Reconstituted Postsynaptic Density as a Molecular Platform for Understanding Synapse Formation and Plasticity. Cell 174, 1172-1187.e16. https://doi.org/10.1016/j.cell.2018.06.047

Zeng, M., Shang, Y., Araki, Y., Guo, T., Huganir, R.L., Zhang, M., 2016. Phase Transition in Postsynaptic Densities Underlies Formation of Synaptic Complexes and Synaptic Plasticity. Cell 166, 1163-1175.e12. https://doi.org/10.1016/j.cell.2016.07.008

Zeng, Y., Yang, J., Zhang, B., Gao, M., Su, Z., Huang, Y., 2021. The structure and phase of tau: from monomer to amyloid filament. Cell Mol Life Sci 78, 1873–1886. https://doi.org/10.1007/s00018-020-03681-x

Zhao, Y.G., Zhang, H., 2020. Phase Separation in Membrane Biology: The Interplay between Membrane-Bound Organelles and Membraneless Condensates. Developmental Cell 55, 30–44. https://doi.org/10.1016/j.devcel.2020.06.033

Zhu, M., Fink, A.L., 2003. Lipid binding inhibits alpha-synuclein fibril formation. J Biol Chem 278, 16873–16877. https://doi.org/10.1074/jbc.M210136200

Zhu, M., Li, J., Fink, A.L., 2003. The association of alpha-synuclein with membranes affects bilayer structure, stability, and fibril formation. J Biol Chem 278, 40186–40197. https://doi.org/10.1074/jbc.M305326200

Zhu, X., Siedlak, S.L., Smith, M.A., Perry, G., Chen, S.G., 2006. LRRK2 protein is a component of Lewy bodies. Ann Neurol 60, 617–618. https://doi.org/10.1002/ana.20928

Ziaunys, M., Sakalauskas, A., Mikalauskaite, K., Smirnovas, V., 2021. Polymorphism of Alpha-Synuclein Amyloid Fibrils Depends on Ionic Strength and Protein Concentration. Int J Mol Sci 22, 12382. https://doi.org/10.3390/ijms222212382

Ziltener, P., Rebane, A.A., Graham, M., Ernst, A.M., Rothman, J.E., 2020. The golgin family exhibits a propensity to form condensates in living cells. FEBS Letters 594, 3086–3094. https://doi.org/10.1002/1873-3468.13884

Ziv, N.E., Fisher-Lavie, A., 2014. Presynaptic and Postsynaptic Scaffolds: Dynamics Fast and Slow. Neuroscientist 20, 439–452. https://doi.org/10.1177/1073858414523321

# LIST OF PUBLICATIONS

## Papers published during graduate studies:

(*equal contribution)

- **Sansevrino R**, Hoffmann C, Milovanovic D. Condensate biology of synaptic vesicle clusters. Trends Neurosci. 2023 Apr;46(4):293-306. doi: 10.1016/j.tins.2023.01.001. Epub 2023 Jan 30. PMID: 36725404.
- Stempels FC, Jiang M, Warner HM, Moser ML, Janssens MH, Maassen S, Nelen IH, de Boer R, Jiemy WF, Knight D, Selley J, O'Cualain R, Baranov MV, Burgers TCQ, **Sansevrino R**, Milovanovic D, Heeringa P, Jones MC, Vlijm R, Ter Beest M, van den Bogaart G. Giant worm-shaped ESCRT scaffolds surround actin-independent integrin clusters. J Cell Biol. 2023 Jul 3;222(7):e202205130. doi: 10.1083/jcb.202205130. Epub 2023 May 18. PMID: 37200023; PMCID: PMC10200693.
- Freitag K, Sterczyk N, Wendlinger S, Obermayer B, Schulz J, Farztdinov V, Mülleder M, Ralser M, Houtman J, Fleck L, Braeuning C, **Sansevrino R**, Hoffmann C, Milovanovic D, Sigrist SJ, Conrad T, Beule D, Heppner FL, Jendrach M. Spermidine reduces neuroinflammation and soluble amyloid beta in an Alzheimer's disease mouse model. J Neuroinflammation. 2022 Jul 2;19(1):172. doi: 10.1186/s12974-022-02534-7. PMID: 35780157; PMCID: PMC9250727.
- Hoffmann C*, **Sansevrino R***, Morabito G, Logan C, Vabulas RM, Ulusoy A, Ganzella M, Milovanovic D. Synapsin Condensates Recruit alpha-Synuclein. J Mol Biol. 2021 Jun 11;433(12):166961. doi: 10.1016/j.jmb.2021.166961. Epub 2021 Mar 25. PMID: 33774037.
- Trnka F*, Hoffmann C*, Wang H*, **Sansevrino R**, Rankovic B, Rost BR, Schmitz D, Schmidt HB, Milovanovic D. Aberrant Phase Separation of FUS Leads to Lysosome Sequestering and Acidification. Front Cell Dev Biol. 2021 Oct 22;9:716919. doi: 10.3389/fcell.2021.716919. PMID: 34746121; PMCID: PMC8569517.

## Manuscripts in preparation/pre-prints:

- Methorst J, Verwei N, Hoffmann C, Chodnicki P, **Sansevrino R**, Wang H, van Hilten N, Aschmann D, Kros A, Andreas L, Czub J, Milovanovic D, Risselada HJ. Physics-based inverse design of cholesterol attracting transmembrane helices reveals a paradoxical role of hydrophobic length. bioRxiv 2021.07.01.450699; doi: https://doi.org/10.1101/2021.07.01.450699
- **Sansevrino R**, Hoffmann C, Chen J, Korobinikov A, Brosius P, Jackson J, Aguilar Pérez G, Wang H, Le Gros M, Rizzoli SO, Outeiro T, Bano D, Larabell C, Milovanovic D. Sequestering of Membrane-Bound Organelles by the Aberrant Condensates of Alpha-Synuclein. Under review.